uOttawa

L'Université canadienne
Canada's university

FACULTÉ DES ÉTUDES SUPÉRIEURES ET POSTOCTORALES

uOttawa

L'Université canadienne
Canada's university

FACULTY OF GRADUATE AND POSDOCTORAL STUDIES

Weihong Li

AUTEUR DE LA THÈSE / AUTHOR OF THESIS

M.A.Sc. (Civil Engineering)

GRADE / DEGREE

Department of Civil Engineering

FACULTÉ, ÉCOLE, DÉPARTEMENT / FACULTY, SCHOOL, DEPARTMENT

Adhesive Applied Roofing System Resistance Evaluation and its Quantification

TITRE DE LA THÈSE / TITLE OF THESIS

Hiroshi Tanaka

DIRECTEUR (DIRECTRICE) DE LA THÈSE / THESIS SUPERVISOR

Bas Baskaran

CO-DIRECTEUR (CO-DIRECTRICE) DE LA THÈSE / THESIS CO-SUPERVISOR

Beatriz Martin-Perez

Magdi Mohareb

David Lau

Gary W. Slater

Le Doyen de la Faculte des etudes superieures et postdoctorales / Dean of the Faculty of Graduate and Postdoctoral Studies

Adhesive Applied Roofing System Resistance Evaluation and its Quantification

By

Weihong Li

Thesis submitted to the Faculty of Graduate and Postdoctoral Studies of University of Ottawa in partial fulfillment of the requirements for

The Degree of Master of Applied Science

in Civil Engineering

The M.A.Sc. program in Civil Engineering is a joint program
with Carleton University administered by the
Ottawa-Carleton Institute for Civil Engineering

Department of Civil Engineering
University of Ottawa, Ottawa, Ontario, Canada
June, 2010

Your file Votre référence
ISBN: 978-0-494-73791-0
Our file Notre référence
ISBN: 978-0-494-73791-0

Abstract

Adhesive Applied Roofing System (AARS) is a new generation of built-up roof, gaining popularity in the North American low-slope roofing market. All components of AARS are integrated using adhesives. Wind flow creates suction over a low-slope roof, which exerts uplift forces on the roof system. The components of AARS are subjected to the combined action of tensile and shearing forces due to the dynamic wind uplift action. As part of a research project, to quantify the wind performance of AARS, three different test methods, namely, pullout (to simulate the tensile force), peel (to simulate the shear force), and wind uplift tests were developed by Current (2009), Wu (2008) and Murty (2010), respectively. Three test methods have been submitted to standard development organizations for industrial applications.

The present study proposes a correlation among these three different test methods, namely, *"Higher resistance in both peel and pullout tests will result in the same or higher wind uplift resistance"*. The present proposal is being verified through experimental study. For four different scenarios, two set of samples were constructed by varying only one component between the samples. For each sample, more than eight specimens were tested in all three test methods. Data from peel, pullout and wind uplift test methods were compared and it successfully verified the present hypothesis. It is concluded that the test results obtained from the small-scale pullout and peel experiments can be used to predict the effectiveness of full-scale system behaviour. This finding is very useful to assess the wind uplift performance of AARS that are already in service. It is also applicable to the situation where the component substitution for AARS is needed at the construction site.

To help the industrial partners, a portable tester was designed such that it can be used for pullout and peel tests in the field. The design specifications of the portable tester were extracted from the requirements of the pullout and peel test

methods based on the laboratory tests. The tester was manufactured by SAI Design Inc. First, the functionality of the portable tester was verified by testing the resistance of roofing fasteners. To further validate the portable tester, more than two hundred AARS specimens of different configurations were constructed and tested by using both the portable tester and Instron machine. The test results and observed failure modes were compared. The data confirmed that the portable tester is a useful and valid equipment in performing both the pullout and peel tests. The device can be used in the field for the evaluation of system response under wind action. Thus it will be useful in quantifying the impact of environmental conditions on the AARS specimens and to examine the effects of component substitutions.

Acknowledgments

This study was part of the collaborative research project between the University of Ottawa and the National Research Council Canada (NRCC), titled *"Development of wind uplift standard for adhesive applied low slope roof systems",* supported by the Natural Sciences and Engineering Research Council (NSERC - CRD 3065819-04). This research was also supported by four Canadian roofing industry partners: Bakor Inc.; IKO Industries Ltd.; Soprema Inc. and Tremco Inc., as well as the Roofing Contractors Association of British Columbia, (RCABC).

I am heartily thankful to my research and academic supervisors, Dr. Bas Baskaran and Dr. Hiroshi Tanaka for their excellent supervision, great encouragement, and continuous support.

Dr. Bas Baskaran provided me tremendous advice and guidance from the beginning of this study as well as giving me extraordinary experiences throughout the work. His true intuition as a scientist, down-to-earth spirit and rich research experience have made a crucial contribution to this research project, which exceptionally inspired and enriched my growth as a student, a researcher and a scientist, which I wanted to be. He provided me with encouragement and support in various ways including the financial subsidy.

Dr. Hiroshi Tanaka gave me enormous guidance and valuable advice in scientific research and thesis writing with his extensive and profound knowledge. Out of his busy schedule, he made a huge effort and spent precious time to read the draft thesis very carefully and gave his critical comments, corrections on it rapidly. Without him, this thesis would have been unintelligible for the readers. I am really grateful to him for the generous financial support he gave me.

It is a pleasure to express my gratitude to Dr. Ralph Paroli, Director of the Building Envelope & Structure of NRC-IRC, for allowing me to carry out the research work at NRC-IRC.

I gratefully thank Helen Yew and Jayson Current for training me how to operate the Instron machine to carry out the peel, pullout and other ASTM standard tests. I would also like to thank them for their practical suggestions on preparation of specimens.

I am very grateful to Steven Ko and Bona Murty for their advice and willingness to share their bright thoughts and great experience with me. I appreciate it very much for the perfect laboratory management by Steven Ko so I could optimally carry out the experiments.

I also benefited by outstanding works from Amor Duric's help with his particular skills in handling different equipment at the work shop of NRCC. The tested specimens would not have been ready without him.

Many thanks go to Sudhakar Molleti, Pascal Beaulieu, and Gordon Sherrer for their valuable advice in scientific discussion. It was a pleasure working together with them. They provided me various types of assistance throughout the development of this thesis.

I convey special acknowledgement to Manon Racine, Lise Rousseau and Yolande Hogan at the Department of Civil Engineering, University of Ottawa for their indispensable help dealing with the administration.

Finally, I would like to thank everybody who was important to the successful realization of this thesis, and express my apology that I could not mention personally one by one.

Contents

List of Tables

List of Figures

Glossary

Symbols

C_e	exposure factor
C_g, C_{gi}	external and internal gust effect factors
C_p, C_{pi}	external and internal pressure coefficients
H	the height of building
I_w	importance factor, provided in NBCC 2005
L	the length of building
p	the measured pressure on a building surface
P_e, P_i	specified external and internal pressure acting statically and in the direction normal to the surface
q	reference velocity pressure
V	the mean wind speed
V_0	building internal volume, in m^3
W	the width of building
α	roof pitch
ρ	density of the air at the temperature and barometric pressure measured

Abbreviations

AARS	Adhesive Applied Roofing Systems
ACB	Asphalt Core Cover Board
Adh	Adhesive
Adh/SD	Adhesive on Steel Deck failed
Adh/BS-CB	Adhesive between BaseSheet-CoverBoard failed
Adh/BS-ISO	Adhesive between BaseSheet and Insulation

AF	Acrylic Facer Insulation
ASTM	American Society for Testing and Materials
BRS	Ballasted Roofing System
BUR	Built-Up Roof
CB	Cover Board
CB/B	Cover Board Brittle
CB/Se	Cover Board Separation
CB/Sp	Cover Board Splitting
CMHC	Canada Mortgage and Housing Corporation
FB	Fiber Board
FBRS	Fully Bonded Roofing System
FOV	Failure Occurrence Value
ISO	Insulation
ISO Facer/D	Insulation Facer Delamination
ISO Facer/R	Insulation Facer Rupture
ISO Facer/T	Insulation Facer Tearing
ISO-R	Insulation Rupture
MARS	Mechanically Attached Roofing Systems
PF	Paper facer Insulation
SD	Standard Deviation
VB	Vapour Barrier

Chapter 1: Introduction

1.1 Low Slope Roofing System

A roof of a building protects its occupancies and contents from environmental natural conditions such as rain, wind and solar radiation. It has to be, therefore, designed with utmost care considering its functional effectiveness and maintenance under these conditions. In terms of the roof slope, the roof systems can be divided into two groups - low slope and steep slope roofing systems. Typically, residential roofs belongs to the steep slope roof system, whereas the commercial or industrial buildings such as office buildings, warehouses, retail buildings and plants and factories often have low slope roofs, see Figures 1.1 (a) and (b).

Canadian Asphalt Shingle Manufacturers' Association defines the low slope when the slope is less than 4:12 or 18.5°. However, according to the *Building Envelope Design Guide* (Tom Smith, 2009), low slope roof is defined as the roof slope of less than 3:12 or 14°. Most of the so-called low slope roofs are about ¼:12 (or 1.2°), which is much more flat compared to these definitions. When the roof slope is very low, the roofs tend to be exposed to more sever wind uplift, wind-driven rain and ice dams, and they are particularly vulnerable under the Canadian climate conditions.

According to the locations where the membranes are placed in a roof assembly, the low slope roofing systems are divided into two types: the conventional roofing assembly for which the membrane is on top of the insulation and the inverted roofing assembly for which the membrane is below the insulation. Based on the type of the coverings, the conventional roofing assemblies can be further classified as:

- Built-up (BUR) roofing system;
- Modified bitumen membrane roofing system;
- Thermoplastic (TPO & PVC) roofing system; and
- Thermoset (EPDM) roofing system.

From the point of view of the roof component attachment methods, the conventional roofing assemblies can also be classified as:

- Ballasted roofing system (BRS);
- Mechanically attached roofing system (MARS);
- Fully bonded roofing system (FBRS); and
- Adhesive applied roofing system (AARS).

The features of these roofing systems are illustrated in Sections 1.2 and 1.4. Furthermore, the market survey of the low slope roofing systems based on the coverings is also analyzed in Section 1.3. Section 1.5 gives a scope of the present AARS research project. The objectives of this thesis are provided in Section 1.6. The outline of the thesis is given in Section 1.7.

(a) Steep slope roof for residential house

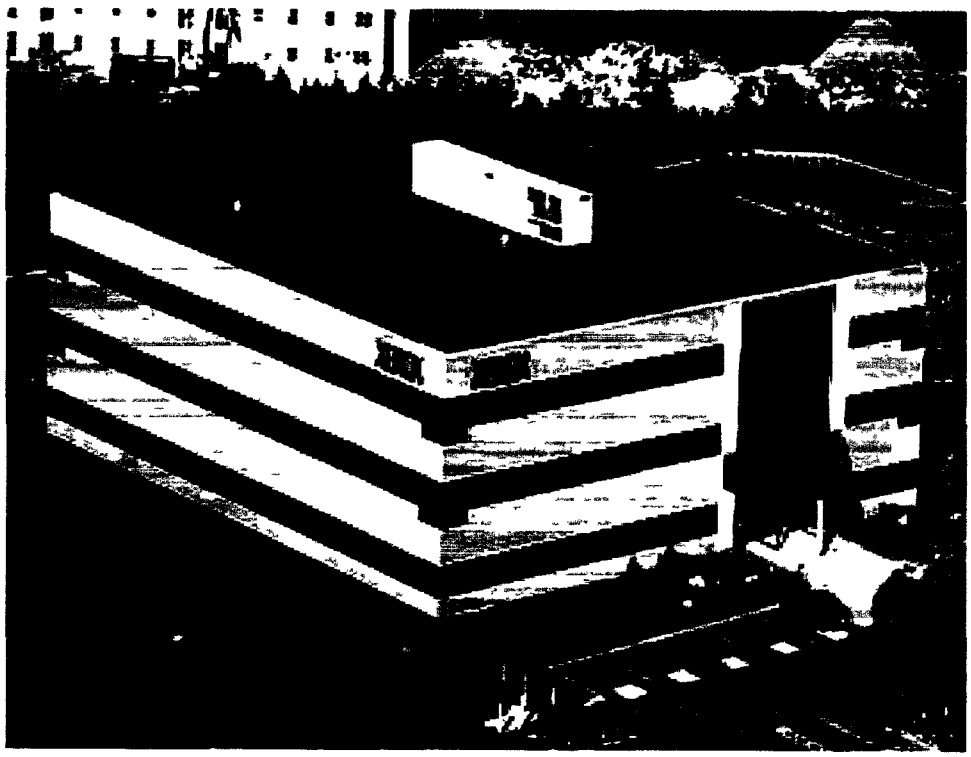

(b) Low slope roof for commercial building

Figure 1.1: Low slope roof system vs. steep slope roof system

1.2 Classification of Low Slope Roofing System by Coverings

Among the low slope roofing systems, the built-up roof (BUR) was the most conventional roofing system employed in North America. However, since mid-to-late 1970s, a variety of low slope roof systems started competing with the traditional built-up roofs. These newer systems include the modified bitumen, PVC & TPO, EPDM roofing system and so on, according to their covering types. Their features are illustrated in the following sub-sections.

1.2.1 Built-Up Roofing System (BUR)

BUR is by far the oldest of the modern low-slope roof systems and is still popular in commercial application. BUR systems generally are composed of multiple layers of bitumen and reinforcing fabrics that create a finished membrane in field. The reinforcing fabrics are called roofing felts or ply sheets. Roofing systems are also classified based on the number of plies. Four plies of felt are recommended generally and it is known as a four-ply roofing system. The bitumen typically used in BUR roof systems is asphalt, coal tar or cold-applied adhesives. Fiberglass felts are typically used for asphalt BURs. The asphalt is typically hot-applied, as seen in Figure 1.2, but cold-applied asphalt is also available. The membrane is either adhered to the substrate in bitumen, or a base sheet (i.e., a heavy felt), which is mechanically attached. When a BUR is installed over the polyisocyanurate insulation, it is recommended by the National Roofing Contractors Association (NRCA) that a suitable cover board be installed over the polyisocyanurate insulation.

The exposed asphalt membrane is susceptible to relatively rapid weathering. Therefore, BURs are surfaced with aggregate, a field-applied coating or a mineral surface cap sheet, mostly.

1.2.2 Modified Bitumen Membrane Roofing System

Modified bitumen membranes are typically composed of the pre-fabricated polymer-modified asphalt sheets. Polymers are added to bitumen to enhance various properties of the bitumen. Modified bitumen membrane is manufactured into a roll material. Modified bitumen is essentially a "factory assembled" built-up roof. The quality of the modified bitumen products is highly dependent on the quality and compatibility of the bitumen and polymers, and the recipe used during the blending process.

Modified bitumen roof system membranes are composed of multiple layers, much like BUR membranes. Modified bitumen roofing systems are typically installed as a two-ply system (Cap Sheet and Base Sheet) and almost always are fully adhered, see Figure 1.3. The examples for the base sheet and cap sheet material are shown in Figure 1.6 (a) and (b). The surfacing for modified bitumen membranes include aggregate surfacing, mineral surfacing, metal foil-laminate surfacing etc. Modified bitumen membranes exhibit general toughness and resistance. There are two primary types of modified bitumen membrane:

(1) Atactic Polypropylene (APP)

APP polymer is blended with asphalt and fillers. The mixture is then factory-fabricated into rolls that are typically one meter wide. The polymer-modified bitumen membranes are typically heat-welded or torch-applied. Generally, APP modifiers impart a "plasticized" quality to asphalt.

(2) Styrene - Butadiene - Styrene (SBS)

SBS polymer is blended with asphalt and fillers. The mixture is then factory-fabricated into rolls with reinforcement. SBS sheets generally have good low-temperature flexibility. The SBS polymer-modified bitumen membranes are commonly installed by hot mopping of asphalt, similar to BUR systems, or as cold adhesive. Some SBS modified membranes are self-adhesive, or they

contain an adhesive backing. Generally, SBS modifiers impart a "rubberized" quality to asphalt.

1.2.3 Thermoplastic Roofing System (PVC & TPO)

The most common thermoplastic roof membranes are PVC (polyvinyl chloride) and TPO (thermoplastic polyolefin), shown in Figures 1.7 and 1.8, respectively. These membranes can be repeatedly softened by heating or hardened when cooled. Because of the materials' chemical nature, thermoplastic membranes are seamed by heat welding with hot air or solvent welding. PVC membranes are among the oldest single-plies, which are still available. Sheet width ranges from 6 feet to 12 feet (1.83 m to 3.66 m). Sheets are typically 45 mils to 90 mils (1.14 mm to 2.29 mm) thick. TPO is the latest thermoplastic membrane introduced into the market. It was commercialized in North America in the early 1990s. Sheet width ranges from 6 to 12 feet (1.83 m to 3.66 m). Sheets are typically 40 mils to 100 mils (1.02 mm to 2.54 mm) thick.

1.2.4 Thermoset Roofing System (EPDM)

Thermoset materials solidify, or "set," irreversibly after heating. EDPM (Ethylene Propylene Diene Monomer) is a synthetic rubber sheet, see Figure 1.9. EPDM roof system is one of the common types of low-slope roofing. It has been in use for roofs in Canada since the 1960's. The sheets are available typically in width of 10, 20 and 45 or 50 feet (3.05, 6.10 and 13.72 or 15.24 m) and 45 mils to 60 mils (1.14 mm to 1.52 mm) thick.

PVC, TPO and EPDM membranes are factory-manufactured sheet membranes and installed in a single layer on low slope roofs. Therefore, they also are categorized as single-ply roofing system. Single-ply membranes can be installed fully adhered, mechanically attached or held down with ballast. In many instances, a combination of attachment methods is used to secure a roof system.

Most single-ply roof systems do not receive surfacing. The photos of a PVC roof system and an EPDM roof system are shown in Figures 1.4 and 1.5.

In comparison to BUR or the modified bitumen membrane system, the singly-ply system is light weight, relatively simple to install and inexpensive. However, it does not offer nearly as much toughness and resistance to abuse (or mechanical damage of membrane) as the BUR and modified bitumen membranes do.

Figure 1.2: Built-up roofing system
http://products.construction.com

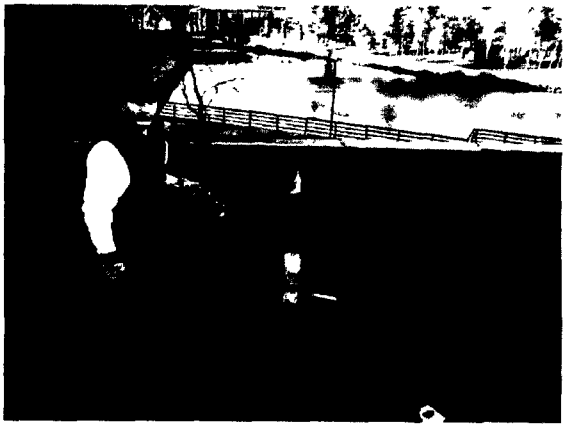

Figure 1.3: Modified bitumen roofing system
http://www.bellaremodeling.net

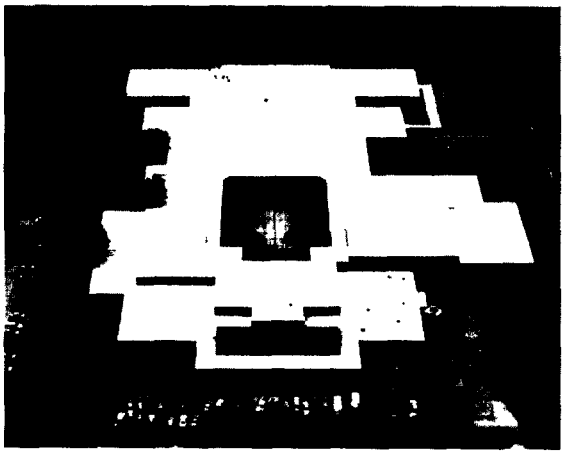

Figure 1.4: PVC roofing system
http://greensolinc.com

Figure 1.5: EPDM roofing system

(a) Base sheet membrane

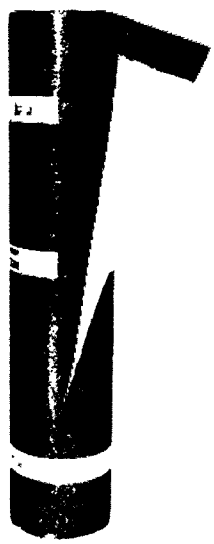

(b) Cap sheet membrane with granules surface

Figure 1.6 Modifier bitumen membranes
(http://www.soprema.ca)

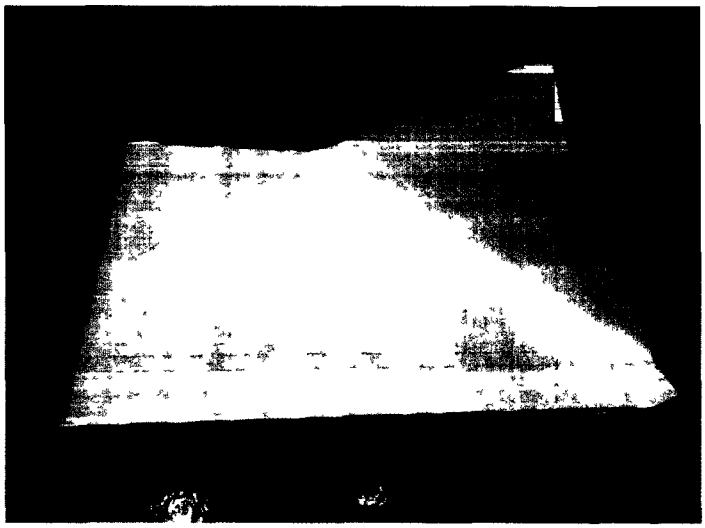

Figure 1.7: PVC membrane

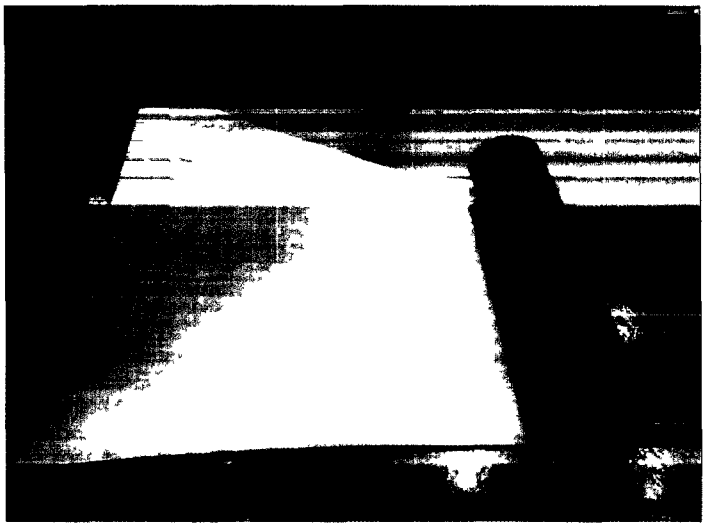

Figure 1.8: TPO membrane

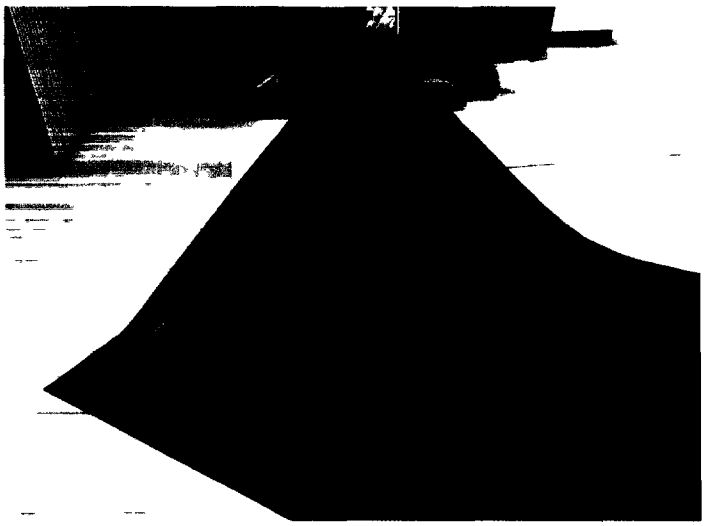

Figure 1.9: EPDM membrane

1.3 Roof Market of Low Slope Roofing System based on Coverings

Roofing community in North America has undergone much changes over the last 25 years along with advances in material science, computer-aided design and engineering application. Roofing systems have been changing from the traditional type of BUR-coal tar hot applied to modified bitumen multiply and polymer-base single-ply. Their market shares also changed with time.

The *Canadian Roofing Contractors' Association (CRCA)* and the *National Roofing Contractors Association (NRCA)* are continuously monitoring the reality of roofing market. According to the CRCA survey in 2000, the new construction and re-roofing of low slope roofing systems had an equal market share in Canada. The modified bitumen roofing systems dominated the low slope roof market in 2000 by occupying 55% of the new construction and re-roofing, whereas the traditional BUR roofing covered 27% of the total market. The single-ply including the PVC, TPO and EPDM roofing systems had a total of 13% and other types held only 5% of the new construction and re-roofing. Figure 1.10 shows the three main low slope roofs in Canada and their market shares for new construction and re-roofing.

In the same year in the United States, the new construction and re-roofing of the low slope roofing systems had somewhat different market shares between different types. As per the 2000–2001 market survey held by the National Roofing Contractors Association (NRCA), the average sales of the three main low slope roof systems for new and re-roofing were: the modified bitumen roofs 23%, BUR 25%, single-ply 40%, and others 3%, as seen in Figure 1.11. Apparently the single-ply roofs dominated the market percentages and the BUR roofs had more sales percentage than the modified bitumen roof system.

As time goes on, the tendency started changing. Figures 1.12 (a) and (b), which were developed based on the 2008–09 NRCA market survey, show the same

variation tendency on market sales during the historical record of 2000 to 2008, no matter for the new construction or re-roofing for the low slope roofing systems. That is, the sales percentages of single-ply roofing system kept increasing and the sales percentages of BUR roofing system kept dropping. Meanwhile, the sales percentages of modified bitumen roofing system and other roof system types hold at around 20% and 13% without obvious changes. During these eight years, the single-ply roofing for new construction has increased 11 growth points from 40% to 51% in the market, while 10 growth points from 36% to 46% for re-roofing projects. It is also noted that starting from 2002, the annual market share of modified bitumen roofing surpass BUR roofing about an average of 3% for both new construction and re-roofing.

Clearly, the single-ply roof systems enjoy the largest market share for service in United States in recent years. Based on the NRCA market survey of 2008-09, the market distribution among the single-ply roof systems in 2008 is: EPDM 49%, TPO 37%, and PVC 14%, see Figure 1.12 (a). EPDM membrane roofs occupied almost a half of the single-ply market volume. The TPO roofs had the second largest portion of single-ply market in 2008 and were expected to be more active in 2009 with 5% increase, while the PVC roof system kept the market share without change. Figure 1.12 (b), shows that the low slope roofing sales for re-roofing had the same trend. Also, the market share of PVC roof systems stayed in steady. The sale of TPO roof system was expected to have 2% increases.

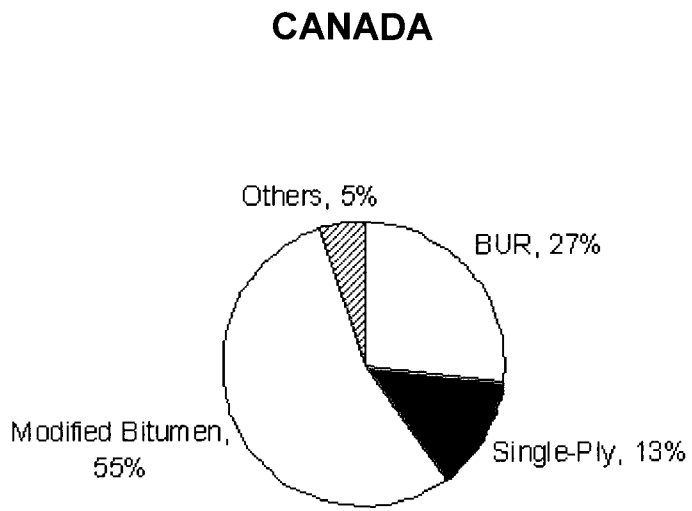

Figure 1.10: Average market share for low-slope roofs in Canada in 2000 (Canadian Roofing Contractors' Association, 2000–2001 Annual Market Survey)

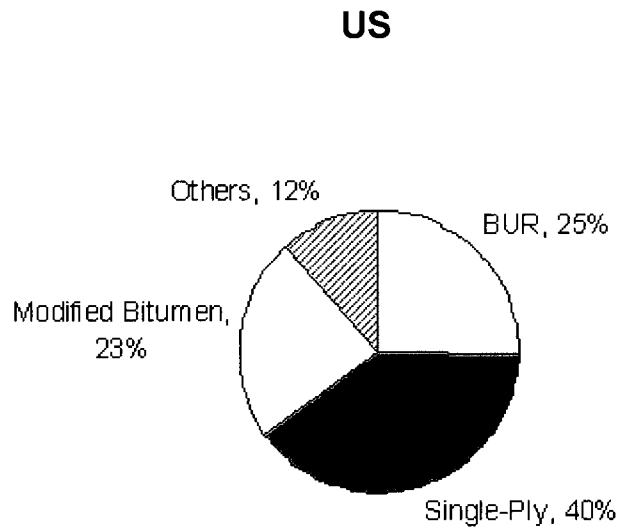

Figure 1.11: Average market share for low slope roofs in United States in 2000 (National Roofing Contractors Association, 2000–2001 NRCA Market Survey)

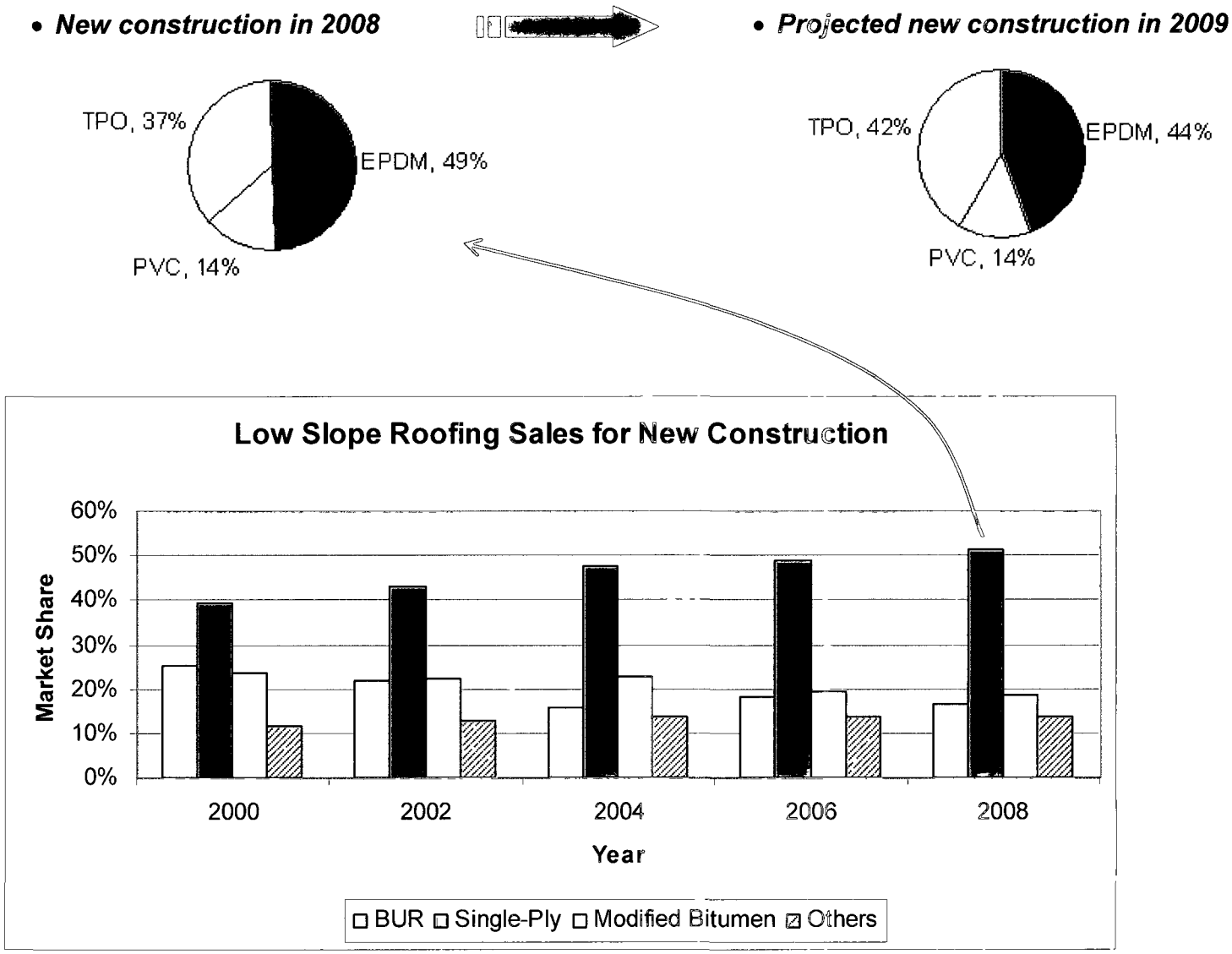

(a) Historical data for new construction

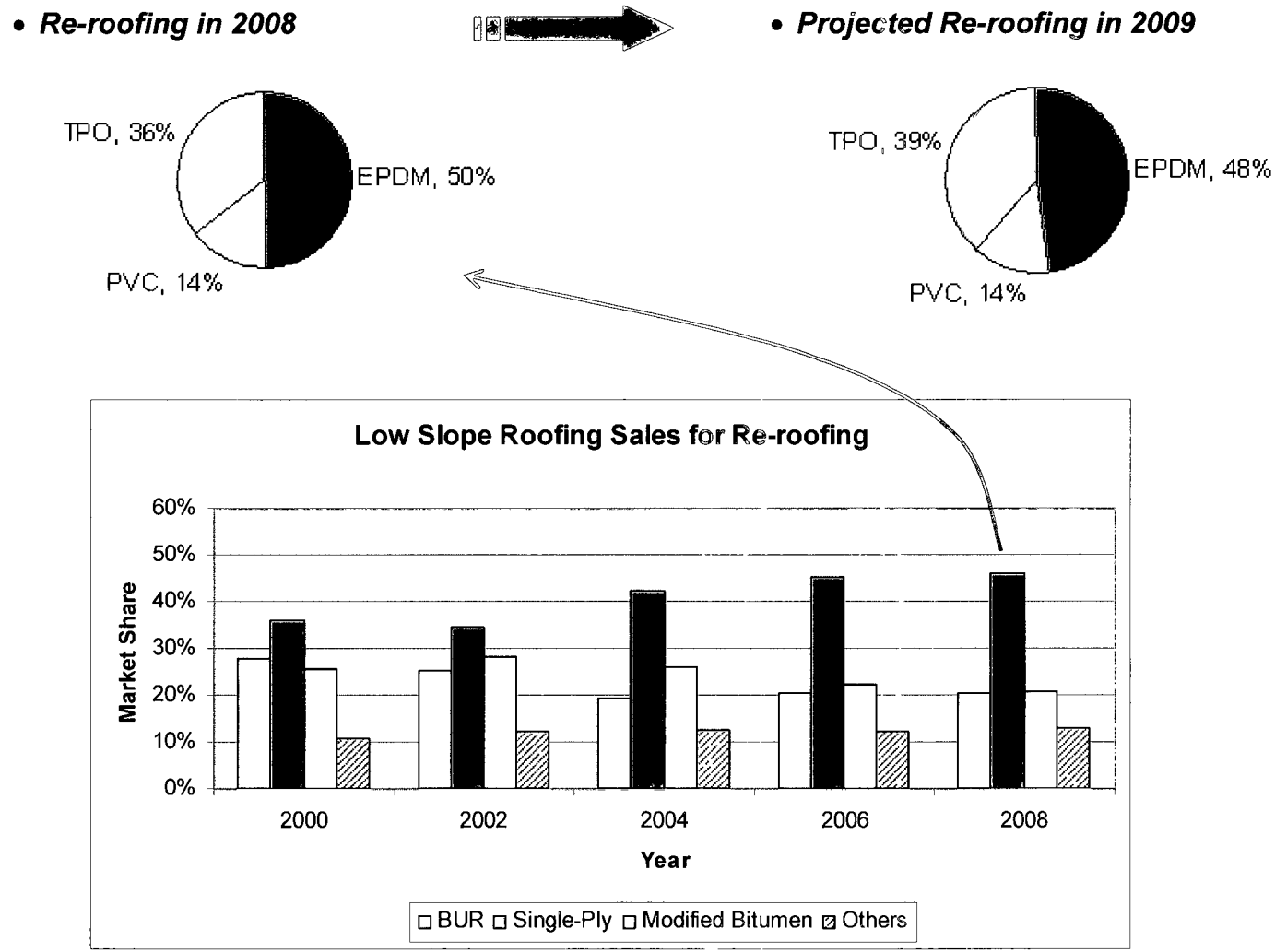

(b) Historical data for Re-roofing

Figure 1.12: Historical average market share for low slope roofs in United States and distribution of EPDM, PVC and TPO roofing for single-ply system (National Roofing Contractors Association, 2008–09 NRCA Market Survey)

1.4 Classification of Low Slope Roofing System by Attachment

In accordance with the attachment methods of the roof components, the conventional roofing can be further divided into four categories:

(1) Ballasted roofing system (BRS);
(2) Mechanically attached roofing system (MARS);
(3) Fully bonded roofing system (FBRS); and
(4) Adhesive applied roofing system (AARS).

In the following sub-sections, their structural features are explained orderly with examples.

1.4.1 Ballasted Roofing System (BRS)

The membrane is loose-laid over the insulation and then held in place with ballast to resist wind uplift forces, see Figure 1.13. At the roof perimeters, the membranes are attached to the roof/wall junctions. Ballast can either be large, well rounded aggregates (for example, 1-½ to 2-½ inches (38 mm to 64 mm) in nominal diameter, depending upon the design wind speed, or concrete pavers weighing 18 to 25 psf (88 to 122 kg/ m^2), or specially designed lightweight interlocking concrete pavers weighing approximately 10 psf (49 kg/m^2). For this group, the insulation is loosely laid or mechanically fastened to the roof deck.

Ballasted roof can have either single-ply membranes including PVC, TPO, EPDM, or Modified Bitumen. This system has a great versatility in the selection of single-ply membranes; compatible with most roof insulation materials. However, the self-weight of the system is relatively heavier than other systems. Also the availability of suitable gravels may be limited, as it has to be well rounded to prevent puncture of the membrane. Also, this system is limited to a maximum roof deck slope of 2:12, or the slope angle of 9.5°, to prevent gravels slipping down *(ANSI/SPRI RP-4 2008)*, whereas the slope of low slope roofing may go up to 4:12 (angle of 18.5°) according to the Canadian Asphalt Shingle Manufacturers' Association as mentioned earlier. Figure 1.14 shows the ballasted roofing system.

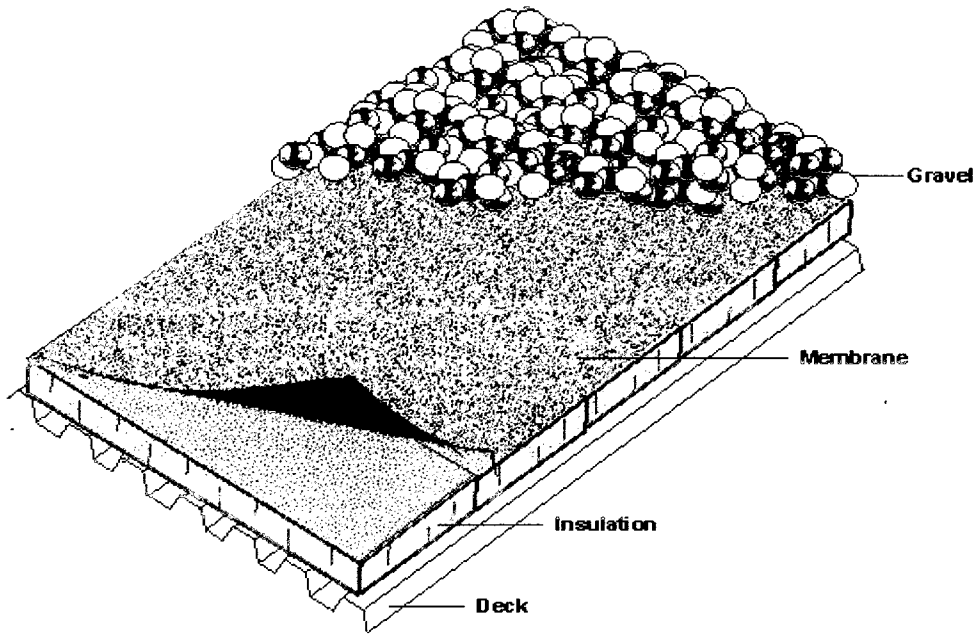

Figure 1.13: Membrane loose-laid, held in place by gravel weight

Figure 1.14: Typical view of the ballasted roof system

1.4.2 Mechanically Attached Roofing System (MARS)

All the roof components of this system are mechanically fastened to the roof deck with fasteners and stress plates or metal / polymer batten. The membrane is loose-laid over substrate except for discrete rows of fasteners at joint seam positions, see Figure 1.15. There are a variety of fastening and seam fabrication with this method, as described in *A Guide for the Wind Design of Mechanically Attached Flexible Membrane Roofs* (Baskaran & Smith 2005).

This system mostly has single-ply membranes including PVC, TPO and EPDM, or two-ply modified bituminous membrane. It is ideal for large production facilities such as manufacturing plants and warehouses. The light self-weight of this system allows lighter structures, thus saving on overall building construction cost can be expected. A potential shortcoming of this system is that the risk of mechanically damaging the membrane is higher because the membrane is fully exposed. Figure 1.16 shows the construction methods of MARS for a TPO membrane at the position of seam.

1.4.3 Fully Bonded Roofing System (FBRS)

Figure 1.17 displays a 3D view of the fully bonded roof configuration. Similar to the mechanically attached system (MARS), insulation is mechanically fastened to the roof deck by using fasteners and stress plates or metal / polymer batten, but in this system, the roof membrane is secured in place with a continuous layer of solvent / water-based or hot bitumen adhesives.

This type of roofing system can be constructed with a variety of single-ply membranes such as PVC, TPO, EPDM, and the modified bitumen membrane. Some self-adhesive membranes are also available for easy construction, eliminating on-site guessing by the installer at the same time, resulting in more uniform application and less chance of adhesive-related failure under the wind uplifting. Figures 1.18 (a) and (b) show two main application methods for membrane assembly. In Figure 1.18 (a), the cold adhesive is fully coated on top

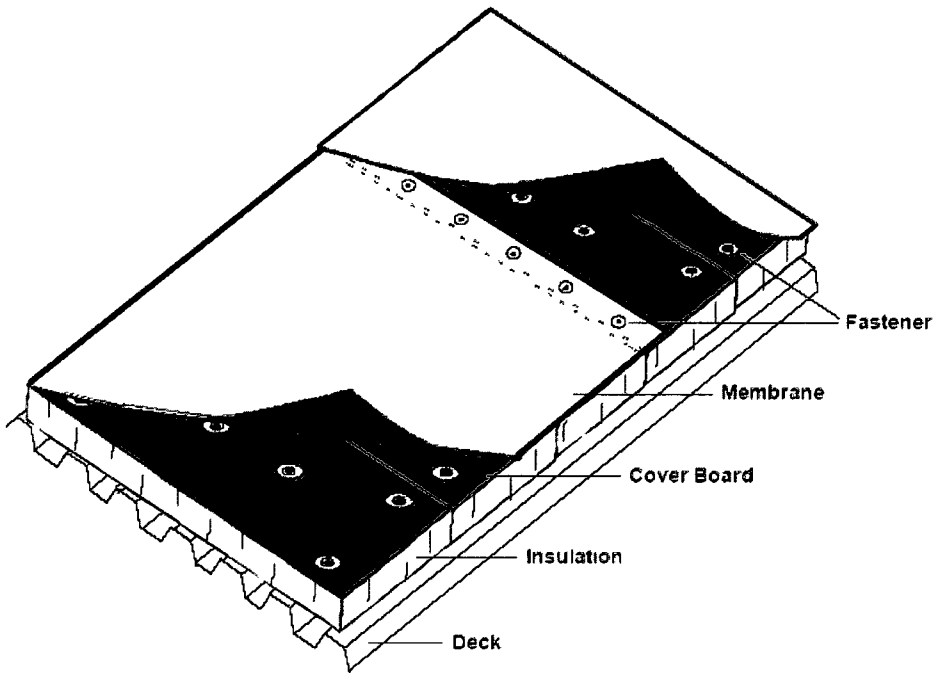

Figure 1.15: Membrane and substrates are fastened to roof deck

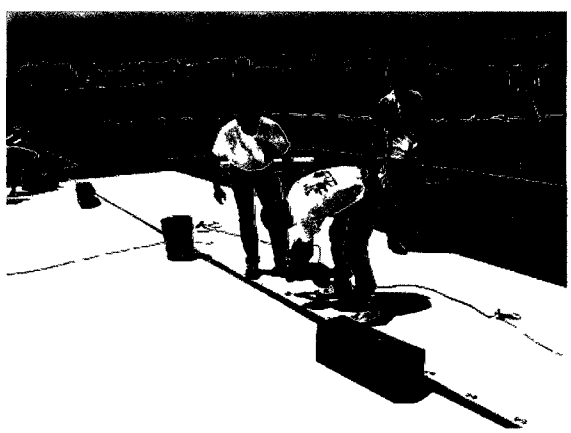

(a) Fastener were installed at the membrane overlap

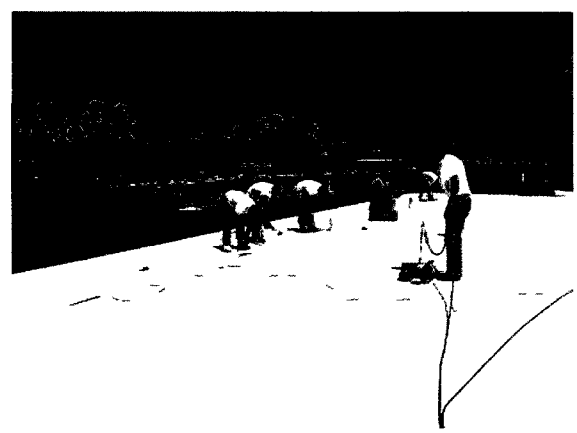

(b) Hot air welding was used at the seam of membrane

Figure 1.16: Typical components of a mechanically attached roofing system (http://www.sdcarruthers.com/)

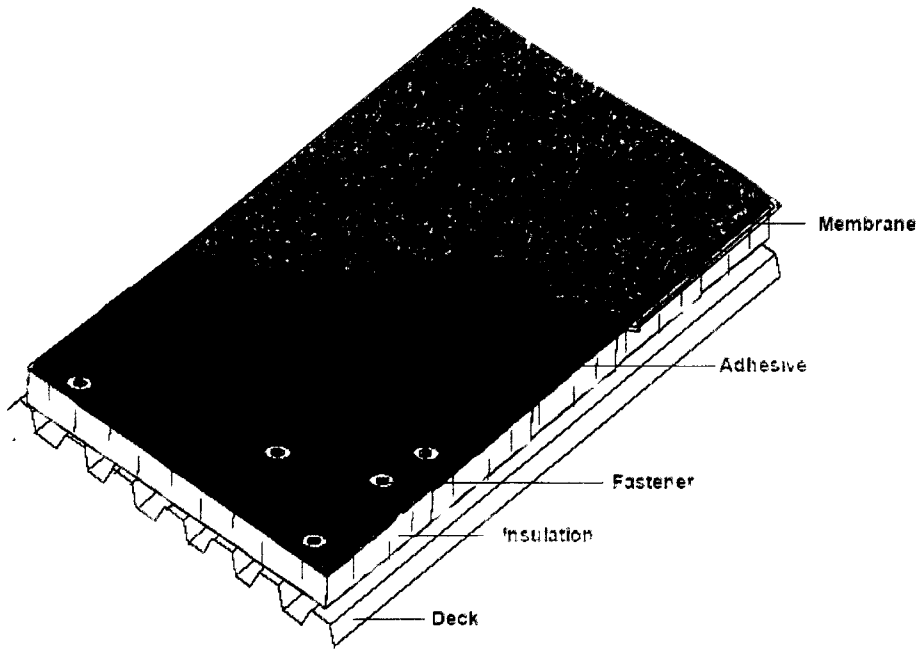

Figure 1.17: Membrane glued by using adhesive, while substrates are fastened to the roof deck

(a) Fully coated cold adhesive for adhering the membrane http://31-81.com/FlatRoofDetails.asp

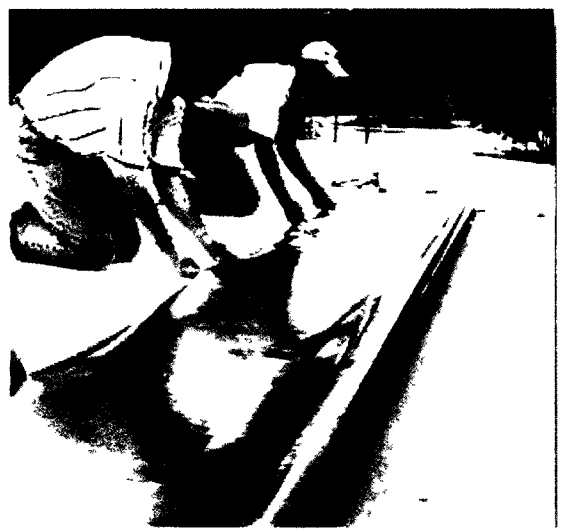

(b) Self-adhered membrane sheet was selected here http://www.trylock.com

Figure 1.18: Typical components of two types of fully bonded roofing systems

of the insulation to bond the membrane. In Figure 1.18 (b), a self-adhesive membrane is applied. The dead load of FBRS is relatively small, which allows for a lighter supporting structure, resulting in savings on overall building construction cost. Similar to MARS, there is more risk of mechanically damaging the membrane, since it is fully exposed to the outdoor environmental conditions.

1.4.4 Adhesive Applied Roofing System (AARS)

In modified bitumen or sing-ply membrane roofing systems, if all components (i.e., the cap sheet, base sheet, insulation board and cover board) are integrated by the application of adhesives, then they are called as Adhesive Applied Roofing Systems (AARS). For AARS, unlike the conventional mechanically attached roofing systems, there are no fasteners used. Thus, AARS offers less thermal bridging, air intrusion, air leakage, moisture migration and corrosion problems.

The format of adhesives applied between layers is either as beading in ribbon or full coating, but at the membrane level it must be always fully coated. Torching as an alternative construction method is used in certain cases for attaching modified bitumen membranes such as cap sheet and base sheet. A typical AARS with modified bitumen membranes is shown in Figure 1.19. The adhesive applied on top of the vapour barrier and insulation is in ribbon format, while the membranes are attached to substrates by fully coated adhesives. Another typical AARS with modified bitumen membrane is shown in Figure 1.21, where all adhesives between the components at different levels are fully coated. Photos (Figures 1.20 and 1.22) illustrate these two different application formats for cold adhesive. One is using the foamy polyurethane roof adhesive on the roof deck to bond the polyisocyanurate insulation; while the other is spreading the cold modified bitumen adhesive on top of the insulation material for bonding its cover board.

In accordance with the nature of membrane materials used, AARS is classified as PVC, TPO, EPDM, modified bitumen roofing systems and so on. PVC, TPO

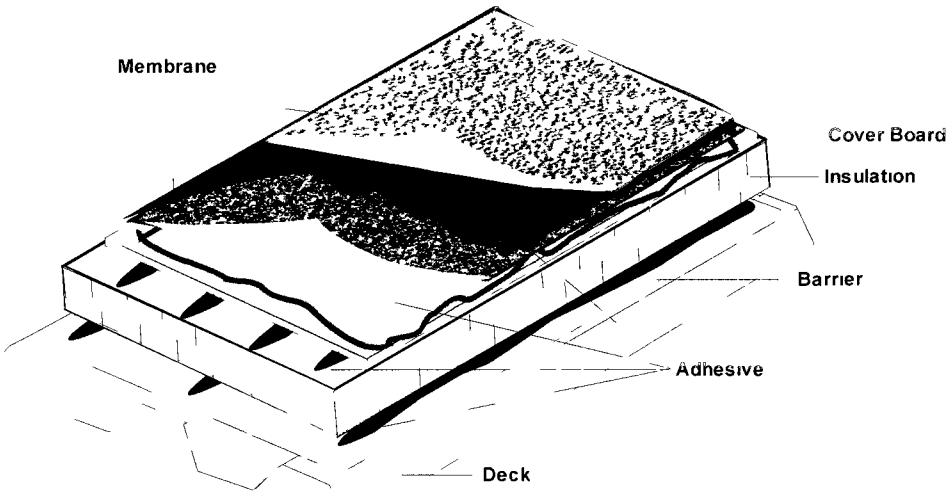

Figure 1 19: Typical configuration of AARS with adhesive in ribbon format

Figure 1 20 Typical components of AARS with adhesive in ribbon format (http://building.dow.com)

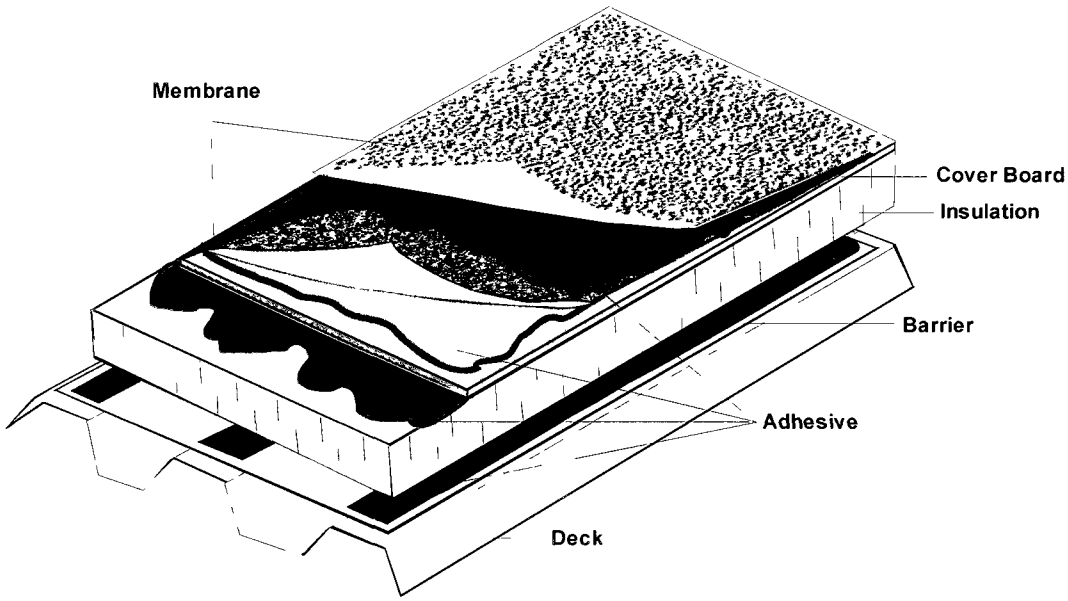

Figure 1.21: Typical configuration of AARS with adhesive full coated

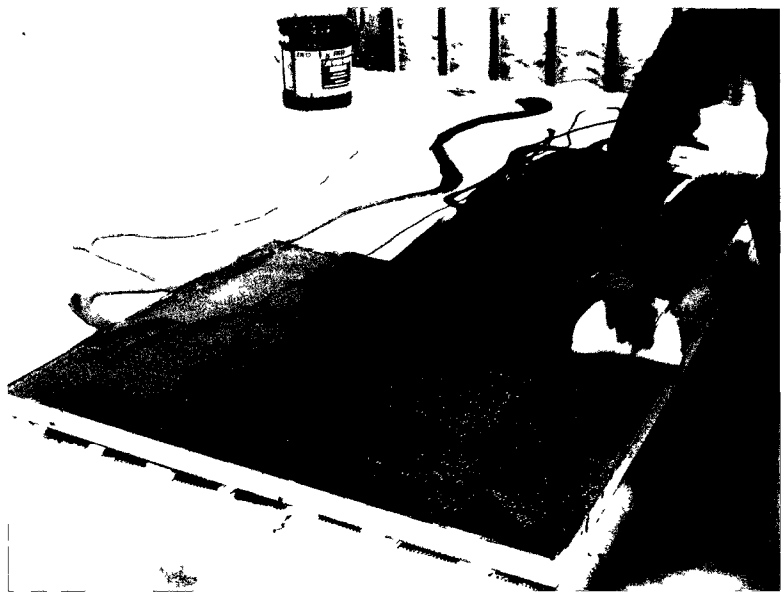

Figure 1.22: Typical components of AARS with adhesive in full coat format

and EPDM roofing systems are also known widely as the single-ply membrane roofing systems, and modified bitumen roofing system is called the multi-ply membrane roofing system. Usually, professional cold adhesive is chosen to glue the roof components of AARS together. To avoid the roof failure occurring at the adhesive level, specific cold adhesive should be selected for different components to attain suitable functions. Sometimes, appropriate primer corresponding to the cold adhesive is also applied on the component to strengthen the bonding effect.

1.5 AARS Project at a Glance

AARS are getting more and more popular in North American roofing market as a type of low slope roofs. To develop the wind uplift resistance standards for the AARS, a collaborative research and development project entitled "Development of Wind Uplift Standard for Adhesive Applied Low Slope Roof Systems" was initiated by the Department of Civil Engineering, University of Ottawa, and the National Research Council Canada (NRCC), in collaboration with the Canadian roofing industry partners, Bakor Inc., IKO Industries Ltd, Soprema Inc., Tremco Inc., and the Roofing Contractors Association of British Columbia. The project has been supported by the NSERC (Natural Sciences and Engineering Research Council) CRD (Collaborative Research and Development) grant (CRDPJ 3065819-04) and has the following tasks:

- Task 1: Pullout Testing
- Task 2: Peel Testing
- Task 3: Wind Uplift Testing
- Task 4: Numerical Modeling
- Task 5: Development of Design Guidelines

Task 1 objective was to establish a pullout testing procedure that can be used to evaluate small scale samples of AARS for uplift resistance performance

evaluation. Similar to Task 1, Task 2 objective was to develop a peel testing procedure for the peel resistance performance evaluation of AARS. Task 3 and Task 4 focus on the development of a dynamic full scale testing method and numerical modelling of AARS for wind uplift performance evaluation. Tasks 1, 2, 3 and 4 were successfully completed and reported by Wu (2008), Current (2009) and Murty (2010). The developed testing procedures have been proposed to the ASTM International (American Society of Testing Materials) to develop a standardized test method. Task 5 can be achieved by combing deliverables from all preceding tasks together with input from the industry partners. The existing standard *CSA123.21-04* is expected to be enhanced by including the AARS research achievements.

1.6 Thesis Objectives

Varieties of experimental configurations were investigated based on the AARS with modified bitumen membranes in the above mentioned project. The pullout, peel and wind uplift test methods have been developed individually. The pullout and peel resistance represent the effects of tensile and shearing forces due to wind on AARS. The dynamic wind uplift test method gives the overall evaluation of wind performance on AARS in full-scale. One of the major contributions of the present study is developing correlation among the above three test methods.

Previous research efforts of Wu (2008) and Current (2009) on peel and pullout testing were respectively carried out in a laboratory condition. Participating industrial partners for the research project agreed that the development of a portable tester would be of great benefit to the roofing industry for these testing. Once such equipment is developed and properly validated with the existing laboratory test data. The roofers can make use of the device in the field. Having an equipment to evaluate the actual response of the system in the field will help identifying the influence of any variation in the applications as well as the impact

of environmental conditions such as the relative humidity and temperature to the system response.

In addition, to have a safe and reliable roofing system, the selected roof assembly and its respective components should have resistance higher than the wind load. A database called WindCAD was originally developed by Baskaran and Borujerdi (2001) by extracting the wind pressure coefficients from the open research literature from 1970 to 2000. This database provides supplementary information for roof wind load design for cases that are not available in the NBCC 2005.

Based on the above, the present thesis project can be classified into three parts:

- Part 1: Update the existing WindCAD database;
- Part 2: Correlating the full-scale system wind uplift response with small scale peel and pullout resistance;
- Part 3: Development of a portable tester and its validation.

In Part 1, open literatures published from 1996 to 2008 were reviewed and useful wind pressure coefficients were extracted from the papers. Graphs for the distribution of wind pressure coefficients were developed. The WindCAD database was expanded successfully to include these collected data.

In Part 2, the developed pullout, peel and wind uplift test methods were reviewed fist and then were applied in an experimental program. The correlation between the test results were analyzed and led to a conclusion that the pullout and peel test by using small-scale specimens would be an effective means to make prediction of the wind uplift behavior of AARS in full-scale.

To fulfill Part 3, the design specifications for fabricating a portable tester was extracted from the developed pullout and peel test methods and the pullout and peel test results obtained from AARS samples in a variety of configurations.

Withdrawal resistance of roofing fasteners test (ANSI/SPRI FX-1-2006) was used to examine the operational capacity of the portable tester in the primary stage of the portable tester development because it has the elementary roof structure, single failure mode, and straight uplift force transfer mechanism. It can offer stable test data for the performance evaluation of the portable tester. After that, the actual AARS samples for pullout and peel tests were constructed and tested on the portable tester and the Instron machine respectively. Their test results of maximum loads and failure modes were compared to benchmark the performance of the portable tester.

1.7 Thesis Outline

In addition to this introductory chapter, this thesis report consists of the following chapters:

- Chapter 2 is a summary of the literature review. The first part describes the wind load calculation method offered by the National Building Code of Canada (NBCC) 2005 in appreciation of acquiring the wind pressure coefficients on various building shapes, heights, roof pitches, locations, and the wind orientations relative to the building itself. The NRC developed WindCAD database allows searching the mean and peak wind pressure coefficients obtained under various conditions, which are made available in public documentation ranging 1970 ~ 2000. Further knowledge on the pressure coefficients were also extracted from open literatures between 1996 ~ 2008 and was formed into 151 pages of results in figures. They are added to the new version of WindCAD 5.0. At the end of the chapter, three case studies are presented to demonstrate how convenient is to use the C_p value searched from WindCAD 5.0 to calculate the wind loads on roofs in some particular situations.

- Chapter 3 illustrates the structural features of the four most popular low slope roof systems which are the ballasted roofing system (BRS), mechanically attached roofing system (MARS), fully bonded roofing system (FBRS), and adhesive applied roofing system (AARS). Their response to the wind uplift loading is illustrated with figures. The details of the force development in AARS are explained in particular.

- Chapter 4 gives an overview of the formerly developed test methods of pullout, peel and wind uplift evaluations. Their experimental parameters are summarized. The specimen setup for pullout, peel and wind uplift tests are presented with figures, which are applied to the one component variation tests to look into the correlation between the test results in the following chapter.

- Chapter 5 develops a correlation between the results of one component variation tests and presented in four scenarios. Failure modes, resistance capacities of peel, pullout and wind uplift specimens were obtained and analyzed. It was proved that the higher resistance observed in peel and pullout tests is in good correlation with the higher wind uplift resistance, which is very useful knowledge for making component substitution at the construction sites.

- Chapter 6 illustrates the design and functionality of the portable tester which will be deployed in field. The portable tester experimental setup for the pullout and peel was described specifically. The operational capacity of the portable tester was examined by using the withdrawal resistance of roofing fasteners test (ANSI/SPRI FX-1-2006). The initial verification for the performance of the portable tester was attempted by using the pullout and peel samples of AARS.

Chapter 2: Wind Loads on Low Slope Roofs

2.1 Introduction

Wind flow interacts with buildings, creating both negative and positive pressure fluctuation over a roofing system. Changes in roof slope affect the wind load greatly. As wind blows over and around the building, if the roof slope is steep enough to force the streamlines upward, the wind exerts positive pressures on the windward slope. Reducing the roof slope reduces the pressures on the windward roof slope progressively to zero at about 30° slope (Griffin et al, The manual of low-slope roof system). The positive pressure on steep roof can turn into negative pressure, or suction, as further reducing the roof slope to low-slope or flat roof with respect to the same wind flow. This is because the wind flow separation develops at the windward eave and vortices are generated while the reattachment of the separated flow also takes place. The wind flows are influenced by any changes in the building shape, e.g. length, width, height, with/without parapets, and in particular, the critical slope at which the maximum suction will occur. Also, wind direction to the building plays an important role. The worst suction coefficients on low slope roofs are known to occur along the edges of the roof caused by the development of conical vortices due to cornering winds (Banks et al, 2000).

An accurate knowledge of wind-induced pressure loading is important for the design of low-slope roof buildings. In this chapter, a review of the wind load calculation procedures offered by NBCC 2005 is presented first. Then follows the description of wind pressure coefficient and the database called WindCAD, which is a collection of pressure coefficients as a reference for the optimal design. Furthermore, three case studies are presented to illustrate how to design wind loads on low slope roof building using the collected data in details.

2.2 Wind Load Calculation

The National Building Code of Canada 2005 (NBCC 2005) offers two methods to define wind loading on buildings – the static method and dynamic method. For most of the low- and medium-rise buildings as well as the structural components and claddings, the static method is used to determine their wind loads. For tall buildings and slender structures that are susceptible to dynamic wind effects, the dynamic method is recommended. The format of the dynamic method is much the same as that of the static method except that the gust effect factor, C_g, and the exposure factor, C_e, are determined differently. The pressure coefficients, C_p, for both methods are the same. In fact, pressure coefficients, C_p, for calculating wind load on building structures are derived from wind-tunnel tests on small-scale models or field monitoring of the full-scale buildings.

Compared to NBCC 1995, the 2005 version of the code introduces the importance factor, I_w, for calculating the specified external/internal pressure due to wind. The updated formulas are:

$$P_e = I_w q C_e C_g C_p \qquad P_i = I_w q C_e C_{gi} C_{pi} \tag{2.1}$$

where P_e, P_i = specified external and internal pressure acting statically and in the direction normal to the surface,

I_w = importance factor, provided in NBCC 2005,

q = reference velocity pressure (reference dynamic pressure at 10 m at the weather station), provided in NBCC 2005 Appendix C,

C_e = exposure factor,

C_g, C_{gi} = external and internal gust effect factors, and

C_p, C_{pi} = external and internal pressure coefficients.

The expose factor C_e takes into account the height and terrain roughness. The gust-effect factor C_g takes into account not only the change of wind speed and wind pressure due to gusts, but it is also an adjustment for the complex dynamic

response of the structure to the gust. The equations of C_e, C_g, C_{gi} for the static and dynamic procedures are given in NBCC 2005.

The pressure coefficients are defined by the measured pressure value divided by the dynamic pressure corresponding to the wind speed V. That is,

$$C_p = \frac{p}{(\frac{1}{2})\rho V^2} \tag{2.2}$$

in which

p = the measured pressure on a building surface,

ρ = density of the air at the temperature and barometric pressure measured, and

V = the mean wind speed.

Obviously, pressure coefficients are dimensionless. They account for the effects of aerodynamic shape of the building, orientation of the surface with respect to the wind flow, and profile of the wind velocity. Since there is a wind-speed gradient, the dynamic pressure varies with height. It is important to claim what the reference height is for the specified wind pressure coefficient.

Wind pressure coefficients are based on measured data obtained from scaled model wind-tunnel tests or verified against full-scale measurements. Different building shapes, heights, wind direction, wind velocity, with/without parapet, parapet heights will result in different pressure coefficients. It could turn into negative (suction) from positive (pressure) wind load that may be critical for structural designing.

Wind pressure coefficients C_p or C_pC_g of nine types of low-rise building structures are recommended in NBCC 2005 (Figures I-7 to I-15) for the design of roofs and secondary structural members. It includes single-span gable roofs, multi-span

gabled (folded) roofs, hipped roofs, stepped roofs, monosloped roofs, sawtooth roofs, and flat-roofs. These data are obtained from systematic boundary-layer wind-tunnel studies. They are most appropriate for buildings with height-to-width ratio of less than 0.5 and the reference height of less than 20 m. The roof slopes are limited within a specific range and the wind direction is unspecified. All these general types of structures have no openings on the wall or roof top, no roof overhangs and parapets. Actually, the shapes of buildings and the styles of roof tops are diverse and their types are far beyond the range of nine types. Canopy roof, cylinder, spherical dome, parabolic dome are commonly used selections for building structures. Moreover, an unexpected case may occur when wind flow changes direction with respect to building roof. Finding out the worst wind direction toward the building roof is significantly important for building design.

Research papers concerning the study of wind pressure coefficient C_p are published unceasingly to demonstrate the wind effects on versatile building structures. It is useful and valuable to collect these achievements and refer them for calculating the wind loads under various conditions.

2.3 Data Extraction for Wind Pressure Coefficient

Although the building code provides wind pressure coefficients of general structural types for design against wind, wind tunnel testing and field data monitoring further offer more specific information about the design of a particular structure than the standard codes. In fact, the codes used in North America recommend wind tunnel tests for buildings that have unusual geometries or are located in particularly high-wind regions. Wind tunnel tests address the specific complexities of each case. They are a key tool for safe, reliable, economical structural design. A database to collect the experimental wind pressure coefficients in different kinds of situations will contribute to optimal structural design.

A survey documenting the boundary layer wind-tunnel research and full-scale measurement of the roof design has been accomplished extensively by Baskaran and Borujerdi (2001). It covers a large number of sources that became available in journals and international conferences etc. between 1970 and 2000, addressing the wind effects on buildings and structures. Wind induced pressure coefficients were extracted and the wind speeds were all converted to the eave height level. Conventional diagrams showing the building dimensions and wind pressure coefficient distribution on the roof were drawn by using the Corel Draw graphics program and converted to the PDF format. Later, the computer aided database for roof wind uplift pressures called WindCAD was developed (CNRC-Client Report #B1010.1). All the collected figures are searchable for the author's name or building height (see Figure 2.1, 2.2, 2.3).

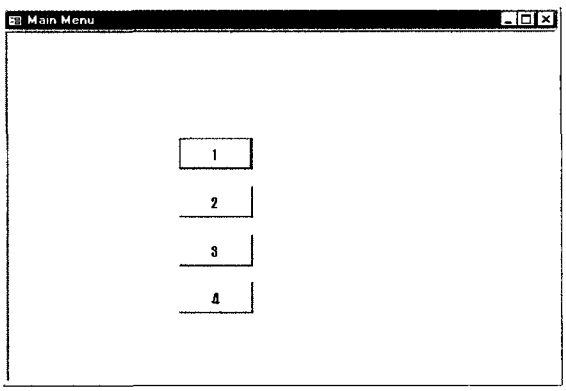

Figure 2.1: Papers were searchable by WindCAD Database

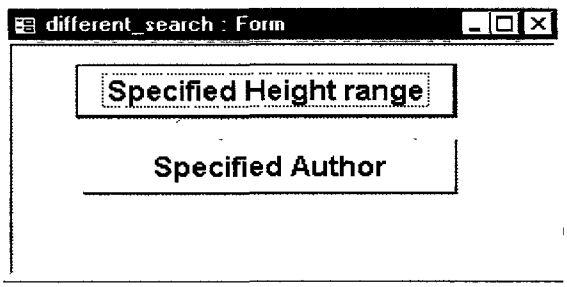

Figure 2.2: Papers can be searched by specified author or building height

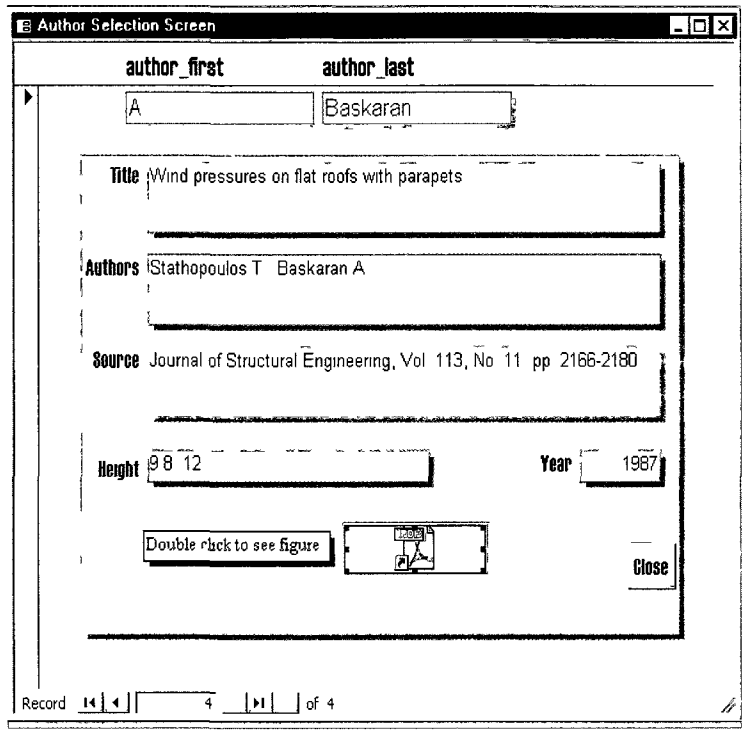

Figure 2.3: Search result by specified author

Following the same procedure, open literatures from 1996 to 2008 were explored to look into useful data for knowledge extraction. More than 40 papers were found that provided roof wind uplift pressure distributions for different roof configurations. The details of paper title, author, publication year, source, building height, terrain category were shown as *Appendix 1: Paper List of Additionally Collected Articles for WindCAD 5.0*. Mean or peak pressure coefficients on various building roofs were extracted from 29 out of 41 articles base on a further comprehensive review. More than 150 pages of Core Draw graphics of coefficient diagram denoted with full-scale building dimensions were prepared to state the wind load and their distribution. Additional works have been performed to keep consistency in units and graphic symbols with the previous collected format. As a result, the original database was successfully expanded to include 41 additionally collected papers and 151 page graphics. The new version of the WindCAD database renders wind pressure coefficient research achievements of close to 40 years from 1970 to 2008 In Figure 2.4, a new page of graphics extracted from the paper published in 1998 is presented.

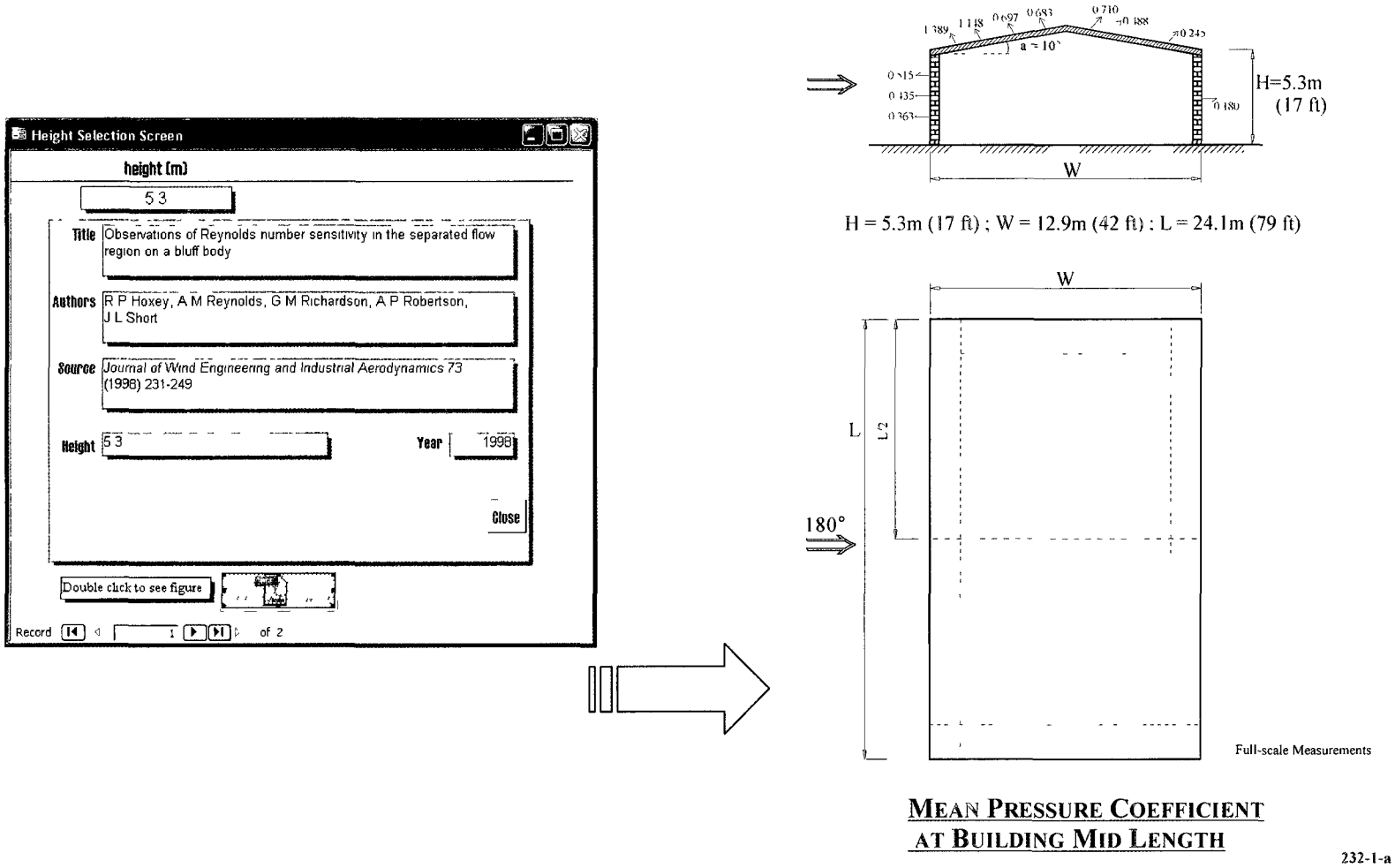

Figure 2.4: Paper published in 1998 was found from updated WindCAD database based on building height

2.4 Reference Height Conversion

As defined earlier

$$C_p = \frac{p}{(½)\rho V^2} \tag{2.2}$$

It is a dimensionless coefficient but its magnitude varies with the reference height since the wind speed varies with the height. For most collected research papers, the reference pressure is taken at the eave height of the building. However, some papers report wind pressure coefficients based on the levels other than eave height. Conversion has to be processed then to place the same eave height reference as NBCC 2005.

Figure 2.5 shows how source data of a wind tunnel study was extracted from the paper: *The assessment of wind loads on roof overhang of low-rise buildings* (Tore Wiik et al, 1997) and converted to eave height for the roof designer. The original reference point for the dynamic pressure was chosen to be at 10 m corresponding to full-scale height. Assume the wind pressure coefficients before and after conversion are C_{p1}, C_{p2}, respectively. So that,

$$C_{p1} = \frac{p}{(½)\rho V_1^2} \qquad C_{p2} = \frac{p}{(½)\rho V_2^2} \tag{2.3}$$

where,

V_1 = the wind speed at original reference height,

V_2 = the wind speed at eave height for new reference.

Hence,

$$\frac{C_{p2}}{C_{p1}} = \left(\frac{V_1}{V_2}\right)^2 \tag{2.4}$$

However, according to the power law, the variation of mean wind speed is

$$\frac{V_1}{V_2} = \left(\frac{Z_1}{Z_2}\right)^{\alpha} \tag{2.5}$$

Hence,

$$\frac{C_{p2}}{C_{p1}} = (\frac{Z_1}{Z_2})^{2\alpha} \tag{2.6}$$

In this example, Z_1 = 10 m is the original reference height and Z_2 = 5.335 m is the eave height for the new reference point, and α = 0.15 is the power law exponent for open country terrain.

Therefore,

$$C_{p2} = C_{p1}(\frac{Z_1}{Z_2})^{2\alpha} = C_{p1}(\frac{10}{5.335})^{2\times 0.15} = 1.207 C_{p1}$$

For instance, the original maximum uplift net wind pressure coefficient on the overhang roof which was located at the top left corner is C_{p1} = -1.17 (see Figure 2.5b). After converting, C_{p2} = 1.207 x (-1.17) = -1.412 (see Figure 2.5c.).

Converted wind pressure coefficient and wind direction are graphically shown in Figure 2.5c. W, L, H, α parameters represent structure width, length, eave height and roof pitch respectively. The wind direction to the building is normal to the gable wall. Net mean pressure coefficients at corner, perimeter and field regions display the wind load effect on a roof with overhang.

In some of the figures, mean or peak pressure coefficients are shown as arrows on top of the roofs which represent the wind force direction.

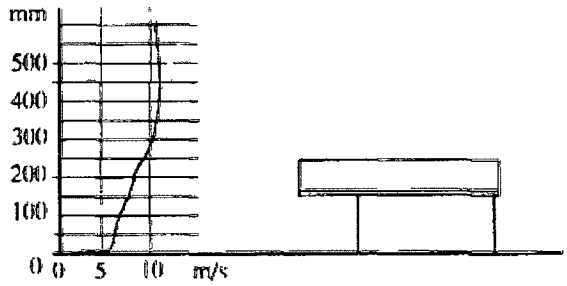

(a) The velocity profile and a model with overhang scale 1:30 configuration in the wind tunnel.

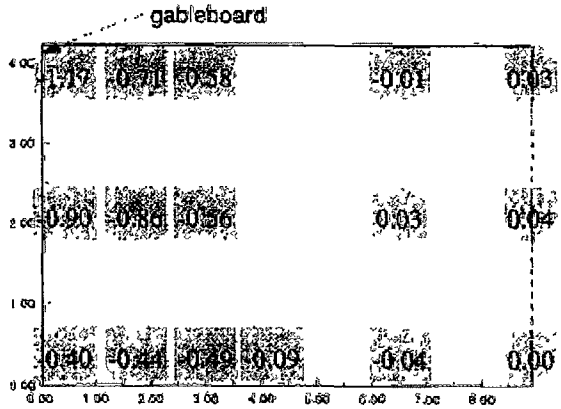

(b) Total measured C_p values on the roof for the house with overhang

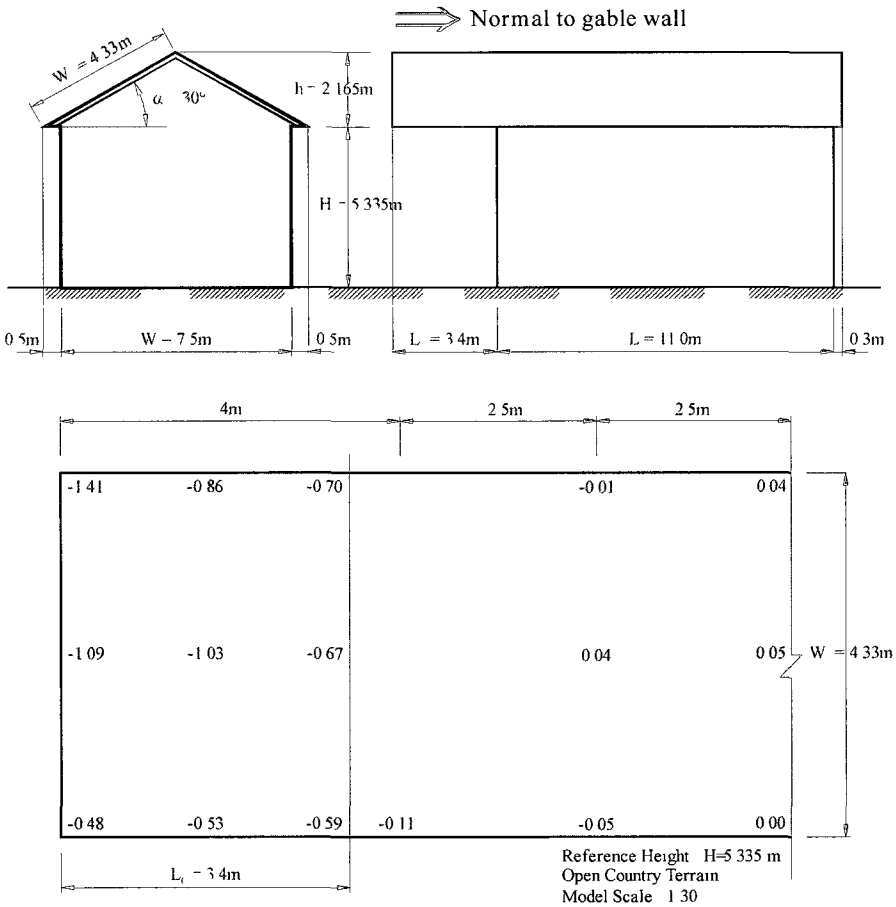

(c) Graph of pressure coefficient distribution with converted data

NET PRESSURE COEFFICIENT ON THE ROOF

Figure 2.5: Example of the extracted design knowledge from the source data

2.5 Case Study 1: Design Wind Load Calculation of Building with Oblique Wind Directions

Referring to the wind flow orientation to building in the National Building Code, it is generally perpendicular or parallel to the ridge of roof. It notes that the directionality effects have been accounted for in the factored loads. Stathopoulos et al (1999) studied the wind direction effect for a building with flat roof through field measurements and wind-tunnel tests with a 2-year period. The average wind pressure coefficients were extracted and added to the WindCAD database.

Figure 2.6 shows the geometries of the building. Its height-to-width ratio is: $H/D = 3.3/2.6 = 1.3 > 1.0$ which is beyond the limits of Figures I-7 to I-14 in the Code. The given value of C_pC_g are no longer a match to this case. Checked with the recommend external pressure coefficient C_p provided in Figure I-15, the wind direction is parallel to the smaller building plan dimension and the advised external pressure coefficients at the corner area is C_p = - 2.3.

Figure 2.7 (a), (b) and (c) present the mean pressure coefficients measured near the flat roof edges for different wind directions ranging from 35° to 60° which were the most critical azimuths. For 45° wind direction their mean suctions were slightly larger than those of 35° and 60°. They revealed the wind pressure variation and the tendency on flat roof under different wind directions. The highest wind uplift load on the flat roof induced by oblique wind can be well approximated by using this extracted knowledge. It is a convenient and reliable reference for a structural designer.

The maximum suction due to wind at 35° on the flat roof corner can be calculated using the following equation:

$$P = I_w q C_e C_g C_p$$

Reasonably set the importance factor I_w for this small rectangular building is 1.0 (say), or

$$I_w = 1.0$$

The measured building was located beside a football field on the Loyola Campus of Concordia University, approximately 8 km west from downtown Montreal. It was exposed to open country type of terrain for winds. The 1-in-50-year hourly wind pressure in that area is,

$$q_{ref} = 0.40\,kPa$$

The converted wind velocity pressure at building height is:

$$q = (\frac{Z}{Z_{ref}})^{2\alpha} q_{ref} = (\frac{3.3}{10})^{2\times 0.15} \times 0.40 = 0.29\,kPa$$

According to Paragraph 7 of Commentary I in NBCC 2005, the reference height h for calculating the exposure factor C_e for this low-rise building with flat roof is: h = 3.3 m. So that,

$$C_e = (h/10)^{0.2} = (3.3/10)^{0.2} = 0.8 < 0.9 \qquad \textit{No Good}$$

Based on the Sentence 4.1.7.1.(5) in NBCC, the exposure factor, C_e shall not be less than 0.9 for open terrain. Thus, assign

$$C_e = 0.9$$

The gust effect factor is (see NBCC 2005, Sentence 4.1.7.1. (6)):

$$C_g = 2.0$$

Therefore,

$$P = I_w q C_e C_g C_p = 1.0 \times 0.29 \times 0.9 \times 2.0 \times 3.2 = 1.67\,kPa = 34.88\,psf$$

Following the same procedure, the highest wind load on the flat roof at the wind directions of 45° and 60° are calculated as well. The advised value C_p = - 2.3 in the Building Code is adopted for comparison. Their results are shown in the Table 2.1.

	I_w	q_{ref} (kPa)	q (kPa)	C_e	C_g	C_p	P (kPa)	P (psf)
$\theta = 35°$	1.0	0.40	0.29	0.9	2.0	**- 3.2**	1.67	34.88
$\theta = 45°$	1.0	0.40	0.29	0.9	2.0	**- 3.4**	1.77	36.97
$\theta = 60°$	1.0	0.40	0.29	0.9	2.0	**- 3.0**	1.57	32.79
Building Code	1.0	0.40	0.29	0.9	2.0	**- 2.3**	1.20	25.06

Table 2.1: Wind uplift pressure at roof corner for building subjected wind from different directions

Measurement of the full-scale flat roof shown that very high mean wind pressure occurred on flat roof corners at points near the roof edge for particular oblique wind directions. The study provided useful insight into the effect of wind direction on roof corner wind loadings. In addition to the Building Code, the research achievements found in public literatures are also good references for wind load design.

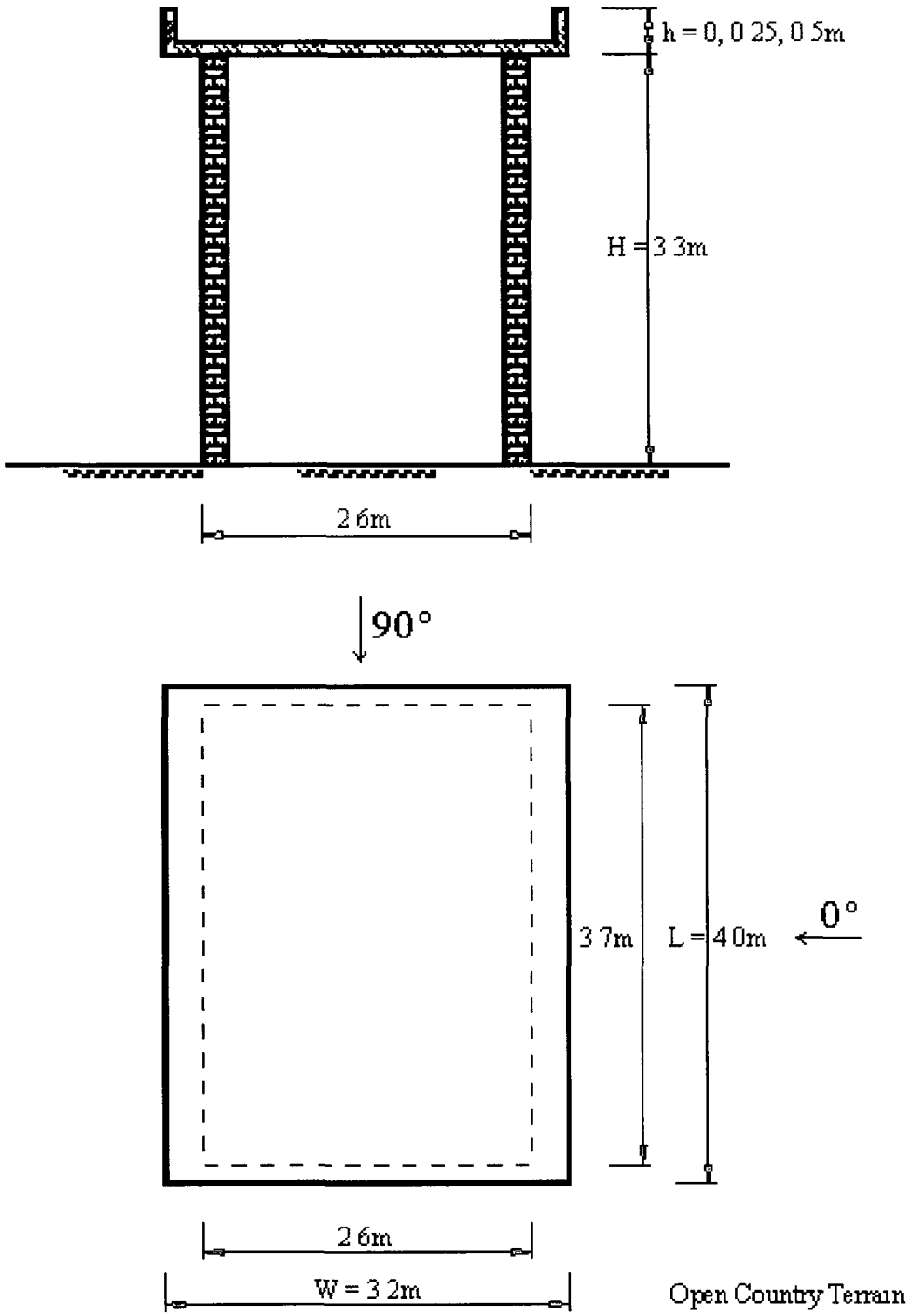

Figure 2.6: Building geometry and the layout

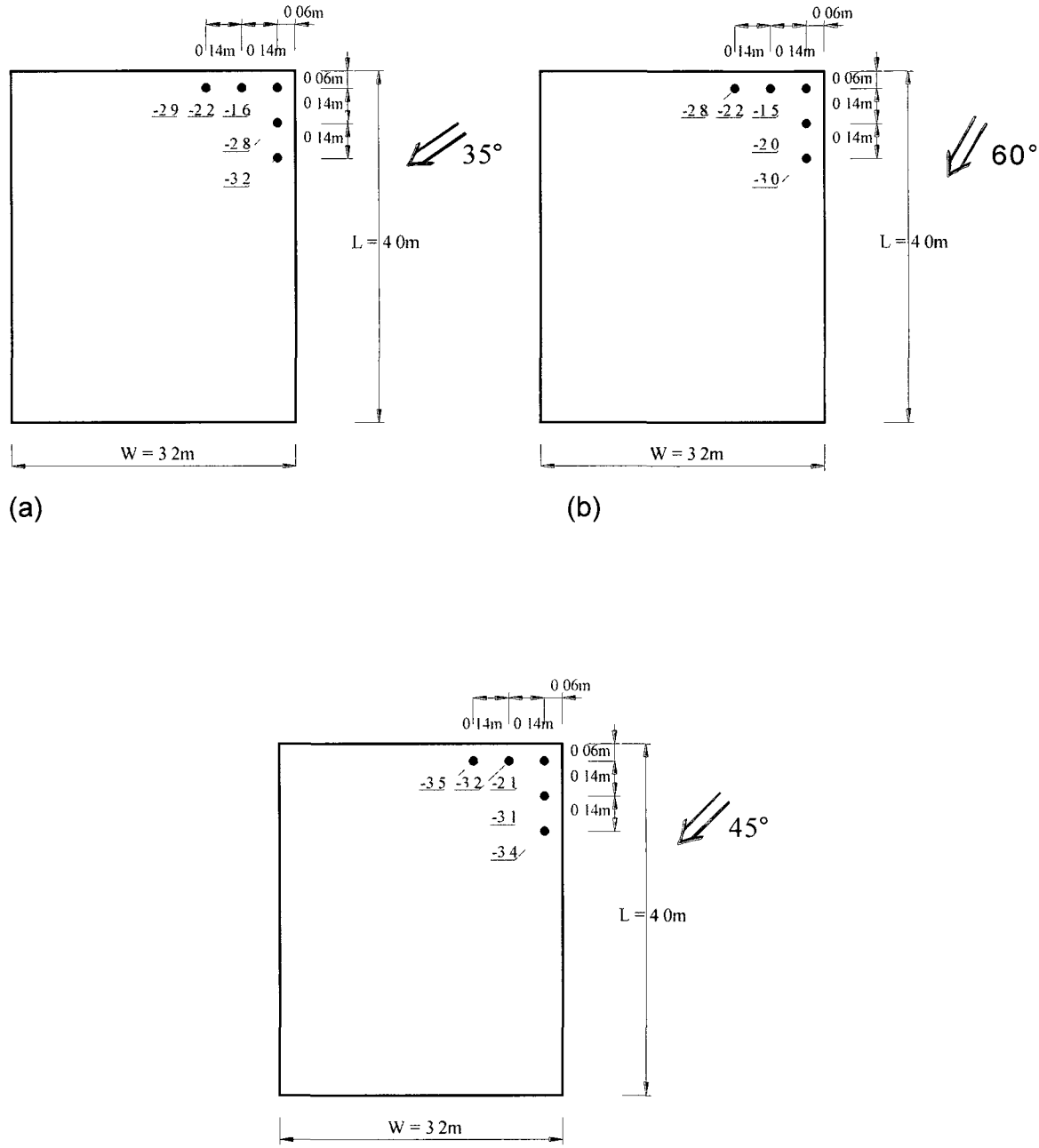

Figure 2.7: Building subjected wind from different directions

2.6 Case Study 2: Design Wind Load Calculation of Building with Parapet

Parapets alter the suction loads on the roof by raising the vortices away from the roof surface, changing the location of the corner vortex relative to the roof and the type of vortex formed. According to Kopp et al (2005), the higher continuous parapets decrease the local suction. However, with the lower parapets, the loads are even increased above those without parapets. Generally, it is agreed that the higher perimeter parapets (h > 1 m) act to reduce the mean and peak pressure coefficients by up to 50% in the corner region (Baskaran and Stathopoulos, 1988). Although most of the parapets allow some reduction in pressures, the building codes do not account for these differences. It is simply recommended the corner coefficients can be reduced for certain type of buildings with the perimeter parapet referring to Figures I-9, I-15 of NBCC 2005 conditionally.

Figure 2.8 shows the beneficial effect of the perimeter spoiler and porous parapet on the wind uplift load reduction. All these data were extracted from Kopp et al (2005). Spoilers and porous perimetric parapets are effective means of mitigating roof suctions. In contrast, leaving the corner open for a solid parapet is worse than the case of the building without parapet. The location of Povungnituk in Quebec is chosen for wind load design where hourly wind pressure q_{ref} is 0.91 kPa. By using the collected C_p value, the maximum external wind uplift pressure around the corner is listed in Table 2.2 for comparison.

Meanwhile, the building with a 0.9 m high perimetric solid parapet is also calculated by using the advised external peak composite pressure-gust coefficient C_pC_g in Figure I-9 of NBCC 2005. The result is shown in Table 2.2 too for reference.

	I_w	q_{ref} (kPa)	q (kPa)	C_e	C_g	C_p	$C_p C_g$	P (kPa)	P (psf)
Perimetric spoiler (h = 0.192 m)	1.0	0.91	0.79	0.9	2.0	**- 0.2**	**- 0.4**	- 0.28	- 5.85
Porous parapet (h = 0.9 m)	1.0	0.91	0.79	0.9	2.0	**- 0.85**	**- 1.7**	- 1.21	- 25.27
Without parapet	1.0	0.91	0.79	0.9	2.0	**- 0.85**	**- 1.7**	- 1.21	- 25.27
Solid parapet without corner (h = 0.9 m)	1.0	0.91	0.79	0.9	2.0	**- 1.45**	**- 2.9**	- 2.06	- 43.02
Perimetric solid parapet (h = 0.9 m) (Building Code)	1.0	0.91	0.79	0.9	/	/	**- 4.0**	- 2.84	- 59.31

Table 2.2: Wind uplift pressure at roof corner for building having dissimilar parapet

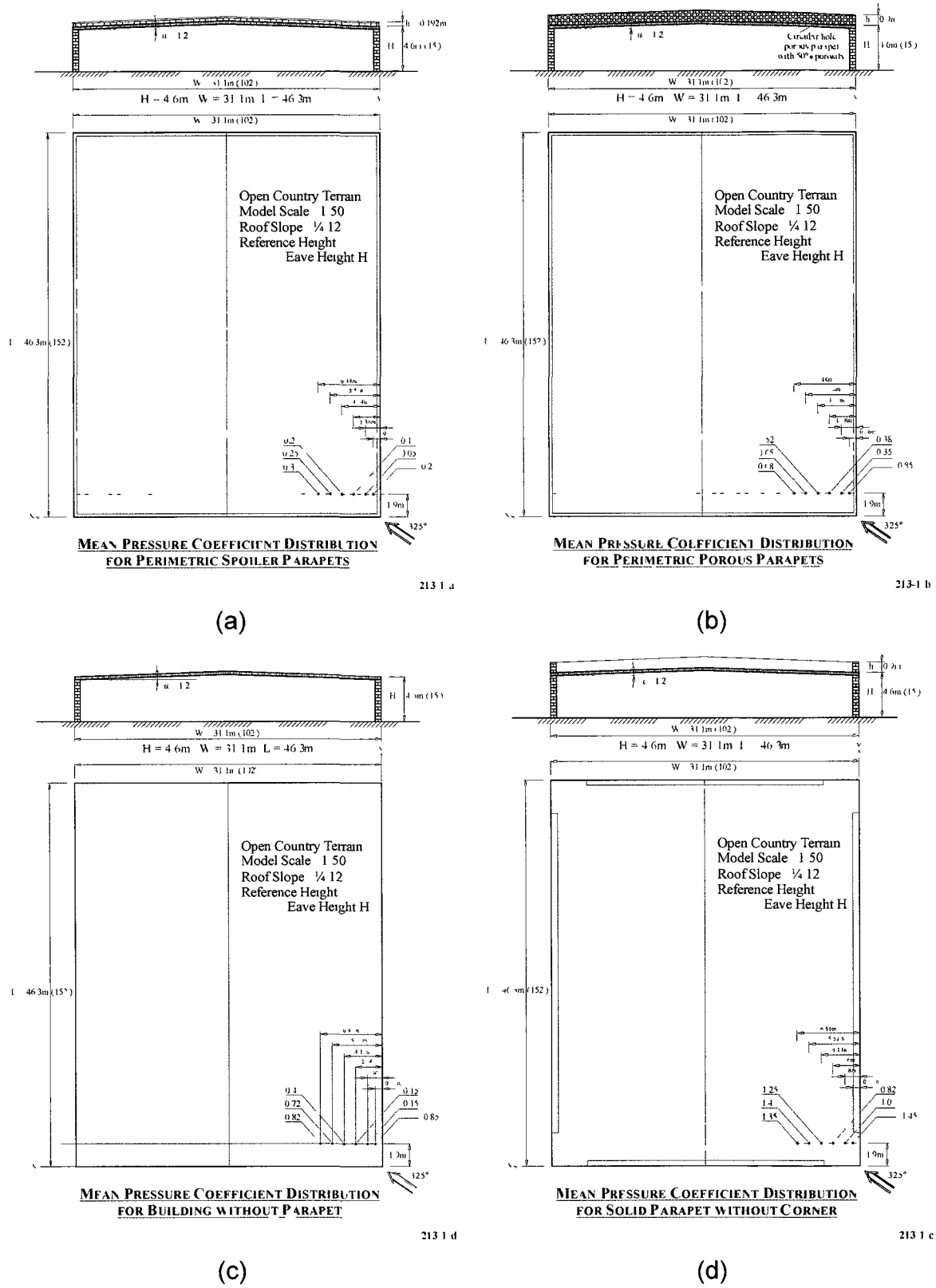

Figure 2.8: Mitigation of corner loads with alternative parapet geometries

2.7 Case Study 3: Design Wind Load Calculation of a Building with Opening

Understanding the impact of internal pressure upon the loads on building envelope is of significance for structural design. The magnitude of internal pressure coefficient depends on the distribution and size of the leakage paths and openings that vent the internal air space to the exterior (NBCC 2005, Commentary I). Internal pressures in the presence of dominant wall openings can contribute greatly to the overall loading on the roof and other building structure. Figure 2.9 shows a building with a single windward opening. The internal pressure effect complements external suction and in particular increase the net loading on the roof. Because of the size and distribution of openings are always changeable and uncertain for buildings, internal pressure coefficients can be wide ranging. The more cases of openings collected the more helpful for designing.

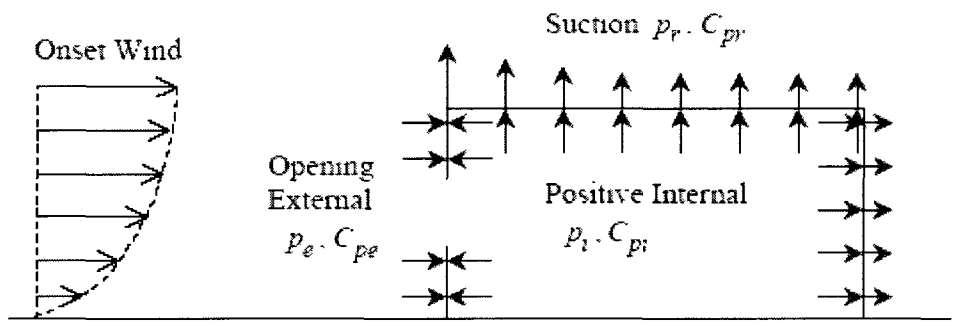

Figure 2.9: Envelope pressures under a dominant windward wall opening (R.N. Sharma, P.J. Richards, 2005)

The dimensions of a low-rise building considered here are show in Figure 2.11. Its worst net wind pressure coefficients at the corner and edge zone are extracted from Sharma et al (2005). Suppose a designed building with the same geometry is located in an open terrain of Toronto, Ontario. The wind velocity pressure will be $q_{ref} = 0.52$ *kPa.* Table 2.3 exhibits the calculation of the

maximum net wind uplift pressure for the corner and edge regions of the flat roof using the extracted knowledge directly.

		I_w	q_{ref} (kPa)	q (kPa)	C_e	C_g	C_p	P_{net} (kPa)	P_{net} (psf)
Corner	RF1 - WO1	1.0	0.52	0.40	0.9	2.0	**- 1.90**	- 1.37	- 28.61
	RF1 - WO2	1.0	0.52	0.40	0.9	2.0	**- 2.17**	- 1.56	- 32.58
Edge	RF2 - WO1	1.0	0.52	0.40	0.9	2.0	**- 2.26**	- 1.63	- 34.04
	RF2 - WO2	1.0	0.52	0.40	0.9	2.0	**- 2.01**	- 1.45	- 30.28

Table 2.3: Calculation for wind load of corner and edge zones with corner or central wall opening location

Meanwhile, using the NBCC 2005 to calculate the net peak wind pressure at the same corner and edge locations of the roof is considered under the same conditions. Referring to Figure I-9 in NBCC 2005, the peak composite pressure-gust coefficient C_pC_g value for the corner and edge is obtained for the tributary area for the zone of corner and edge, respectively (see Figure 2.10). The computation of the external peak wind load is displayed in Table 2.4 (a).

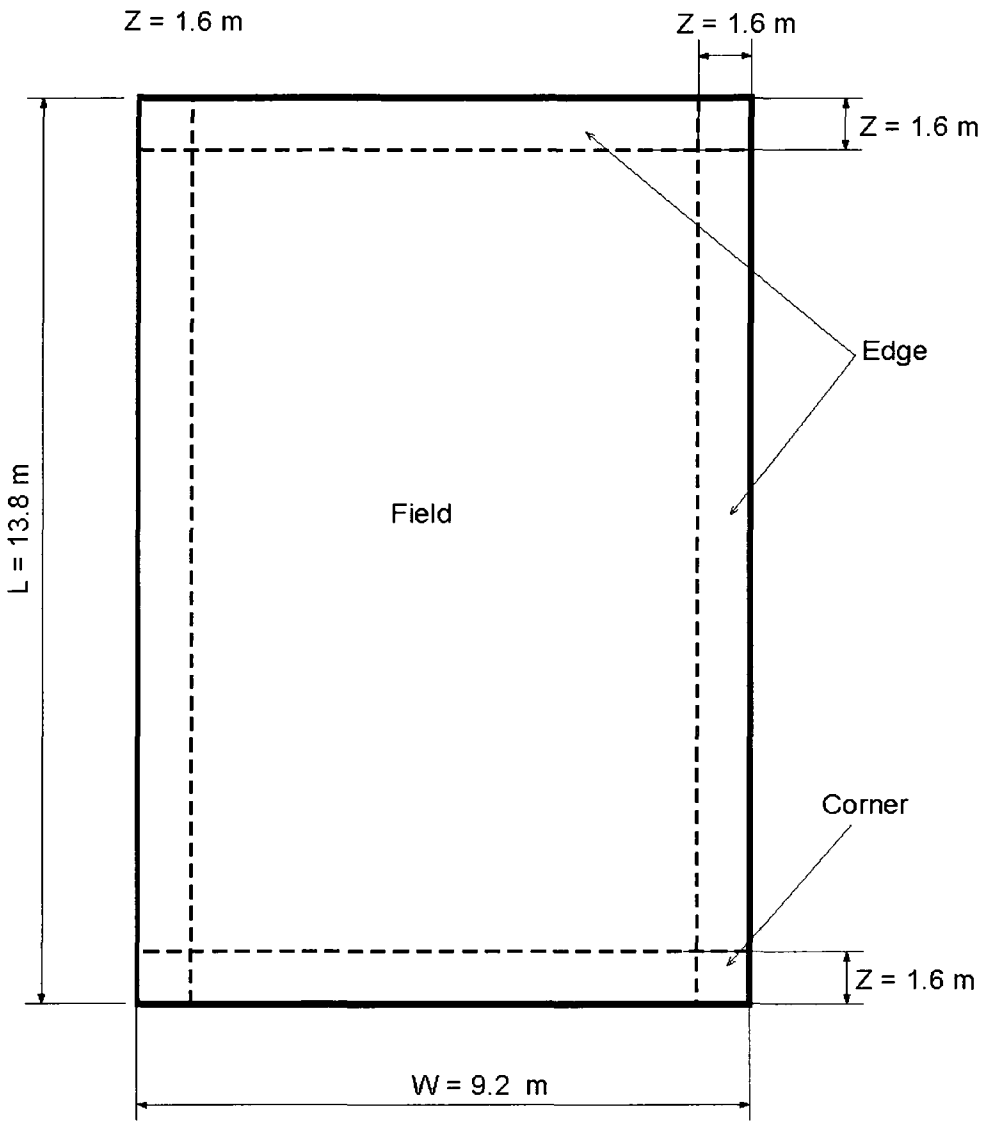

Figure 2.10: Corner, edge zone distribution on roof plan

The internal gust effect factor C_{gi} can be obtained using formulas provided in the Building Code as follows:

$$C_{gi} = 1 + \frac{1}{\sqrt{1+\tau}} \; ; \qquad \tau = \frac{V_0}{6950A}[1 + 1.42 \times 10^5 \frac{A_s}{V_0}\delta]$$

Where

V_0 = internal volume, in m^3,

A = total area of all exterior openings of the volume, in m^2,

A_s = total interior surface area of the volume (excluding slabs on grade), in m^2,

$\delta = 5 \times 10^{-5} m^3 / N$.

For the present building,

V_0 = 13.2 x 8.6 x 3.35 = 380.292 m^3

A = 2 x 1 = 2 m^2

A_s = (13.2 + 8.6) x 2 x 3.35 + 13.2 x 8.6 = 259.58 m^2

$$\tau = \frac{380.292}{6950 \times 2}[1 + 1.42 \times 10^5 \times \frac{259.58}{380.292} \times 5 \times 10^{-5}] = 0.15995$$

$$C_{gi} = 1 + \frac{1}{\sqrt{1 + 0.15995}} = 1.93$$

The default value of the internal gust effect factor is also recommend in the Code as C_{gi} = 2.0. To be conservative, C_{gi} is taken as 2.0.

For the internal pressure coefficient C_{pi}, this building with large openings matches the basic design Category 3 in NBCC 2005. The recommended internal pressure coefficient C_{pi} = 0.7.

Table 2.4 (b) and (c) present the internal peak wind load and net peak wind load calculation respectively.

(a) External peak wind load		I_w	q_{ref} (kPa)	q (kPa)	C_e	C_pC_g	P_e (kPa)	P_e (psf)
	Corner	1.0	0.52	0.40	0.9	**- 4.25**	- 1.53	- 31.95
	Edge	1.0	0.52	0.40	0.9	**- 2.0**	- 0.72	- 15.04

(b) Internal peak wind load		I_w	q_{ref} (kPa)	q (kPa)	C_e	C_{gi}	C_{pi}	P_i (kPa)	P_i (psf)
	Corner	1.0	0.52	0.40	0.9	**2.0**	**0.7**	0.50	10.44
	Edge	1.0	0.52	0.40	0.9	**2.0**	**0.7**	0.50	10.44

(c) Net peak wind load		P_e (kPa)	P_i (kPa)	P_{net} (kPa)	P_{net} (psf)
	Corner	- 1.53	0.50	- 2.03	- 42.40
	Edge	- 0.72	0.50	-1.22	- 25.48
	$P_{net} = P_e - P_i$				

Table 2.4: External, internal and net peak wind load calculations

The designed net peak wind uplift loads applied to the corner and edge of the flat roof using the two methods are listed in Table 2.5. Comparison between the result derived from NBCC 2005 and the extracted knowledge from the experimental measurement reveals that, at the edge zone, the building code is less conservative in predicting the peak wind uplift load. In the experimental method, the largest net uplift pressure coefficient at the edge zone was 2.26 with the corner wall opening case and wind angle $\theta = 30^{\circ}$. Corresponding wind uplift load was 1.63 kPa (34.04 psf). This is 34% higher than the largest net uplift pressure, which is 1.22 kPa (25.48 psf) based on the Building Code. This is due to the non-conservative internal pressure coefficients C_{pi} provided in the code. At the corner zone, the largest net uplift pressure defined by using the code is somewhat higher in magnitude.

		P_{net}				Difference
		WindCAD Database		Building Code		
		(kPa)	*(psf)*	*(kPa)*	*(psf)*	
Corner	RF1 - WO1	- 1.37	- 28.61	- 2.03	- 42.40	conservative
	RF1 - WO2	- 1.56	- 32.58			
Edge	RF2 - WO1	- 1.63	- 34.04	-1.22	- 25.48	34%
	RF2 - WO2	- 1.45	- 30.28			

Table 2.5: Result comparison between two methods

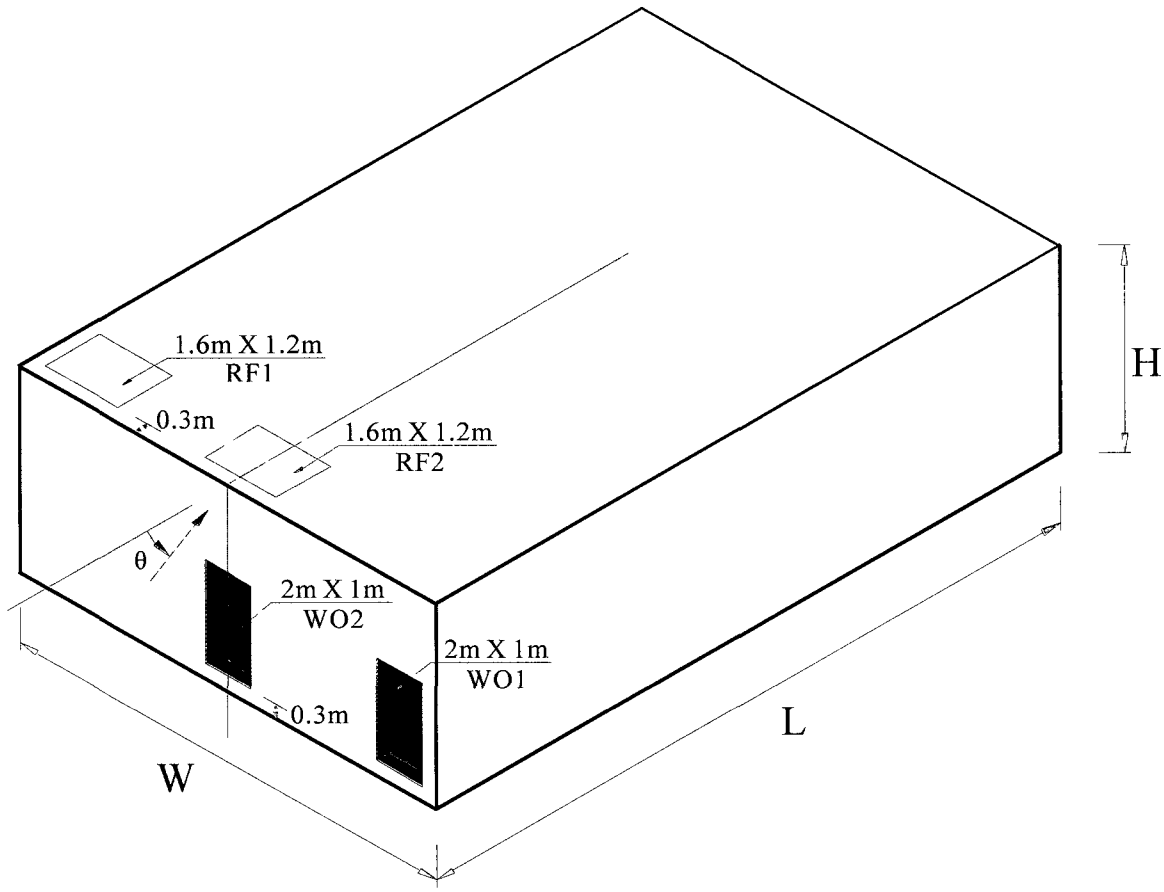

H = 4.0m
open country terrain
model scale: 1:50

RF1: Corner Roof Region
RF2: Centre Roof Region
WO1: Corner Wall Opening
WO2: Centre Wall Opening

External: 13.8 m L x 9.2 m W x 4 m H

Internal: 13.2 m L x 8.6 m W x 3.35 m H

Figure 2.11: Building geometry and the layout of opening door in two cases

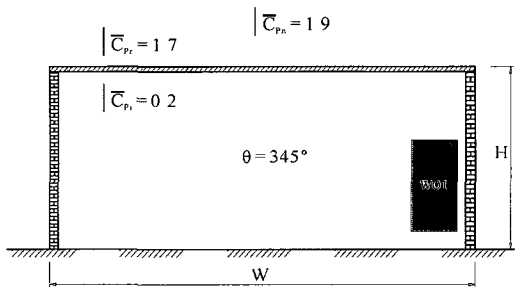

H = 4 0m W = 9 2m , L = 13 8m

LARGEST NET UPLIFT PRESSURE COEFFICIENT FOR RF1-WO1

208-1-d

(a)

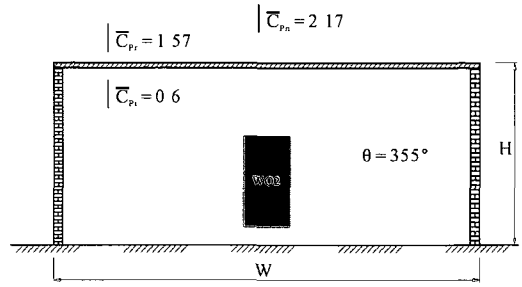

H = 4 0m , W = 9 2m L = 13 8m

LARGEST NET UPLIFT PRESSURE COEFFICIENT FOR RF1-WO2

208 1 g

(b)

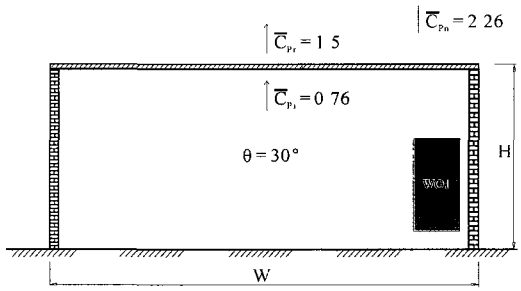

H = 4 0m , W = 9 2m , L = 13 8m

LARGEST NET UPLIFT PRESSURE COEFFICIENT FOR RF2-WO1

208-1-j

(c)

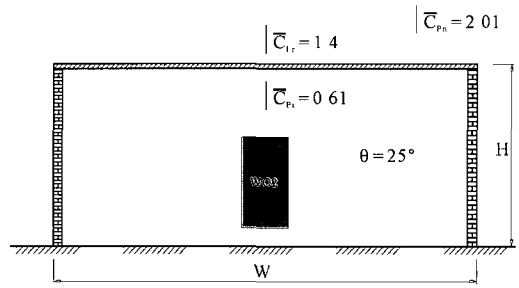

H = 4 0m W = 9 2m L = 13 8m

LARGEST NET UPLIFT PRESSURE COEFFICIENT FOR RF2-WO2

208-1-m

(d)

Figure 2.12: Corner and edge wind pressure coefficients in two cases of door opening

Chapter 3: Wind Uplift Resistance of Low Slope Roofs

3.1 Introduction

As discussed in Chapter 1, the conventional roofing for low slope roofs can be classified into four categories in accordance with the attachment methods of the roof components. They are ballasted roofing system (BRS); mechanically attached roofing system (MARS); fully bonded roofing system (FBRS); and adhesive applied roofing system (AARS). The component features for these four systems are also explained in Chapter 1.

When wind flows over a low-slope roof, it creates suction which exerts uplift force on the roof system. This force tends to pull the roof system away from the roof structure deck. Assuming that the roof deck structure is engineered properly, the wind uplift load could cause the roof system to fail if the wind resistance of the roof system is insufficient. BRS, MARS, FBRS and AARS can react differently when exposed to the same magnitude of wind uplift due to their particular load transferring mechanisms or response. These reactions are caused by different attachment methods, configurations, and application technologies of roofing system.

Chapter 2 presented how to calculate the wind loads on low slope roofs. This chapter discusses the roof response to the wind uplift loads. Sections 3.2 to 3.5 summarize the wind uplift effect and wind load transferring mechanisms on four roof systems, respectively. Adhesive applied roofing system (AARS) as the new trend roofing system is known to show good response to wind uplift loads. How the forces are developed in AARS under wind action is further discussed in Section 3.6.

3.2 Ballasted Roof System (BRS)

A conventional ballasted roof system consists of membrane or membrane and substrate material (insulation, slip sheet, etc.) loose laid over a deck using ballast to hold the system in place. In BRS, the ballast is used to provide wind uplift resistance for the roofing system that are not adhered or mechanically attached to the roof deck. It comes in the form of large stones, typically river bottom stone 3/4 in to 1-1/2 in (19mm to 38mm) diameter, size No. 4 per ASTM D448.

Wind exerts aerodynamic drag force on the exposed ballast. At a certain critical value, it topples some ballast away from their nested positions. Through a complex interaction of forces, upward motion of a rolling ballast combined with the increased aerodynamic drag force, wind will blow some ballast off the roof (Griffin & Fricklas, 2000). Once the gravels are lifted away, the loose laid membranes can be blown off followed by loose insulations, resulting in the complete failure of the roof. Figure 3.1 displays the failure occurred at the corner and around the parapet of a large retail building with ballasted roof.

Figure 3.2 illustrates the moment balance for a ballast lying loose at the roof surface. At the critical condition, the moment due to the drag force equals to that due to the ballast weight, which $D_c k_1 d = W k_2 d$ (k_1 and k_2 are constants of proportionality which depend on stone shape). Therefore, the critical wind speed V_c which exerts the aerodynamic drag force has the relationship with the ballast size as $V_c = \sqrt{d}$. The design procedures for the BRS are available in *Wind Design Standard for Ballasted Single-ply Roofing Systems (ANSI/SPRI RP-4, 2008).*

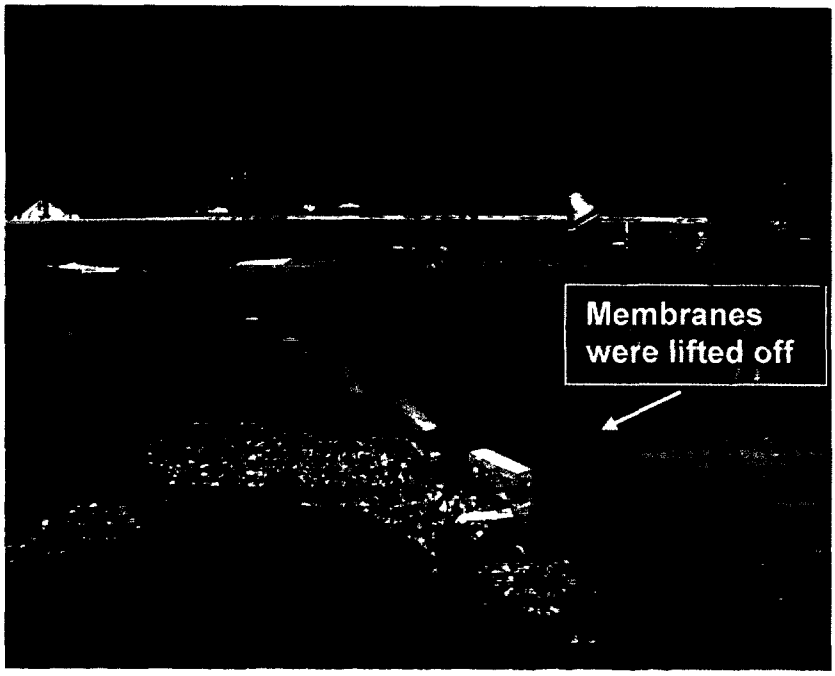

(a) At corner

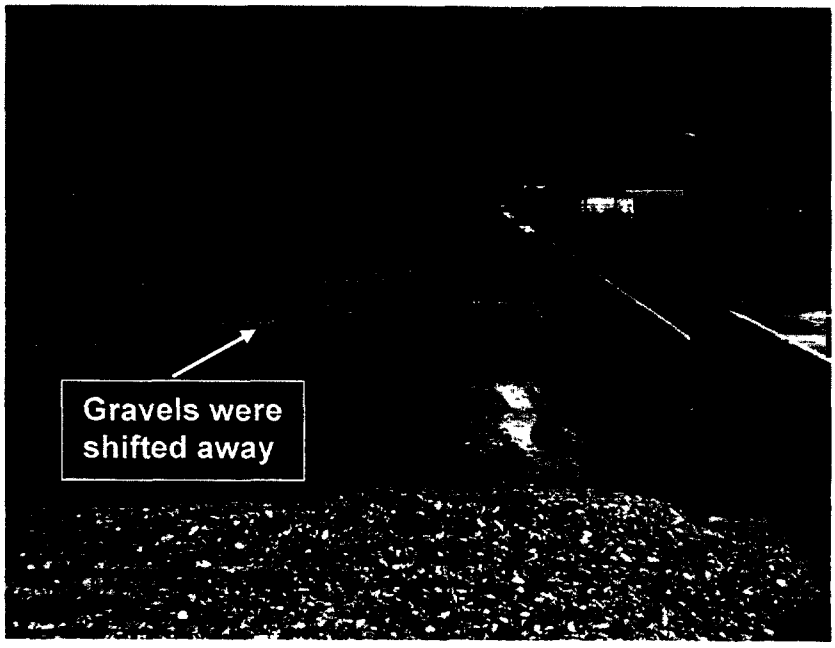

(b) Around parapet

Figure 3.1: Wind uplift failure of BRS

(Hurricanes Charley and Ivan Investigation Report, RICOWI, March 2006)

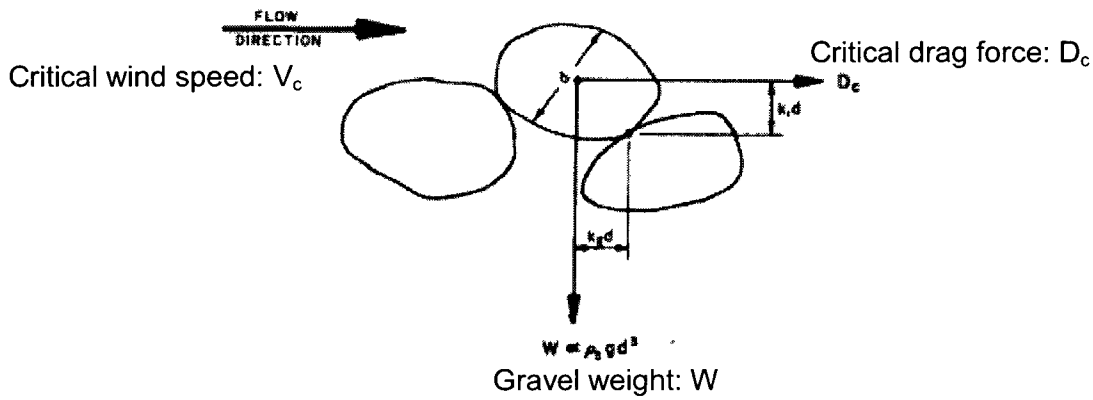

Figure 3.2: Moment balance on stone at critical condition (Kind and Wardlaw, 1977)

3.3 Mechanically Attached Roof System (MARS)

The membrane of this system is attached directly to the roof deck using mechanical fasteners and stress plates along the laps. The insulation may also be attached to the deck using mechanical fasteners and plates. With a mechanically fastened system, all of the wind uplift forces are exerted directly upon the membrane. This means that the negative wind pressure would try to pull the membrane away from the deck. Moderate-to-strong winds can cause the membrane to lift and billow between attachment points or rows as seen in Figure 3.3. The reaction to wind uplift of MARS is simplified in Figure 3.4. The billow height is determined by the combination of wind load, the fastener row spacing, the load-strain modulus of the membrane, and the presence of an air retarder/vapour barrier in the roof system (Baskaran, et al, 2006). This force membrane withstood is transferred directly to the membrane fasteners. Since the membrane attachment to the roof structure is independent of the insulation attachment, the insulation is not really exposed to a great deal of wind uplift forces.

Due to the fastener penetrations and joints of the steel deck and insulation, the indoor conditioned air intrudes into the assembly. The insulation pressure (also named as low pressure/bubble pressure) builds up to 40 ~ 60% of the membrane pressure. The weakest link of the wind uplift resistance comes to the membrane level. Figure 3.5 shows the typical failure mode of MARS.

The details for designing a proper MARS to resist the wind uplift load are provided in *A Guide for the Wind Design of Mechanically Attached Flexible Membrane Roofs* (Baskaran & Smith, 2005).

Figure 3.3: Field performance of a MARS

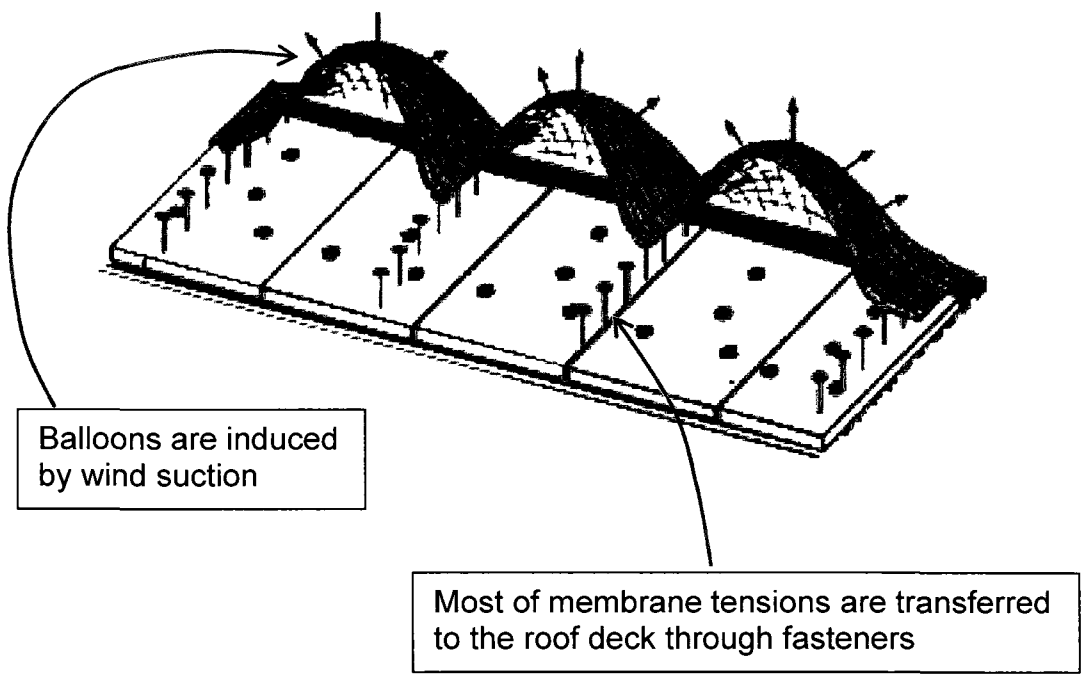

Figure 3.4: Flexible response of MARS

(a) Failure overview

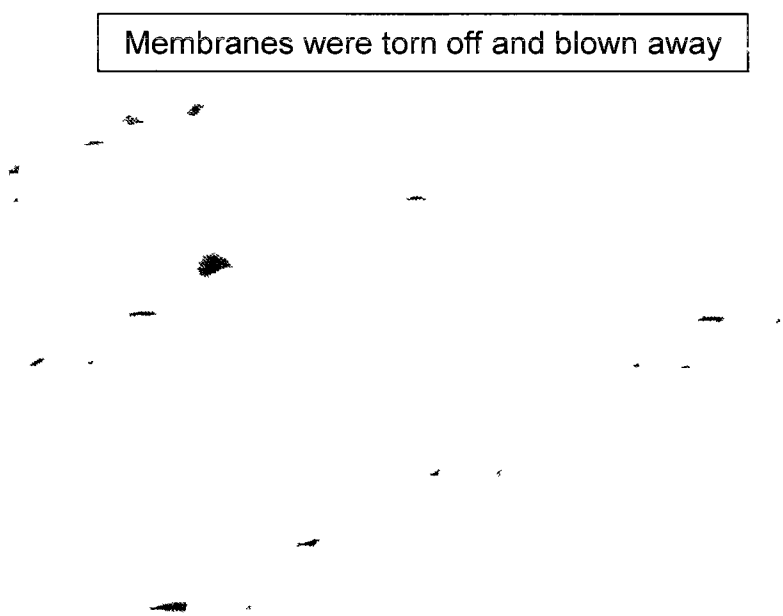

(b) Close-up view of the failure

Figure 3.5: Wind uplift failure of MARS
(Hurricane Katrina Investigation Report, RICOWI, August 2007)

3.4 Fully Bonded Roof System (FBRS)

This type roofing assembly is a combination of mechanical attachment and adhesive application. It is comprised of the following components: membrane, adhesive, fastener, fastener plate, insulation, barrier, and roof deck. The membrane is glued directly to the insulation by solvent or water-based adhesive or hot bitumen, instead of being fastened to the roof deck by using fasteners and plates like MARS. The insulation is mechanically attached to the structural deck. Therefore, the wind uplift force on the membrane is first transferred to the insulation and the securing fastener plates of the insulation, then to fastener and structural deck as seen in Figure 3.6. When wind uplift exerts on this type of system, its membranes are kept attached with under-layer surface through adhesive without billowing as those of the MARS membranes. The entire roofing assembly acts as a composite unit, and each roofing component offers certain resistance against the wind uplift, see Figure 3.7. The wind uplift resistance of FBRS depends on the application and bonding strength of the adhesive itself; bonding compatibility of the adhesive with the membrane, insulation and fastener plates; fastener density of the insulation board; configuration (shape & material) of the fastener plate; insulation thickness and curing time of the assembly.

From the research achievement of *NRCC-45613* (Baskaran, Molleti & Sexton, 2006), it is confirmed that the optimal curing time of the assembly appears to be 28 days, at which the maximum adhesive bond is achieved between the membrane and the insulation facer. With the same curing time, a larger bonding area or contact area between the membrane and fastener plates increases the bonding strength and therefore results in higher wind uplift resistance. Thicker insulation board contributes to higher compressive strength, lower deformation and better airflow intrusion control into the assembly, which allow the assembly to sustain higher wind uplift pressures. Figure 3.8 presents a FBRS failed during the hurricane Charley in Florida, 2004.

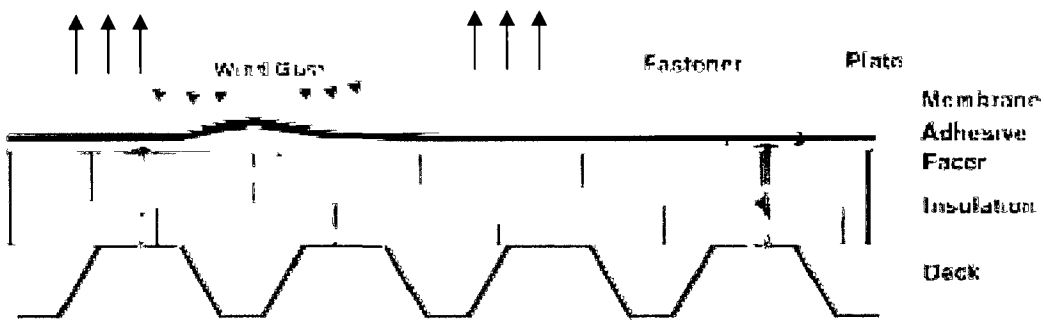

Figure 3.6: Force diagram of FBRS
(NRCC-45613, Baskaran; Molleti & Sexton, 2007)

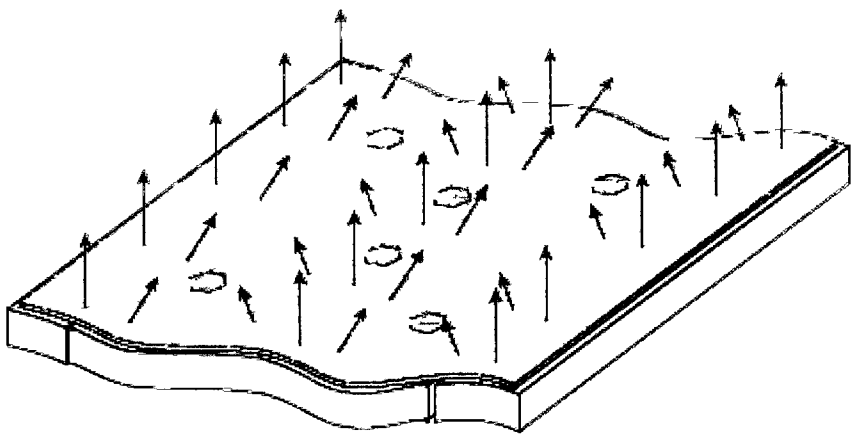

Figure 3.7: Response of FBRS under Wind uplift load
(NRCC-45613, Baskaran; Molleti & Sexton, 2007)

(a) Insulations rupture at high wind uplift pressure

(b) Insulation facers peeled away from the insulation boards and blown off with modified bitumen membrane

Figure 3.8: Wind uplift failure of FBRS
(Hurricanes Charley and Ivan Investigation Report, RICOWI, March 2006)

3.5 Adhesive Applied Roof System (AARS)

All components of the AARS roof systems are integrated by using adhesive. There are no fasteners used for components' attachment. The general configuration of AARS includes membrane, cover board, insulation, vapour barrier and roof deck from top to the bottom layer in this sequence. Cover board and vapour barrier may be neglected depending upon the design requirements. Like the case of single-ply PVC membrane roof system applied widely in the United States, the PVC membrane, insulation and steel deck are assembled by using the PVC bonding adhesive and professional polyurethane insulation adhesive. Components such as cover board and vapour barrier are not included in this roof system. As there is no fastener used, AARS can not only offer advantages of reduction in moisture migration and thermal bridges of the roof assemblies but also provide higher wind uplift resistance.

Comparing to the flexible response of MARS under wind uplift load, the AARS provides the rigid reaction. The wind uplift response of AARS is simplified as shown in Figure 3.9. All components of AARS are bonded together by using adhesive and work together as a whole to against the wind uplift load. Its membranes and other components are kept attached with their underlayments by means of adhesive without billowing as those of the MARS membranes until failure. The uniform wind uplift loads applied on the roof system are fully transferred from the membrane layers, cap sheet and base sheet, to the cover board, insulation and other layers underneath in sequence through adhesive in between. If the adhesive at all levels are compatible with their adjacent components in high-coherence, very few indoor air flows would intrude up to the membrane level. The low/bubble pressure appearing in MARS will not occur on insulation of AARS. In other words, the substrate layer of membrane, namely the insulation, takes over 100% of the upper membrane pressure and passes it to the next underlying layers if there is no component deformation taking place. Figure 3.10 exhibits the AARS failure at insulation and membrane level during a hurricane.

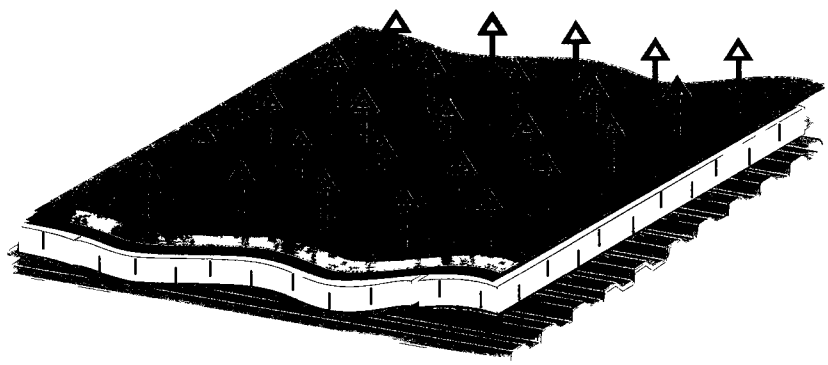

Figure 3 9: Rigid response of AARS.

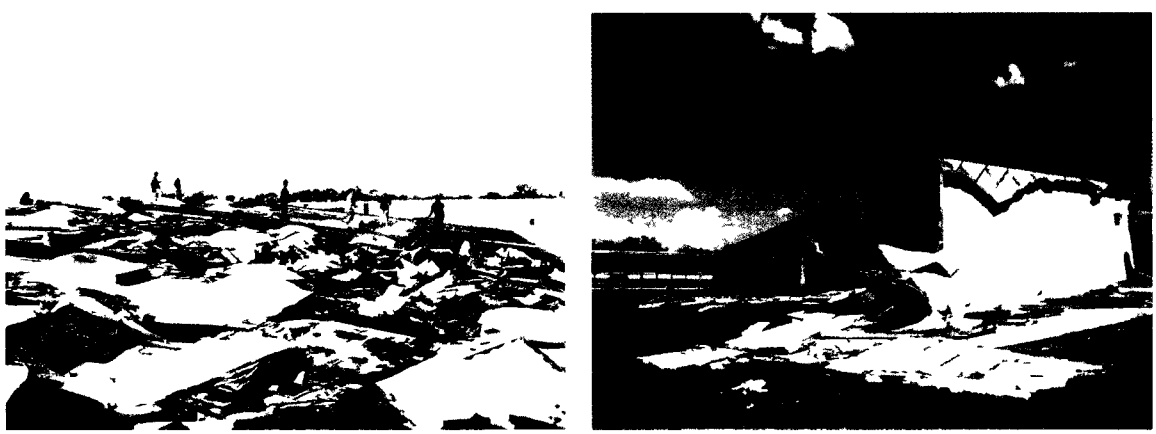

(a) Roof insulation failed during Hurricane Charley (Hurricanes Charley and Ivan Investigation Report, RICOWI, March 2006)

(b) Roof membrane and insulation failed during Hurricane Katrina (Hurricane Katrina Investigation Report, RICOWI, August 2007)

Figure 3.10: Wind uplift failure of AARS

3.6 Force Development in AARS

The dynamic wind uplift effects on different types of low slow roof are illustrated in the previous sections. To understand the force development in AARS, the typical wind induced failure is shown in Figure 3.11. It shows the wind induced shear and tensile forces on AARS. The tensile force can cause the uplift of the components. The membrane pulling without rupture can be correlated to the shear forces.

Figure 3.11 (b) shows the field example collected after the hurricane Katrina in 2005. The membrane and its substrate layers are lifted up by the effect of tensile and shear forces induced by dynamic wind uplift loads. The photo of Figure 3.12 shows the failed roof system. Membranes were completely peeled from the fibre boards which were used as cover board for AARS, and the fibre boards were separated due to pullout of the wind uplift load. The vortex streets induced by wind acted as a combination of tensile and shear forces applying on the roof continuously. Gradually, roof failed when the accumulating deformation for one of the roof components exceeded its acceptable limit due to the combination effect of pullout and peel from the dynamic wind.

In general, wind uplift loading on AARS roof places the roof components in the status of shear and tensile stress state. Shear force results in peeling failure and tensile force result in pullout failure. The shear and tensile forces development in AARS are illustrated in Figure 3.13.

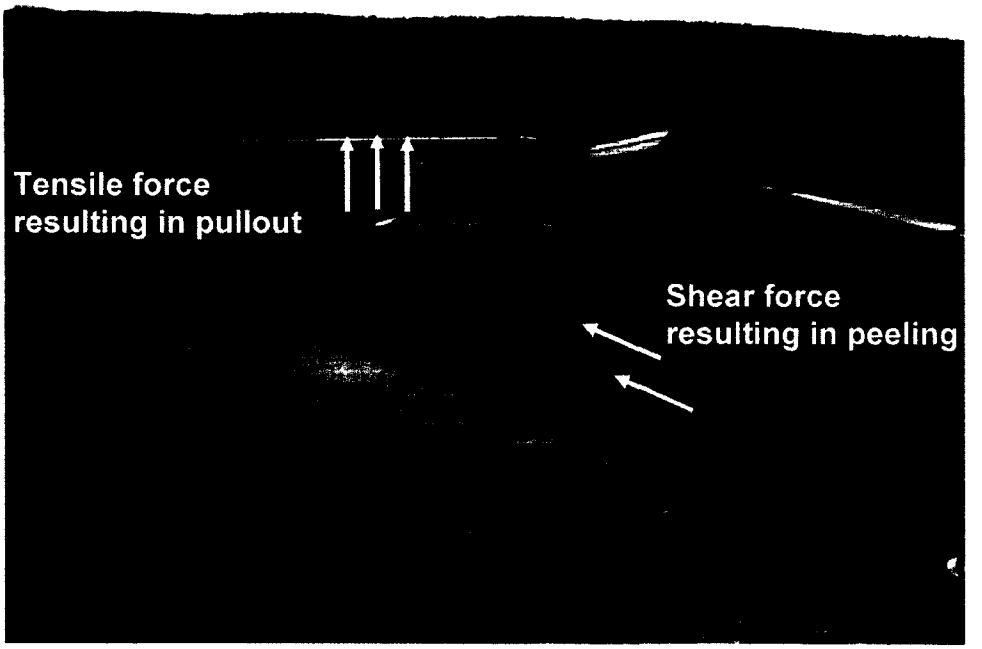

(a)

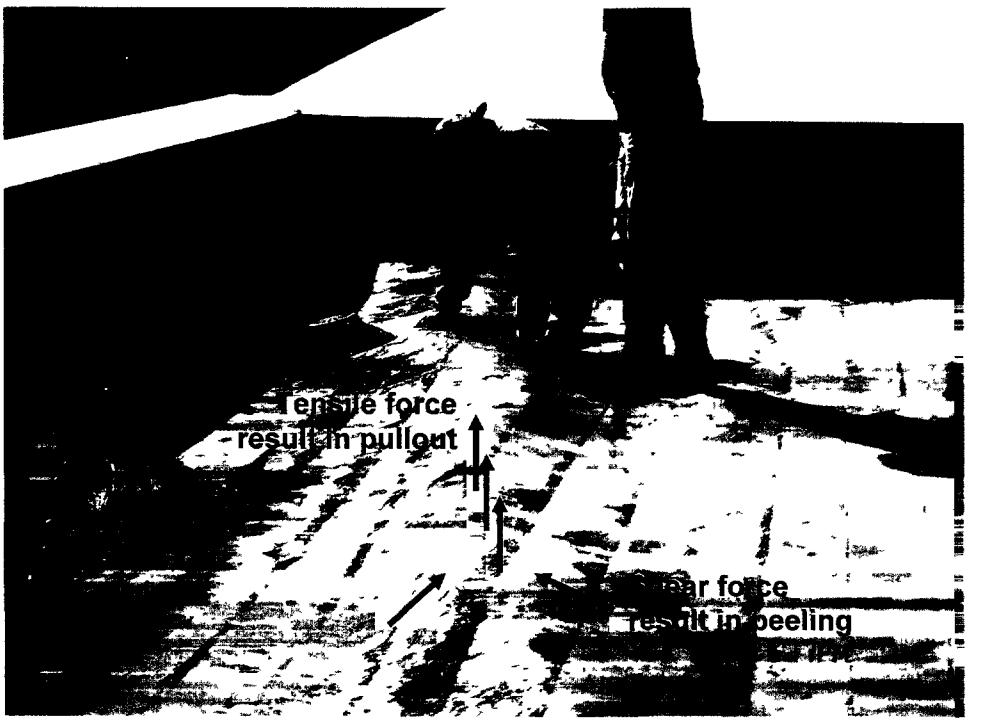

(b)

Figure 3.11: Wind Induced Shear and Tensile Forces on the AARS

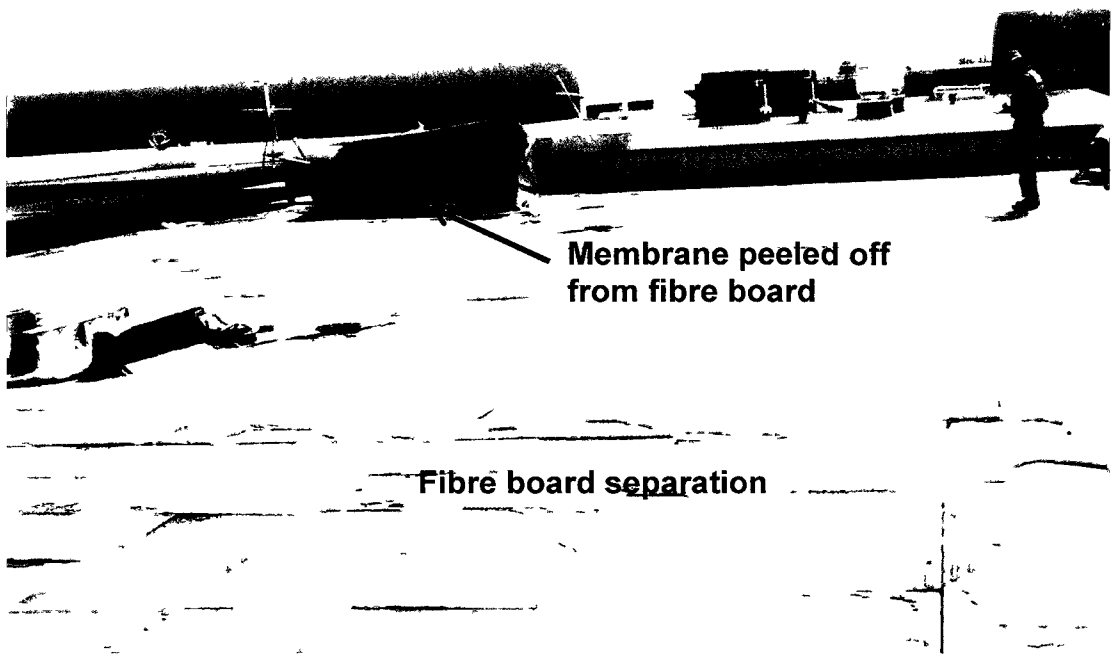

Figure 3.12: Weakest Link in the AARS for Shear and Tensile Forces

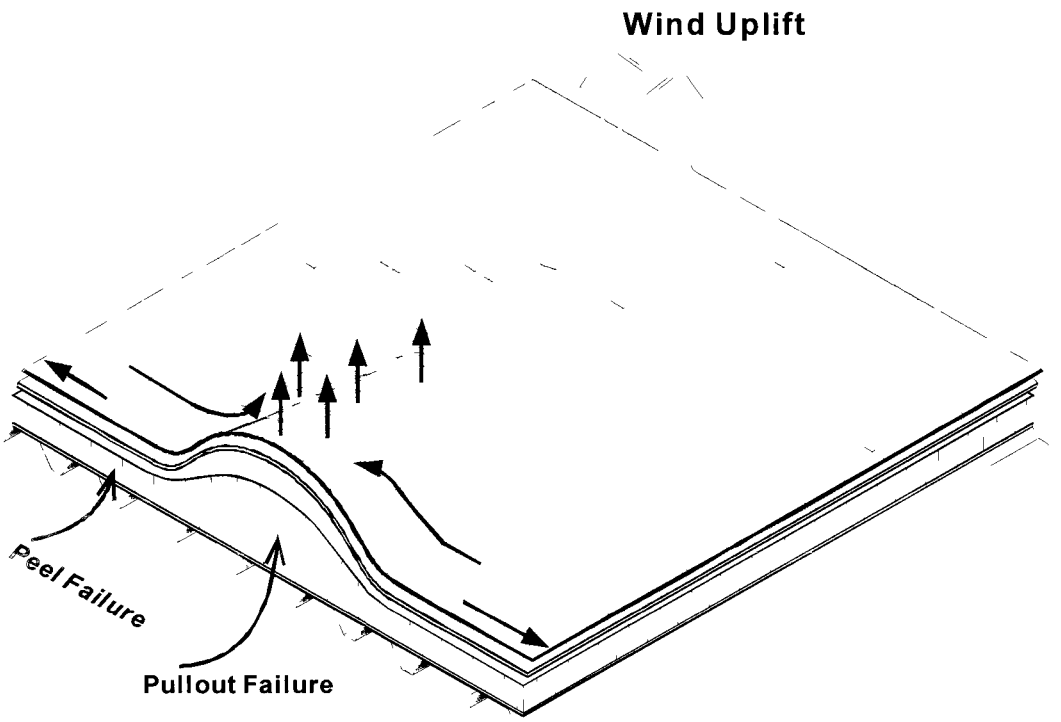

Figure 3.13: Force development in AARS and resultant failures

How does the dynamic wind develop the tensile and shear forces on AARS? Wind load is a random and dynamic process. When it separates from the roof edges or corners, it creates zones of suction or negative pressure on a low slope roof. It varies from one zone of the roof to the other and fluctuates from one period of time to other (NRCC-48676, Baskaran, 2006). As discussed in Chapter 2, e.g. Figure 2.5, the wind loads acted on the roof were not uniform. In this situation, the highest uplifting forces occurred near the corner and perimeter of the roof. The pressure decreases as wind blows across the roof. The spatial variations can be distinguished from zones of higher to lower suctions as corner, edge and field.

Wind also fluctuates with respect to time. The time fluctuations can be simplified through statistical approach by calculating mean, peak and standard deviation. Figure 3.14 shows typical wind induced pressures on a roof location in terms of time history. Taking a certain time segment, the actual wind loading at that instance can be decomposed into vertical wind force F_V and horizontal wind force F_H. The vertical force F_V can induce tensile forces on the roof system. It can be simulated in the laboratory by subjecting AARS specimens under pullout forces. The horizontal force F_H is the shear force acting on the components of the roofing system. It can be simulated in the laboratory by subjecting AARS specimen under shear forces with an angle. These simplifications can simulate the dynamic wind uplift loads on low slope roof of AARS.

A pull out test method was developed by Current (2009) in order to imitate the tensile force on roof components of AARS. It quantifies the pullout resistance of the roof of AARS. A peel test method was developed by Wu (2008), which simulates the shear force acting on the roof component of AARS. It can be used to quantify the peel resistance of the AARS. The experimental parameters and setup of the peel and pullout tests are reviewed in Chapter 4.

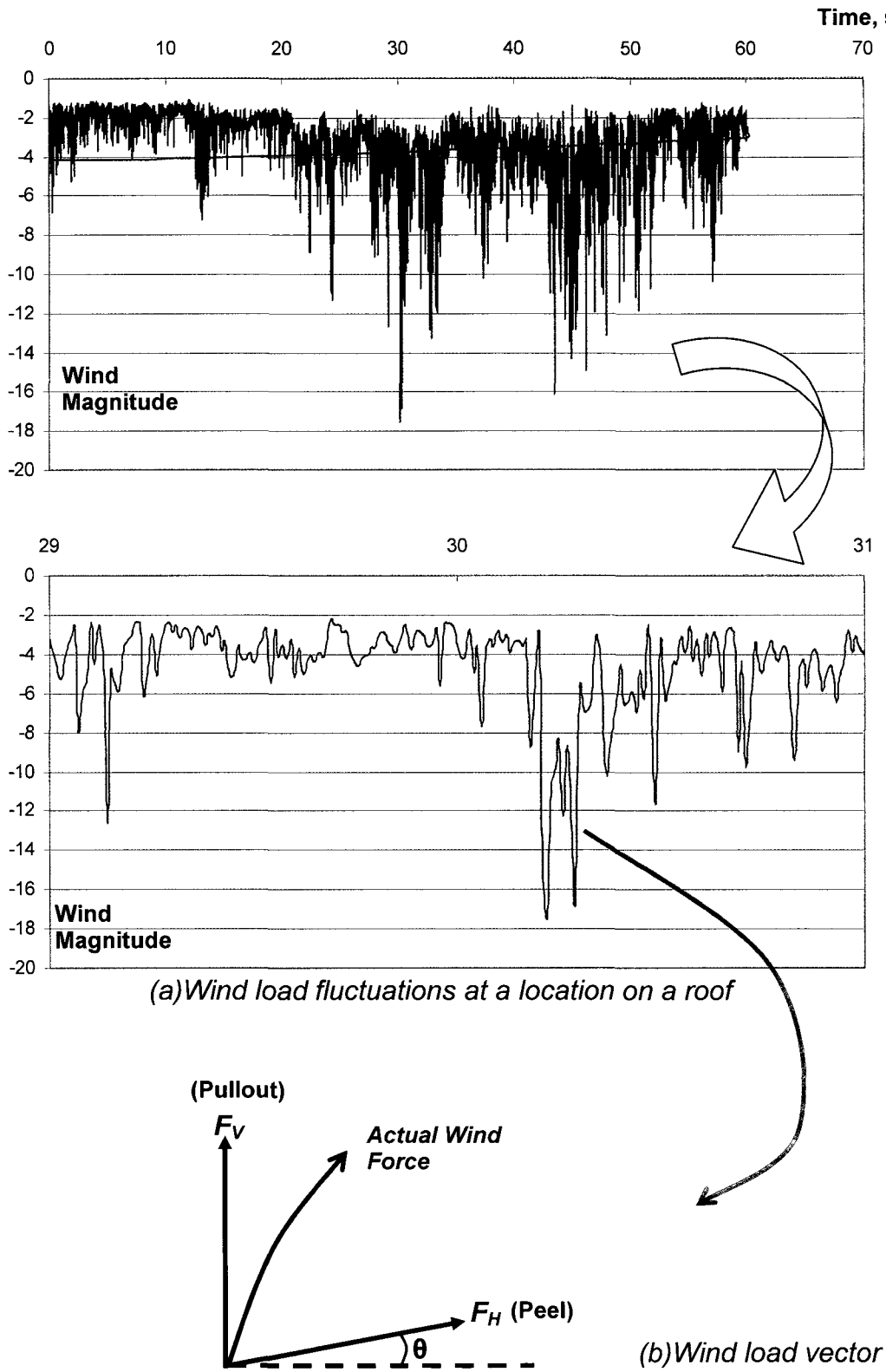

Figure 3.14: Vertical and horizontal wind force from dynamic wind load

3.7 Summary of Low Slope Roof Types

The structural characters and wind uplift resistance of four types of low slope roofing systems are introduced and explained in Section 1.4 of Chapter 1 and Section 3.2 of Chapter 3. Here are a few general guidelines for roofing design: BRS are the most cost effective if there are no weight load restrictions and high wind speed is not an issue. MARS are the most economical when dead load is an issue and medium to high wind speeds are expected. FBRS and AARS are typically the most expensive but would perform very well over time and can handle extremely high wind speed with the proper insulation attachment. Furthermore, there is no air intrusion for AARS that will result in higher wind uplift resistance if proper materials are assembled with well-matched adhesives.

Chapter 4: Review of the Existing Test Methods

4.1 Introduction

Though the AARS have been in use for a long time, there exists no standard to quantify its wind-uplift performances. This type of system tends to suffer serious shear and tensile forces due to dynamic wind uplifting loads. Shear force together with the tensile force could fail the weakest part along the resistance link first, resulting in the whole roof system failure.

As an achievement of the previously carried out research projects, in order to quantify the wind performance of AARS, three testing methods were developed and submitted to a standard development organization. These three testing methods are called the pullout, peel and dynamic wind uplift methods. Pullout and peel test methods evaluate the resistance of AARS under tensile and shear actions using small size specimens. The dynamic wind uplift test method assesses the wind uplift resistance of the roof system in full scale mockups. Thus the wind performance of AARS is quantified in three different ways, namely pullout, peel and full-scale dynamic wind uplifts individually. The full details of the three standard testing methods and procedures are given by Wu (2008), Current (2009) and Murty (2010).

This chapter presents the review of these three testing methods. The pullout test method is illustrated in Section 4.2 first. Then Section 4.3 displays the peel test method. In Section 4.4, the dynamic wind uplift test method is explained. Their respective experimental setup is also presented in the above sections, which will be used for the continuous AARS research at the next stage. The characteristics of three testing methods are summarized in Section 4.5.

4.2 Review of Pullout Test Method

To develop the standardized test methods for AARS, which are assembled by using adhesives, experimental investigations were carried out for specimens provided by four participating industrial partners who supplied their own materials and methods currently used for AARS construction. Varieties of specimens were tested and analyzed in various sizes and configurations combined with different loading rates.

The pullout specimens for testing have the same component configurations as the full-scale AARS roof. They are constructed with components of Cap Sheet, Base Sheet, Cover Board, Insulation, Vapour Barrier or Retarder, and the Deck. Cold adhesives are applied to bond all layers together. Adhesives are applied either as beading (ribbon format) or in fully coated format. Torching is sometimes used as an alternative to cold adhesives at the membrane level (Cap Sheet and Base Sheet). A minimum of 28 days is required for adhesives to cure.

4.2.1 Experimental Parameters

The research on the small-scale pullout test method of AARS was conducted by Current (2009). To achieve the consistent test results in terms of the maximum load, the load–extension relationship and the failure modes, three sensitive testing parameters were considered. They are the pullout rate, specimen size, and attachment condition to the deck, and they were carefully analyzed through the tests.

The maximum load, load–extension relationship and failure mode of pullout specimens reflect the wind uplift performance of the AARS specimen in small scale. Based on the detailed comparative analysis, the study concluded the following:

(1) Tensile loading rate of 0.25 in/min (6.35 mm/min);

(2) Specimen size of 12 in x 18 in (305 mm x 457 mm); and

(3) The steel deck secured on 4 flutes.

The above parameters were considered to be the most appropriate conditions for conducting the pullout tests in order to obtain consistent experimental results for evaluating the AARS behaviour in the field.

Through the use of the rigid top and bottom plate-flanged housings, which are attached on the stress plate and specimen mounting platform respectively, the boundary condition for the pullout tested specimen is both ends fixed. Figure 4.1 (e) shows a 12 in x 18 in (305 mm x 457 mm) specimen, which was set up on the Instron machine in this way and ready for the pullout test.

4.2.2 Experimental Setup for Pullout Test

The steps introduced in the developed pullout test methods are shown as below.

Step 1:

The male end of the bottom plate-flanged housing on the specimen mounting platform is plugged into its mating female component inside the Instron frame. The two are then rigidly connected by a pin-lock. With the specimen mounting platform properly attached, the steel stress plate is placed on top of the specimen mounting platform. The crosshead is then jogged down so that the male end of the top plate-flanged housing, which is connected to the stress plate, slid into the female component on the crosshead and the two are also stiffly connected by a pin-lock (Figure 4.1 (a) and (b)).

Step 2:

Jog upward the crosshead until there is enough space to install the specimen on the mounting platform. Then slot the attachment strips into the female flutes of the specimen. A visual inspection is needed to ensure that the female flutes are aligned with the 8 holes on the specimen mounting platform while keeping the center alignment between the stress plate, specimen and mounting platform at the same time (Figure 4.1 (c)).

Step 3:

Once the specimen is properly aligned, using ¼" (6.35 mm) bolts and nuts fasten the attachment strips to the mounting platform – ensuring that the specimen is rigidly fixed to the platform. Jog downward the crosshead until the steel stress plate is sitting on top of the specimen and then remove the pin-lock from the top plate-flanged housing. This is to release the stress plate and left it sitting directly on top of the specimen plywood dummy.

Step 4:

Jog upwards the crosshead so that a cordless drill can be used to fasten down the 10 #10 1" (25.4 mm) Robertson head wood screws to the stress plate to the specimen plywood dummy (Figure 4.1 (d)). Once the stress plate is secured to the specimen, jog the crosshead back down to reconnect the stress plate through the top plate-flanged housing. Replace the pin-lock in the top plate-flanged housing therefore re-attaching the specimen to the crosshead and the load cell. At this point the specimen is setup and ready for testing (Figure 4.1 (e)).

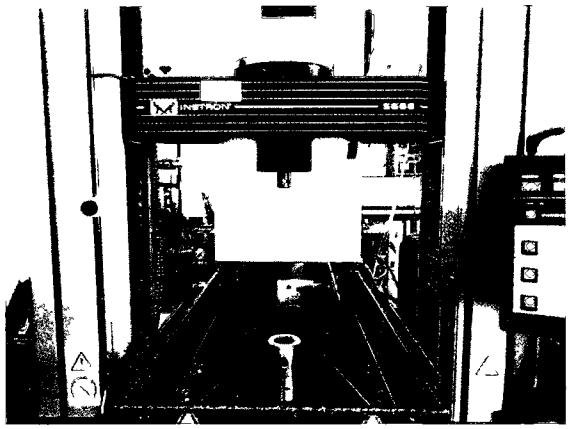

(a) The original Instron machine without attachment

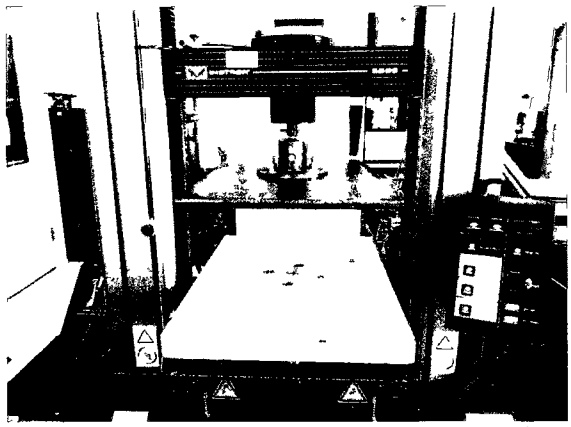

(b) Attachment of the steel stress plate & mounting platform by using the top and bottom plate-flanged housings

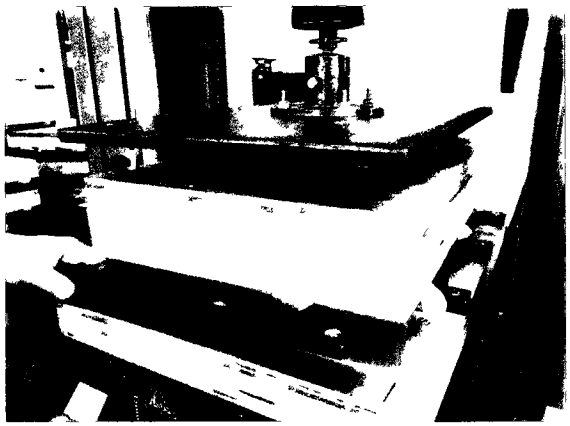

(c) Installation of specimen on the mounting platform & alignment check

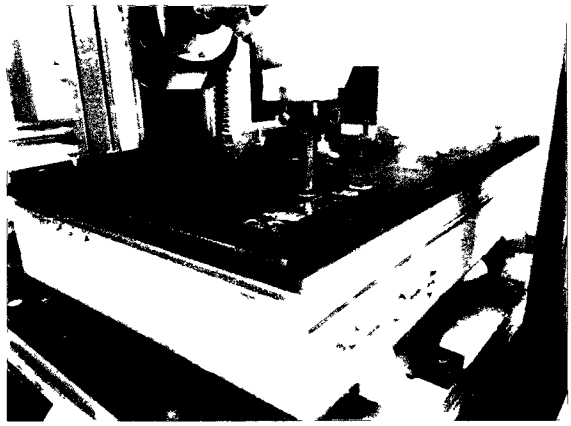

(d) Attaching the steel stress plate to the specimen plywood dummy

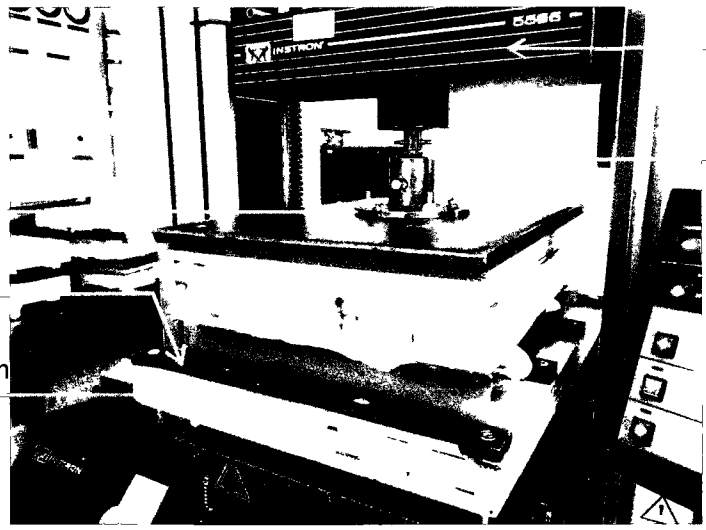

(e) Specimen ready for testing

Figure 4 1: Procedure of pullout specimen setup

4.3 Review of Peel Test Method

Wind uplift loads acting on AARS lead to shear force working on the components of AARS. The shear force becomes weaker as the increasing of the depth from the top layer surface. It is considered that the shear force effect intrude the components upon to the layer of insulation. Thereby, a standard peeling specimen configuration includes base sheet, cover board, and insulation from the top layer to the bottom layer. The bottom insulation and the cover board are cut into 6 in x 6 in (152 mm x 152 mm) squares, then the top membrane is cut into 6.5 in x 6 in square which is 0.5 in (13 mm) longer than the layer underneath at the edge so that a 0.5 in (13 mm) overhang is available to grip the specimen during the test. These layers are glued together by the same cold adhesive type as in the full size AARS tests.

4.3.1 Experimental Parameters

The peel test method was developed by Wu (2008) and the study recommends the following test parameters:

(1) Peeling rate was 1.0 in/min or 25.4 mm/min;
(2) Peeling angle set to be 15 degrees;
(3) Peeling at the edge position; and
(4) The suggested sample curing time was 28 days after assembly.

The proposed machine for standard peel test was the Instron machine 5566, which has the capability to offer constant rate of extension (CRE) with a crosshead speed of 1.0 in/min or 25.4 mm/min, recording the force-time relationship. To exert a peeling force on the specimen, a set of special fixer and angle controller were evolved and produced during the research. The fixer, which is made of steel plates, holds the specimen stable during the test. The fixer's size is 16 in x 14 in x 4 in, or 406 mm x 356 mm x 102 mm for length,

width and height, respectively. The angle controller serves to alter the vertical tension to peeling at desired angles.

4.3.2 Experimental Setup for Peel Test

The steps introduced in the developed peel test method are shown below.

Step 1:

The pneumatic action jaw is chosen to attach with the Instron machine's load cell, which can provide high clamping force for the wire under peeling. Secure the angle controller in the Instron frame by rigid coupling. Place the specimen in the center of the fixer and make alignment check with the angle controller (Figure 4.2 (a)). Adjust the three steel threaded rods of the fixer to hold the specimen tightly.

Step 2:

Use the gripper to grasp the overhang edge of the base sheet. Adjust the gripper position and the clamp-screws slightly to make sure the clamp-force along the overhang is uniform and symmetric (Figure 4.2 (b)).

Step 3:

Perform the Instron machine's pneumatic action jaw to clamp the peeling wire, which is tied to the gripper at one end and then goes through the roller of the angle controller (Figure 4.2 (c)).

Step 4:

Straighten the peeling wire by jogging up the crosshead of the Instron machine. Measure the peel angle and make the adjustment at the same time by altering the height of the angle controller until the required 15 degree is reached (Figure 4.2 (d)).

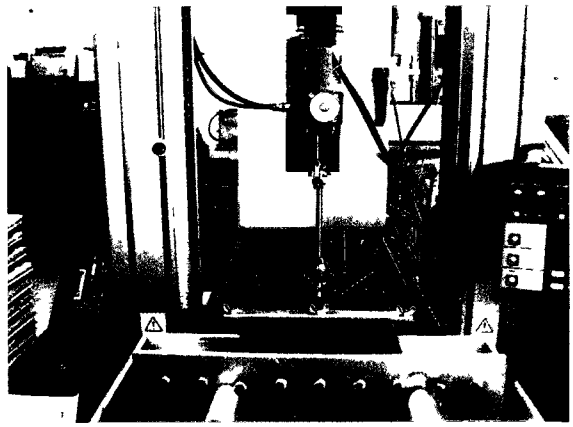

(a) Installation of specimen and alignment check

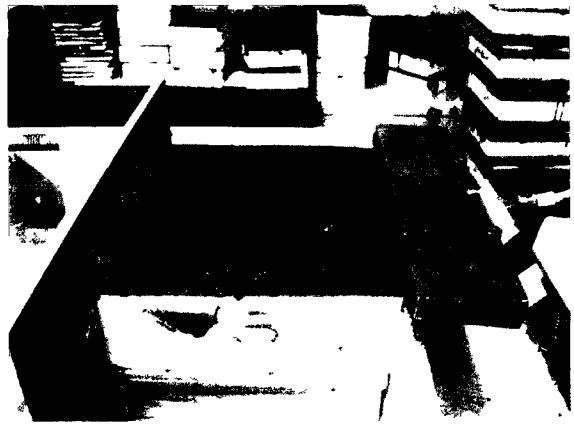

(b) Connection of gripper with specimen base sheet

(c) Connection of gripper with load cell through angle controller

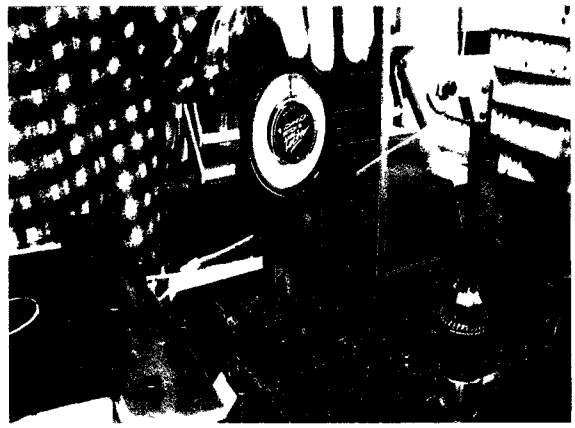

(d) Angle adjustment for the 15 degree

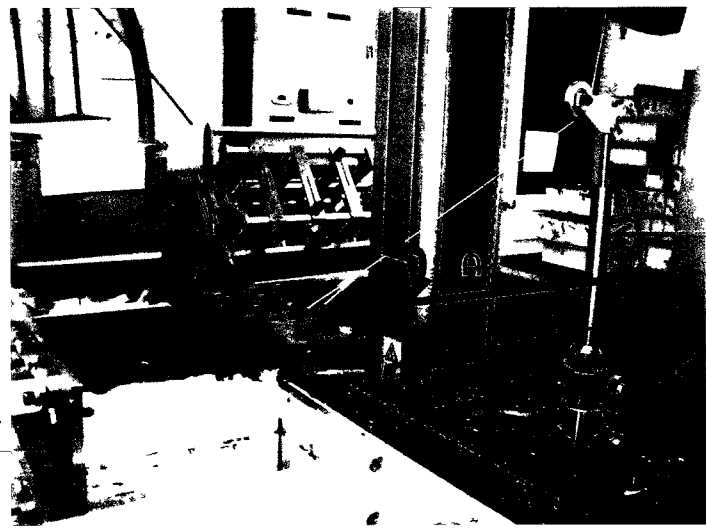

(e) Specimen ready for peel test

Figure 4.2: Procedure of peel specimen setup

4.4 Review of Full-scale Test Method

Accompanying the small-scale pullout and peel experimental studies, the full-scale experimental research on how to quantify the AARS wind uplift load resistance was carried out simultaneously and the dynamic test method was established by Murty and Baskaran (2010). The test method simulates the wind uplift effects on a full-scale AARS model to evaluate its dynamic performance.

4.4.1 Experimental Parameters

As to the definition of "full-scale", the width of the specimen should have a minimum of 2 component joints and the length of the test specimen should accommodate a minimum of 2 structural spans. Hence, a minimum specimen dimension of 8 ft x 10 ft or 2438 mm x 3048 mm was recommended.

Based on the boundary layer wind tunnel studies using rigid models, a time-dependent or dynamic load cycle was developed to simulate the dynamic wind effects to some extent. The models were made to consider the different building height, building aspect ratio and wind direction, which are three major factors to affect the wind pressure distribution on a low-slope roof. Three aspect ratios (L/W) of 1.0, 0.5 and 2.0 were tested for two different wind directions, 0 and 45 degrees at three different full-scale equivalent heights, namely 20 ft (6.1 m), 40 ft (12.2 m) and 60 ft (18.3 m). In total, there were 18 model configurations tested.

Figure 4.3 (a) shows the developed wind load cycles for the dynamic wind uplift test. The developed time-dependent wind load cycles were used to evaluate five different levels of AARS wind uplift resistance, from Level A to Level E. There were eight loading sequences, two groups for each level. Group 1 represents the wind-induced suction over a roof assembly. It consists of four sequences, where the pressure level alternates between zero and a fixed pressure. Group 2 represents the effects of exterior wind fluctuations combined with a constant interior pressure, or the static pressure, on a building. In group 2, while the roof

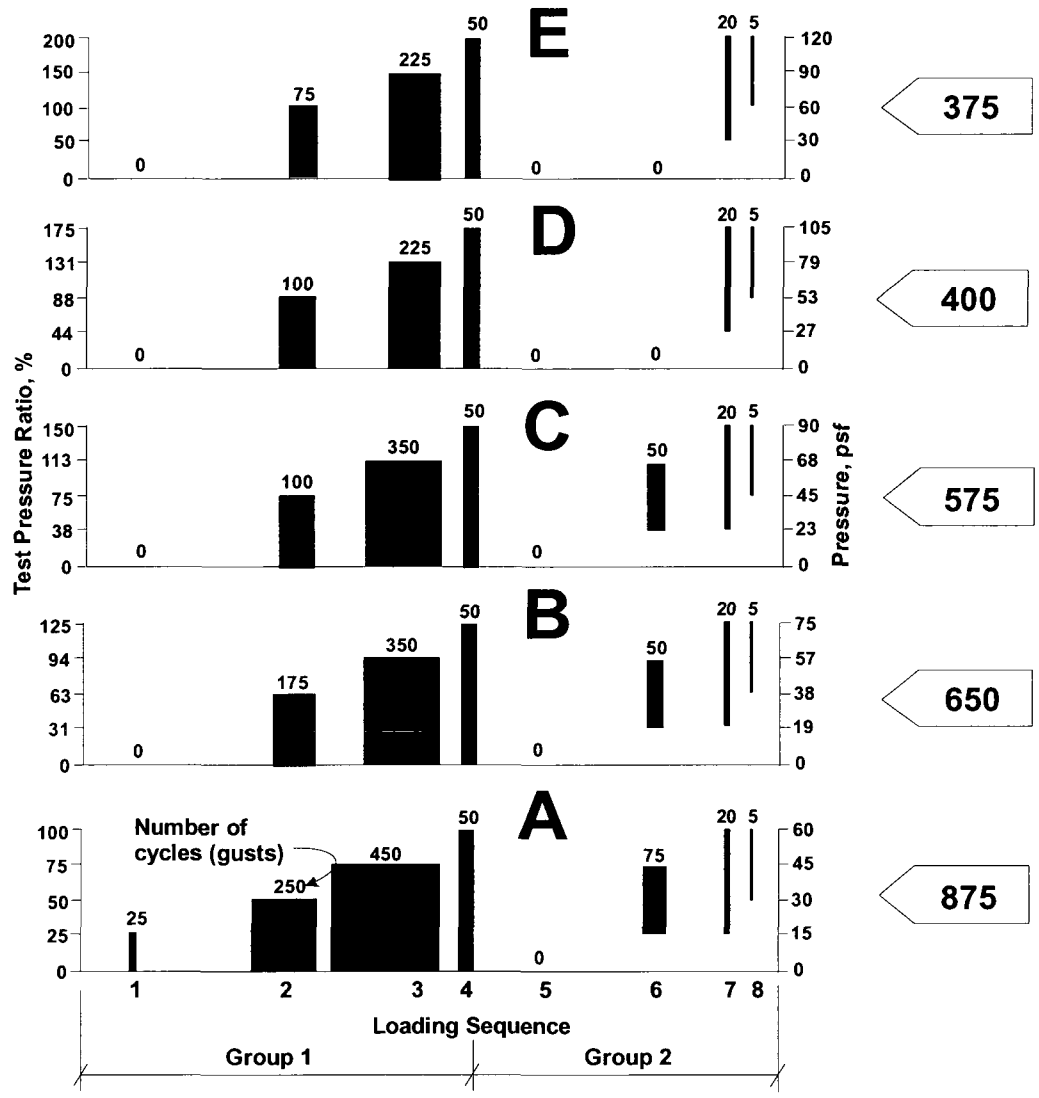

(a) Dynamic wind load cycles

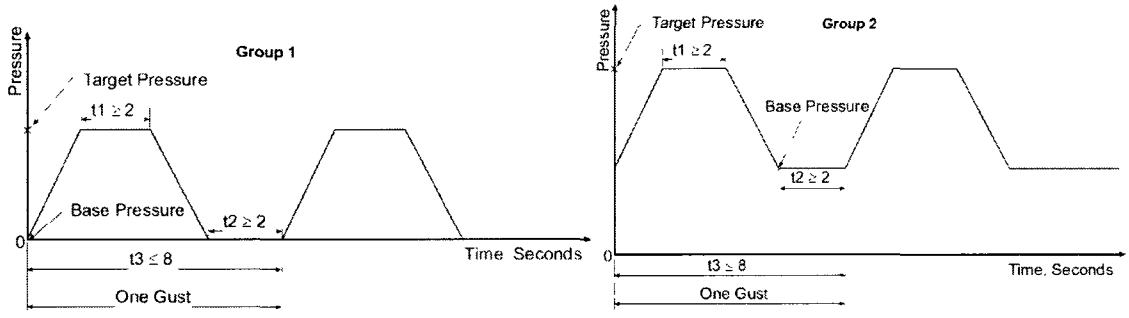

(b) Time requirement of gust cycle

Figure 4.3: The developed load cycle for AARS wind uplift test

membrane was to be lifted by static pressure, the wind gust was also considered on top of the constant static pressure. As shown in Figure 4.3 (b), test pressures of each gust shall be applied and maintained for no less than 2 s. The pressure is then released, with the system remaining at base pressure for at least 2 s. The total duration of every gust, including time to reach the required pressure, shall not exceed 8 s. To obtain a rating, all specified numbers of gusts of eight loading sequences in each level were to be completed.

All experiments were carried out at the Dynamic Roofing Facility (DRF) (see Figure 4.4). The DRF consists of a pressure chamber, a gust simulator and a suction box to simulate the desired wind loads. The pressure chamber contains a bottom frame of adjustable height upon which the roof specimens are installed and a removable top chamber. By following the developed load cycle for AARS, the wind uplift loads are applied on the specimen to simulate the wind effects on membrane roof assemblies. Figure 4.5 displays the structure of the pressure chamber with a 16 ft x 32 ft (4.9 m x 9.8 m) PVC roofing system mock-up on the testing table. The setup steps for a mock-up introduced in the developed dynamic wind uplift test method are shown in the following sub-section.

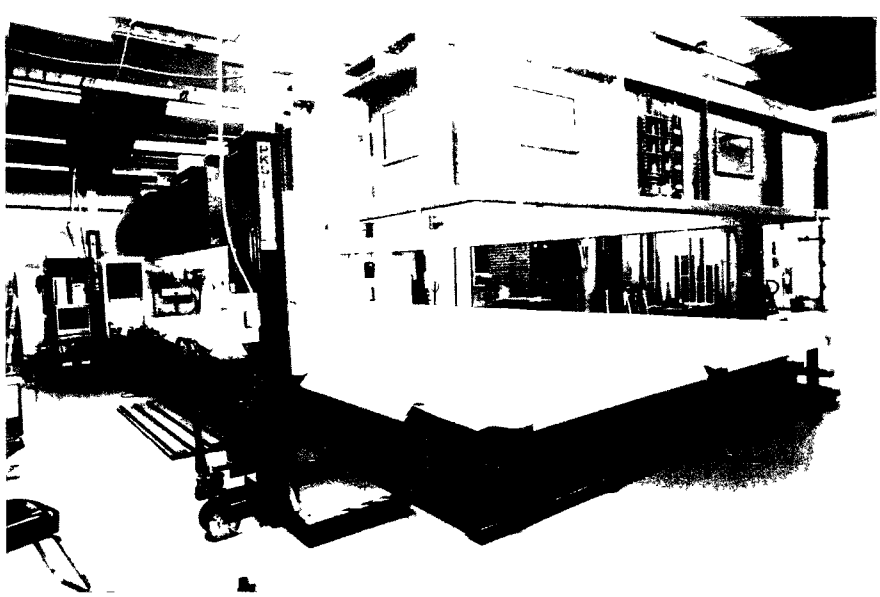

Figure 4.4: Dynamic Roofing Facility

4.4.2 Experimental Setup for Wind Uplift Test

Step 1:

Construct a mock-up on the individual full-scale roof deck with two joists underneath and cure the adhesives applied at room temperature with a specific time period, see Figure 4.5 (a).

Step 2:

Once the mock-up is ready for the testing, it is transported to the testing table by using a forklift. Place the mock-up into the testing table with the aid of a small portable hydraulic jack.

Step 3:

In order to easily monitor the membrane deformation visually, grid the surface with squares and position them by marking numbers (Figure 4.5 (b)). One of the failure mode definitions for the wind uplift test is based on the observation of membrane deformation. When the 15% squares are deformed, it is deemed that the whole roofing system failed.

Step 4:

Secure the mock-up on the steel joists of the bottom frame. To minimize any air leakage into the assembly during testing, the edges along the perimeter of dummy sections are sealed using foams, air sealant tape, additional edge fasteners, and clamps as shown in Figure 4.5 (c).

Step 5:

Clean the testing table by using a pressure-air gun (Figure 4.5 (d)). Move down the moveable-top chamber and leave it sitting on the bottom frame freely. It is also necessary to set up a recorder to trace the specimen appearance changing for post-test analysis (Figure 4.5 (e)).

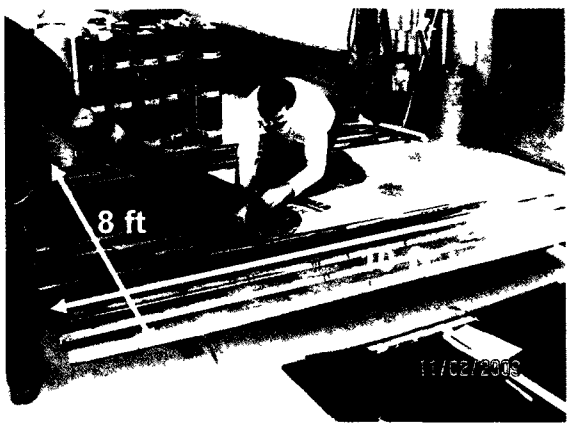

(a) Construction of a mock-up and curing with a specific time period

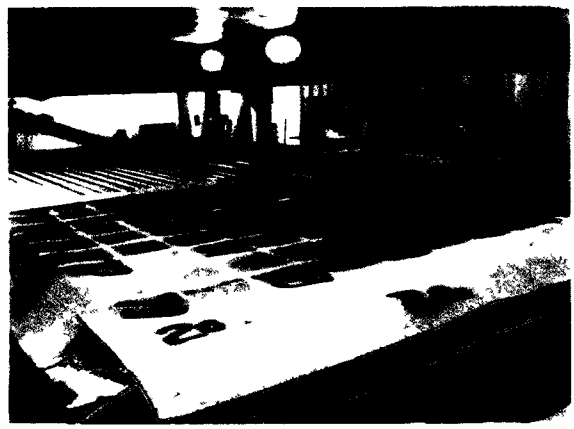

(b) Placing the mock-up on the testing table and marking with square grid for helping the deformation monitoring

(c) Edge treatment along the perimeter of dummy to minimize air leakage

(d) Cleaning the testing table by using pressure-air

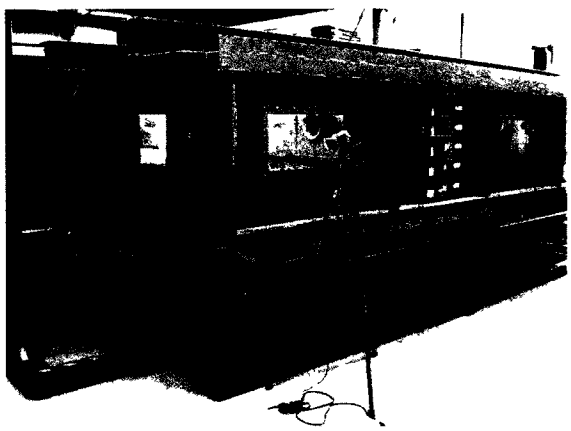

(e) Mounting the top chamber on the bottom frame directly

Figure 4.5: Procedure of wind uplift mock-up setup

4.5 Summary of the Three Developed Test Methods

Three test methods, namely the pullout, peel and wind-uplift test methods, were developed to quantify the wind performance of roofing components bonded together by adhesives. These three test methods were developed separately by Wu (2008), Current (2009) and Murty (2010). Now the correlation between the results of these three different test methods must be discussed carefully.

Table 4.1 highlights the main features and differences between the three developed test methods. The pullout test imitates the tensile force, while the peel test simulates the shear force applied on AARS components induced by wind uplift load. The dynamic wind uplift test method simulates the actual dynamic wind uplift load at varied magnitudes. That is to say that the pullout and peel test methods evaluate the partial performance of AARS against wind load while wind uplift test presents the overall wind performance of a roof.

Pullout test and peel test examine AARS using small-size specimens, whereas the wind uplift test examines AARS in full-scale size. For the preparation of the specimen and testing, it is obvious that the full-scale test costs more for materials, labor and it is also more time consuming than the small-scale pullout and peel tests. A practical question is if it is worth pursuing any particular testing method for evaluation of the wind uplift performance of AARS?

The weight of specimens used for pullout test and peel test was much less. The test methods are relative simple and easy to operate. The mock-up size for the full-scale wind uplift test is at least 8 ft x 10 ft or 2438 mm x 3048 mm, which is also heavy and not easy to handle. It should be tested in a special chamber, which is sophisticated for both setup and operation.

All of the pullout, peel and dynamic wind uplift tests were established based on the experimental investigation of modified bitumen roofing system. A question remains if it is suitable to test only the single-ply roofing system for drawing any

conclusions. It is necessary to apply pullout, peel and wind uplift tests to other types of AARS to further verify the pullout, peel and wind uplift test methods.

In summary, the pullout and peel tests can reflect the properties of both tensile and shearing resistance of the AARS roof, which are two significant indicators of the roof wind performance. It may be possible to use the pullout and peel test data to estimate the dynamic wind uplift performance in full-scale so long as their test results are well-correlated. It would certainly save the cost of labor, time and materials for building up full-scale experiments but would be also an effective way to assess AARS wind uplift performance for a roof already constructed or in service. Therefore, it is meaningful to find out the relationship of test results between pullout, peel and wind uplift test methods for practical engineering applications. An intensive study about the correlation among the pullout, peel and wind uplift test methods is continued in Chapter 5.

		Pullout Test	Peel Test	Wind Uplift Test
Characteristic of a Force		Tension	Shear	Combined
Specimen Size		12 in x 18 in (305 mm x 457 mm)	6 in x 6 in (152 mm x 152 mm)	8 ft x 10 ft (2438 mm x 3048 mm)
Component Considered		Cap Sheet Base Sheet Cover Board Insulation Vapour Barrier Steel Deck	/ Base Sheet Cover Board Insulation / /	Cap Sheet Base Sheet Cover Board Insulation Vapour Barrier Steel Deck
Loading Rate		0.25 in/min 6.35 mm/min	1 in/min 25.4 mm/min	2 sec Loading 2 sec Unloading 8 sec Gusts
Duration	**Setup**	30 min	15 min	4 hrs
	Testing	5 min	2 min	8 ~ 10 hrs
Approximate Cost Ratio		4	1	200

Table: 4.1: Summary of the three developed test methods for AARS

Chapter 5: Correlating Pullout, Peel and Wind Uplift Resistances

5.1 Introduction

The pullout, peel and wind uplift test methods were developed to assess the pullout, peeling and wind uplift resistance of AARS roof. They respectively reflect the tensile, shear and wind forces acting on AARS roof. The wind performance of AARS roof were simulated using full-scale experiments, whereas the pull and peel resistances were examined in small-scale experiments. The next step is to examine the correlation among the three testing methods.

Experimental studies on various roof configurations are carried out to investigate the relationship among the pullout, peel and wind uplift test results. For instance, an AARS with modified bitumen membrane, acrylic facer insulation and asphalt core board was constructed and tested. Its pullout, peel and wind uplift resistance were 379 lbf (1686 N), 85 lbf (378 N) and 45 psf (2155 Pa), respectively. A new configuration was constructed by changing the insulation component to paper facer insulation, while maintaining all other components same. The respective resistance were enhanced to 518 lbf (2304 N), 102 lbf (534 N) and 60 psf (2873 Pa). As a preamble, from the preliminary data analysis, the following hypothesis is proposed: *Higher resistance in both peel and pullout tests will result in the same or higher wind uplift resistance*. If this hypothesis is found acceptable, the simple and easy pullout and peel test methods can be used in lieu of the wind uplift test method to judge the wind performance of AARS. It will be a significant advantage for the practical application when making the component changes in AARS on site. If only one component in a roof is substituted in constructing a new roof, the new roof can maintain the same wind

uplift resistance as long as its pullout and peel resistance are higher than those of the original roof.

To verify this hypothesis, an experimental validation of one component change between two groups of samples was attempted by using the pullout, peel and dynamic wind uplift tests. The strategy of this validation is explained in Section 5.2. Section 5.3 illustrates the one component variation tests based on the AARS with modified bitumen membrane by considering three different scenarios. As Scenario 4, the one component variation tests based on the AARS with PVC membrane are presented in Section 5.4.

5.2 One Component Variation Test Strategy

A clarification is required to differentiate between the terms "component" and "material". The term "component" would refer to the element integrated in AARS that fulfils a defined specific purpose. For example, a component that is used to protect insulation from physical and chemical damages is a cover board. The "material" refers to the item that performs a specific role. Returning to the example, an adhered fibre board provides a barrier for roof constructers to walk on and prevent impact damage to the insulation once it has been placed during construction.

One component variation for the pullout and peel tests was conducted for comparison of two samples, each of which consisted of 8 or 12 specimens. The term "specimen" refers to an individual model built up in the laboratory for testing. The term "sample", on the other hand, refers to a group of specimens that were built under the same conditions and have common geometry and test variables. Corresponding to the same one component variation for the wind uplift test, the tested full size specimen is termed "mock-up", which keeps the same concept as the term "sample".

Four different scenarios were designed for the one component variation tests. The component substitutions for the four scenarios were selected at the membrane, cover board, support board and insulation level respectively which are the core elements of AARS. The first three scenarios use modified bitumen membranes and the fourth one has PVC membrane. Although the pullout, peel and wind uplift test methods were all established on the results using the modified bitumen roofing systems, they should be applicable to other types of AARS roofs as well. Investigations on the PVC membrane roof system were conducted to further confirm the application of the three testing methods. Another point of view is that the modified bitumen roofing system selected here belongs to the multi-ply roofing family, while the PVC membrane roofing is the single-ply roofing system. The research on PVC membrane roofing system and the results will thus reinforce the three proposed standard test methods and make a supplementary contribution to AARS.

For each scenario, two groups of samples namely Sample 1, Sample 2 were constructed for the complete set of testing matrix, which includes the pullout, peel and dynamic wind uplift tests. In these two samples, only one component was made different for comparison. The material source, application format of adhesive, assembly method, curing time, curing temperature and relative humidity for Samples 1 and 2 were kept identical. In total, 72 peel specimens, 72 pullout specimens and 8 wind uplift mock-ups were constructed and tested. Figure 5.1 is the flow chart indicating the validation procedure and the variables of roofing components.

Both the pullout and peel specimens prepared for the one component variation tests were examined by using the Instron machine 5566. The wind uplift mock-ups were tested by using the specific pressure chamber at the NRCC laboratory. The load-extension curves from the pullout tests, time history of loading curves from peel tests and dynamic time history of loading files from the wind uplift tests were produced by the testing machines. The maximum load and failure mode for

each tested specimen were recorded. The mean resistance of pullout and peel tests for every set of specimen was calculated for the subsequent data comparative analysis between sample sets. The pullout and peel specimen failure mode were identified according to the failure categorization defined by Wu (2008) and Current (2009). The failure mode for wind uplift mock-up was classified according to Appendix 2. Configuration details, test data and failure modes are illustrated in the following sections according to each Scenario.

5.3 Experimental Procedure for AARS with Modified Bitumen Membrane

One component variation tests for the AARS with modified bitumen membrane was set as Scenarios 1, 2 and 3. The changed components among them were membrane adherence, support board and cover board, respectively. The exact altered constituents for the three scenarios are shown in Figure 5.2.

Comparative samples of Scenarios 1, 2, and 3 for one component variation tests were constructed by three industrial partners. Each industrial partner carried one pair of sample construction with their own materials and assembly method. For each Sample, 8 peel specimens in the size of 6 in x 6 in (152 mm x 152 mm), 8 pullout specimens in the size of 12 in x 18 in (305 mm x 457 mm), and one wind uplift mock-up in the size of 8 ft x 10 ft (2438 mm x 3048 mm) were fabricated.

The experimental configuration, validation data and failure mode for Samples 1 and 2 of Scenarios 1, 2 and 3 are presented in the following sub-sections. The emphasis of the description is on the variation between Samples 1 and 2.

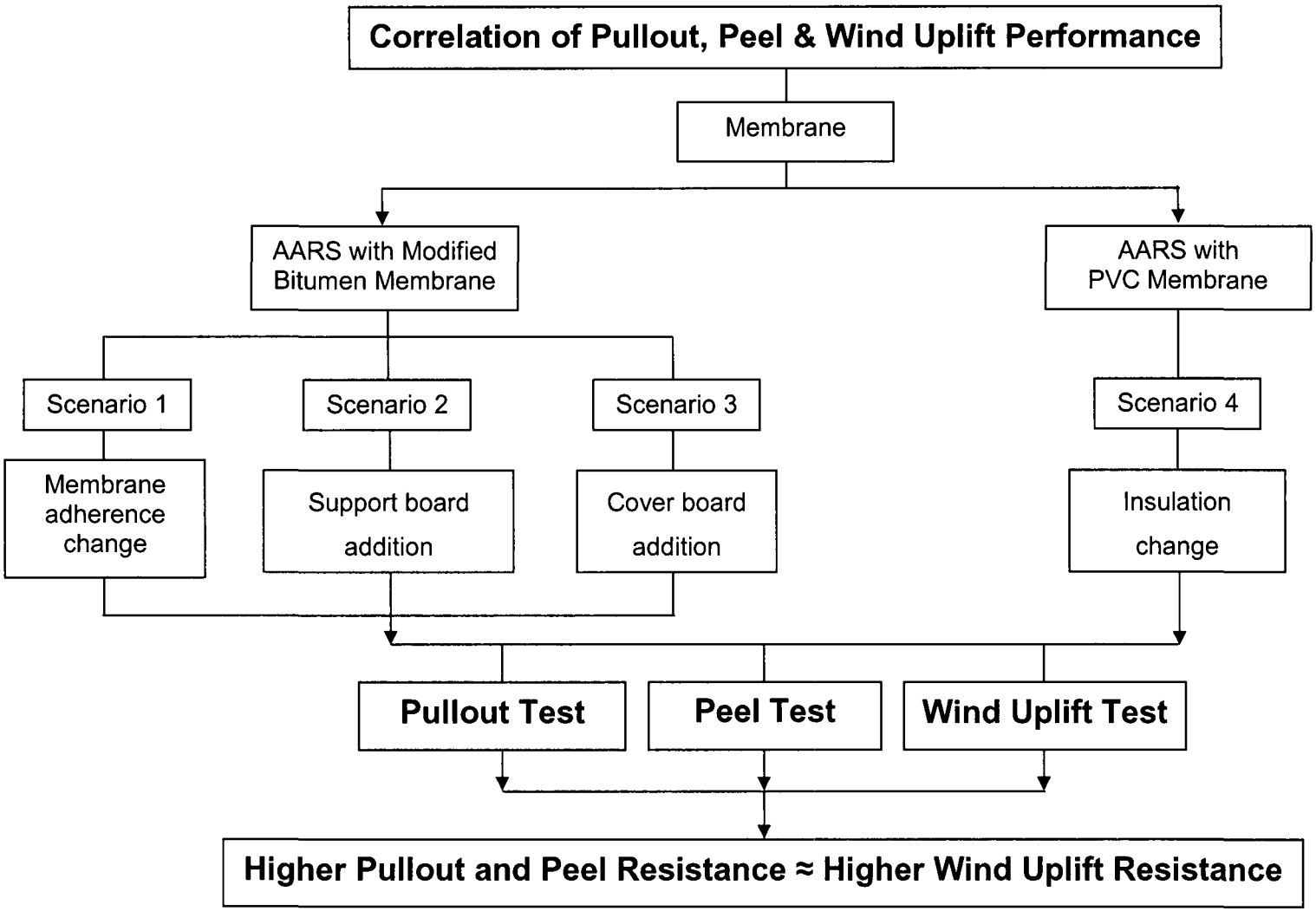

Figure 5.1: Flow chart for one component variation tests

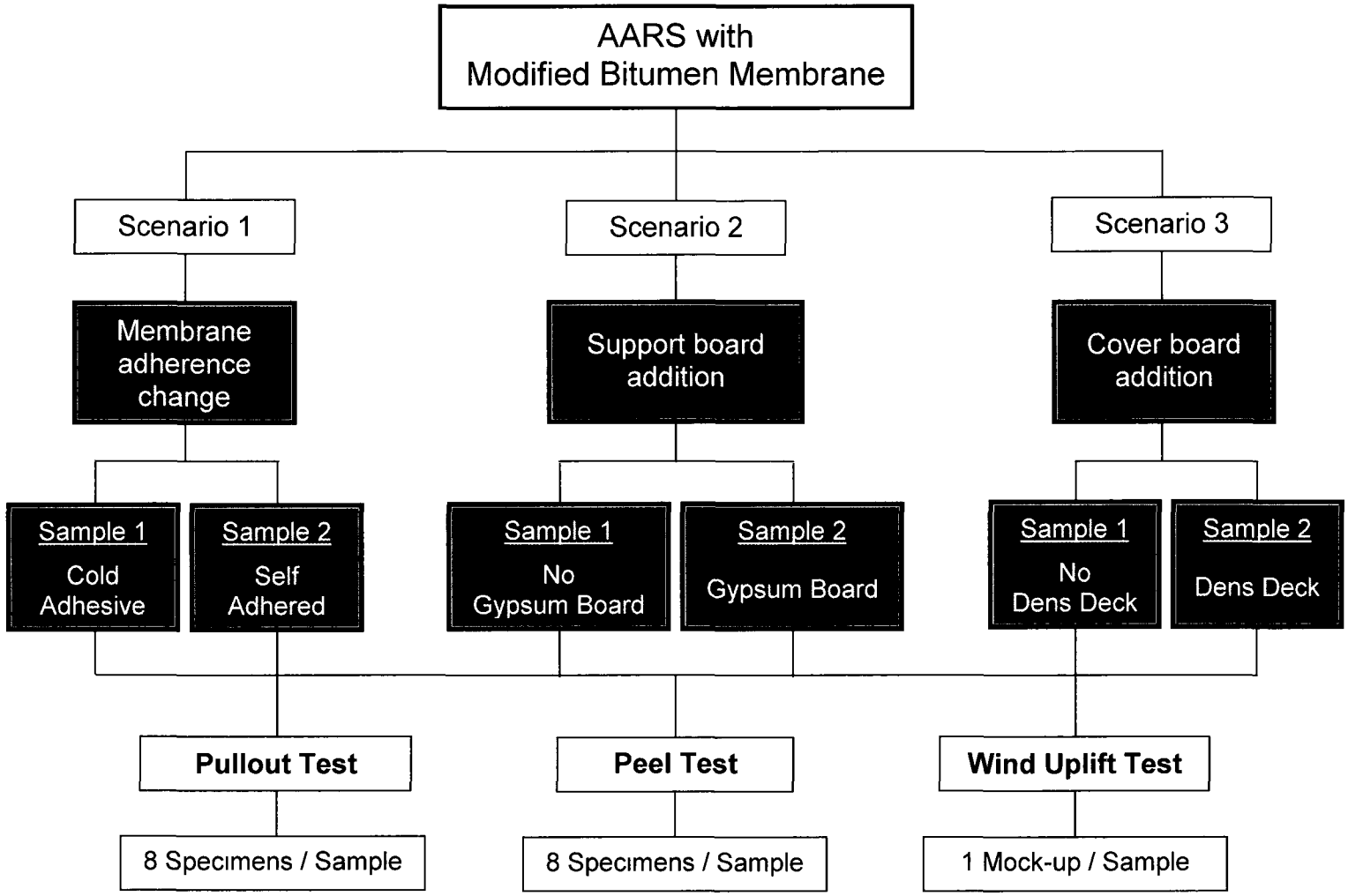

Figure 5.2: Validation for AARS with modified bitumen membrane

5.3.1 Scenario 1 – Membrane Adherence Change

(1) Experiment Configuration for Scenario 1

The substituted component in the Scenario 1 was the adherence of the base sheet. The roofing configuration for Scenario 1 includes modified bitumen membranes (cap sheet and base sheet), DD Prime board and steel deck. There was no insulation and vapour barrier used. The DD Prime roof board is a kind of standard Dens Deck roof board with enhanced surface treatment, which results in stronger and more consistent bond by allowing uniform spread of adhesives.

For Sample 1, the regular base sheet was integrated with the DD Prime board with cold adhesive in fully coated format, whereas Sample 2 chose the self-adhered base sheet. The specific primer was rolled over on the DD Prime surface first and dried up before laying the self-adhered base sheet. All other components were the same in both Samples. Their cross-sections and the construction processes of the mock-ups for the wind uplift test of Samples 1 and 2 are presented in Figure 5.3 (a) ~ (d), respectively.

(2) Validation Data Achieved by Scenario1

Scenario 1 compares the cold adhesive vs. self adherence and the varied components were arranged at the membrane level. Cold adhesive was fully coated for Sample 1 to bond the base sheet with DD Prime board. Self adhered base sheet was selected to build up the specimens for Sample 2.

As shown in Table 5.1, the mean resistance values of the pullout, peel and wind uplift test results for Sample 1 were: 680 lbf (3025 N), 136 lbf (605 N) and 90 psf (4309 Pa), respectively. After the regular base sheet was substituted in Sample 2 by self-adhered base sheet, the entire pullout, peel and wind uplift resistance were increased to: 1108 lbf (4929 N), 197 lbf (876 N) and 120 psf (5746 Pa), respectively, which were much higher than the resistance obtained for Sample 1.

Sample 1	Sample 2
Cap Sheet *Torch* Base Sheet ***Clod Adhesive Full Coat*** 1/2" DD Prime Board *Adhesive Beading* Steel Deck	Cap Sheet *Torch* Base Sheet ***Self-adhered*** 1/2" DD Prime Board (coated with blue primer) *Adhesive Beading* Steel Deck
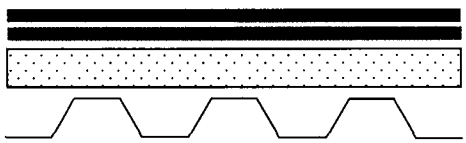	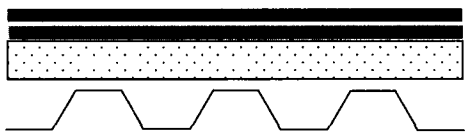
(a) Sample 1 cross-section	*(b) Sample 2 cross-section*
	
(c) Full coating of cold adhesive was applied on the DD Prime board	*(d) Self-adhered base sheet was installed on the DD Prime board*

Figure 5.3: Scenario 1 experiment configuration

A resistance ratio of Sample 2 to Sample 1 for the quantitative comparison was developed and expressed by a column chart in Figure 5.4. It normalizes the pullout, peel and wind uplift resistance of Samples 1 to 1.0. The ratio of test result of Sample 2 is then calculated as the pullout, peel and wind uplift resistance of Sample 2 divided by that of Sample 1. It clearly shows the trend that the pullout and peel resistance of Sample 2 is higher than that of Sample 1, when the self-adhered membrane is used instead of the cold adhesive bonded membrane. The pullout resistance of Sample 2 was found 1.6 times of the pullout resistance of Sample 1 while its peel resistance was increased by 45% from 136 lbf (605 N) to 197 lbf (876 N). The dynamic wind uplift rate of 120 psf for Sample 2 was 1.3 times higher than the original rate of 90 psf for Sample 1. This scenario validation data complies with the hypothesis that higher resistance of peel and pullout tests is associated with the higher wind uplift resistance.

(3) Failure Mode of Scenario1

Failure modes in pullout test

For pullout testing, basically, specimens of Samples 1 and 2 exhibited the same failure mode with rupture of the DD Prime board facer. The failed position was at the interface between the bottom facer of the DD Prime board and the flutes of steel deck, except for one out of sixteen specimens where the top facer delaminated from the DD Prime. The typical failure mode of Sample 1 and 2 are shown in Figure 5.5 (a) and (b).

Failure modes in peel test

For peel testing, the failures of Sample 1 occurred on the top facer of the DD Prime board, which was either delaminated or ruptured. The failures of Sample 2 were always at the base sheet, which was torn first due to exceptionally strong attachment between the self-adhered base sheet and the DD Prime board. The photos for their failure mode are displayed in Figure 5.5 (c) and (d).

Resistance	Sample 1 cold adhesive	Sample 2 self adhered membrane
Pullout	680 lbf (3025 N)	1108 lbf (4929 N)
Peel	136 lbf (605 N)	197 lbf (876 N)
Wind uplift	90 psf (4309 Pa)	120 psf (5746 Pa)

Table 5.1: Comparison of Scenario 1 results

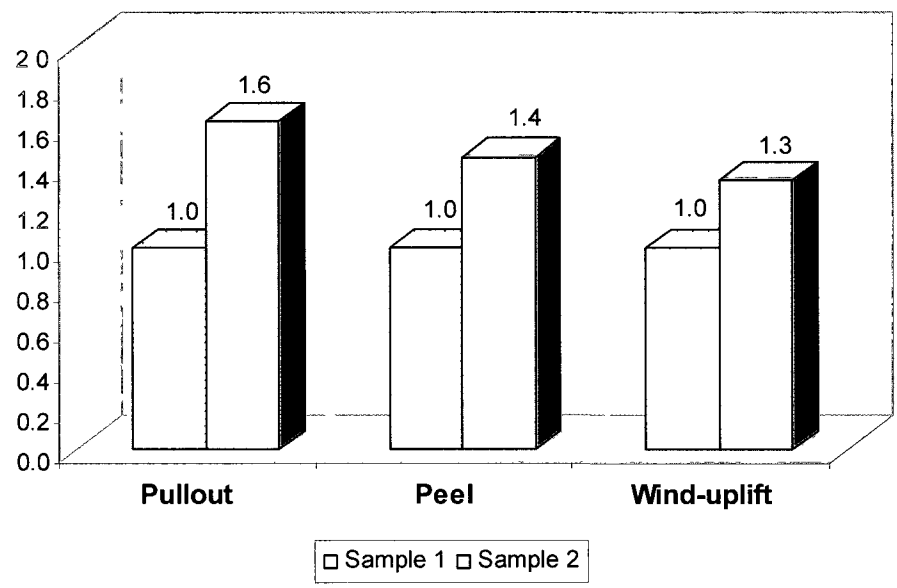

Figure 5.4: Comparison of pullout, peel and wind uplift resistance for Scenario 1

Failure modes in wind uplift test

For the wind uplift testing, Sample 2 passed the rating of 120 psf (5746 Pa) without failure. The mock-up of Sample 1 sustained 90 psf (4309 Pa). The primary failure was at the adhesive between the steel deck and DD Prime board which is shown in Figure 5.5 (e). The cracks in the dens deck are not part of the system failure. They are due to the sampling taking during the failure mode investigation.

5.3.2 Scenario 2 – Support Board Addition

(1) Experiment Configuration for Scenario 2

The variation for this group of validation is the additional support board (gypsum board) which is placed under the insulation. Sample 1 was constructed with a traditional configuration. The component layers from top to bottom were the cap sheet, base sheet, fibre board, paper facer insulation, vapour barrier and steel deck. In addition to these components, a layer of ½ in (12.7 mm) thick gypsum board was added between the vapour barrier and the steel deck for Sample 2. Thus, Sample 2 has one additional component compared to Sample 1 in pullout specimens and wind uplift mock-ups, but has the same configuration as Sample 1 in peel specimens because the components of peel specimen just contain the layers from base sheet to insulation. The detailed configurations for both Samples, their cross-sections and construction photos are demonstrated in Figure 5.6.

Sample 1	Sample 2
	
(a) Pullout failure mode: DD Prime board facer rupture	*(b) Pullout failure mode: DD Prime board facer rupture*
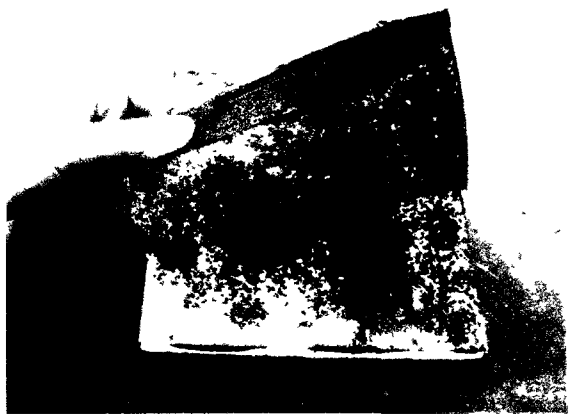	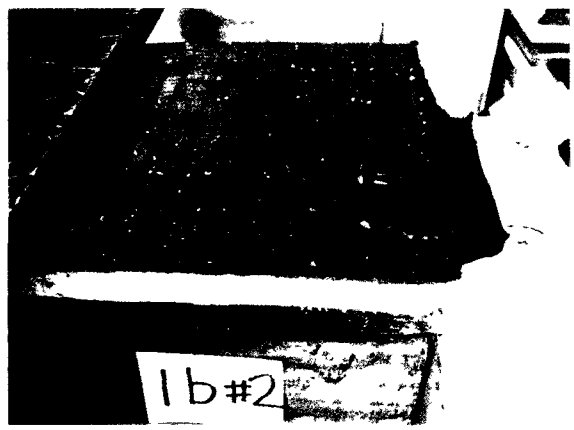
(c) Peel failure mode: DD Prime board facer rupture	*(d) Peel failure mode: base sheet was torn off*
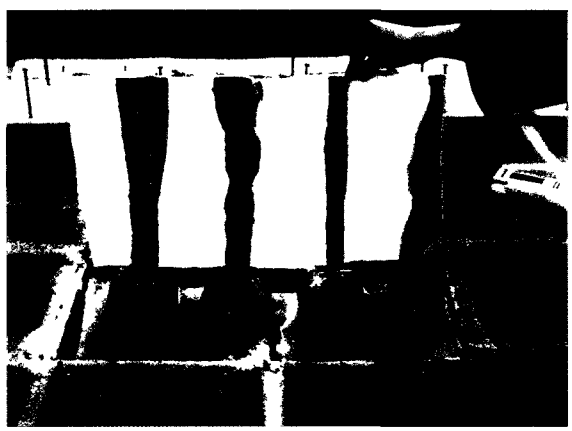	No failure for the mock-up of Sample 2
(e) Primary failure mode in wind uplift test: Adhesive failure between Steel Deck & DD Prime	

Figure 5.5: Failure mode comparison for Scenario 1

Sample 1	Sample 2
Cap Sheet *Adhesive Full Coat* Base Sheet *Adhesive Full Coat* Cover Board (Fibre Board) *Adhesive Beading* Paper Facer Insulation (2" thick) *Adhesive Beading* Vapour Barrier *Adhesive Beading* Steel Deck	Cap Sheet *Adhesive Full Coat* Base Sheet *Adhesive Full Coat* Cover Board (Fibre Board) *Adhesive Beading* Paper Facer Insulation (2" thick) *Adhesive Beading* Vapour Barrier *Adhesive Beading* **Gypsum Board (½")** ***Adhesive Beading*** Steel Deck
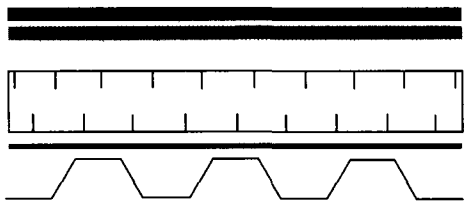	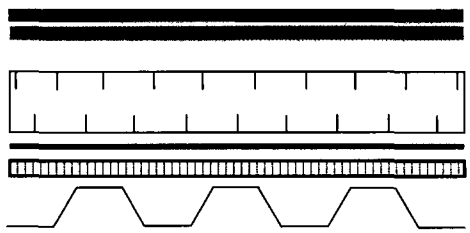
(a) Sample 1 cross-section	*(b) Sample 2 cross-section*
	
(c) Vapour barrier glued directly on the Steel Deck in Sample 1	*(d) Gypsum board attached to the Steel Deck first in Sample 2*

Figure 5.6: Scenario 2 experiment configuration

(2) Validation Data Achieved by Scenario 2

Scenario 2 used the additional component - gypsum board as a variable parameter. In addition to the same components as Sample 1, Sample 2 had an additional support board, ½ in (12.7 mm) thick gypsum board, on the steel deck but under the vapour barrier. Gypsum board is widely used for roofs and internal walls by the construction industry for fire protection.

Although the pullout specimens and wind uplift mock-up of Sample 2 were constructed with an additional support board between the steel deck and vapour barrier, its pullout, peel and wind uplift resistance were found similar to those of Sample 1. The pullout resistance of Sample 2 was increased slightly from 416 lbf (1851 N) to 483 lbf (2149 N), which is 16% increase. The peel resistances of both Samples were same due to the same specimen configuration. Sample 2 wind-uplift rate was decreased from 90 psf (4309 Pa) to 75 psf (3591 Pa). However, according to the CSA A123.21, a difference of 15 psf is acceptable between any two tests. The validation data for Samples 1 and 2 are summarized in Table 5.2.

In order to find the general tendency, a column chart of the normalized resistance is presented in Figure 5.7. It shows that the pullout resistance of Sample 2 is somewhat higher than that of Sample 1. Their peel resistance is exactly the same. However, the wind-uplift rate of Sample 2 is somewhat lower than that of Sample 1. In other words, the higher pullout resistance did not mean higher peel and dynamic wind uplift resistance for the Sample 2 experiments. The pullout, peel and wind uplift resistance of two samples were fairly close to each other.

Why were the pullout, peel and wind uplift resistance of Sample 2 close to those of Sample 1 after addition of a support board? The use of gypsum board in Sample 2 for an underlayer of the roof system provides the effective fire protection through the roof. From the viewpoint of roof structure, the attached

Resistance	Sample 1 without support board	Sample 2 with support board
Pullout	416 lbf (1851 N)	483 lbf (2149 N)
Peel	151 lbf (671 N)	151 lbf (671 N)
Wind uplift	90 psf (4309 Pa)	75 psf (3591 Pa)

Table 5.2: Comparison of Scenario 2 results

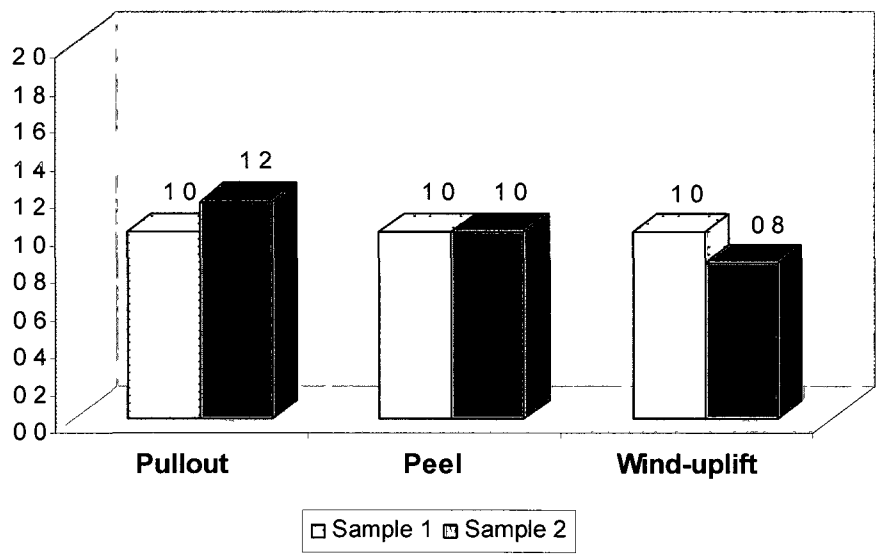

Figure 5.7: Comparison of pullout, peel and wind uplift resistance for Scenario 2

gypsum board on the steel deck strengthens the stiffness of the steel deck. However, there was no influence on other components above it. In other words, the additional support board does not stiffen the entire roof system. Since the roof components above the gypsum board were identical between Sample 1 and Sample 2, the two roof samples had the same configuration and construction methods except they were given two different stiffness of the deck. Generally, the roof decks are secured properly as a part of the building structure. The shear and tensile stresses in the components above the roof decks had no difference between Samples 1 and 2 under the same wind load. For this scenario, the weakest link was the fiber board. Once the weakest link among them failed, the roof systems failed as well. Therefore, Sample 1 and Sample 2 had the same failure modes and resistances on pullout, peel and wind uplift tests.

(3) Failure Mode of Scenario 2

Failure modes in pullout test

In both Samples 1 and 2, half of the pullout specimens failed due to the cover board separation. The cover board used in Scenario 2 was a fibre board. Fibre board was always found to be the weakest link according to earlier research (Current 2009). The other failure modes include the failure of adhesive layer on the steel deck, insulation facer tearing and/or gypsum board facer rupture. The comparison for pullout failure mode between Samples 1 and 2 is shown in Figure 5.8.

For this scenario, the cold adhesive was applied on the steel deck in the beading format. It results in non-uniform distribution of adhesion and stress concentration between the steel deck and its adjacent layer, namely the vapour barrier for the case of Sample 1 and the gypsum board for the case of Sample 2. Hence, the adhesive, insulation facer or gypsum board facer failed earlier than the fibre board separation took place.

Sample 1	Sample 2
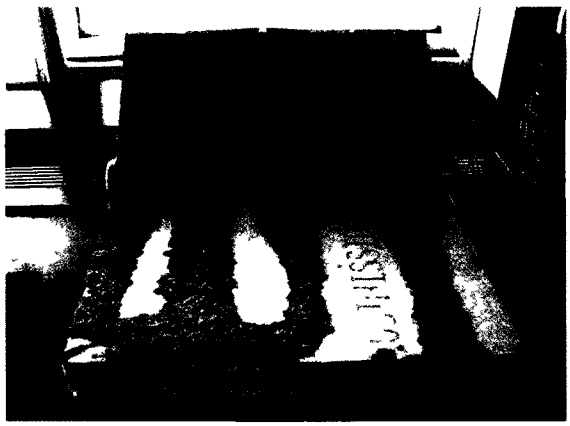	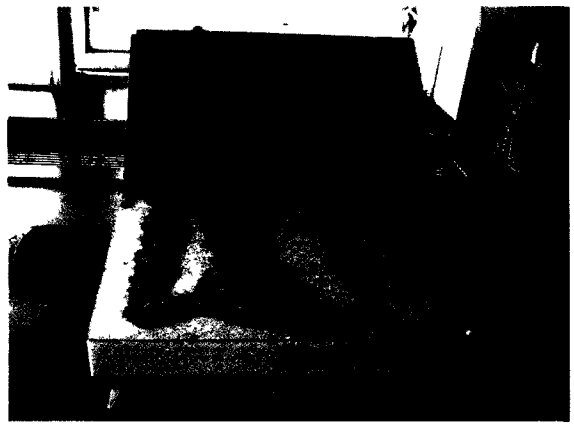
(a) Primary pullout failure mode: cover board separation	*(b) Primary pullout failure mode: cover board separation*
	
(c)Secondly pullout failure mode: insulation facer tearing	*(d) Secondly pullout failure mode: gypsum board facer rupture*

Figure 5.8: Pullout failure mode comparison for Scenario 2

Sample 1	Sample 2
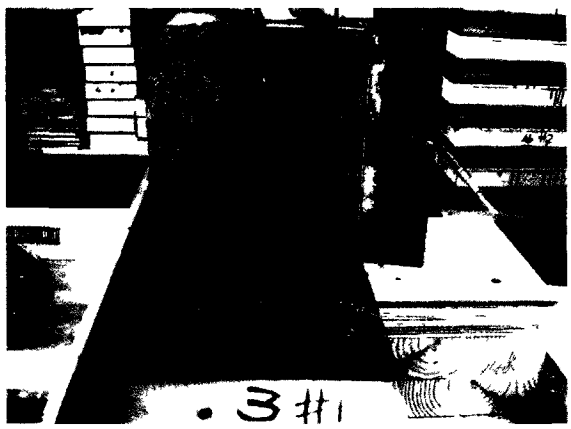	
(a) Peel failure mode Fibre Board separation	*(b) Peel failure mode: Fibre Board separation*
	
(c) Wind uplift failure mode: Fibre Board separation	*(d) Wind uplift failure mode: Fibre Board separation*

Figure 5.9: Peel and wind uplift failure mode comparison for Scenario 2

Failure modes in peel test

As mentioned earlier, the peel specimen configuration was composed of the base sheet, fibre board and insulation. The addition of a support board underneath the insulation layer was not included. This led to the result that Samples 1 and 2 had the same peel specimen configuration. Almost all the failure modes of peel tests were the fibre board separation with only one exception which was the base sheet tearing. Peel specimen failure modes of Scenario 2 comply with the results of peeling experiment by Wu (2008) that fibre board is the weakest link in peel tests. The failure modes are displayed in Figures 5.9 (a) and (b).

Failure modes in wind uplift test

The wind uplift test failure modes of Samples 1 and 2 are displayed in Figures 5.9 (c) and (d). They all failed by the separation of the fibre board. The wind uplift mock-up failure modes coincide with the former wind uplift experiment results by Murty (2010).

5.3.3 Scenario 3 – Cover Board Addition

(1) Experiment Configuration for Scenario 3

The factor to be compared for this set of Samples is with or without a cover board, which is placed on top of the insulation. Sample 1 was fabricated with membranes (cap sheet, base sheet), paper facer insulation, vapour barrier and steel deck but without any cover board. In contrast to it, an additional ¼ in (6.35 mm) thick dens deck layer was placed between the base sheet and paper facer insulation, while keeping other components consistent to Sample 1. Figure 5.10 displays the difference between Sample 1 and Sample 2 with their detailed configurations, cross-sections and photos when they were fabricated in full-size 8 ft x 10 ft (2438 mm x 3048 mm) mock-ups for the wind uplift tests.

Sample 1	Sample 2
Cap Sheet *Adhesive Full Coat* Base Sheet *Adhesive Full Coat* Paper Facer Insulation (2" thick) *Adhesive Beading* Kraf Vapour Barrier *Adhesive Full Coat* Steel Deck	Cap Sheet *Adhesive Full Coat* Base Sheet *Adhesive Full Coat* **¼" Dens Deck** ***Adhesive Full Coat*** Paper Facer Insulation (2" thick) *Adhesive Beading* Kraf Vapour Barrier *Adhesive Full Coat* Steel Deck
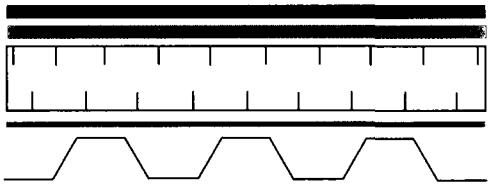	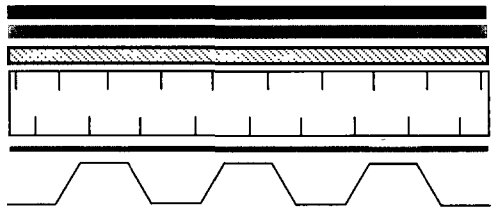
(a) Sample 1 cross-section	*(b) Sample 2 cross-section*
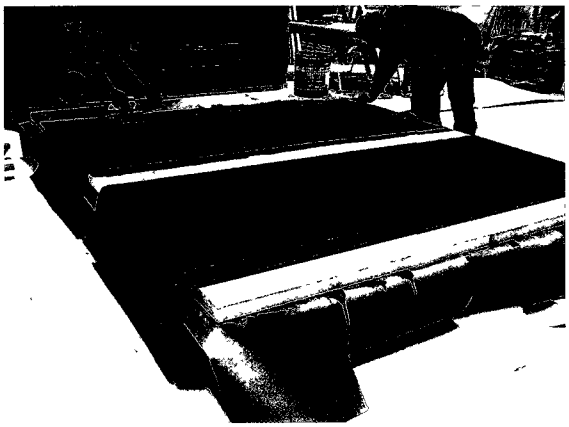	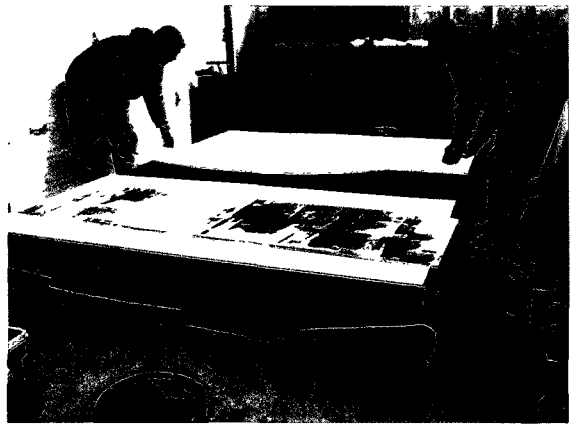
(c) Base sheet was laid on the insulation	*(d) Dens deck was placed on the insulation before installing base sheet*

Figure 5.10: Scenario 3 experiment configuration

(2) Validation Data Achieved by Scenario 3

The factor to be compared in this set of Samples was the existence of the cover board (Dens Deck). Sample 1 was constructed without any cover board. For Sample 2, ¼ in (6.4 mm) thick dens deck as a cover board was added to the roofing system just on top of the insulation. All other components were consistent between two Samples. The Dens-Deck roof board is an effective fire barrier, thermal barrier and recovery board used in various commercial roofing systems.

The average pullout and peel resistance of Samples 1 and 2 are listed in Table 5.3. After adding the cover board, the pullout resistance of Sample 2 did not change from that of Sample 1. However, the peel resistance was more than twice of that of Sample 1. Sample 2 obtained the same dynamic wind uplift rating as Sample 1, which was 120 psf (5746 Pa). The variation of the pullout, peel and wind uplift resistances for Samples 1 and 2 is expressed with the normalized resistance ratio in column chart, Figure 5.11.

The experiment of Scenario 3 demonstrated that the wind performance of AARS is determined by both the shear and tensile resistance of AARS. The shear resistance of Sample 2 was enhanced greatly by adding a stiff cover board, namely the dens deck. While keeping the pullout resistance as before, the wind uplift resistance of Sample 2 maintained at least the same rating as the Sample 1. The experimental results of Scenario 3 fortified the proposed hypothesis.

Resistance	Sample 1 without cover board	Sample 2 with cover board
Pullout	719 lbf (3198 N)	712 lbf (3167 N)
Peel	110 lbf (489 N)	241 lbf (1072 N)
Wind uplift	120 psf (5746 Pa) No Failure	120 psf (5746 Pa) No Failure

Table 5.3: Comparison of scenario 3 test results

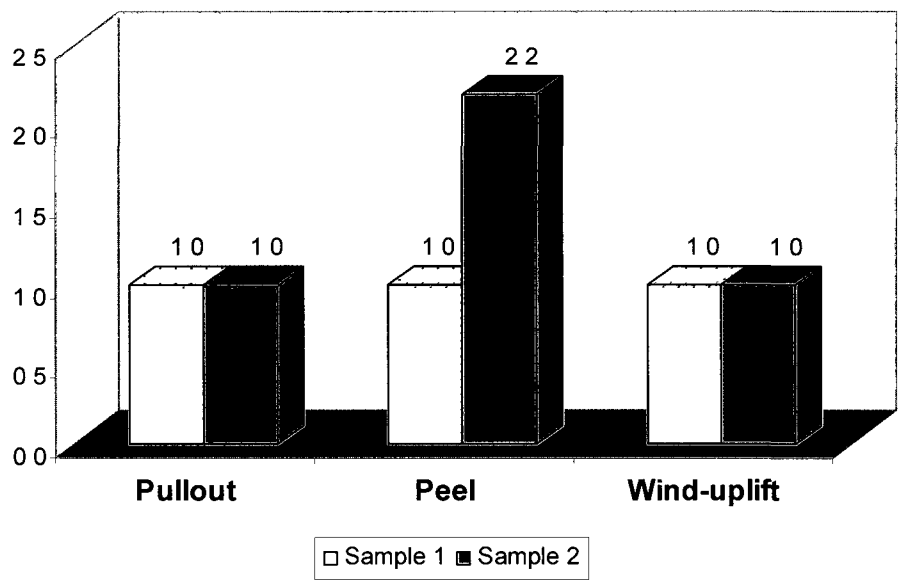

Figure 5.11: Comparison of pullout, peel and wind uplift resistance for Scenario 3

(3) Failure Mode of Scenario 3

Failure modes in pullout test

Samples 1 and 2 had the same failure mode in pullout tests. All failure modes of Samples 1 and 2 were at the insulation, without exception, either by rupture or facer delamination. The cold adhesive applied on every level of component was fully coated and spread out carefully so that adherence was good. There was no failure related to the adhesives in pullout tests. The typical pullout failure modes for Sample 1 and 2 are shown in Figure 5.12 (a) ~ (d). By examing the pullout specimen failure, it was noticed that the locations of foam insulation ruptures were mostly happened above the male flute of steel deck. This was because the steel deck was fixed at the female flutes. The deformations only occurred at male flute locations as well only the male flute surfaces were the actual contact area with the insulation. The transferred forces within the insulation were distributed to the male flutes. Increased in the deck deformation at the male flute places caused the insulation ruptured.

Failure modes in peel test

The failure mode of Samples 1 and 2 was found completely different in the peel tests. The peel specimen configuration of Sample 1 included only the base sheet and insulation without any cover board. Its typical peel failure was the insulation facer delaminaiton, see Figure 5.12 (e). For Sample 2, a piece of dens deck was added to the specimen. The base sheet was attached to the dens deck rather than the insulation. This combination effectively increased the shear resistance of peel specimens of Sample 2. Dens deck became the main component to resist against shear action. In most cases, the membrane was torn off before the dens deck facer delaminated, see Figure 5.12 (f). No insulation failure was observed in the peel tests of Sample 2.

Sample 1	Sample 2
	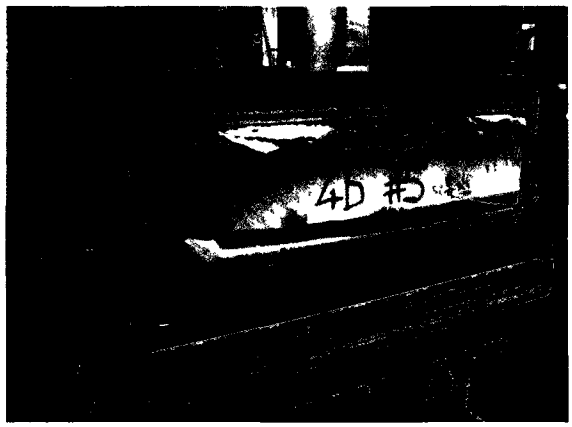
(a) Pullout failure mode: insulation rupture	*(b) Pullout failure mode: insulation rupture*
	
(c) Pullout failure mode: insulation facer delaminaiton	*(d) Pullout failure mode: insulation facer delaminaiton*
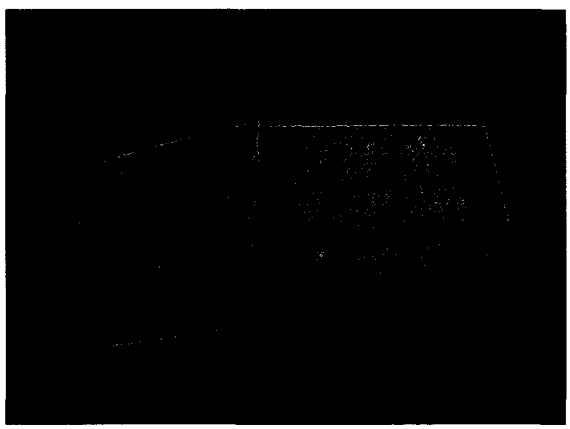	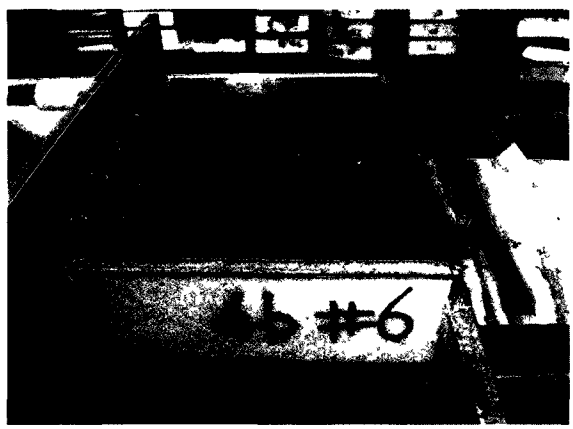
(e) Peel failure mode: insulation facer delaminaiton	*(f) Peel failure mode: membrane was torn off*

Figure 5.12: Failure mode comparison for Scenario 3

Failure modes in wind uplift test

Wind uplift rates of both Samples 1 and 2 were over 120 psf (5746 Pa) without failure, which was the highest rate that could be achieved by the testing machine.

5.4 Experimental Procedure for AARS with PVC Membrane

One-component variation test was also carried out on the Single-Ply Roofing Systems, which are widely used in the United State. It is set as Scenario 4 for the hypothesis validation. Generally, the configuration of single-ply roof system is in the sequence of membrane – insulation – steel deck from the top layer to the bottom layer. Due to less number of layers of components, the single ply roofing systems result in a cleaner, quicker and more economical system for installation compared to the multi-ply modified bitumen roofing system.

The membranes used for variation test was 40 mils (0.04", or 1.0 mm) thick white color Duro-Last specially formulated roofing membrane, which is comprised of a polyvinyl chloride polymer blend commonly known as PVC membrane. The validation flow chart is presented in Figure 5.13. Twelve peel specimens in 6 in x 6 in, twelve pullout specimens in 12 in x 18 in and one wind uplift mock-up in 8 ft x 10 ft (2438 mm x 3048 mm) for each Sample were constructed.

In this validated PVC membrane roofing system, the membrane was fully adhered with insulation by using the specific PVC bonding adhesive. A professional roof insulation adhesive was applied to attach the roof insulation boards to steel deck. It is single-component polyurethane foam adhesive and can provide fast adhesion.

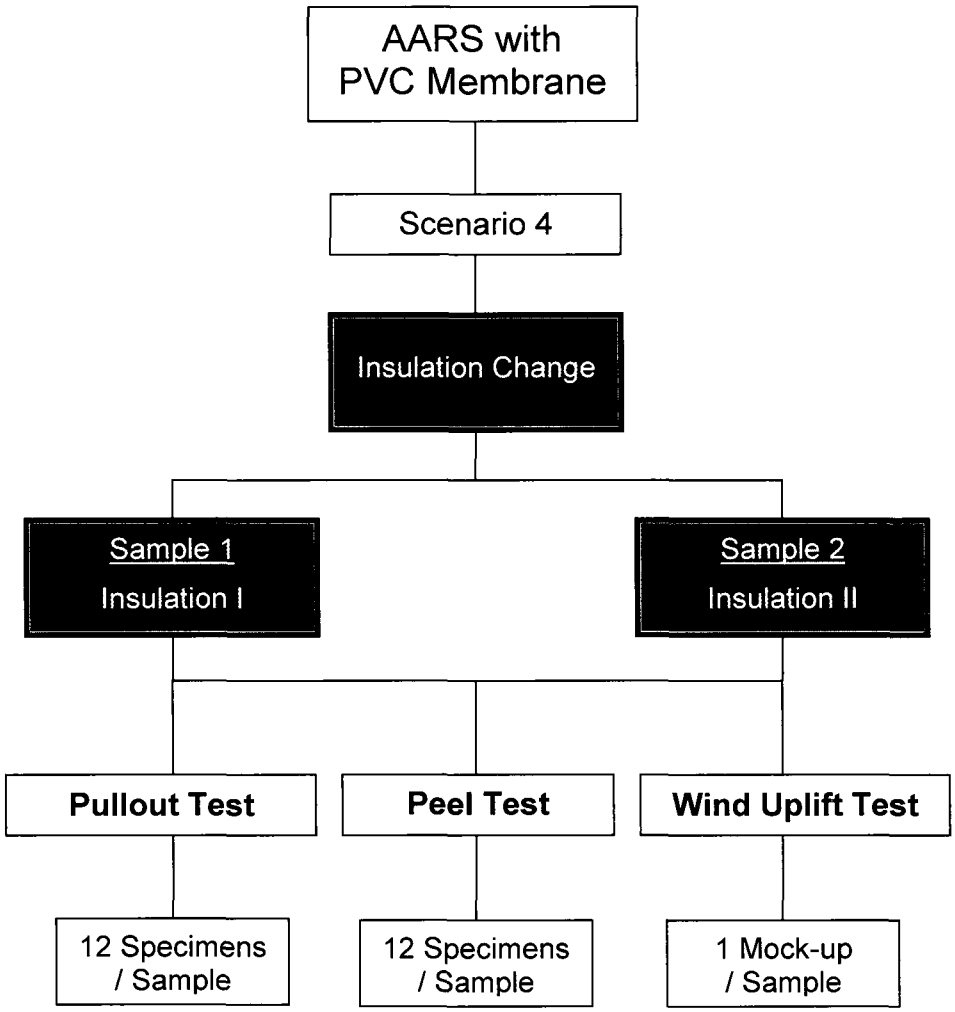

Figure 5.13: Validation for AARS with PVC membrane

5.4.1 Scenario 4 – Insulation Change

1) Experiment Configuration for Scenario 4

The roof configurations for Scenario 4 are much simpler than Scenarios 1, 2 and 3. They are the PVC membrane roofing system which belongs to the single-ply roofing system. The changed component in validation experiments for this set was the insulation. The Paper facer insulation from two different material manufacturers were selected and marked as insulation I and insulation II for the specimen fabrication of Sample 1 and 2, respectively.

The pullout and peel specimens and wind uplift mock-ups of Samples 1 and 2 were constructed by the NRC laboratory technicians according to the PVC roof system criteria. The detailed configurations, cross-sections of Sample 1 and 2 and two kinds of insulations used in Samples 1 and 2 are displayed in Figure 5.14. All the pullout and peel specimens and wind uplift mock-ups were cured under the room temperature with 30% humidity for 7 days according to the fast-dried attribute of the foamy polyurethane adhesive and the PVC bonding adhesive. For the modified bitumen adhesives, a minimum of 28 days is advised for curing in the proposed standard test methods of AARS.

(2) Validation Data Achieved by Scenario 4

The altered component for comparison in this scenario is Polyiso insulation. Specimens of Sample 1 were made with paper facer insulation I, while specimens of Sample 2 were constructed with paper facer insulation II.

The use of foam quick-set professional roof insulation adhesive resulted in much stronger adhesion between the insulation materials and steel deck compared to the modified bitumen cold adhesive. Its expandable foamy nature eliminated the influence of uneven surface of the steel deck. The insulation was adhered to the flutes of steel deck completely and uniformly. There was no adhering skip on the interface of the insulation and steel deck, which promotes the adherence loss.

Sample 1	Sample 2
PVC Membrane *PVC Bonding Adhesive (Full Coat)* **Insulation I** *Foamy polyurethane Insulation adhesive* Steel Deck	PVC Membrane *PVC Bonding Adhesive (Full Coat)* **Insulation II** *Foamy polyurethane Insulation adhesive* Steel Deck
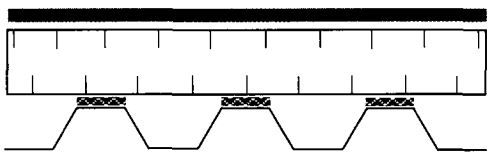	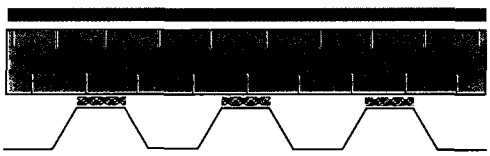
(a) Sample 1 cross-section	*(b) Sample 2 cross-section*
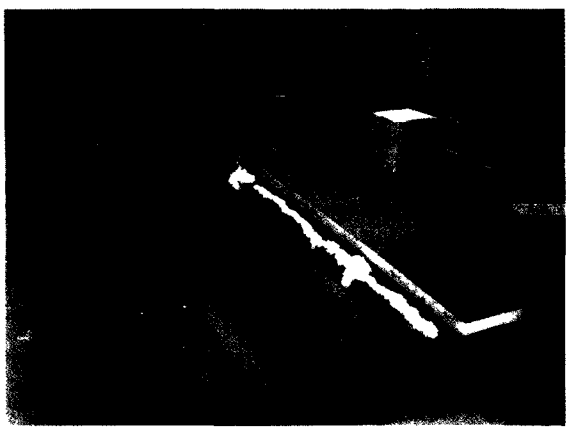	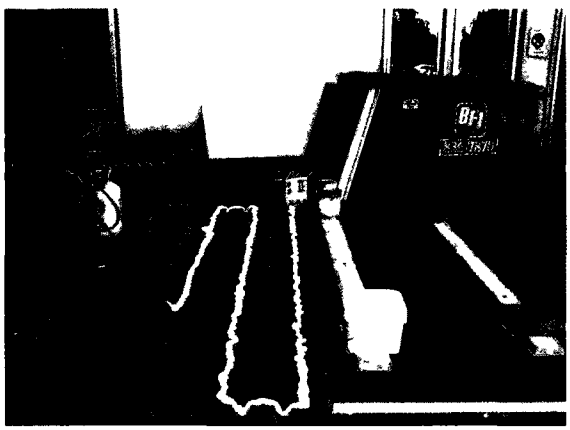
(a) Insulation I used for Sample 1 construction	*(b) Insulation II used for Sample 2 fabrication*

Figure 5.14: Scenario 4 experiment configuration

Resistance	Sample 1 Insulation I	Sample 2 Insulation II
Pullout	578 lbf (2571 N)	1061 lbf (4720 N)
Peel	90 lbf (400 N)	114 lbf (507 N)
Wind uplift	180 psf (8618 Pa) No Failure	180 psf (8618 Pa) No Failure

Table 5 4· Comparison of scenario 4 test results

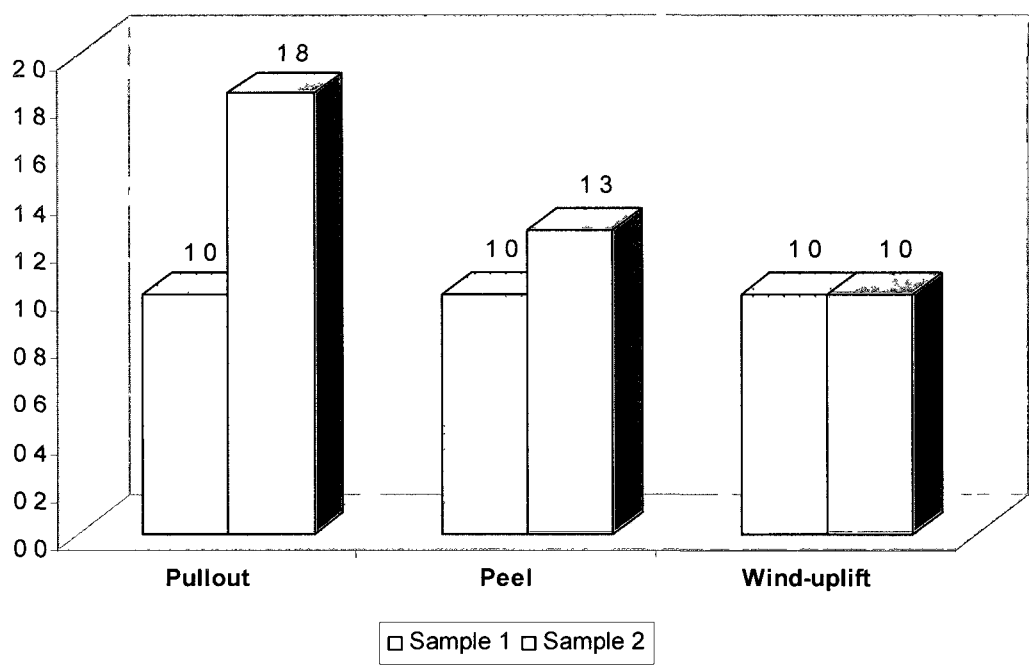

Figure 5.15: Comparison of pullout, peel and wind uplift resistance for Scenario 4

The mean values of each of the pullout, peel and wind uplift resistance of Samples 1 and 2 are presented in Table 5.4. Their variation tendency is displayed in normalized resistance ratio by a column chart in Figure 5.15. It is clear that both pullout and peel resistance of Sample 2 was found higher than those of Sample 1. When the normal paper facer insulation was used for Sample 1, the pullout and peel resistance were found to be 578 lbf (2571 N) and 90 lbf (400 N), respectively. After taking insulation II for Sample 2, the pullout and peel resistance were upgraded to 1061 lbf (4720 N) and 114 lbf (507 N), respectively. The pullout resistance of Sample 2 was almost twice as much compared to that of the pullout resistance of Sample 1 and its peel resistance was also increased by 30%. According to the hypothesis presented earlier, the wind uplift rate of Sample 2 is expected to be higher than that of Sample 1. The test results show that both of them reached the highest rate 180 psf (8618 Pa) that the testing machine could attain. The one component change validation of Scenario 4 by using PVC membrane roofing system also supports the proposed hypothesis and verify that pullout, peel and wind uplift test methods can be applied to examine single-ply roofing system.

(3) Failure Mode of Scenario 4

Failure modes in pullout test

Both Samples 1 and 2 had the same failure mode for pullout tests. PVC bonding adhesive and foamy polyurethane roof insulation adhesive were selected for integrating the three components; namely, the PVC membrane, insulation and steel deck. Their high binding moved the weakest link in pullout to the insulation layer. All the pullout specimens failed by rupture at the insulation facer for both Sample 1 and Sample 2. No failure at the adhesive was observed. Figures 5.16 (a) and (b) show the photos of their failure mode.

Failure modes in peel test

Samples 1 and 2 also showed the same failure mode in the peel tests. The peel resistance of PVC membrane and the cohesion between PVC membrane and

Sample 1	Sample 2
	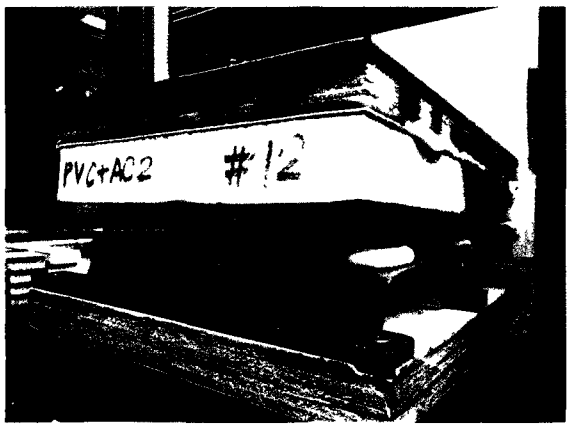
(a) Pullout failure mode: insulation facer rupture	*(b) Pullout failure mode: insulation facer rupture*
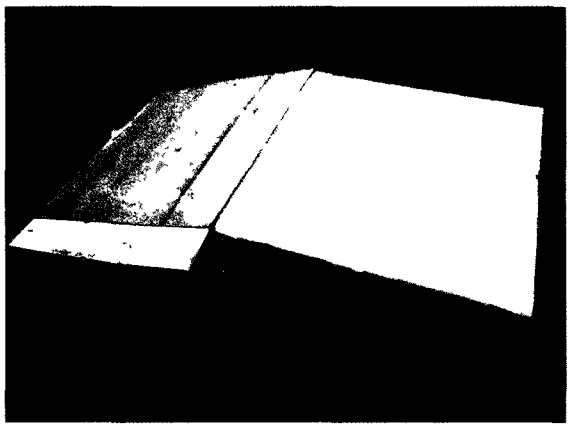	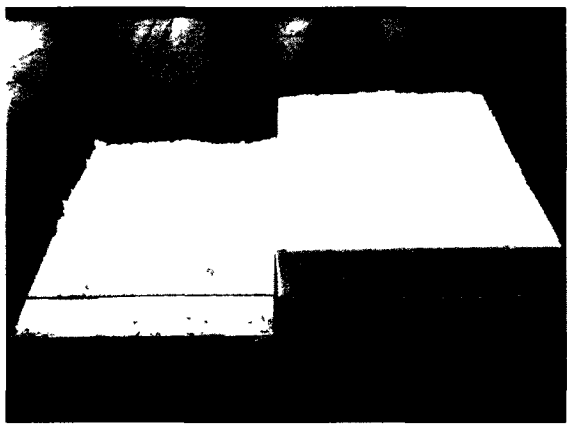
(c) Peel failure mode: insulation facer delaminaiton	*(d) Peel failure mode: insulation facer delaminaiton*

Figure 5.16: Failure mode comparison for Scenario 4

insulation provided by PVC bonding adhesive were stronger than the adhesion between insulation and its facer. Hence, the insulation facer became the weakest link under peeling. All the peel test failures for both Sample 1 and Sample 2 were insulation facer delaminaiton, see Figures 5.16 (c) and (d).

Failure modes in wind uplift test

For dynamic wind uplift tests using full-scale mock-ups, both Samples 1 and 2 passed the maximum attainable rating of 180 psf (8618 Pa) without failure.

5.5 Conclusion

The comparative study in four scenarios was carried out for one component variation of them. The component change of membrane (Scenario 1), cover board (Scenario 3), insulation (Scenario 4) and support board (Scenario 2) were tried. The correlation between the pullout, peel and dynamic wind uplift test results was examined through one component change tests. The results are applicable to both the modified bitumen roofing system and single-ply roofing system.

Experimental data obtained in Scenarios 1 and 4 proved that the proposed hypothesis is acceptable; i.e., *Higher resistance in both peel and pullout tests will result in the same or higher wind uplift resistance*. Test results from Scenario 2, with and without the support board, illustrate that a roof with higher pullout resistance does not necessarily mean a higher peel resistance and better wind uplift rating. Similarly a roof with higher peel resistance does not mean a higher pullout resistance or a better wind uplift rating as it was demonstrated in Scenario 3, the tests with and without dens deck.

It is also proved by the one component variation tests that it is a joint action of shear and tensile forces that leads the AARS roofing to its failure. Once the weakest link fails, the whole roof system fails. Projecting on the test methods, the peel and pullout test methods for small-scale specimens can be used to

evaluate the wind performance of AARS in full-size. The peel test result should be combined with the pullout test result together for predicting the wind performance of AARS. If the small-scale roof specimen exhibits higher resistance in both pullout and peel tests, the roof will result in relatively higher wind uplift rating or maintain at least the same wind uplift rate as the roof before component replacement.

A large number of pullout, peel and wind uplift experiments with various specimen configurations were carried out at the NRCC laboratory. For practical purposes, it is easy to perform the component substitution for AARS roof construction in field by referencing to these accumulated laboratory data. Based on the validated correlation between test results of pullout, peel and wind uplift tests, if the peel and pullout resistance of the roof after component substitution are higher than the roof with original configuration, the roof with new configuration can maintain at least the same, if not higher, wind uplift rate as the original one.

In fact, the dynamic wind uplift test by using the full-scale mock-ups is more expensive and time-consuming. Sometimes it is even not possible to perform such tests because of the facility requirement. The peel and pullout tests by using small-scale specimens are effective alternatives for the prediction of the roofing system behaviour under wind action. It is particularly useful for the assessment of AARS wind uplift performance of a roof already in existence or in service.

Chapter 6: Design and Functionality of a Portable Tester

6.1 Introduction

By using an Instron 5566 electromechanical testing machine, the pullout and peel test methods of AARS have been established and submitted to a standard development organization, e.g. ASTM. The pullout and peel resistance of AARS specimens were found out, and the failure modes were identified for various configurations. The Instron testing machine can measure a wide range of mechanical properties including the tensile, compressive and shear properties, as well as flexural, creep-relaxation and other properties. It is an equipment suitable to well prepared laboratories.

The participating industrial partners of this research project agreed that development of a portable tester would be of great benefit to the roofing industry. After the development and validation with the existing laboratory experimental data, they can also make use of the device in the field. With a tool to evaluate actual response of the system in the field, the influence of design alteration, for example, as well as the impact of environmental conditions such as the relative humidity and temperature can be easily evaluated in the field. Also, it is possible to use the portable tester in the field for a quick and handy way to evaluate the quality control of roof constructions.

This chapter presents the design and fabrication of a portable tester and its achievement in testing functions. Section 6.2 provides the design specification of the portable tester. Section 6.3 illustrates the working principle of the portable tester. Section 6.4 addresses the design and fabrication of the tester attachment for performing the peel test. Section 6.5 examines the functionality of the fabricated portable tester by testing the resistance of roofing fasteners against pulling (ANSI/SPRI FX-1-2006). Section 6.6 and Section 6.7 present the

experimental setup for the pullout and peel tests of the portable tester, respectively. The functionality of the developed tester is summarized in Section 6.8.

6.2 Design Specification of Portable Tester

The portable tester was designed to carry out the pullout and peel tests at the construction site in accordance with the standard pullout and peel test methods developed by Current (2009) and Wu (2008). The portable tester must be deployable in the field and give the reasonable test results and proper failure modes. By referencing the experimental data for the AARS obtained earlier on the Instron machine, the tester should meet the following requirements:

(1) The tension speed must be constant and independent of the magnitude of loading;
(2) The tension speed is expected to be in the range of 0.25 to 1.00 in/min, or 6.35 to 25.4 mm/min;
(3) The speed tolerance should not exceed ± 5% of the set speed to ensure the stability of loading;
(4) The applied pulling force should not be less than 900 lbf, or 4003 N;
(5) The travel length in pulling test is no less than 3 in, or 76.2 mm; and
(6) The data storage of loading history must be in digital format and compatible with the *Excel* application.

6.3 Working Principle of Portable Tester

The photo of the tester which was manufactured by SAI Design Inc. according to the specification is shown in Figure 6.1 with indication of the parts. It is made of high strength steel. A flat portal frame with a testing platform composes the main structure of the tester. A motor connecting with a gear screw jack is mounted on the cross-girder of the frame. A thread shaft inside the screw jack sleeve, or housing, is named lifting screw and links up with one end of the load cell through

an adapting connector. When the motor spindle rotates clockwise or counter-clockwise with constant speed, it drives the lifting screw moving upward or downward smoothly at certain speed. In other words, the motor provides a rotary motion, and the screw jack converts it into a linear movement. By using suitable positioning controller system and computer software, the prescribed loading speed can be achieved independent of the loading magnitude. By connecting the load cell to the signal conditioning equipment, the load cell outputs are digitalized and saved in the dedicated computer. The work flow chart of the portable tester is given in Figure 6.2. When the direction of the pulling force is changed by an angle controller, the peel test function can be given, which is shown by a dash line in Figure 6.2. How the portable tester implements the speed control and data storage is described in Appendix 3 in detail.

Figure 6.3 demonstrates a 12 in x 18 in (305 mm x 457 mm) pullout specimen of AARS, which is set up properly on the testing platform and connected with the load cell through a set of connectors. If setting is for the lifting screw shaft to move upward at the speed of 0.25 in/min (6.35 mm/min), the installed specimen on the platform linked with the load cell will be in the status of the standard pullout test.

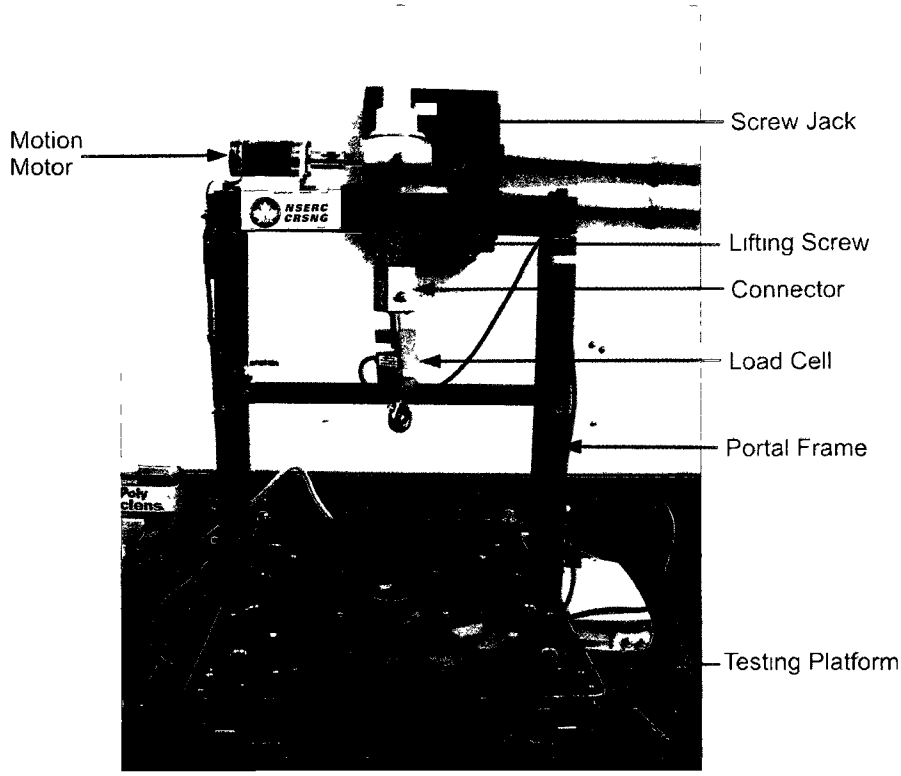

Figure 6.1: Components of the portable tester

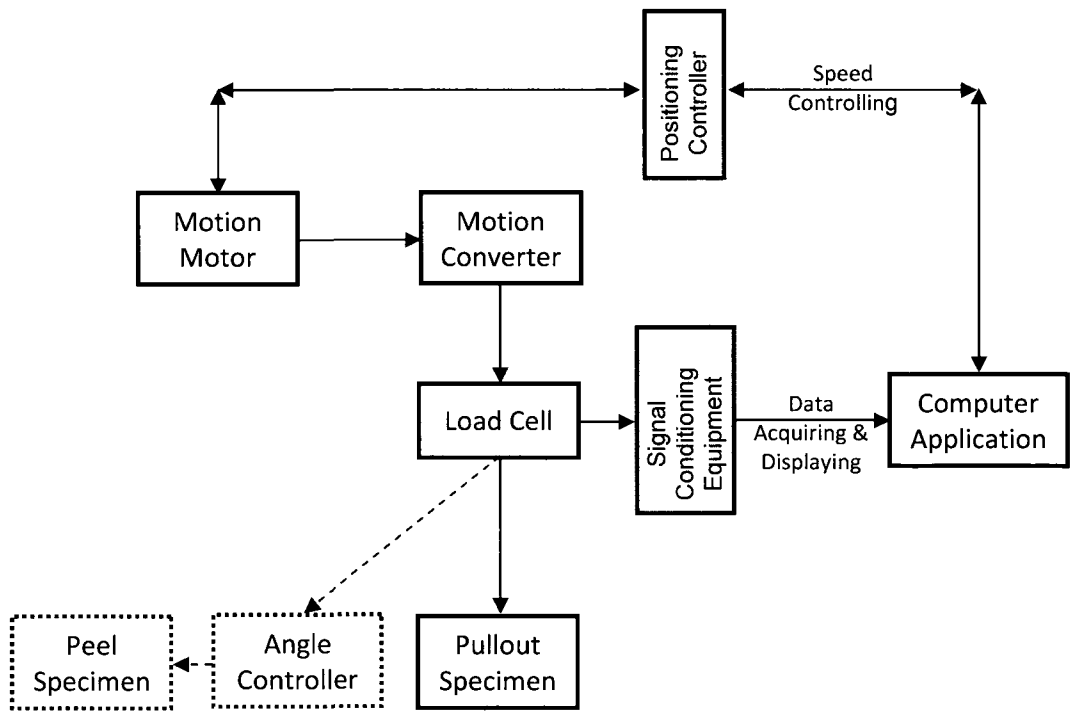

Figure 6.2: Workflow diagram of portable tester

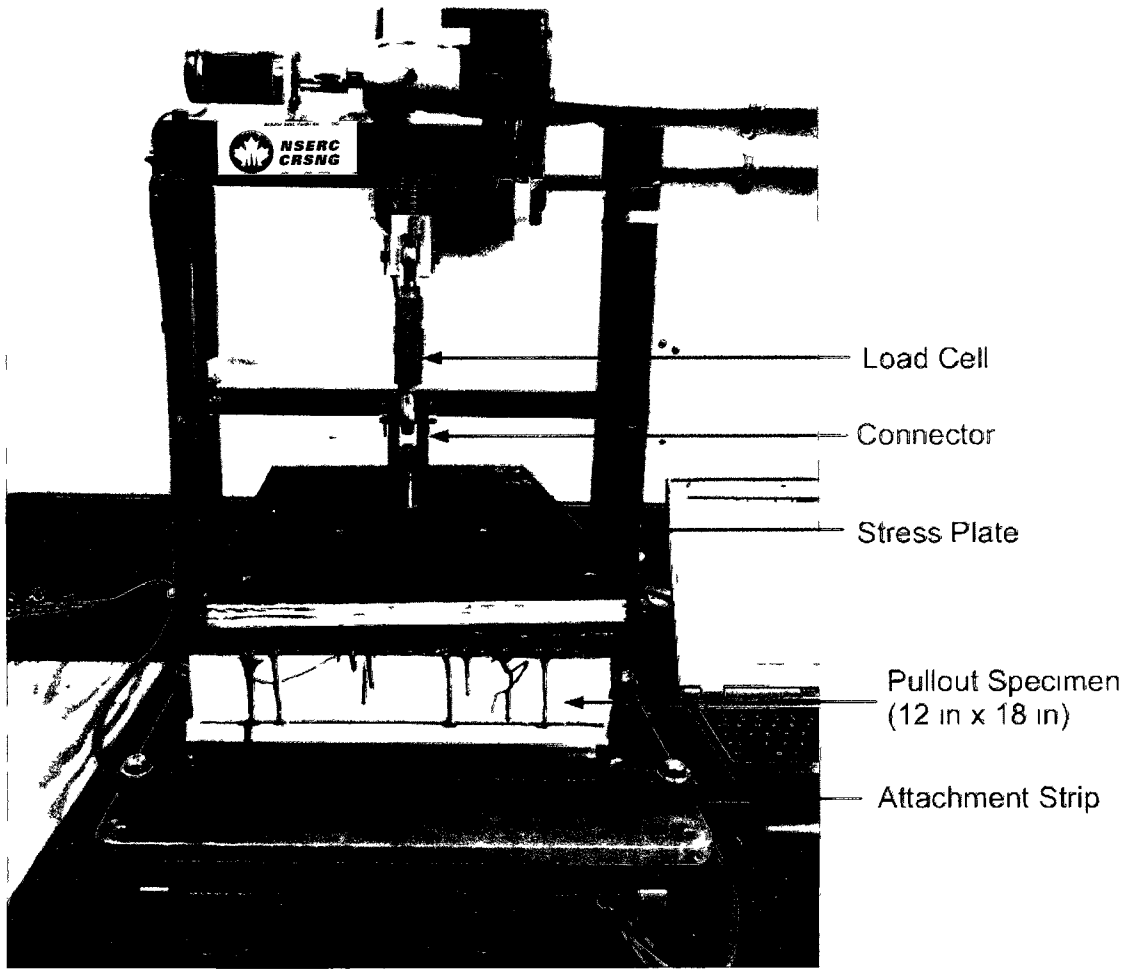

Figure 6.3. AARS specimen set up on portable tester

6.4 Peeling Attachment Design and Fabrication

Similar to the Instron machine, by means of altering the pulling direction, a pullout test can be converted to a peel test. In addition to the specimen fixer mentioned in Chapter 4, a suitable angle controller for the potable tester is required to realize the peel test function.

The design drawings of an angle controller which was specific for the portable tester were generated as in (a), (b), (c) of Figure 6.4. The angle controller can be installed on the platform of the portable tester with four pieces of bolts in 3/8 in (9.5 mm) diameter. The base plate of the angle controller was designed in the same length as the platform of the portable tester. The stranded wire, of which one end is firmly fixed to the load cell, passes through the wheel rim and then links up with gripped specimen at the other end. The 2 in (50.8 mm) diameter wheel works as a direction guide transmitting the drag force to the specimen. There is a 4 in (101.6 mm) long slot carved on the 3/8 in (9.5 mm) thick upright steel plate that provides adequate range for adjusting the desired peeling angle by relocating the wheel along it. The rod end of the load cell and the center of base plate are in the same vertical axis. It is worth noting that, the vertical axis of the wheel has a radius distance from this axis, see drawing (b). The purpose is to ensure the vertical axis of the load cell and the contact point at the wheel inner edge are on the same line, so that the stranded wire in-between can move vertically. The ultimate objective of this is to prevent the side force application on the load cell which can easily damage it.

To keep the peeling angle stable during loading, the wheel should be securely fixed to against any movement caused by a minimum 900 lbf (4003 N) force transferred from the steel stranded wire. Two threaded bars in ¼ in (6.35 mm) diameter are set up side by side shoring the wheel spindle.

The angle controller for peel testing was fabricated in the Processing Workshop of the University of Ottawa, as shown in Figures 6.5 (a), (b). On the evidence of

a trial test with an AARS specimen, it was proved to work effectively. There was no displacement, deformation and bending observed at all for the attachment parts during the peel tests.

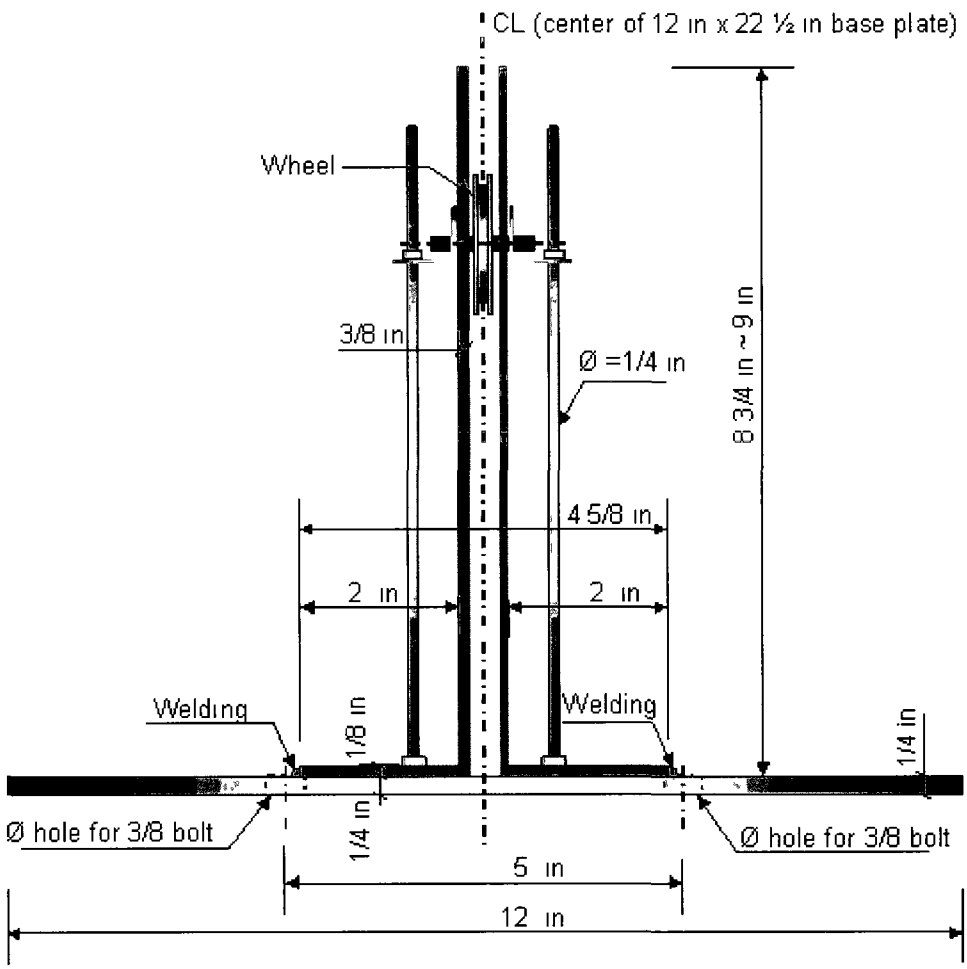

(a) Front view

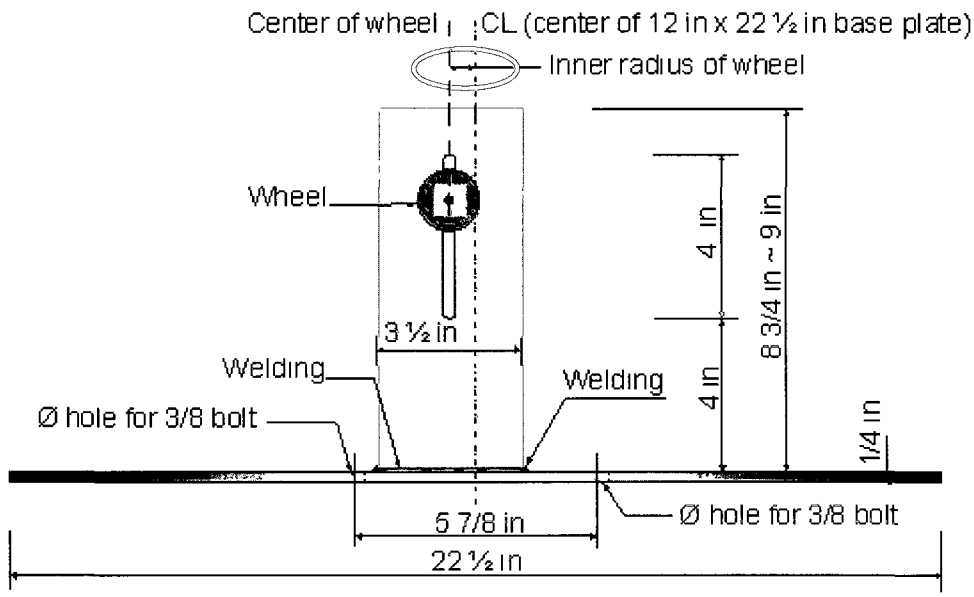

(b) Cross Section

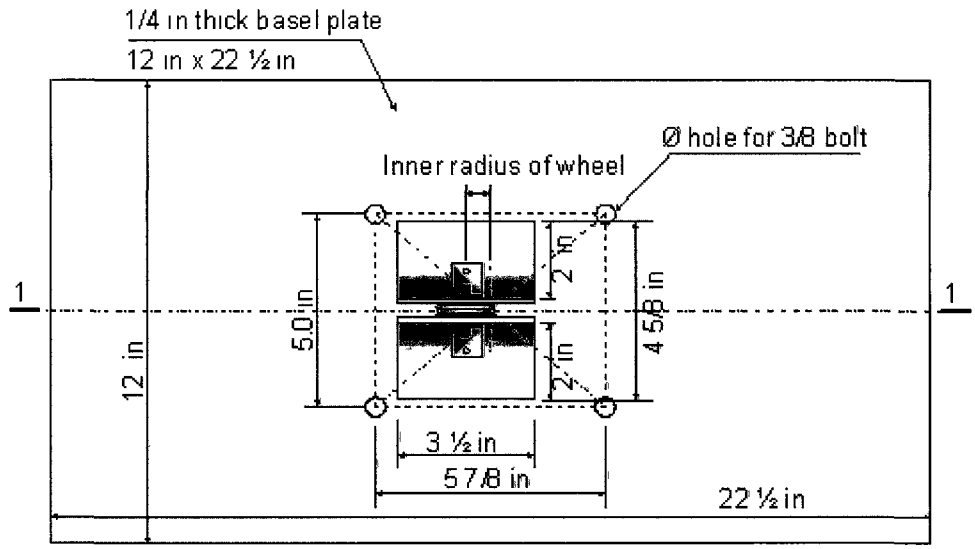

(c) Plan View

Figure 6.4: Design drawings of peel attachment for portable tester

(Note: 1 in = 25.4 mm)

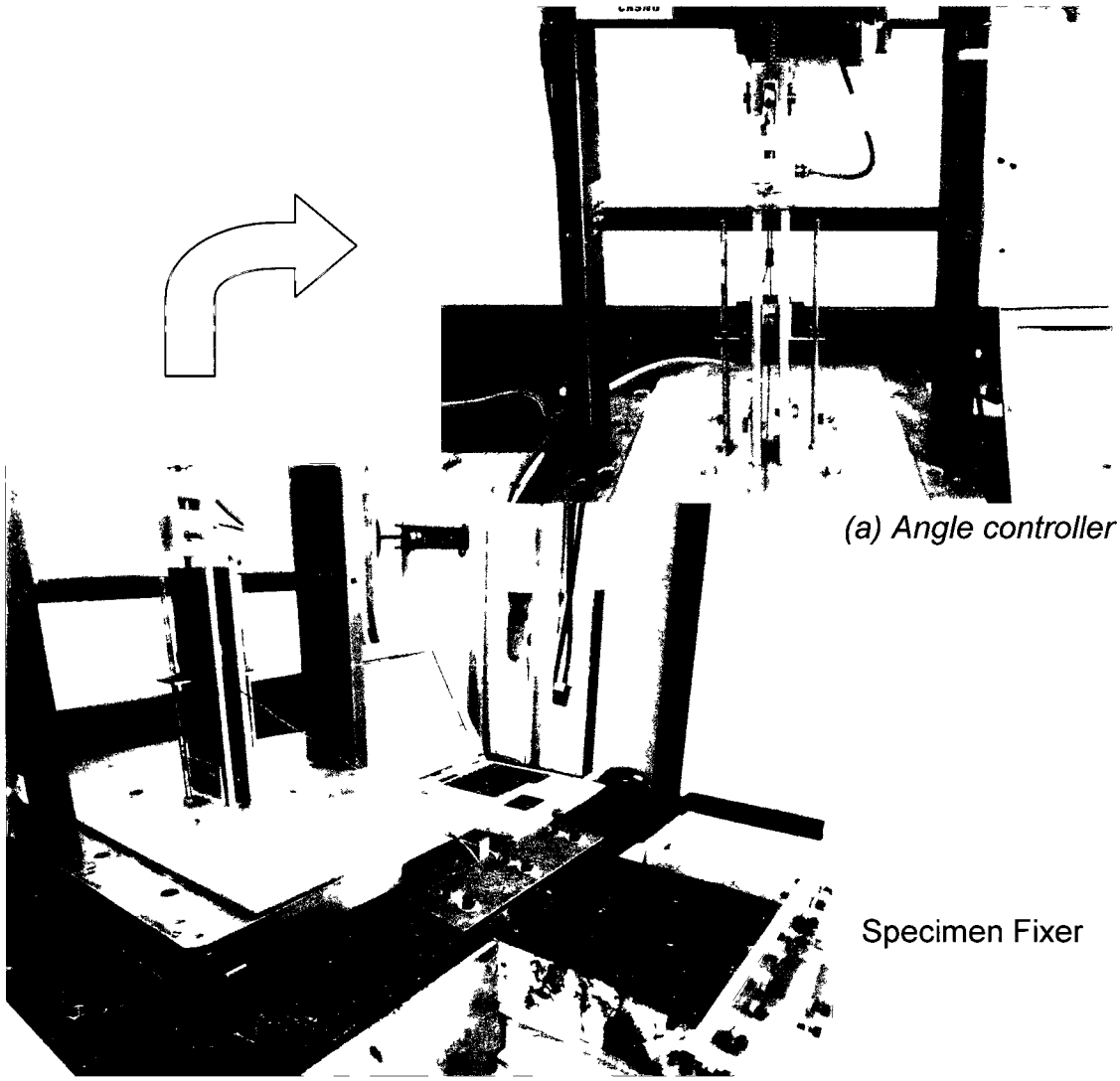

Figure 6 5: Photo of peel test attachment

6.5 Functionality of the Portable Tester

To verify the functionality of the portable tester, a simplified tensile loading experiment was conducted. In this experiment, the resistance of a fastener engaged in a steel deck was determined. Six specimens were tested using both the Instron apparatus and portable tester. Specification of the testing followed the *"Standard Test Procedure for Determining the Withdrawal Resistance of Roofing Fasteners, ANSI/SPRI FX – 1 – 2006"*, (SPRI, 2006). The original aim of the standard was to measure the pullout resistance of roofing fasteners in field conditions that the roofing contractor can use it to evaluate a fastener's pullout resistance with a steel deck's holding strength. This standard test method is widely used on most roofs where the mechanical fasteners are applied. The structure of the fastener-steel deck is simple and clear and the testing specimens are easy to be prepared.

6.5.1 Overall Experiment Setup

The preparation of the roof fastener-steel deck specimen is shown in Figure 6.6 (a). A 3 in (76 mm) long #15-S2 fastener was drilled into a piece of 22 Gage - 80 ksi (550 MPa) Steel Deck in size of 7.5 in x 12 in (191 mm x 305 mm). The penetration length of a fastener, the part that extends beyond the underside of the steel deck is about ¾ to 1 in (19 to 25 mm). The specimen was installed on the testing platform of the Instron machine and portable tester, respectively; and fixed with the attachment strips with bolts and nuts, as shown in Figures 6.6 (b) and (c). The testing rate is set as 0.25 in/min (6.35 mm/min) which is required in the AARS standard pullout test method developed by Current (2009).

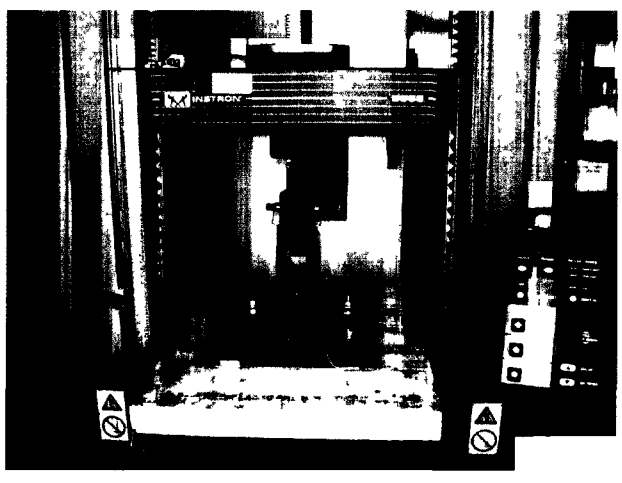

(b) Tested on Instron machine

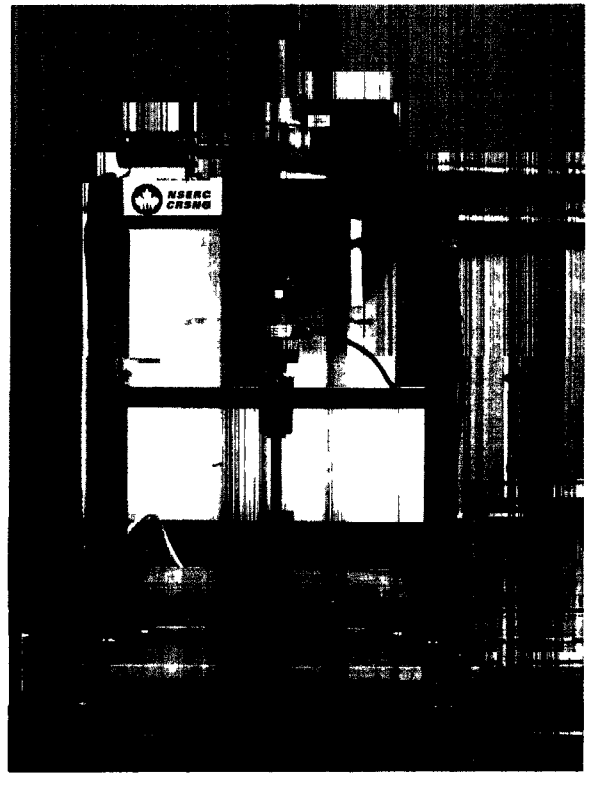

(c) Tested on portable tester

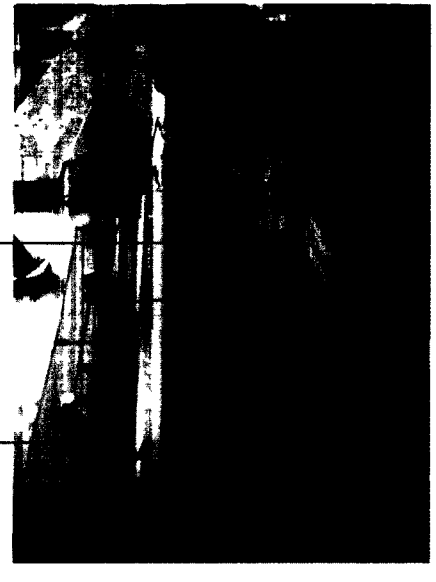

(a) Drilling the fastener into steel deck at the center of the specimen

Figure 6.6: Pullout test for roof fastener-steel deck sample

6.5.2 Data Analysis

Six fastener-steel deck specimens for each test at the Instron machine and portable tester were fabricated and tested. Figure 6.7 is the load-extension diagram to indicate the test results of a specimen which was carried out on the portable tester. The peak load is 714 lbf (3.18 kN). Six loading curves were redrawn in one chart by using the stored raw data and shown in Figure 6.8 (a). Their similar shapes express the repeatability of performance of the portable tester. Comparing them to the load-extension diagrams obtained from the Instron machine, which are displayed in Figure 6.8 (b), they show strong resemblance to each other. Table 6.1 is the data analysis for the two testers. It shows that the difference at maximum, minimum and mean load is merely 0.25%, 3.52% and 0.82% between the two machines.

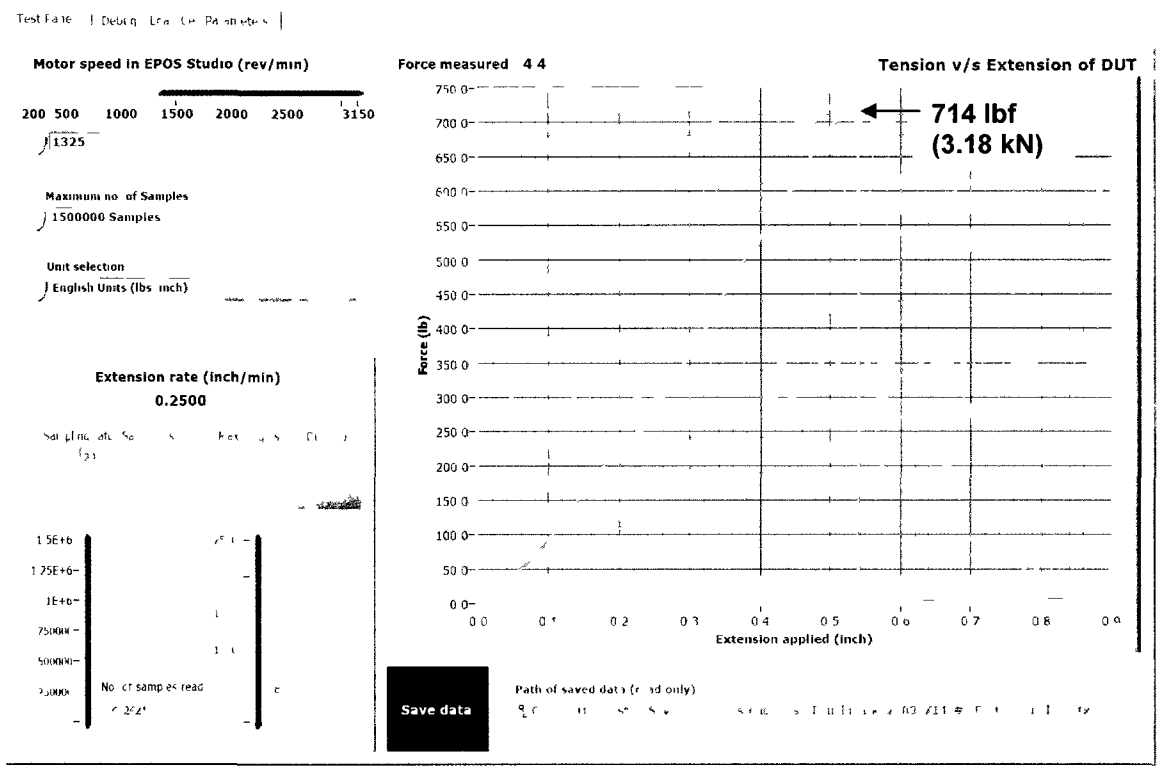

Figure 6.7: A load-extension diagram produced by portable tester

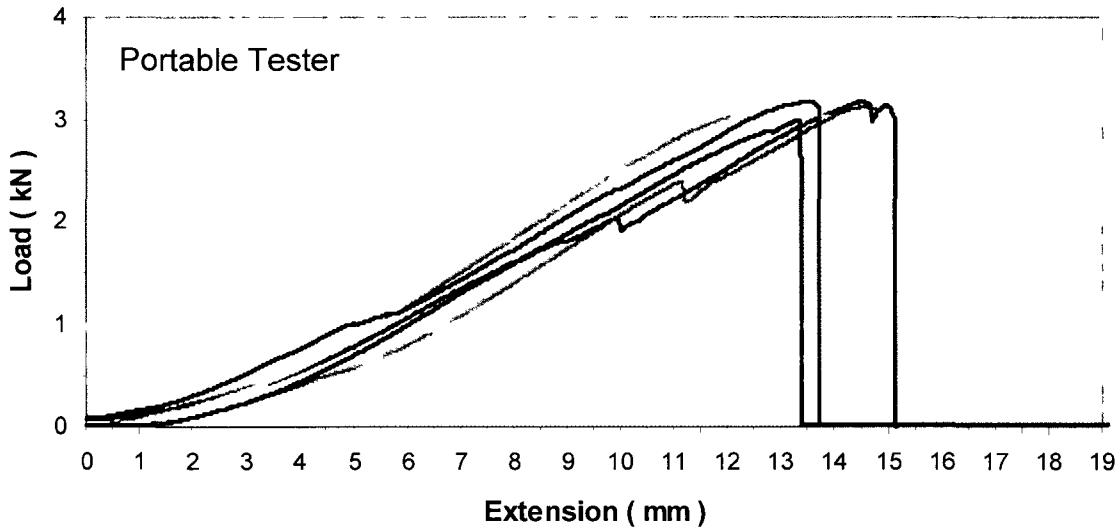

(a) By using portable tester

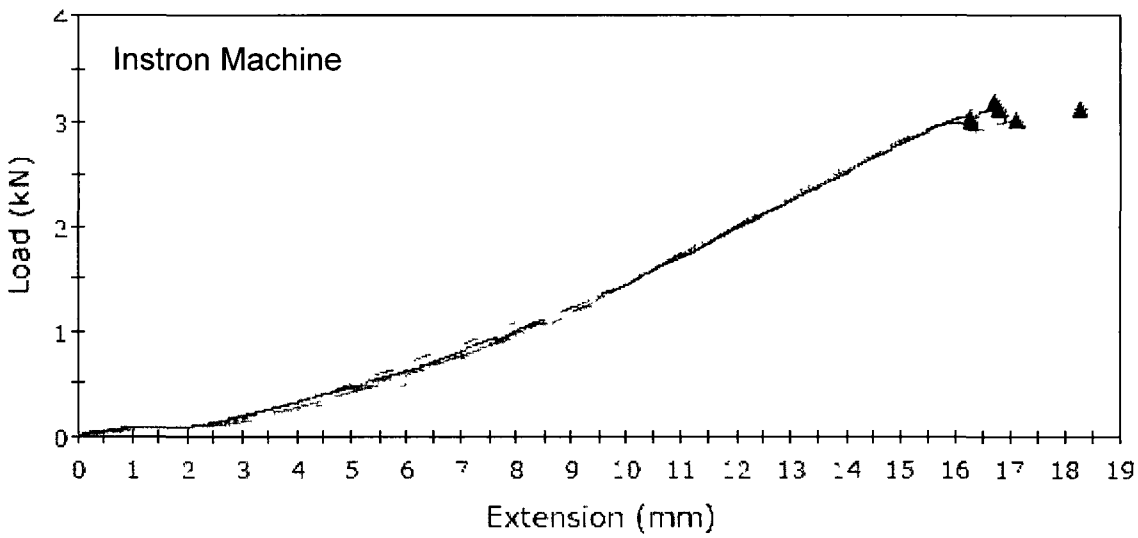

(b) By using Instron Machine

Figure 6.8: Comparison of the load-extension diagram

Table 6.1: Testing data comparison between two testers

	Portable Tester	Instron Machine
Testing Rate	0.25 in/min (6.35 mm/min)	0.25 in/min (6.35 mm/min)
#15 Fastener Length	3 in (76 mm)	3 in (76 mm)
Steel Deck	22 Ga – 80 ksi (550MPa)	22 Ga – 80 ksi (550MPa)
Testing Date	2009-07-14	2009-04-03
Total Specimens	6	6
Maximum Load	714 lbf (3.18 kN)	716 lbf (3.18 kN)
Minimum Load	672 lbf (2.99 kN)	675 lbf (3.00 kN)
Mean Load	695 lbf (3.09 kN)	692 lbf (3.08 kN)
Standard Deviation	15 (0.07)	16 (0.07)

6.6 Pullout Test with AARS Specimen

In the following sub-sections, the procedure to install a pullout specimen on the portable tester is illustrated and the preliminary pullout test function is addressed by using the AARS pullout specimen.

6.6.1 Experimental Setup for Pullout Test with AARS Specimen

Step 1:

First, the specimen is placed on the testing platform and four steel clamp strips are set on the female flutes of the specimen, see Figure 6.9 (a). The specimen and strips are arranged in such a way so that the slotted holes at the end of the strips are aligned with eight bolt holes on the testing platform. Eight ¾" (19 mm) bolts are then screwed in without tightening.

Step 2:

A ¾" (19 mm) thick steel stress plate is put on top of the specimen and a suitable screw rod and the connector are installed to ensure that the travelling distance of the lifting screw is less than 3 inches. The load cell is lowered down and connected to the stress plate by pin-connection, while the position of the stress plate is being adjusted, see Figures 6.9 (b) and (c). The load cell should stay in vertical position with no bending.

Step 3:

The stress plate is jogged upward until it loses its contact with the specimen. The stress plate will be suspended horizontally over the specimen. The specimen is then aligned to the stress plate as exactly as possible, see Figure 6.9 (d). This step is to make sure that the centreline of the stress plate aligns with the centre of the specimen so that uplift load can be transmitted to the specimen vertically and uniformly and reduces the risk of damage caused by the eccentricity of the load. For the same reason, the connecting pin is placed in the lateral direction.

Step 4:

The stress plate is jogged down until it sits directly on top of the specimen. The pin is to be removed from the connector. A cordless driver is used to fasten down ten #10 1" Robertson head wood screws to secure the stress plate to the specimen, see Figure 6.9 (e). The eight of 3/8 in bolts are tightened up to fix the four clamp strips. Then the pin is installed again, re-attaching the specimen to the load cell, see Figure 6.9 (f). It may be needed to jog down the load cell slightly because of the extra compression caused by fastening of screws.

6.6.2 Data Analysis for Pullout Test with AARS Specimen

A trial test for AARS pullout specimen was conducted on the portable tester. The specimen was the one left from the previous one component variation experiments referred to in Chapter 5. The load-extension diagram is displayed in Figure 6.10 (a). A typical load-extension diagram for the previous experiment is presented in Figure 6.10 (b). Basically, they present the same results.

The peak load of the tested specimen was 792 lbf (3.52 kN). It is in the same range as indicated by the former test results from the six specimens, performed on the Instron machine, which were in the range of 617 to 803 lbf (2.74 to 3.57 kN).

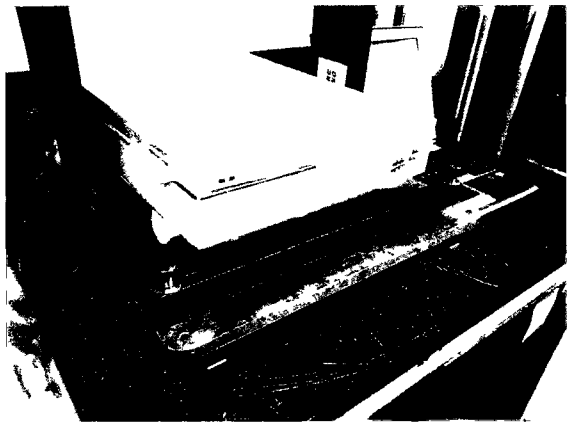

(a) Installation of specimen and attachment strips with alignment check

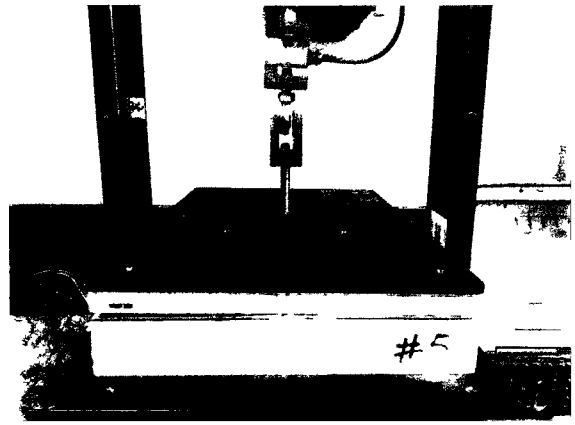

(b) Placement and arrangement of stress plate with screw rod and connector

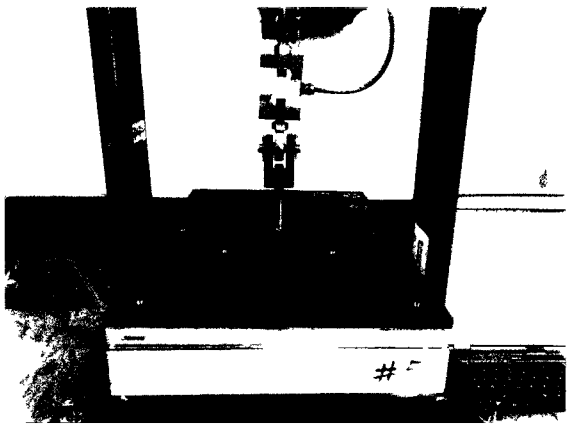

(c) Connecting stress plate with load cell via pin-connection

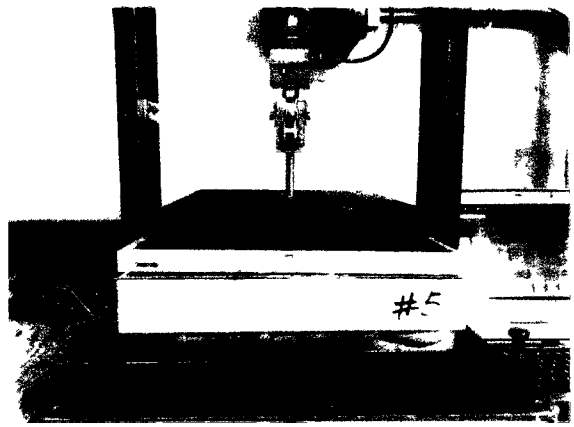

(d) Aligning specimen to the hanging stress plate vertically

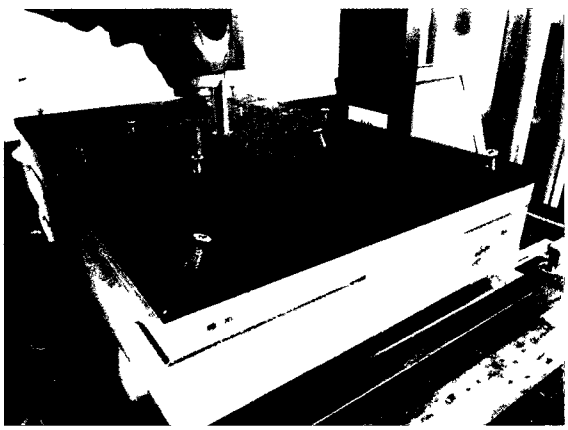

(e) Attaching stress plate to plywood dummy of specimen

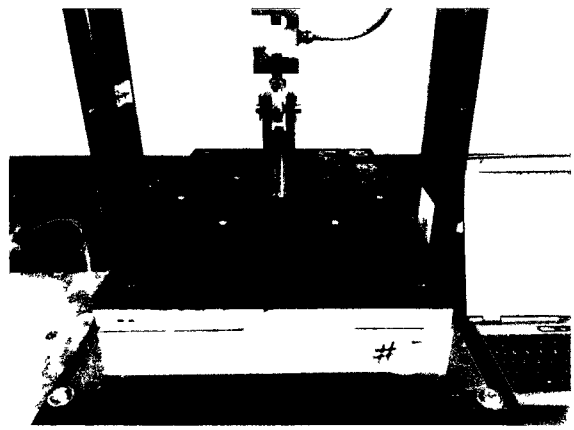

(f) Reinstalling pin and tightening up bolts to secure specimen for testing

Figure 6 9· Steps involved in the pullout experiment setup – Portable Tester

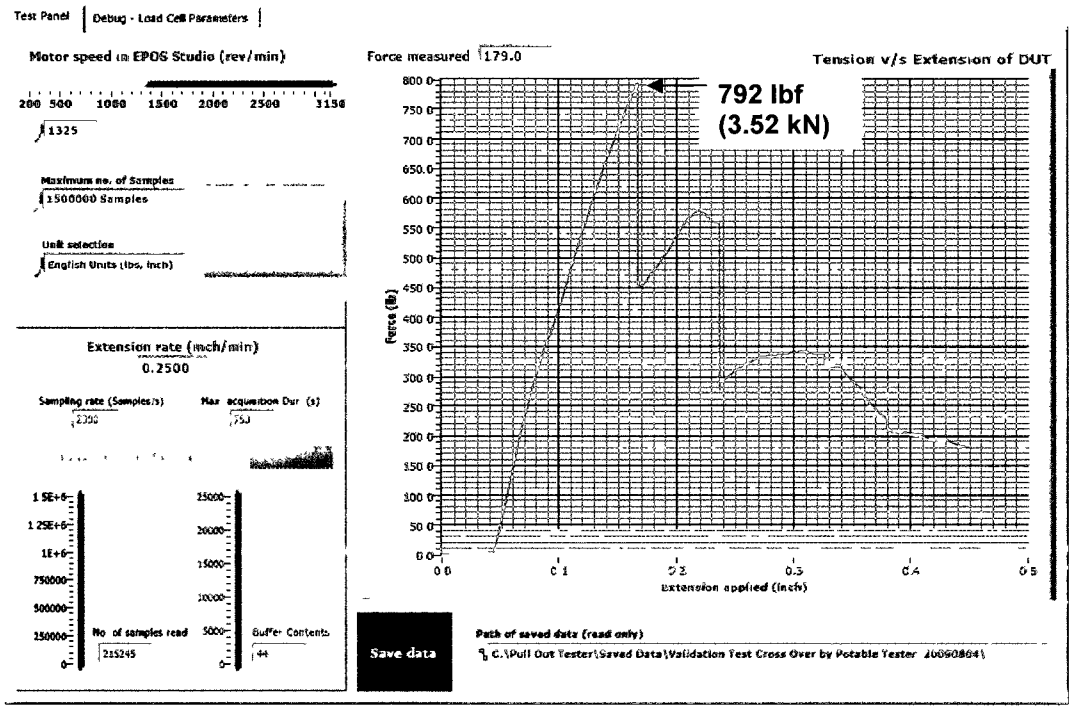

(a) The load-extension diagram produced by portable tester

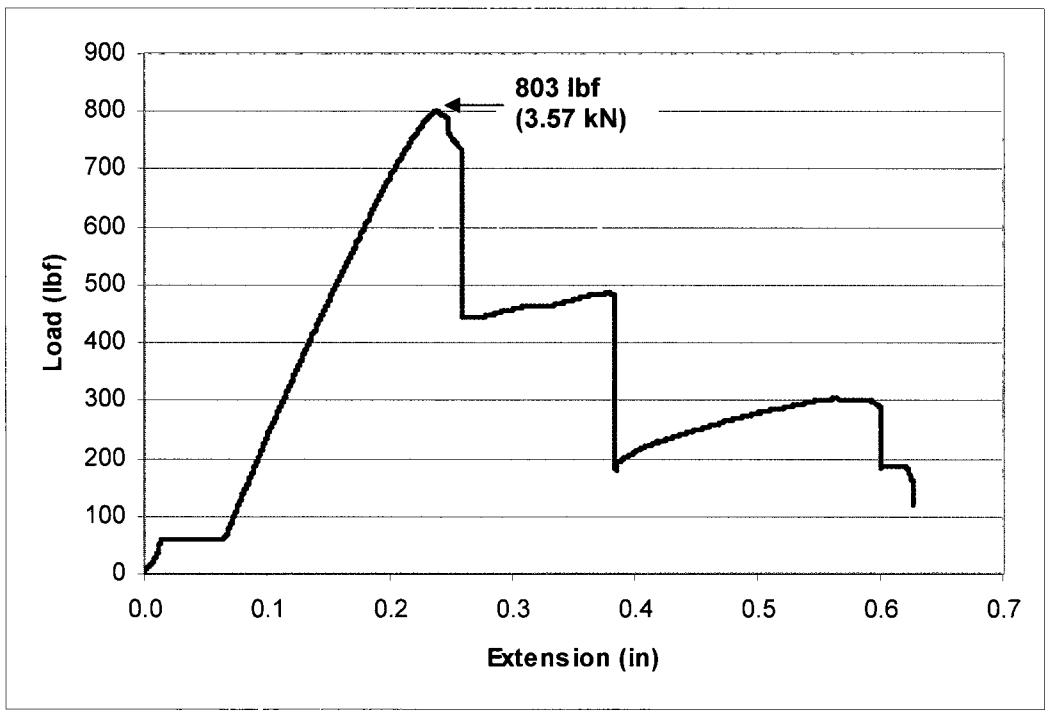

(b) A typical diagram obtained from Instron machine

Figure 6.10: The load-extension diagram of pullout test

6.7 Peel Test with AARS Specimen

An initial trial peel test on the portable tester was also performed by using the AARS peel specimen, which was left from the previous one component variation experiments. In the following sub-sections, the experimental setup for peel test on the portable tester is illustrated first, followed by the test results.

6.7.1 Experiment Setup for Peel Test with AARS Specimen

Step 1:

The peeling attachment is to be placed in the middle of the testing platform of the portable tester, while the alignment of the center of the base plate with the load cell is ensured. It is then fixed by using 4 - 3/8 in bolts, see Figure 6.11 (a).

Step 2:

The grip wire is linked with the load cell along with the wheel, see Figure 6.11 (b). It is important to double check and confirm that the upper part of the wire, which is between the load cell and wheel, is in vertical position so that there would be no side force applied to the load cell during the peel test.

Step 3:

The peel specimen fixer is combined with the portable tester and aligned its centerline with the wheel center. The peel specimen is to be held tightly in the middle of the fixer. The overhang edge is held by using the grip which is linked to the load cell. The grip's position is adjusted to keep the specimen and the center of the wheel in a straight line, see Figure 6.11 (c).

Step 4:

The wire is to be made straight by jogging the load cell upward to examine the wire angle with respect to the horizontal line. By adjusting the height of the wheel, the peel angle can be changed. Once the peel angle is set to 15 degrees, the specimen is ready for the standard peel test, see Figure 6.11 (d).

6.7.2 Data Analysis for Peel Test with AARS Specimen

The graphic output of the specimen tested by using the portable tester and Instron machine are shown in Figures 6.12 and 6.13, respectively. The specimen configuration belongs to Sample 2 of Scenario 1 of the previously performed one component variation test. Figure 6.12 is the load-extension diagram, which was produced by the portable tester. By making use of the stored raw data from the portable tester, the Excel presentation in load-time relationship is displayed in Figure 6.13 (a).

The loading curve shown in Figure 6.12 does not start from the origin of the coordinate system. This is caused by the preloading by the grip when the peeling angle of 15 degrees was set. The Instron machine, on the other hand, has the function to bring the record back to the origin before actual loading starts. As to the portable tester, the preloading offset needs to be manually eliminated when the output data are analyzed, see Figure 6.13 (a). A typical loading diagram obtained from the previous test on the Instron machine is also displayed in Figure 6.13 (b) for comparison.

Overall, they produce very similar test results indicating the peak loads close to each other. However, the time for testing by the portable tester is shorter than that required for the Instron machine. The maximum load of the tested specimen obtained from the portable tester was 192 lbf (0.85 kN). It is within the range of the previous test results out of 6 specimens obtained from the Instron machine, which were in the range of 191 to 202 lbf (0.85 to 0.90 kN).

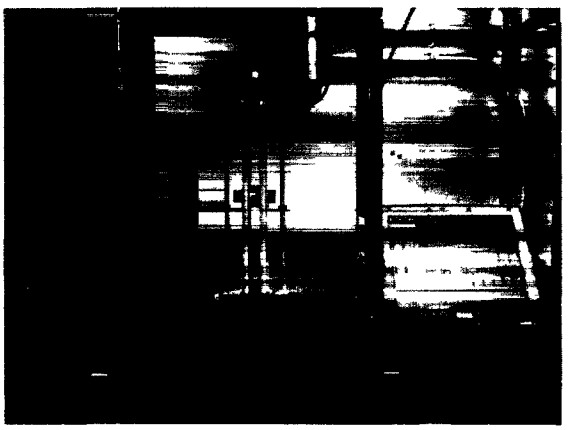

(a) Mounting peel attachment on testing platform

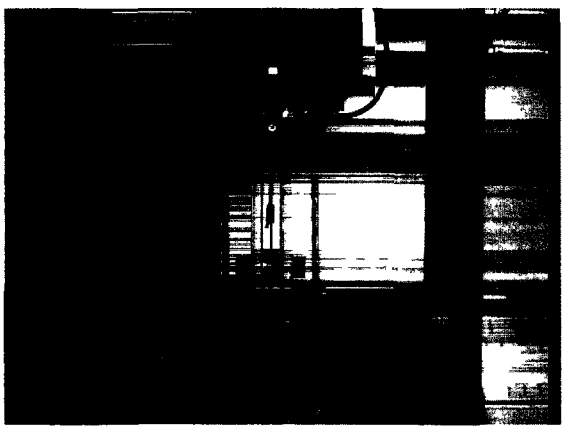

(b) Installing griper stranded wire

(c) Gripping specimen and aligning with the load cell

(d) Adjusting peel angle to 15°

Figure 6.11: Procedure of peel experiment setup

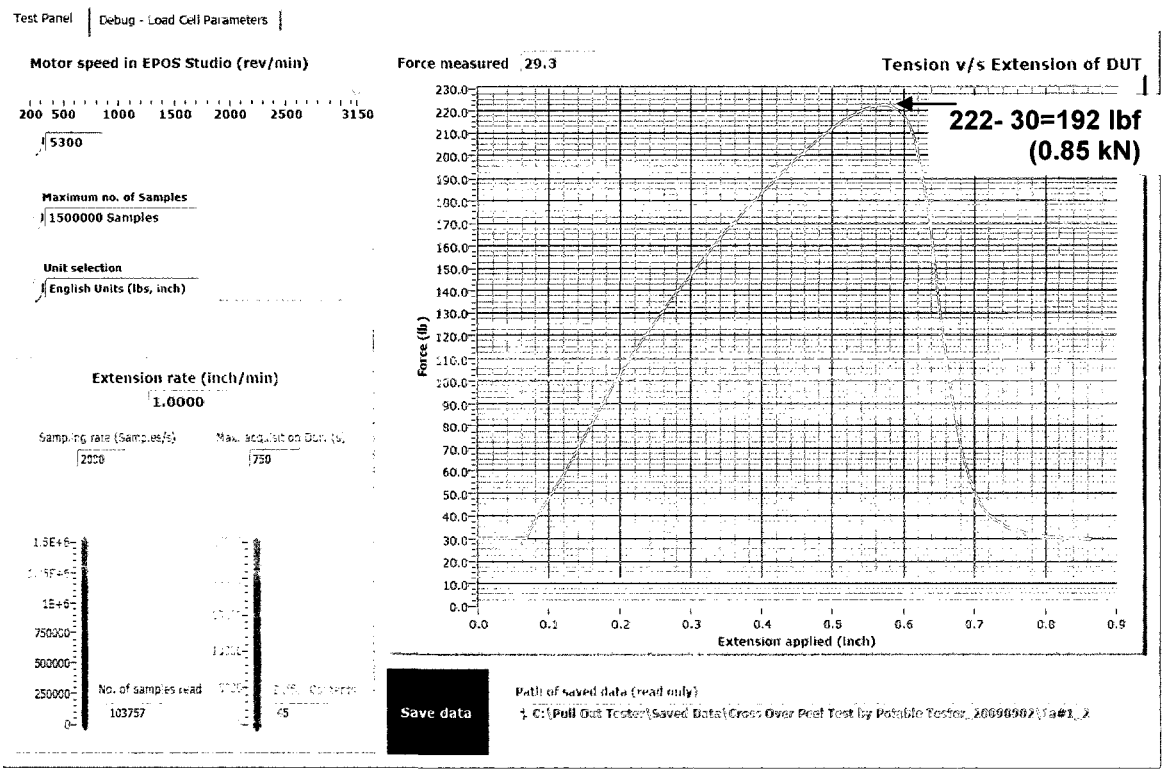

Figure 6.12: The load-extension diagram produced by portable tester

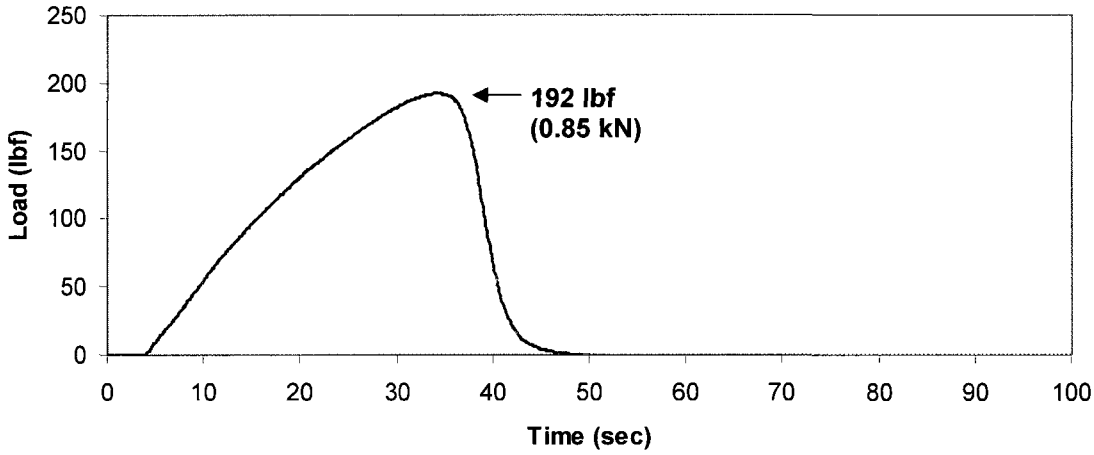

(a) Time history of loading diagram obtained from portable tester

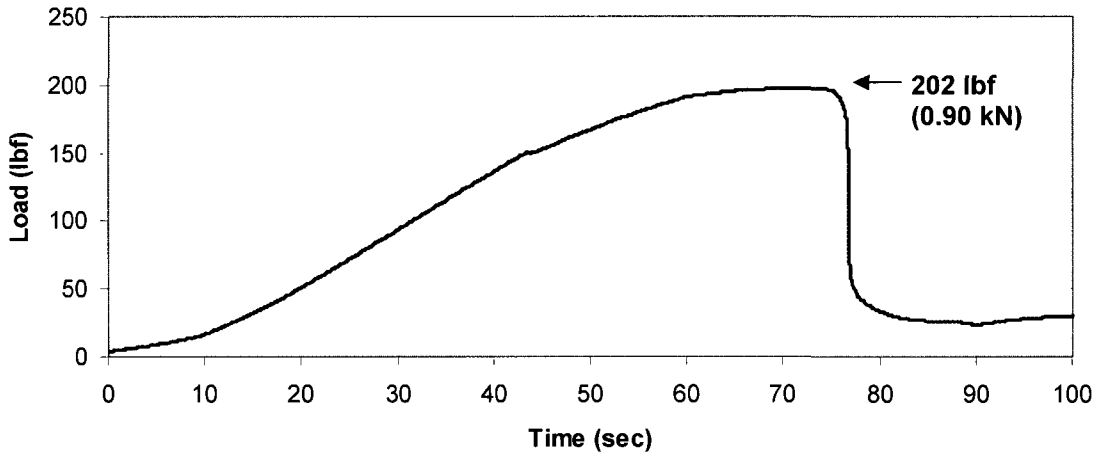

(b) A typical diagram obtained from Instron machine

Figure 6.13: Comparison of the time history of loading diagram

6.8 Summary

Based on the above analysis, the test results of the roof fastener-steel deck samples obtained from the portable tester and Instron machine are in good agreement. It provides the strong evidence that the properly designed and fabricated portable tester meets the objectives. The tester has the ability to provide a constant pulling speed during the test and record the test data, which basically satisfy the design requirements. The two trial tests for pullout and peel by using the AARS specimens also indicated that the portable tester renders the maximum load and gives the proper load-extension curves with reasonable accuracy compared to the previously obtained experimental results.

To further verify the pullout and peeling performance and ensure that the portable tester gives the reasonable and reliable results for AARS, the experimental comparison between the portable tester and Instron machine by using the AARS specimens was carried out. The experimental setup of the portable tester for pullout and peel tests presented in this Chapter is to be applied to the next step of experiments. Various conditions for specimens such as design configurations, materials and curing time were considered. The verifying results and analyses for comparison of the applied load and failure mode are presented in the following chapter.

Chapter 7: Benchmarking Portable Tester Performance

7.1 Introduction

Preliminary results of the benchmark experiment of pullout and peel tests indicated that the developed portable tester was fully operational. Testing of a large number of real roof samples of AARS immediately followed for further verifying the effectiveness and precision of the portable tester. Both peel and pullout tests were performed on the portable tester and Instron machine by using identical test specimens for direct comparison. All specimens were constructed under conditions as similar as possible and cured for the same period at the same room temperature.

The pullout performance of the portable tester was examined by using three different samples and the peel performance was examined by using five different samples. Their verifying processes are presented in Section 7.2 and Section 7.3, respectively. In total, over 200 specimens were constructed and tested. In their respective sub-sections, the detailed experimental configurations and conditions of these samples are described first. Then following is the comparison of the resistance capacity of specimens by using the portable tester and Instron machine. Also, their specimen failure modes were identified and classified according to the specification for the pullout and peel test methods developed by Current (2009) and Wu (2008), respectively. In addition, the failure modes in both pullout and peel performance are compared. The lesson learned during the verifying performance for the portable tester is given in Section 7.4. Section 7.5 concludes the results of verifying tests of the portable tester. The limitation for the use of the portable tester and possible improvements are suggested in Section 7.6

7.2 Pullout Performance of Portable Tester

7.2.1 Experimental Configurations for Pullout Test

The objective of testing a group of pullout specimens of AARS in three different samples is in order to verify the extent of applicability of the new portable tester. These three chosen samples are expected to cover diverse conditions of specimens considering different roofing types, material sources and types of cold adhesives. When fabricating the specimens, two sets of specimens were always constructed on the same day by the same person with the materials from the same source - one set for testing on the portable tester and the other for examining on the Instron machine. It is important to verify not only the resistance capacity but also the observed failure mode by using the portable tester to identify if it agrees with the result from the Instron machine.

Here, the term "specimen" refers to an individual mock-up built up in the laboratory for testing. The term "sample", on the other hand, refers to a group of specimens that were built under the same conditions and have common geometry and test variables. These definitions are the same as those defined in Chapter 5.

The AARS specimens of Samples 1 and 3 had modified bitumen membrane including cap sheet and base sheet, and Sample 2 specimens had the single-ply PVC membrane. The configuration of Samples 1 and 3 also had one more layer of cover board compared to Sample 2. As to the adhesive application, the cold adhesive #1 was employed from the cap sheet to steel deck for the specimens of Sample 1. Considering the unevenness of steel deck surface, insulation and steel deck may not be bonded as firmly as expected by applying only 20 to 30×10^{-3} inches of cold adhesive #1. Therefore, a new professional polyurethane roof adhesive, cold adhesive #3, was applied on steel deck to bond the insulation of Sample 3, while cold adhesive #1 was still used for the attachment of other layers. For the PVC roofing specimens of Sample 2, the specific cold

adhesive #2 was used to bond PVC membranes with the insulation materials according to the instruction for construction. The cold adhesive #3 was also employed on the steel deck following the PVC roofing construction method. All specimens of three samples were cured for 20 days. The detailed configurations of these three samples and their cross-sections are summarised in Table 7.1 and Figure 7.1.

Table 7.1: *Configuration of three samples used in the pullout testing*

	Sample 1	**Sample 2**	**Sample 3**
Cap Sheet	Modified Bitumen Membrane	PVC Membrane	Modified Bitumen Membrane
	Cold Adhesive #1 full coat	*Cold Adhesive #2 full coat*	*Cold Adhesive #1 full coat*
Base Sheet	Modified Bitumen Membrane	*none*	Modified Bitumen Membrane
	Cold Adhesive #1 full coat	*none*	*Cold Adhesive #1 full coat*
Cover Board	Reinforced Asphalt Core Board	*none*	Reinforced Asphalt Core Board
	Cold Adhesive #1 full coat	*none*	*Cold Adhesive #1 full coat*
Insulation	Paper Facer Insulation Source I	Paper Facer Insulation Source II	Paper Facer Insulation Source I
	Cold Adhesive #1 full coat	*Cold Adhesive #3 applied*	*Cold Adhesive #3 applied*
Vapour Barrier	*none*	*none*	*none*
Roof Deck	Steel Deck	Steel Deck	Steel Deck
Curing Time	20 days	20 days	20 days
Cold Adhesive #1: Modified Bitumen Adhesive Cold Adhesive #2: PVC Bonding Adhesive Cold Adhesive #3: Polyurethane Roof Adhesive			

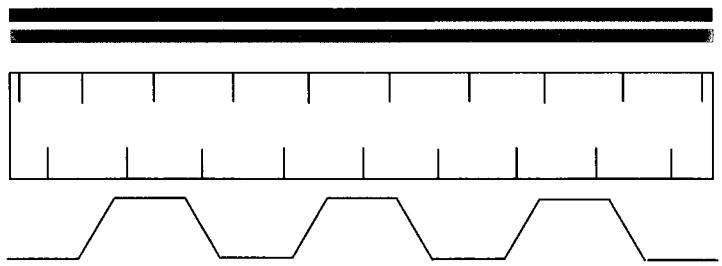

Cap Sheet
Adhesive
Base Sheet
Adhesive
Cover Board
Adhesive
Insulation
Adhesive
Steel Deck

(a) Sample 1 cross-section

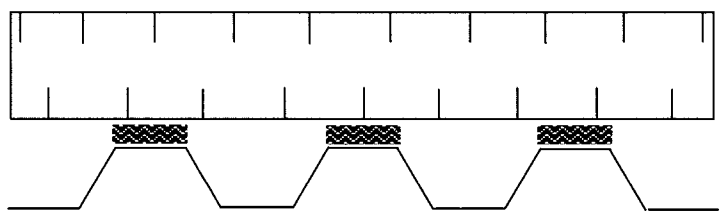

PVC Membrane
Adhesive
Insulation
Adhesive
Steel Deck

(b) Sample 2 cross-section

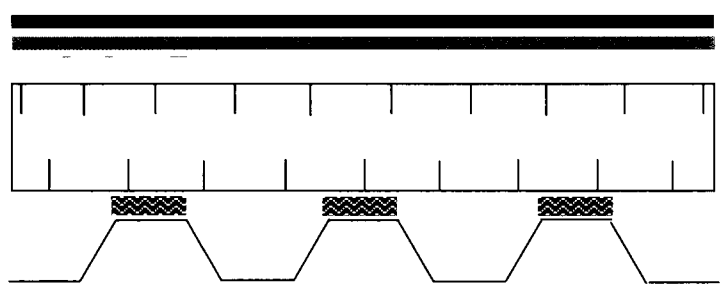

Cap Sheet
Adhesive
Base Sheet
Adhesive
Cover Board
Adhesive
Insulation
Adhesive
Steel Deck

(c) Sample 3 cross-section

Figure 7.1: Cross-sections of three samples used in the pullout testing

7.2.2 Comparison of Capacities for Pullout Test

The resistance capacity of specimens is the most important indicator in the verification test of the portable tester. The following sub-sections compare the pullout resistance capacities obtained from the portable tester and Instron machine. Comparison is carried out, first of all, specimen by specimen for each sample with the use of the two apparatus. Then, sample-to-sample comparison is further carried out.

Pullout Loading History

Figure 7.2 displays two groups of pullout loading history of the tested specimens for Sample 1, which were obtained from the portable tester and Instron machine, respectively. Basically, the portable tester and Instron machine produced the same load-extension diagrams with similar peak loads. They all indicate very similar characteristics and test results are found consistent. The portable tester is capable of providing with the stable loading procedure and magnitude of test loading as those of the Instron machine. However, the slope of their linear part is different. It is recognized that the two testing apparatus render different slopes for the linear section of the curve, though the specimens have identical model configurations and construction methods. Thus, the peak loads attained by the portable tester are used for the subsequent analysis and the stiffness of specimens obtained from the portable tester is used only as a reference for calculating the specimen's stiffness. The reason for having different slopes by different machines is explained in Section 7.4.

Pullout Peak Load Comparison by Specimens

Taking Sample 1 as an example, seven pullout peak loads obtained by using the portable tester and Instron machine are listed graphically in Figure 7.3. It is clearly seen that the results from two testers agree well. The average peak load of specimens tested by using the portable tester was 325 lbf (1.45 kN) with 25 lbf (0.11 kN) standard deviation. Thus, the pullout resistance can range from 300 lbf (1.33 kN) to 350 lbf (1.56 kN). While by using the Instron machine, it was 349 lbf

(1.55 kN) with 27 lbf (0.12 kN) standard deviation. Thus the pullout resistance range was from 322 lbf (1.43 kN) to 376 lbf (1.67 kN). The difference of the average peak load by using two testers is only 7%. As a result, it can be concluded that, for Sample 1, the two testers give very similar pullout test results.

Pullout Average Peak Load Comparison by Samples

Pullout average peak load of Samples 2 and 3 obtained from the portable tester and the Instron machine are displayed in Figure 7.4 in addition to Sample 1. Samples 2 and 3 are also show very close average peak loads and standard deviations by using two different apparatus. The difference of the average peak load for Samples 2 and 3 is 2% and 6%, respectively. Thus it is concluded that two testers can give very close results of the pullout resistance, or the pullout resistance evaluated by using the portable tester is found reliable. The capacity of the portable tester was designed as 900 lbf (4.0 kN). During the testing of Sample 2, the portable tester was stopped manually for some specimens even though they did not fail. This resulted in a reduction in the average peak load. However, as shown in the Figure 7.4, the data set of Sample 2 only differ between 952 lbf (4.23 kN) verses 970 lbf (4.31 kN) between the data from the portable tester to the Instron machin.

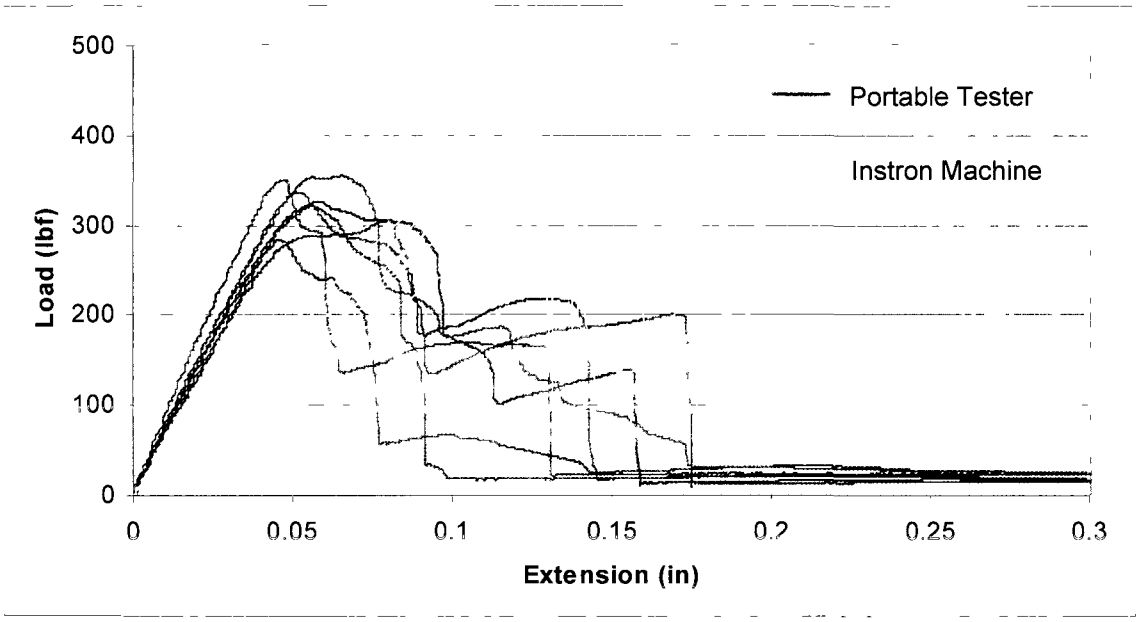

Figure 7.2: Pullout response of Sample 1 produced by using portable tester and Instron machine

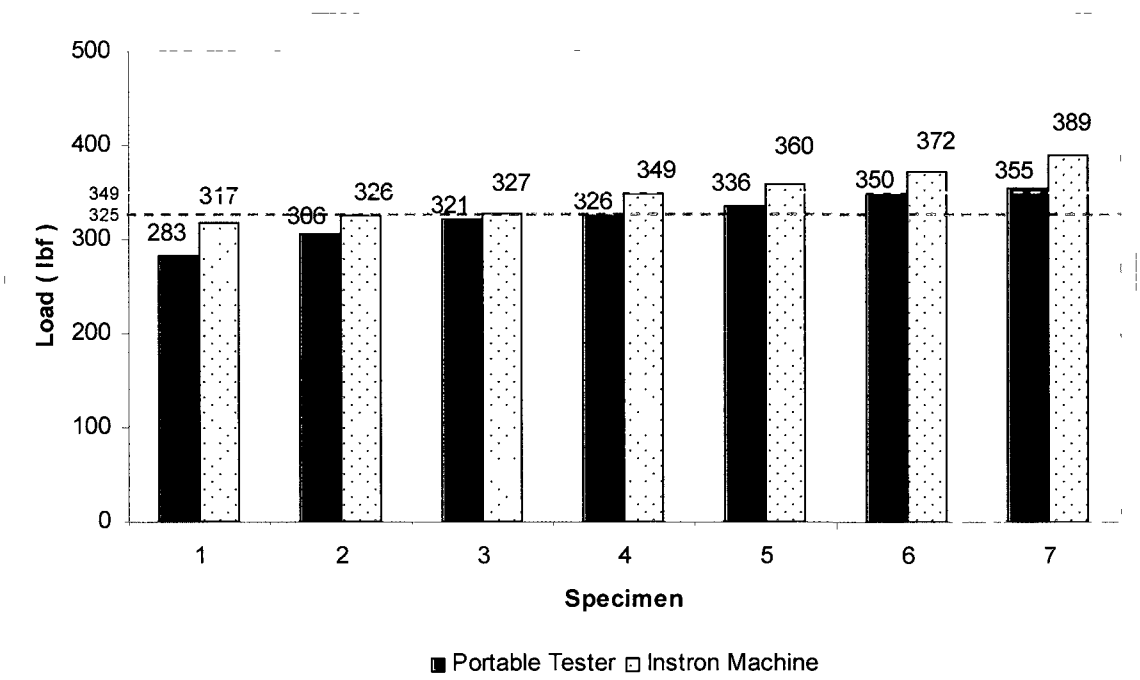

Figure 7.3: Pullout resistance comparison by specimens of Sample 1

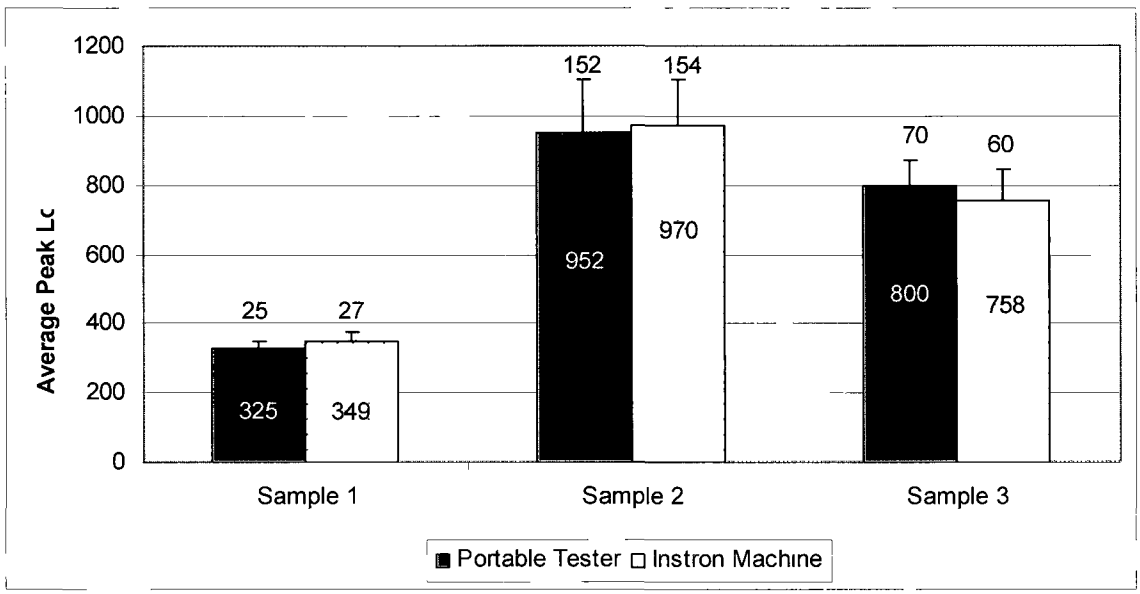

Figure 7.4. Comparison of average pullout peak load of three samples

7.2.3 Comparison of Failure Modes for Pullout Test

In place of the Instron machine for pullout tests, the portable tester is expected to result in not only the same resistance capacity but also the same failure modes as shown by the Instron machine for the same specimen. In the following sections, the failure modes of the pullout specimens acquired from two testers are illustrated and compared. Furthermore, the number of failure occurrence is counted and compared sample by sample.

Failure Modes revealed by both testers

The curing time for Sample 1 experiments was 20 days. Apparently, the applied cold adhesive #1 was still not fully hardened yet when the test was carried out. The failure in pullout tests of these cases, regardless of the testers, all happened at the cold adhesive #1 applied on the steel deck. Figures 7.5 (a) and (b) display the photos of this failure mode obtained from the portable tester and Instron machine, respectively. They show exactly the same failure modes.

Take the failure mode of Sample 3 as another example. Specimens of Sample 3 also had the traditional AARS configuration as Sample 1 specimens. Adhesive applied at all levels was also the cold adhesive #1, except on the steel deck, where cold adhesive #3 was applied. This is a type of foam adhesive and can provide fast adhesion. The weakest link in resisting the pulling force was found at the insulation facer. The bottom insulation facer delaminated on all specimens tested by both the portable tester and Instron machine, see Figures 7.5 (e) and (f).

Referring to Sample 2, the portable tester and Instron machine also gave the same failure modes. The failure always took place at the bottom facer of the insulation in all test cases because cold adhesive #3 was used instead of cold adhesive #1 on steel deck. Figures 7.5 (c) and (d) show their failure modes from testing by the portable tester and Instron machine, respectively.

Portable Tester	Instron Machine
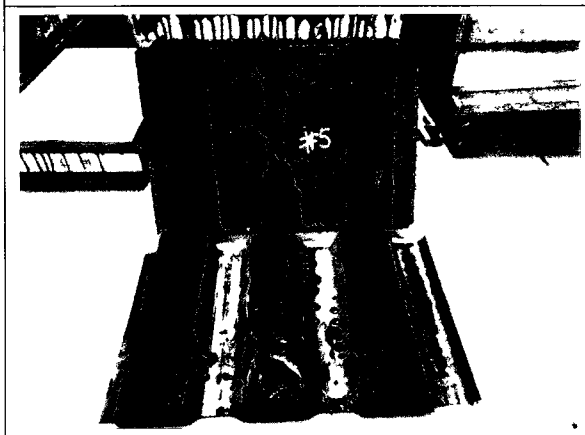	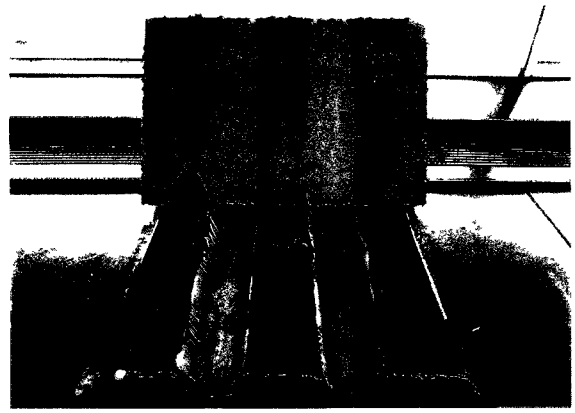
(a) Sample 1: Adhesive on Steel Deck failed	*(b) Sample 1: Adhesive on Steel Deck failed*
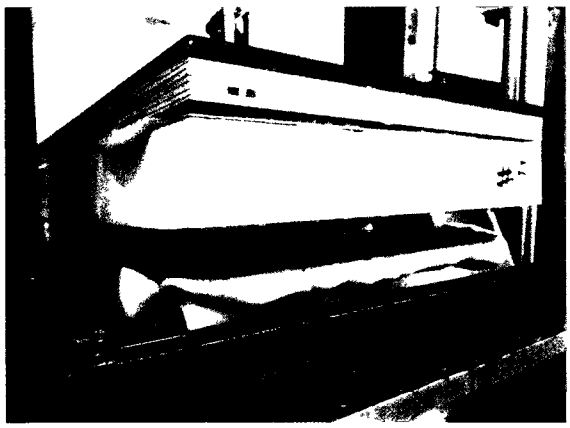	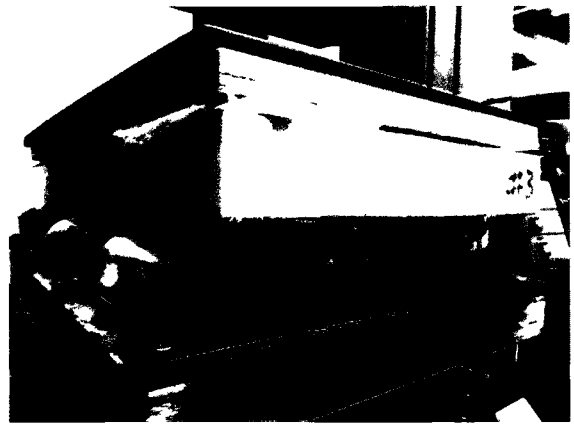
(c) Sample 2: Insulation facer rupture	*(d) Sample 2: Insulation facer rupture*
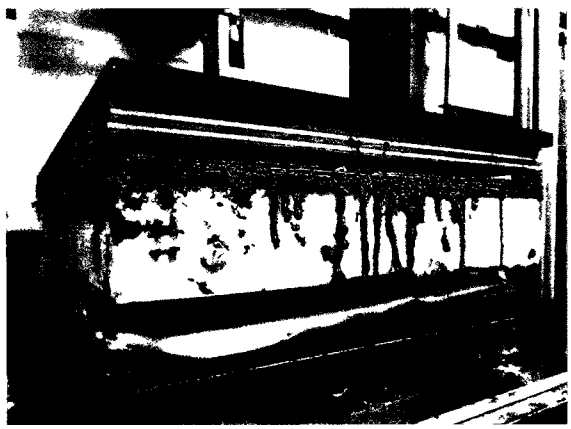	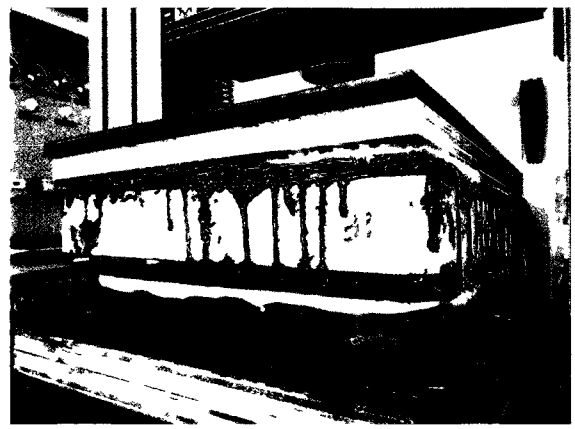
(e) Sample 3: Insulation facer rupture	*(f) Sample 3: Insulation facer rupture*

Figure 7.5: Comparison of pullout test failure modes by the portable tester and Instron machine

Failure Occurrence on Portable Tester and Instron Machine

A statistics analysis of the failure mode is worked out and presented in Table 7.2 for the three samples. The "failure occurrence value" for each sample was calculated. The "failure occurrence value" is defined by the number of failures that took place in various modes, counted for each specimen set. If a specimen fails in a combination of 2 failure modes, 0.5 is assigned to each of the modes. For a set of 7 specimens, there are a total of 7 failures. What is called no failure in Sample 2 in Table 7.2 means the pullout testing was stopped manually before the specimen failed because of the capacity limitation of the load cell of the portable tester.

Table 7.2: Failure mode distribution from the pullout tests

	Failure Mode	Failure Occurrence Value	
		Portable Tester	Instron Machine
Sample 1	**Adh/SD:** Adhesive on Steel Deck failed	7	7
Sample 2	**ISO Facer/R:** Insulation facer rupture	4	6
	ISO Facer/D: Insulation facer delaminaion	0	1
	No Failure	3	0
Sample 3	**ISO Facer/R:** Insulation facer rupture	6.5	6.5
	Adh/BS-CB: Adhesive between BaseSheet and CoverBoard failed	0.5	0.5

The observed failure modes by the portable tester and Instron machine were compared by using pie charts, see Figures 7.6 (a) and (b). The percentage of failure occurrence is indicated for each type of failure. In total, there were five different failure modes including the "No Failure". No matter which tester was used, ISO Facer/R (rupture of the Insulation facer) and Adh/SD (failure of Adhesive on the Steel Deck) were the major failure modes observed in all test specimens. A total occurrence of Adh/SD mode was 33% of all failures, which was consistent for both apparatus.

The distribution of failure modes of the three samples tested by the portable tester and Instron machine are shown in Figures 7.7 (a) and (b). Except for the cases of "No failure" in Sample 2, the failure modes and their percentage value were the same when different testing machines were used. Among the testing of Sample 1, only one Adh/SD mode was observed for the specimens tested by both machines. In Sample 3, two failure modes ISO Facer/R and Adh/BS-CB (failure of Adhesives between the BaseSheet and CoverBoard) were observed for the specimens by both machines. Since the rate of occurrence of these failure modes is consistent between the two machines, it can be concluded that there is no serious difference regarding the failure modes observed by the use of the two testing machines.

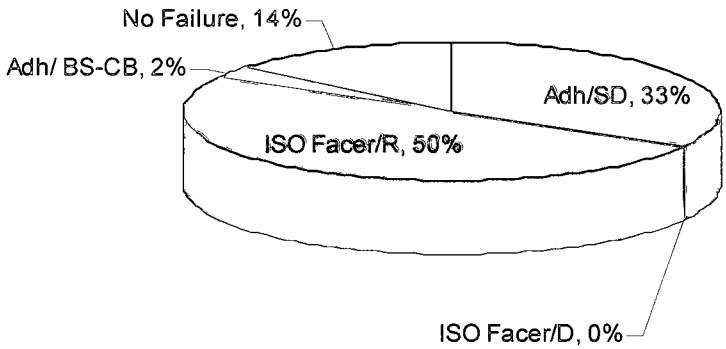

(a) By using the portable tester

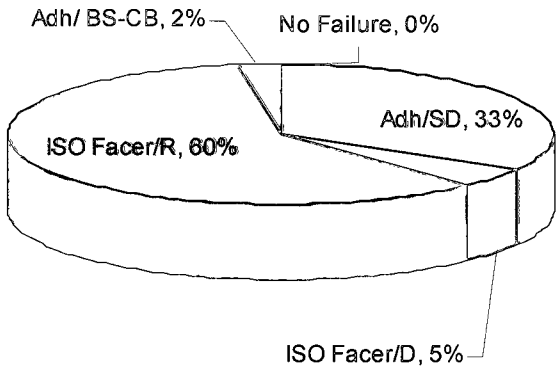

(b) By using the Instron machine

Figure 7.6: Comparison of pullout test failure mode percentage by the portable tester and Instron machine

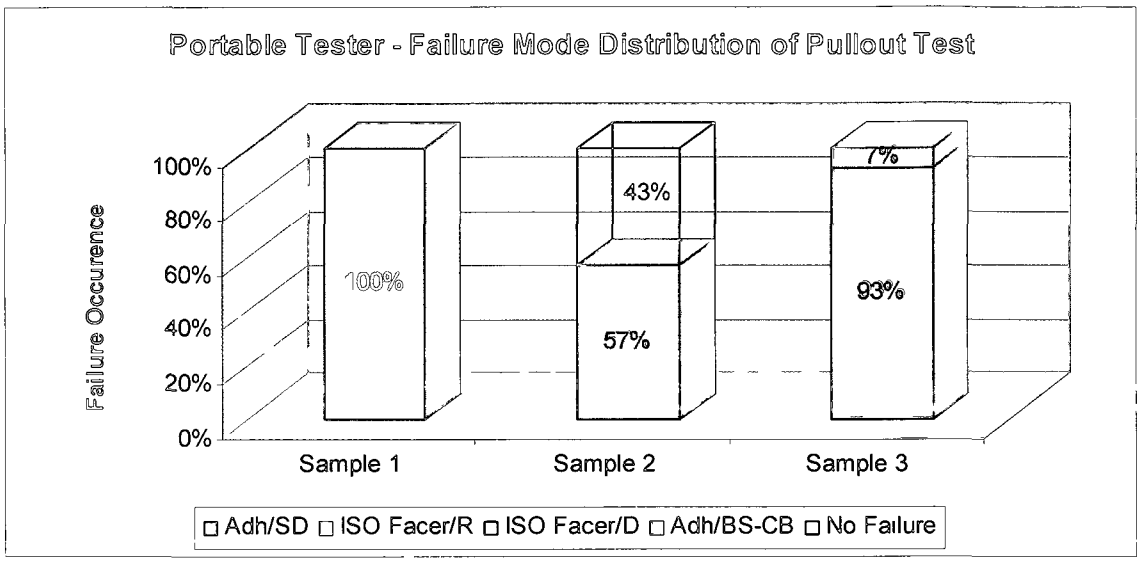

(a) By using the portable tester

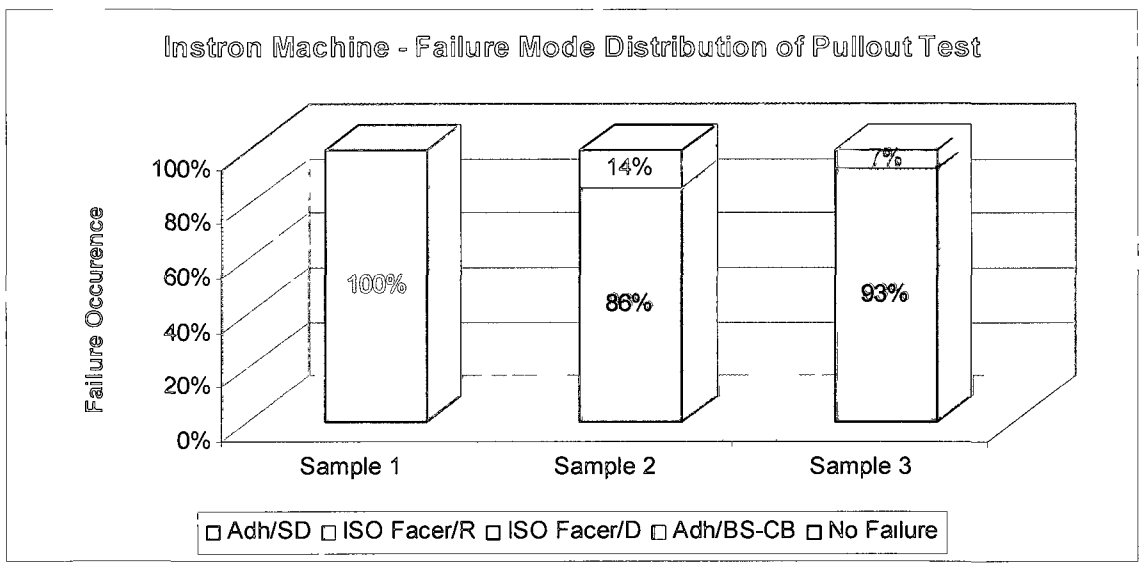

(b) By using the Instron machine

Figure 7.7: Comparison of pullout test failure mode distribution by the portable tester and Instron machine

7.3 Peel Performance of Portable Tester

7.3.1 Experimental Configurations for Peel Test

To verify the peel performance of the portable tester, five samples were chosen, which are expected to cover the diverse conditions of specimens such as the different roofing types, curing time, material source and types of cold adhesives. In the same way as the pullout performance verification, for each sample, when fabricating the specimens for peel testing, always two sets of specimens were constructed on the same day by the same person with the materials from the same source - one set for testing on the portable tester and the other for examining on the Instron machine.

The roof type of all samples other than Sample 4 belongs to the AARS with modified bitumen membrane, which is the most traditional AARS system, dominating the market share in Canada. Sample 4 is the single-ply AARS with PVC membrane, which is popular in USA. Out of the four Modified Bitumen roofing systems, the configuration of Samples 1 and 5 has a cover board. The specimens of Samples 2 and 3 were assembled without using any cover board. As far as the adhesive application is concerned, the cold adhesive #1 was employed from the cap sheet to insulation for the specimens of Samples 1, 2, 3 and 5. For the PVC roofing specimens of Sample 4, the specific PVC bonding adhesive, cold adhesive #2, was used to bond PVC membranes with the insulation materials according to the instruction for construction. The specimens of Samples 1, 2, 4, and 5 were cured for 20 days, while the curing time of Sample 3 specimens was 30 days to examine the portable tester in another aspect. The detailed configurations of these five samples are summarised in Table 7.3. Their cross-sections are shown in Figure 7.8.

Table 7.3: Configuration of 5 Samples used in the peel testing

	Sample 1	Sample 2	Sample 3	Sample 4	Sample 5
Base Sheet	Modified Bitumen Membrane	Modified Bitumen Membrane	Modified Bitumen Membrane	PVC Membrane	Modified Bitumen Membrane
	Cold Adhesive #1 full coat	*Cold Adhesive #1 full coat*	*Cold Adhesive #1 full coat*	*Cold Adhesive #2 full coat*	*Cold Adhesive #1 full coat*
Cover Board	Reinforced Asphalt Core Board	/	/	/	Reinforced Asphalt Core Board
	Cold Adhesive #1 full coat	/	/	/	*Cold Adhesive #1 full coat*
Insulation	Paper Facer Insulation Source I	Paper Facer Insulation Source II	Paper Facer Insulation Source I	Paper Facer Insulation Source II	Paper Facer Insulation Source I
Curing Time	20 days	20 days	30 days	20 days	20 days

Cold Adhesive #1: Modified Bitumen Adhesive

Cold Adhesive #2: PVC Bonding Adhesive

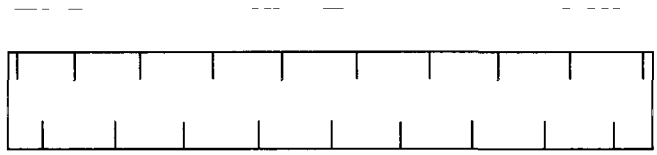

Base Sheet
Adhesive
Cover Board
Adhesive
Insulation

(a) Sample 1 cross-section

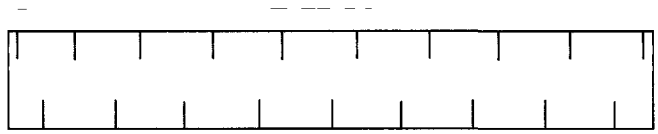

Base Sheet
Adhesive
Insulation

(b) Sample 2 cross-section

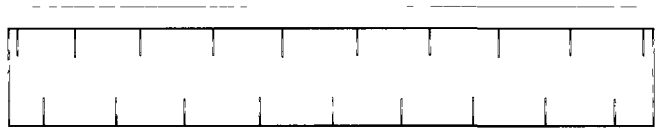

Base Sheet
Adhesive
Insulation

(c) Sample 3 cross-section

PVC Membrane
Adhesive
Insulation

(d) Sample 4 cross-section

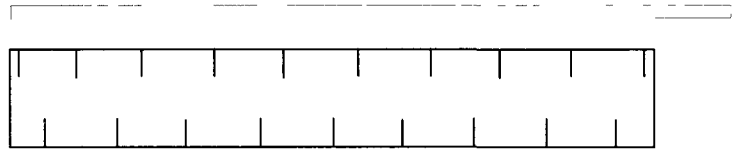

Base Sheet
Adhesive
Cover Board
Adhesive
Insulation

(e) Sample 5 cross-section

Figure 7.8: Cross-sections of five samples used in the peel testing

7.3.2 Comparison of Capacities for Peel Test

Peel Loading History

Following the standard peel test method, the portable tester and Instron machine applied a peel force at the rate of 1 in/min (25.4 mm/min) at an angle of 15 degrees. The loading history of peeling force exerted by the portable tester and Instron machine for Sample 1 is presented in Figure 7.9. The white peel test curves were produced by the Instron machine. The dark blue curves represent the specimen response tested by the portable tester. The loading profiles of the portable tester and Instron machine are similar to each other and have much the same peak values.

However, the portable tester tends to reach the peak loading sooner than that by the Instron machine. The same tendency was observed with all the sample set of seven specimens. The reason for this difference is illustrated in Section 7.4. Hence, like the processing method for the slope of the load-extension diagram achieved by the pullout testing on the portable tester, the time to reach the peak peeling load obtained by the portable tester is again considered merely as a reference.

Peel Peak Load Comparison by Specimens

Figure 7.10 compares the two peak loads of seven specimens from Sample 1. The dark blue columns represent results from the portable tester and the light coloured columns are from the Instron machine. Their average peak loads are 234 lbf or 1.04 kN, with the standard deviation of 25 lbf (0.11 kN), and 218 lbf or 0.97 kN, with the standard deviation of 19 lbf (0.08 kN), respectively. The difference of the two mean values is only 7%. It is evident that both the portable tester and Instron machine generate consistent peel resistance results, and the tests are repeatable.

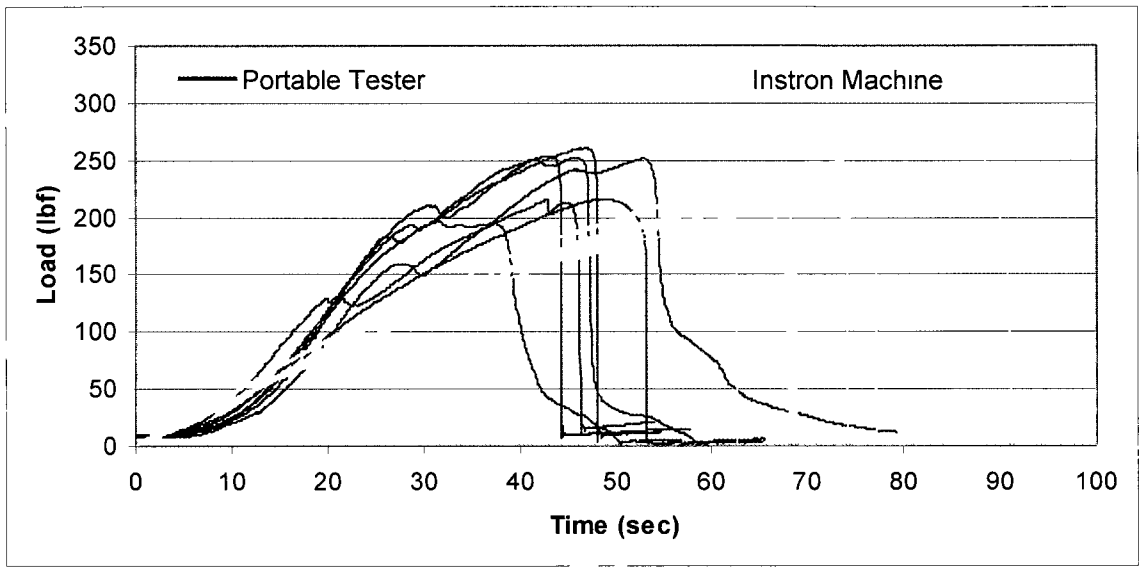

Figure 7.9: Peel response of Sample 1
by using portable tester and Instron machine

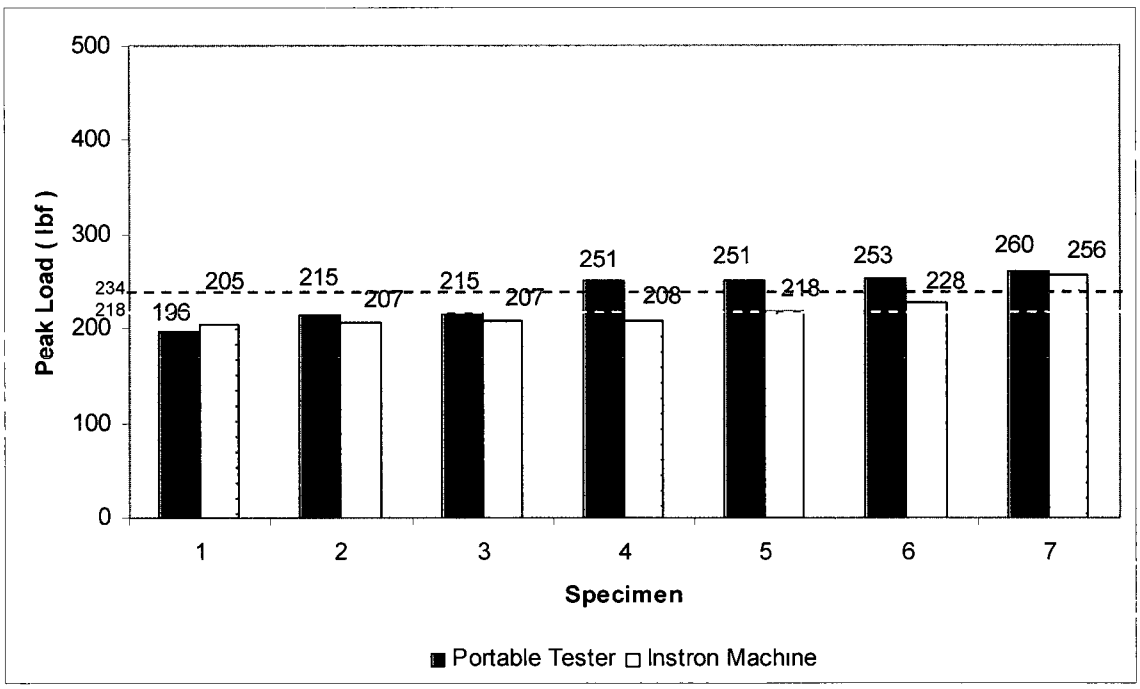

Figure 7.10: Peel resistance comparison by specimens of Sample 1

Peel Average Peak Load Comparison by Samples

Sample 1 proved that the portable tester renders consistent test results of peak peel force as the Instron machine. Following the previously discussed verification strategy, four more samples with various conditions were tested. The average peak loads obtained from the portable tester and Instron machine for all five samples are summarized in Figure 7.11. From Samples 1 through 5, the peak loads obtained from the portable tester showed good agreement with the test results from the Instron machine regardless of the difference of parameters such as the material sources, specimen configurations, adhesives and curing time. Having completed variety of peel tests, it is now concluded that the portable tester is not only effective but also reliable for evaluating the peel peak load in lieu of the Instron machine.

7.3.3 Comparison of Failure Modes for Peel Test

Failure Modes revealed by both testers

The specimen for peel tests consisted of the base sheet to insulation layer. During the series of peel tests, failure modes were categorised immediately following the completion of each test according to the standard peel test method (Wu 2008). The failure modes of all samples were found at the layer of either adhesive or insulation facer. For Sample 1, adhesive between the base sheet and cover board failed due to insufficient curing, see Figures 7.12 (a) and (b). This was testified in peel tests on both the portable tester and Instron machine. For Sample 3, the curing time was increased to 31 days as mentioned earlier. As a result, a part of the specimens failed at the adhesive layer between base sheet and insulation (Adh/BS-ISO). The failure modes for the rest of the specimens were found to be delamination of the insulation facer, see Figures 7.13 (a) ~ (d). This phenomenon was also verified by using both apparatus. For Sample 2, whose specimens were without cover board, the typical failure modes were adhesive between base sheet and insulation or the insulation facer delaminaiton on both the portable tester and Instron machine, see Figures 7.12 (c) ~ (f). Specimens tested on the portable tester exhibited an extra failure mode; i.e., the

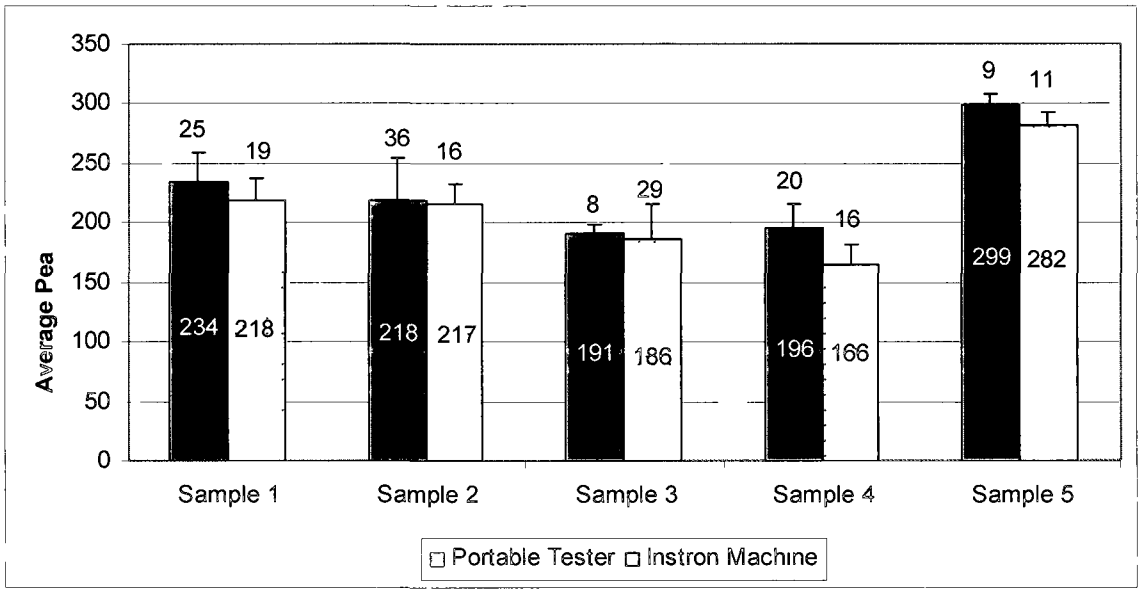

Figure 7.11: Comparison of average peel peak load of five samples

Portable Tester	Instron Machine
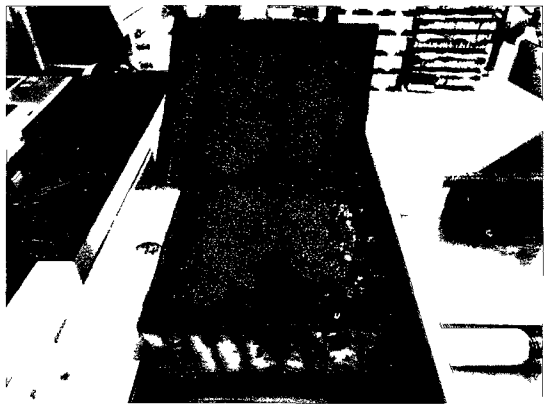	
(a) Sample 1: Adhesive between BaseSheet - CoverBoard failed	*(b) Sample 1: Adhesive between BaseSheet - CoverBoard failed*
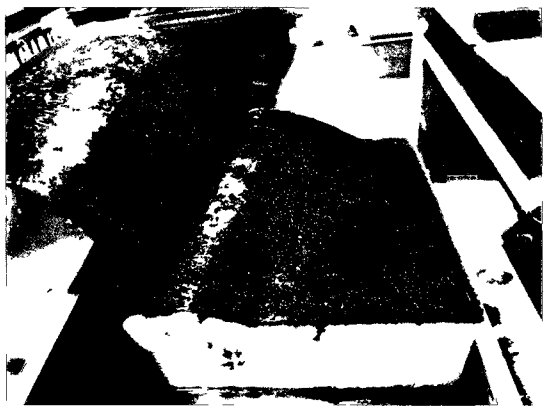	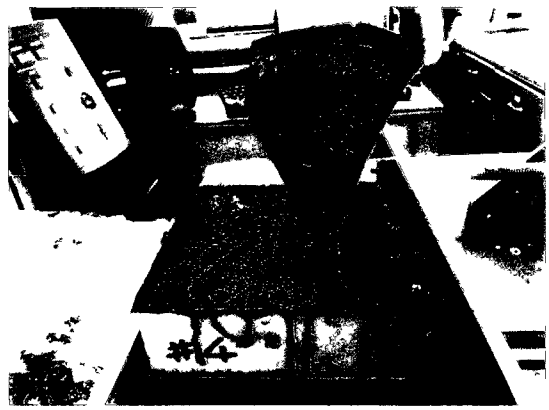
(c) Sample 2: Adhesive between BaseSheet - Insulation failed	*(d) Sample 2: Adhesive between BaseSheet - Insulation failed*
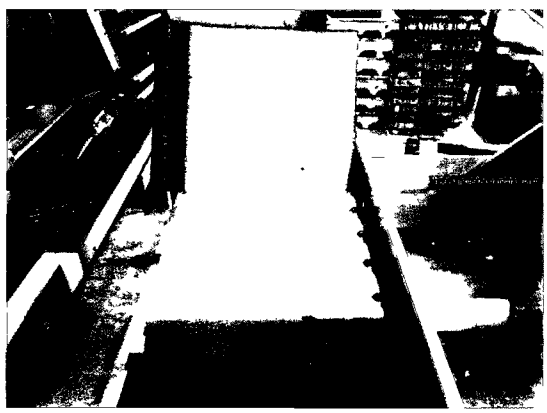	
(e) Sample 2: Insulation facer delamination	*(f) Sample 2: Insulation facer delamination*

Figure 7.12: Comparison of peel test failure modes by the portable tester and Instron machine for Samples 1 and 2

Portable Tester	Instron Machine
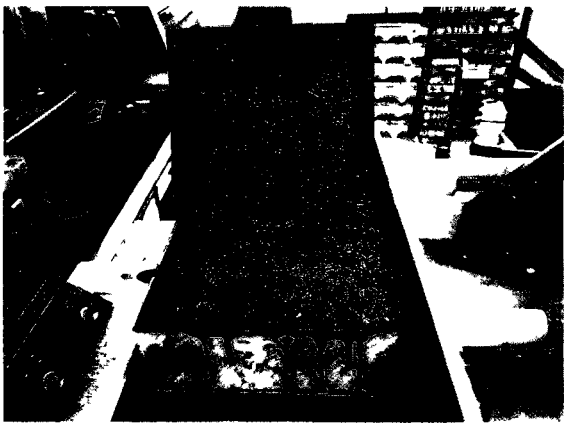	
(a) Sample 3: Adhesive between BaseSheet - CoverBoard failed	*(b) Sample 3: Adhesive between BaseSheet - CoverBoard failed*
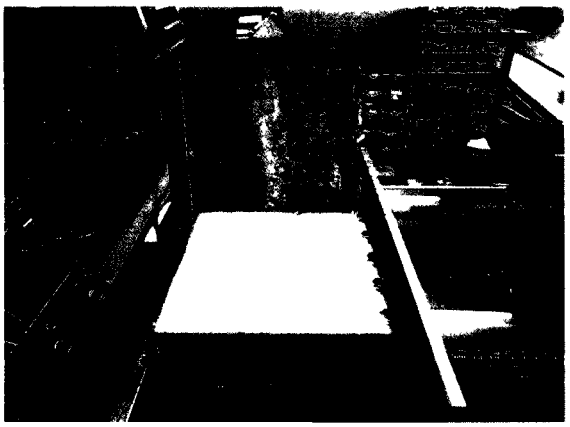	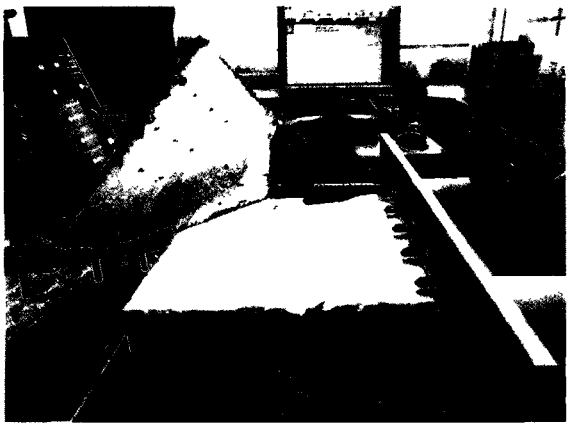
(c) Sample 3: Insulation facer delamination	*(d) Sample 3: Insulation facer delamination*

Figure 7.13: Comparison of peel test failure modes by the portable tester and Instron machine for Sample 3

Portable Tester	Instron Machine
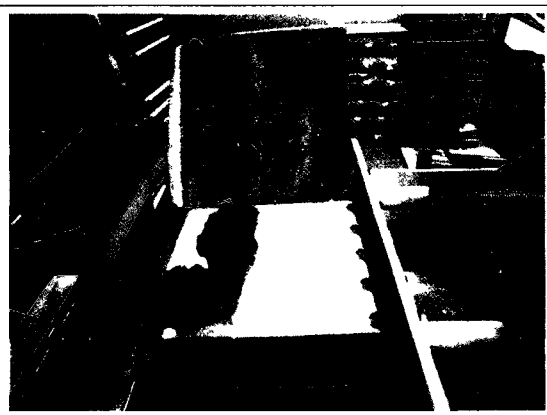	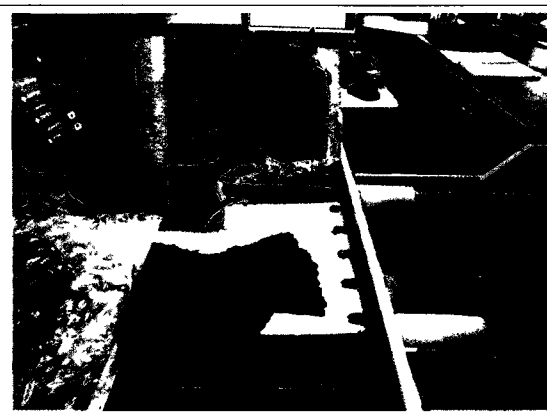
(a) Sample 4: Insulation facer tearing	*(b) Sample 4: Insulation facer tearing*
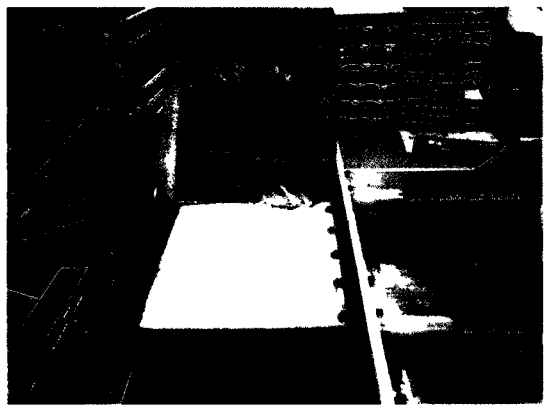	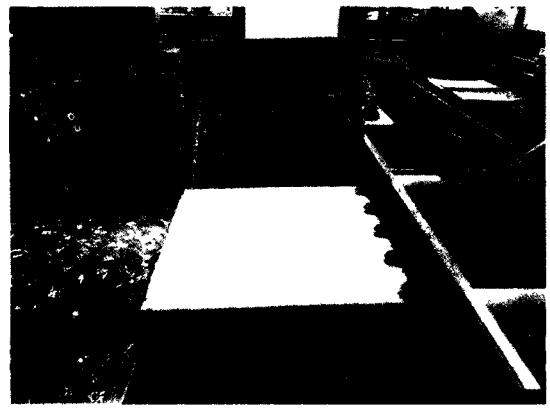
(c) Sample 4: Insulation facer delamination	*(d) Sample 4: Insulation facer delamination*
	
(e) Sample 5: Adhesive between BaseSheet - CoverBoard failed	*(f) Sample 5: Adhesive between BaseSheet - CoverBoard failed*

Figure 7.14: Comparison of peel test failure modes by the portable tester and Instron machine for Samples 4 and 5

insulation rupture (ISO/R) though it was still located at the insulation level. Sample 4 specimens consisted of the single-ply AARS with PVC membrane. The two testers continued to render the same failure modes for them: the tearing and/or delamination of insulation facer, see Figures 7.14 (a) ~ (d). The curing time for Sample 5 specimens was 20 days as that of Sample 1 with the same sample configuration but with different material sources. The location of adhesive failure was also between the base sheet and cover board, see Figures 7.14 (e) and (f). Therefore, from Samples 1 to 5, the two testers demonstrated exactly the same results in terms of the failure modes.

Failure Occurrence on Portable Tester and Instron Machine

A statistical consideration of observed failures by both machines is presented in Table 7.4. Comparing the failure occurrence value, the results from both machines are very consistent. The occurrence value (0.5) assigned to the ISO rupture for Sample 2 is a combination failure with the ISO facer delamination.

Figures 7.15 (a) and (b) are the percentage presentation of the observed failure modes by using the two apparatus. In general, they identify a very similar failure mode category and percentage. For the major failure modes, Adh/BS-CB (failure of Adhesives between BaseSheet and CoverBoard) and Adh/BS-ISO (failure of Adhesives between BaseSheet and Insulation), they were observed for the tested specimens by the use of the two machines with exactly the same percentages, which are 40% and 26%.

Following to the pie charts are the column charts for the peel test failure mode distribution of the five samples by using the portable tester and Instron machine, see Figure 7.16 (a) and (b). They also demonstrate the consistency of test results of the five samples. For Samples 1, 3 and 5, the same failure mode categories with exactly the same ratio were counted by using the portable tester and Instron machine. For Samples 2 and 4, the outcome from the portable tester is comparable to that from the Instron machine. Though the ratio between the

Table 7.4: Failure mode distribution from the peel tests

	Failure Mode	Failure Occurrence Value	
		Portable Tester	**Instron Machine**
Sample 1	**Adh/BS-CB** Adhesive between BaseSheet and CoverBoard failed	7	7
Sample 2	**Adh/BS-ISO** Adhesive between BaseSheet and Insulation failed	3	3
	ISO Facer/D Insulation facer delamination	3.5	4
	ISO/R Insulation rupture	0.5	0
Sample 3	**Adh/BS-ISO** Adhesive between BaseSheet and Insulation failed	6	6
	ISO Facer/D Insulation facer delamination	1	1
Sample 4	**ISO Facer/T** Insulation facer tearing	3.5	2
	ISO Facer/D Insulation facer delamination	3.5	5
Sample 5	**Adh/BS-CB** Adhesive between BaseSheet and CoverBoard failed	7	7

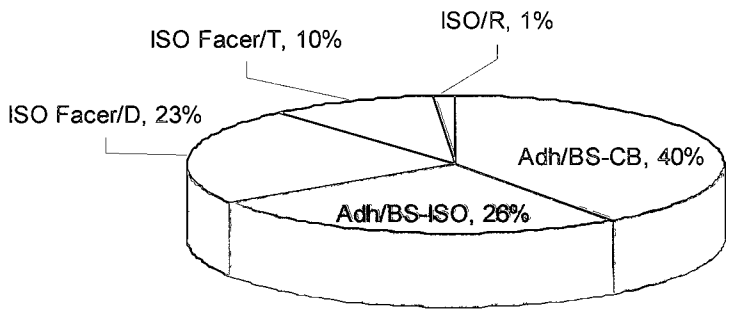

(a) By using the portable tester

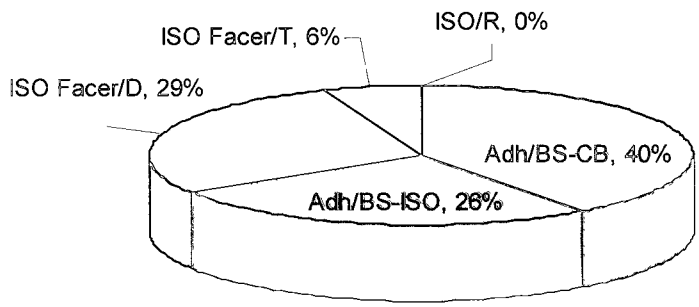

(b) By using the Instron machine

Figure 7.15: Comparison of peel test failure mode percentage by the portable tester and Instron machine

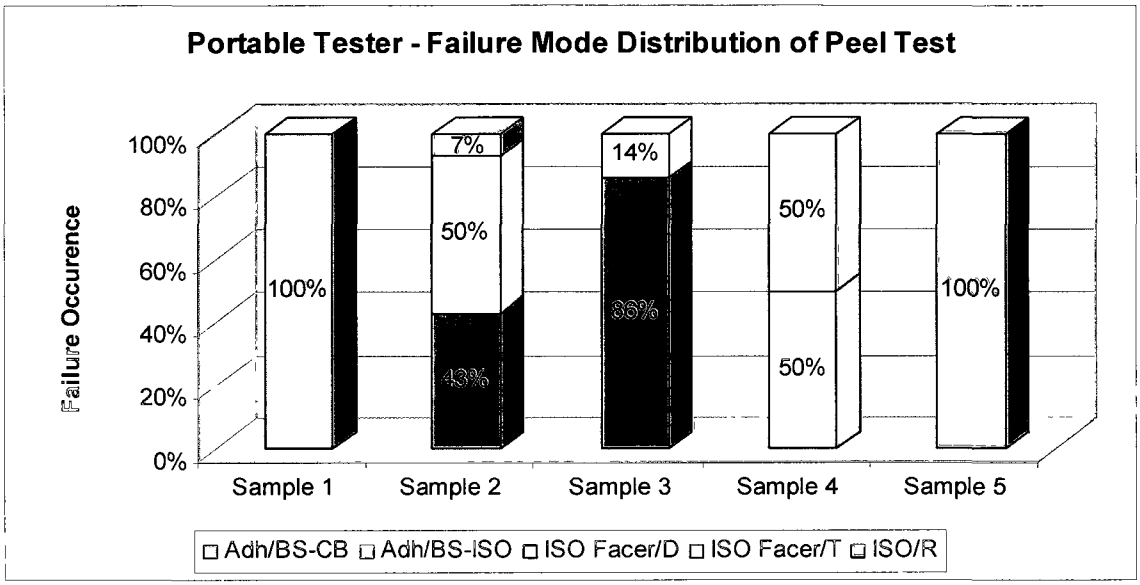

(a) By using the portable tester

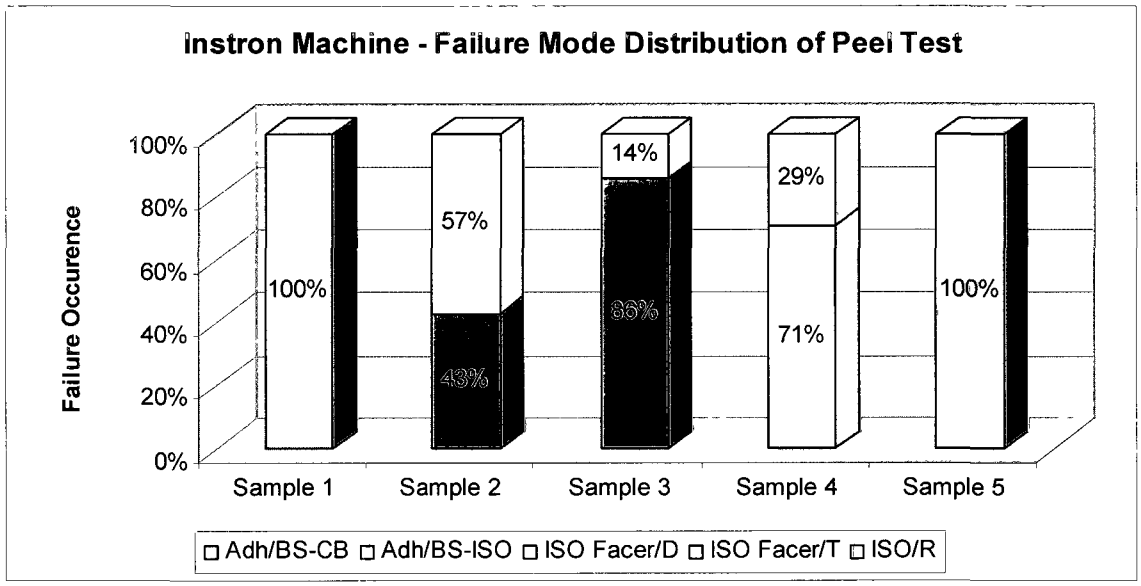

(b) By using the Instron machine

Figure 7.16: Comparison of peel test failure mode distribution by the portable tester and Instron machine

failure modes may be slightly different, the specimen failure locations are same by using two different testing machines. For example, when the Sample 4 was tested by using the portable tester, 50% failure modes were ISO Facer/D (Insulation Facer Delamination), 50% failure modes were ISO Facer/T (Insulation Facer Tearing). When Sample 4 was tested by using the Instron machine, the failure mode ration was 71% ISO Facer/D and 29% ISO Facer/T. However, all the failures occurred on insulation facer. By using the two different testers, we obtained the same conclusion: insulation facer of Sample 4 was the weakest link.

7.4 Lesson Learned from Benchmark Tests

Pullout Load-Extension Diagram

The slope of the linear section of a pullout load-extension diagram represents the stiffness of a roofing sample. The steeper the gradient is, the more rigid the roofing sample is. Figure 7.2 clearly shows that the specimens tested by the portable tester had higher slope or stiffness than the cases tested by the Instron machine with the same sample. Why do they exhibit this difference? The main reason is the different style of connectors used in the two testers to link up the tested specimen with the load cell. For the Instron machine, the connection between the tested specimen and the cross-head load cell is secured by means of rigid coupling. It can be considered as a fixed joint. The bending effect caused by the eccentricity of pullout load to the 12 in x 18 in (305 mm x 457 mm) tested specimen or the imperfect levelling top surface of specimen is absorbed by the fixed joint. However, for the portable tester, a simple loose connection is made by a pin-joint, so that the eccentricity influences directly on the tested specimen and it accelerates the failure at earlier stage compared to the case of the Instron machine. As a result, the specimen tested by using the portable tester looks more rigid than the case of the Instron machine. The other reasons can be attributed to the use of the testing platform and attachments. For the portable tester, the platform is 1 in (25 mm) thick steel plate and the secure fasteners are

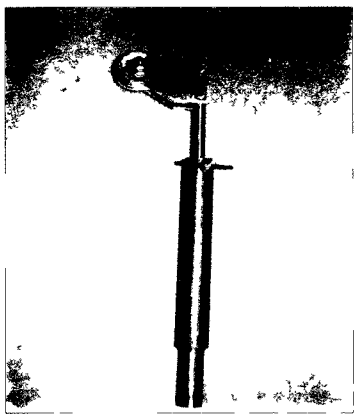

(a) Angle controller with pulley

(b) The shaft of angle controller deformed along peeling test

Figure 7.17: Angle controller for the Instron machine

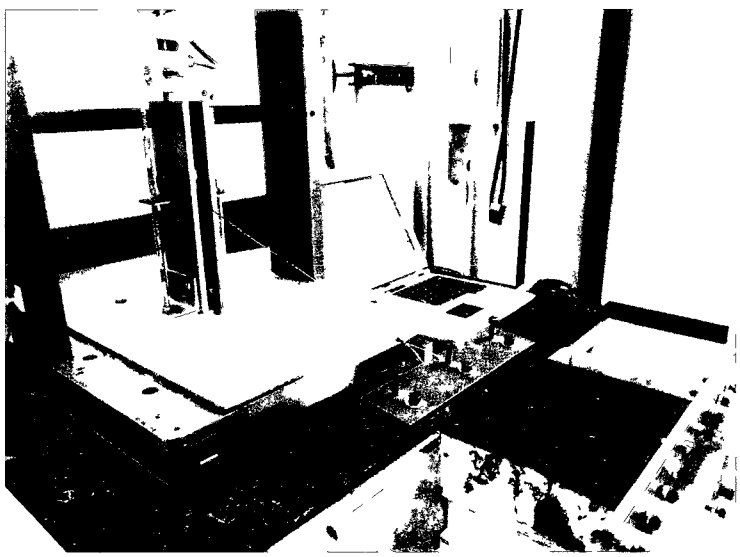

Figure 7.18: Angle controller for the portable tester

¾ in (19 mm) bolts, while the Instron machine has a plywood platform and ¼ in (6 mm) thick bolts instead which are more flexible.

Peel Time History of Loading Diagram

Figure 7.9 shows the portable tester, which tends to reach the peak loading sooner than that of the Instron machine. This is because the angle controllers installed on the two testing machines are different. In Figure 7.17, it is observed that a slender shaft of angle controller on the Instron machine is dragged forward with the increase of peeling force, which delays the failure time for the specimen. As to the angle controller of the portable tester, it consists of two 3½ in (89 mm) wide upright steel plates, which provide sufficient stiffness to work against giving displacement, see Figure 7.18.

7.5 Conclusion for Benchmarking Test

By constructing new sets of specimens, both standard pullout and peel tests were carried out by using the portable tester. In the meanwhile, the same testing was conducted on the Instron machine as a cross reference. For testing of each sample, the results obtained from both testers presented high consistency. They exhibited the same failure locations, similar failure modes and very close peak loads. Tests were found repeatable on the portable tester. Comparing the results, their average peak loads and the failure occurrence for each sample exhibited essentially no difference. Three samples in different configurations for pullout performance, and five samples with various experimental parameters for peel performance, demonstrated that the portable tester provides reliable testing data.

As a prototype of the proposed simple fixture, the portable tester was designed without the load balancing function. The output raw data, therefore, need to be properly treated before coming to the presentable output. The slope of pullout curves developed by using the portable tester was found steeper than that

measured by using the Instron machine. It can be used only as a reference for calculating the stiffness of the specimens.

From the above pullout and peel performance experiments, the portable tester was confirmed to be a useful and valid equipment for pullout and peel tests. It provides accurate maximum load and demonstrates appropriate failure modes for standard pullout and peel tests. It is effective and convenient for evaluating the performance of AARS in field, when it is needed, instead of wasting time by shipping samples for carrying out more expensive testing in an environmentally prepared laboratory. Furthermore, it is possible to use the portable tester in the field for a quick and handy way to evaluate the quality control of roof constructions.

7.6 Limitation of Portable Tester and Improvements

The current portable tester is a functional prototype. As such, it is far from perfect and could be further optimized. There are many potential improvements to have better performance and make it more user friendly.

First of all, the maximum testing capacity of the portable tester and the travel length of its screw jack should be increased. The portable tester was designed and manufactured referencing the technical data of testing the modified bitumen membrane AARS. Hence, the capacity was aimed at 900 lbf (4.0 kN) and the load cell was designed for a maximum load of 1000 lbf (4.5 kN). The ultimate travel length of screw jack was designated to be 3 in (76 mm) long. These design conditions could restrict the testing of AARS specimens in other configurations. For example, the specimens of AARS with PVC membrane would have higher pullout resistance than the modified bitumen membrane system and exceed the tester capacity occasionally. If the testing specimen is made without Insulation, the 3 in (76 mm) travel length may not be adequate enough for specimen set-up.

Secondly, it is inconvenient for the operator to have two separate software applications, EPOS Studio and LabVIEW, to be monitored instead of relying on a single interface with the ability to control both the driving motor and the load cell. The current LabVIEW application could be modified so as to drive the motor directly. The operator would then have no need to use the EPOS Studio software to set the motor speed, turn on or stop the motor. All testing parameters and procedures can be controlled via LABVIEW only.

Thirdly, the current motor uses Hall Effect sensors for speed control. This strategy is more economical but control at lower speed is compromised. Using an additional encoder will allow a more precise speed regulation than the current speed tolerance of ± 5% and a wider range of testing speeds.

Fourthly, the definition of failure and termination of test should be programmed in LabVIEW to make the tester more automatic. For instance, when the load reduces to 90% of the peak load, it can be considered that the specimen has already failed and the test can be terminated. Also, when loading attains the maximum capacity, the test should be terminated automatically in order to avoid any possible damages of the load cell.

During the present experiments, it is noted that it is important to add an emergency switch to stop the motor. It is more convenient to have it particularly when the lifting screw moves close to the extreme ends of the travel distance (see Figure 7.19). Otherwise, a small key inside the jack, namely Key – KFTN, could fall out, causing the trouble in the screw jack movement.

Furthermore, by optimizing the mechanical design and material selection, the 60 kg heavy portable tester could be made lighter and more portable.

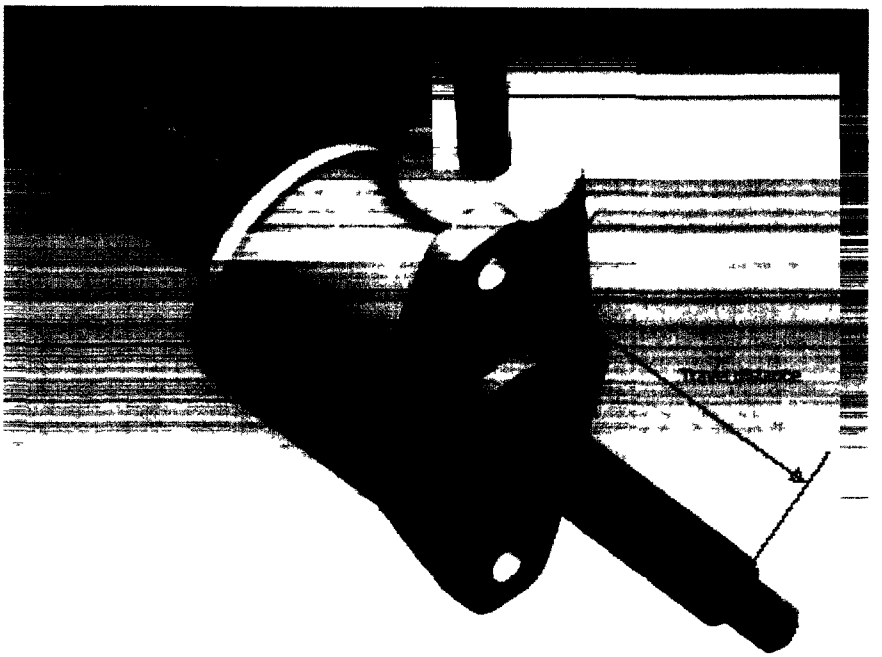

Figure 7.19: Travel distance of the lifting screw
Travel Distance = 3 in (76 mm)

Chapter 8: Conclusions and Future Study

8.1 Scope of the Thesis

The basic nature of wind effects on the roof is dynamic. The wind-induced suction on low sloped roof fluctuates with time, and the way it fluctuates varies from one zone to the other of the roof. The statistical mean and peak readings of wind pressure coefficient distribution reflect the spatial variation of wind pressure over a roof. Information on reliable wind pressure distribution is hence a key factor for the sound design of roofs. Chapter 2 discusses extraction of wind pressure coefficients from open literature to update the WindCAD database, which is designed as a reference for optimal design of roofs.

In Canada, modified bitumen roofing system dominates the low sloped roof market whereas the single-ply roofing system has the biggest market share in the United States. In Chapter 3, the ballasted roofing system, mechanically attached roofing system, fully bonded roofing system and adhesive applied roofing system, as four of the most popular roof types, are introduced. Their structural features and wind uplift responses are briefly described. Adhesive applied roofing system in particular is a focus of the present study. Its behaviour under tension and shear forces subjected to wind uplift load are discussed.

In order to quantify the wind performance of AARS, the pullout, peel and wind uplift test methods were established earlier. A review of these three existing standard test methods is provided in Chapter 4.

In Chapter 5, the correlation between the pullout, peel and wind uplift test results is explored by carrying out the one component variation tests.

A portable tester was developed in Chapter 6, aiming at the evaluation of the roof system behaviour particularly in the field. The developed portable tester is to conduct the pullout and peel tests and they are illustrated.

Chapter 7 presents the validation process and its results of the portable tester. The pullout and peel tests were conducted both on the portable tester and Instron machine respectively for performance comparison.

8.2 Summary of Research

Dynamic wind uplift load on low sloped roof promotes the roof components of AARS in the stress state of tension and shear. AARS deforms gradually under the combination effect of tension and shear. The standard pullout test method simulates the tension force, while the standard peel test method imitates the shear force on AARS. The dynamic wind uplift test method mocks the dynamic effects of wind uplift load at various magnitudes. One component variation tests of four scenarios in Chapter 5 verified that the pullout, peel and wind uplift test methods were applicable to assess both modified bitumen roofing system and single-ply roofing system. The observed relationship between test results of the three methods is:

(1) Shear or peeling force jointly with tensile or pullout force drives AARS into failure. The wind performance of AARS is determined by both tension and shear contributing to it;
(2) Higher resistance in both pullout and peel tests results in the same or higher overall resistance, which is observed in the full-scale wind uplift tests;
(3) Both peel and pullout tests are effective means in predicting the wind performance of AARS in full-scale;
(4) In any component substitution for a new roofing construction, if peel and pullout resistance are found higher than that of the original roof,

the component substituted roof can maintain the same level of wind uplift rating.

The development of the portable tester made it possible to perform small-scale pullout and peel tests in the field for the evaluation of the expected wind-induced response of the system under the impact of the same environmental conditions including the relative humidity and temperature. Experimental study, by using the portable tester and five different scenarios including the modified bitumen roofing system and single-ply roofing system with various adhesives, revealed that the portable tester is capable of

(1) giving equivalent peak loads in the pullout and peel tests as the data obtained by using the Instron machine;
(2) indicating the same failure location and similar failure mode as the Instron machine in the pullout and peel tests; and
(3) producing the load-extension diagram in the pullout test and the loading time history in the peel test, similar to those produced by the Instron machine.

8.3 Future Research

As a major contribution of the current research, a good correction between the pullout, peel and wind uplift test results have been found, based on the experiments of the modified bitumen and PVC membrane roofing systems. It is significant to apply them for the case of material substitution during the roof construction in the field. One component variation tests for the popular EPDM, TOP membrane roofing systems etc. would be necessary as a future study. The change of membranes between modified bitumen, PVC, EPDM and TPO is another supplementary variation in need of research. A large amount of experimental test data for the component changes would provide a broader choice of material substitution applications during the roof construction.

As a proposed instrument, the portable tester was validated for its full functions in the present study. However, all the validation data presented in Chapter 7 is based on the laboratory experiments. Whether or not it works properly at the work-site, giving the accurate testing data and right failure mode under any environmental conditions should be further verified. The portable tester is expected to be deployed at the construction sites, where the environmental control is not so ideal as in the laboratory environment. The change of design must be made to account for fluctuations of field temperature to give reliable test results. Meanwhile, there are also some potential improvements to achieve the optimized system design as below:

(1) Change the current LABVIEW application so as to drive the motor directly. The user would then have no need to use the EPOS STUDIO software to set the motor speed, turn on the motor and stop it. Everything can be done via LABVIEW only;
(2) Add limit switches to stop the motor running any time without damaging the jack;
(3) Using an additional encoder to attain a more precise motor speed regulation than the current which has ± 5% tolerance;
(4) Mechanical optimizations can be carried out to make the instrument lighter and more portable;
(5) Recode the LABVIEW application to display the real-time loading status and demonstrate all the loading curves of one set of specimens within one chart for comparing.

The specimens in small-scale or full-scale size examined in the present research were cured indoor with constant temperature and humidity which did not reflect the actual conditions especially for a building roof. However, what would happen in reality is that following the diurnal changes in temperature, water vapor promotes blister growth by exerting cyclic pumping action to the blister *(A joint*

research project undertaken by NRCA (USA) and NRCC-IRC, March 1998). The formed blisters will accelerate the failure of a roof of AARS under wind load. It is better to have more tests using samples taken from different locations to build up the links of laboratory experiments to actual roof.

Aging resistance is another concern for roofing system, especially for adhesive applied roofing system. All the experimental investigations in the present project were carried out without considering the problem of aging. The specimens were tested immediately when they reached the specified minimum curing time. It is believed that different adhesive and roofing materials used for AARS have different aging conditions, aging temperature, aging rates, aging process and aging schedule. A brand new roof of AARS with strong wind performance may not show the similar performance after a few years. As an integrated system, long-term aging tests combined with weathering and stresses will be helpful to assess the wind performance of AARS in the overall perspective.

Appendix 1: Paper List of Additionally Collected Articles for WindCAD 5.0

ID	Title / Authors	Year	Source	Height (m)
201	***Wind load evaluation system for the design of roof cladding of spherical domes*** Yasushi Uematsua, Raku Tsuruishib	2008	Journal of Wind Engineering and Industrial Aerodynamics 96 (2008) 2054-2066	37.38
202	***Wind loads on free-standing canopy roofs: Part 1 local wind pressures*** Yasushi Uematsua, Theodore Stathopoulosb, Eri Iizumi	2008	Journal of Wind Engineering and Industrial Aerodynamics 96 (2008) 1015-1028	5
203	***Wind force coefficients for designing free-standing canopy roofs*** Yasushi Uematsua, Eri Iizumib, Theodore Stathopoulos	2007	Journal of Wind Engineering and Industrial Aerodynamics 95 (2007) 1486-1510	5
206	***Peak Wind Load Comparison: Theoretical Estimates and ASCE 7*** Henry W. Tieleman, Mohamed A. K. Elsayed, Muhammad R. Hajj	2006	Journal of Structural Engineering © ASCE July 2006	9.8
207	***The UWO contribution to the NIST aerodynamic database for wind loads on low buildings: Part 1.Archiving format and basic aerodynamic data*** T.C.E. Ho, D. Surry, D. Morrish, G.A. Kopp	2005	Journal of Wind Engineering and Industrial Aerodynamics 93 (2005) 1-30	4.88, 7.32, 9.75, 12.19
208	***Net pressures on the roof of a low-rise building with wall openings*** R.N. Sharma, P.J. Richards	2005	Journal of Wind Engineering and Industrial Aerodynamics 93 (2005) 267-291	4
210	***Wind effects of parapets on low buildings: Part 1. Basic aerodynamics and local loads*** Gregory A. Kopp┌, David Surry, Christian Mans	2005	Journal of Wind Engineering and Industrial Aerodynamics 93 (2005) 817-841	4.6

ID	Title / Authors	Year	Source	Height (m)
211	***Wind effects of parapets on low buildings: Part 2. Structural loads***			
	Gregory A. Kopp, Christian Mans, David Surry	2005	Journal of Wind Engineering and Industrial Aerodynamics 93 (2005) 843-855	4.6, 9.1, 18.3
213	***Wind effects of parapets on low buildings: Part 4. Mitigation of corner loads with alternative geometries***			
	Gregory A. Kopp, Christian Mans, David Surry	2005	Journal of Wind Engineering and Industrial Aerodynamics 93 (2005) 873-888	4.6
214	***Effect of building length on wind loads on low-rise buildings with a steep roof pitch***			
	J.D. Gingera, J.D. Holmesb	2003	Journal of Wind Engineering and Industrial Aerodynamics 91 (2003) 1377-1400	22
216	***Wind loads on parapets***			
	T. Stathopoulos, P. Saathoff, X. Du	2002	Journal of Wind Engineering and Industrial Aerodynamics 90 (2002) 503-514	30, 15
218	***Wind tunnel modelling of mean pressures on planar canopy roof***			
	B. Natalini, J.O. Marighetti, M.B. Natalini	2002	Journal of Wind Engineering and Industrial Aerodynamics 90 (2002) 427-439	5.5
219	***Effect of geometry on wind pressures on low-rise hip roof buildings***			
	Shakeel Ahmada, Krishen Kumarb	2002	Journal of Wind Engineering and Industrial Aerodynamics 90 (2002) 755-779	2.8, 2.9, 3.5, 4.2
220	***Occurrence of peak lifting actions on a large horizontal cantilevered roof***			
	K.M. Lam, J.G. Zhao	2002	Journal of Wind Engineering and Industrial Aerodynamics 90 (2002) 897-940	18

ID	Title Authors	Year	Source	Height (m)
221	***Detailed simulation of pressures in separated/reattached flows*** H.W. Tieleman, T.A. Reinhold, M.R. Hajj	2001	Journal of Wind Engineering and Industrial Aerodynamics 89 (2001) 1657-1670	3.95
223	***Behaviour of a hemispherical dome subjected to wind loading*** P. Montes, A. Fernandez	2001	Journal of Wind Engineering and Industrial Aerodynamics 89 (2001) 911-924	12
226	***Mean wind loads on porous canopy roofs*** C.W. Letchford, A. Row, A. Vitale, J. Wolbers	2000	Journal of Wind Engineering and Industrial Aerodynamics 84 (2000) 197-213	5
227	***Wind load effects and equivalent pressures on low-rise house roofs*** J.D. Ginger, G.F. Reardon, B.J. Whitbread	2000	Engineering Structures 22 (2000) 638-646	3.86
228	***Mean and fluctuating wind loads on rough and smooth parabolic domes*** C.W. Letchford, P.P. Sarkar	2000	Journal of Wind Engineering and Industrial Aerodynamics 88 (2000) 101-117	45
229	***Mean wind pressures on flat roof corners affected by parapets: field and wind tunnel studies*** Theodore Stathopoulos, Rajan Marathe, Hanqing Wu	1999	Engineering Structures 21 (1999) 629-638	3.3

ID	Title / Authors	Year	Source	Height (m)
230	***Wind-induced dynamic response and resultant load estimation of a circular flat roof***			
	Yasushi Uematsu, Keisuke Watanabe, Akihiro Sasaki, Motohiko Yamada, Takeshi Hongo	1999	Journal of Wind Engineering and Industrial Aerodynamics 83 (1999) 251-261	20~26, 40~52, 60~78, 70~91, 100~130, 12.5~16.25, 25~32.5, 50~65, 100~130
231	***Net pressures on a low-rise full-scale building***			
	J.D. Ginger, C.W. Letchford	1999	Journal of Wind Engineering and Industrial Aerodynamics 83 (1999) 239-250	4
232	***Observations of Reynolds number sensitivity in the separated flow region on a bluff body***			
	R.P.Hoxey, A.M.Reynolds, G.M.Richardson, A.P.Robertson, J.L.Short	1998	Journal of Wind Engineering and Industrial Aerodynamics 73 (1998) 231-249	5.3
233	***Variations of wind pressure on hip roofs with roof pitch***			
	Y.L.Xu, G.F.Reardon	1998	Journal of Wind Engineering and Industrial Aerodynamics 73 (1998) 267-284	2.9
236	***Wind loads on low buildings with 4 : 12 gable roofs in open country and suburban exposures***			
	P.C. Case, N. Isyumov	1998	Journal of Wind Engineering and Industrial Aerodynamics 77&78 (1998) 107-118	5.69
238	***Wind loads and wind-induced dynamic behaviour of a single-layer latticed dome***			
	Yasushi Uematsu, Motohiko Yamada, Akira Inoue, Takeshi Hongo	1997	Journal of Wind Engineering and Industrial Aerodynamics 74&76 (1998) 675-685	36, 42, 54

ID	Title / Authors	Year	Source	Height (m)
239	***The assessment of wind loads on roof overhang of low-rise buildings*** Tore Wiik, Ernst W.M. Hansen	1997	Journal of Wind Engineering and Industrial Aerodynamics 67&68 (1997) 687-696	10
240	***Wind-induced dynamic response and resultant load estimation for a flat long-span roof*** Y. Uematsu, M. Yamada, A. Sasakil	1996	Journal of Wind Engineering and Industrial Aerodynamics 65 (1996) 155-166	25

Appendix 2: Failure Mode Classification for Wind Uplift Test

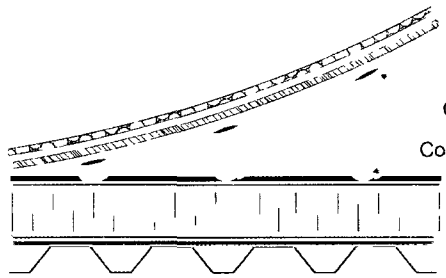

(a) Cover board separation

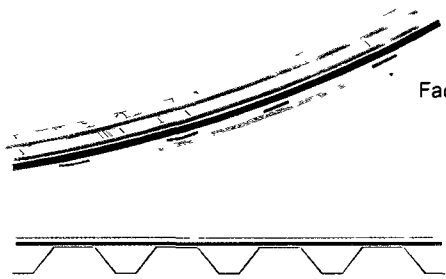

(b) Insulation facer delamination

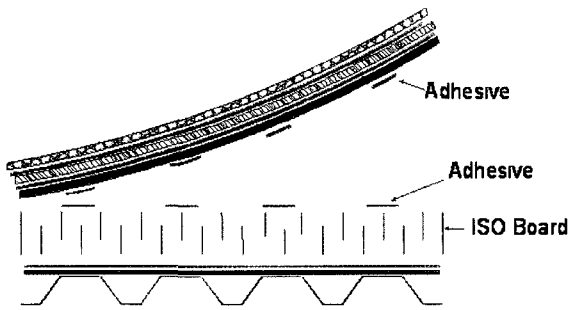

(c) Adhesive failure

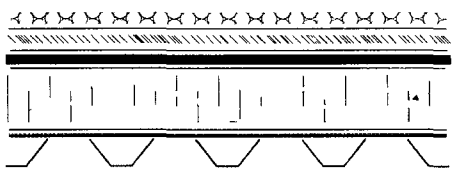

(d) Insulation foam failures

Figure App.2.1: Typical failure mode sketch for wind uplift test

Appendix 3: Speed Control and Data Storage of Portable Tester

App.3.1 Electronic Control System

The mechanical driving system of prototype is electronically operated by maxon motor control system which includes motor, gearbox, EPOS2 positioning controller and the EPOS Studio software. Their connection layout is displayed in Figure App.3.1. The EPOS2 50/5 positioning controller is a small-sized full digital smart motion controller. It is installed in the holding tray underneath the platform plate (see Figure App.3.2). The integrated position-velocity-and current control functionality of EPOS2 allows sophisticated positioning applications. The maxon motor control program contains servo amplifiers for controlling the fast reacting EC motor. The function of the speed servo amplifier is to keep the prescribed motor speed constant and independent of load changes.

The motor used for mechanical driving system is naxon brushless EC motor which made in Switzerland. Cable M1 has motor power lines and motor Hall sensor lines connected with EPOS2 by means of connector J2, J3. The motor is equipped with a digital encoder that connects with EPOS2 through encoder cables M2 provides communication with EPOS2 controller. To achieve the constant prescribed motor speed and independent of load changes, the set value (desired speed) is continuously compared with the actual value (actual speed) in the control electronics of the servo amplifier. The motor is provided with a voltage that is proportional to the applied speed set value. The speed would drop with increasing motor load. The compensation circuitry increases the output voltage with increasing motor current.

Through connecting USB – COM cable to computer application, EPOS Studio program communicates with the motor controller EPOS2. The interface of EPOS Studio 1.41 is shown in Figure App.3.3.

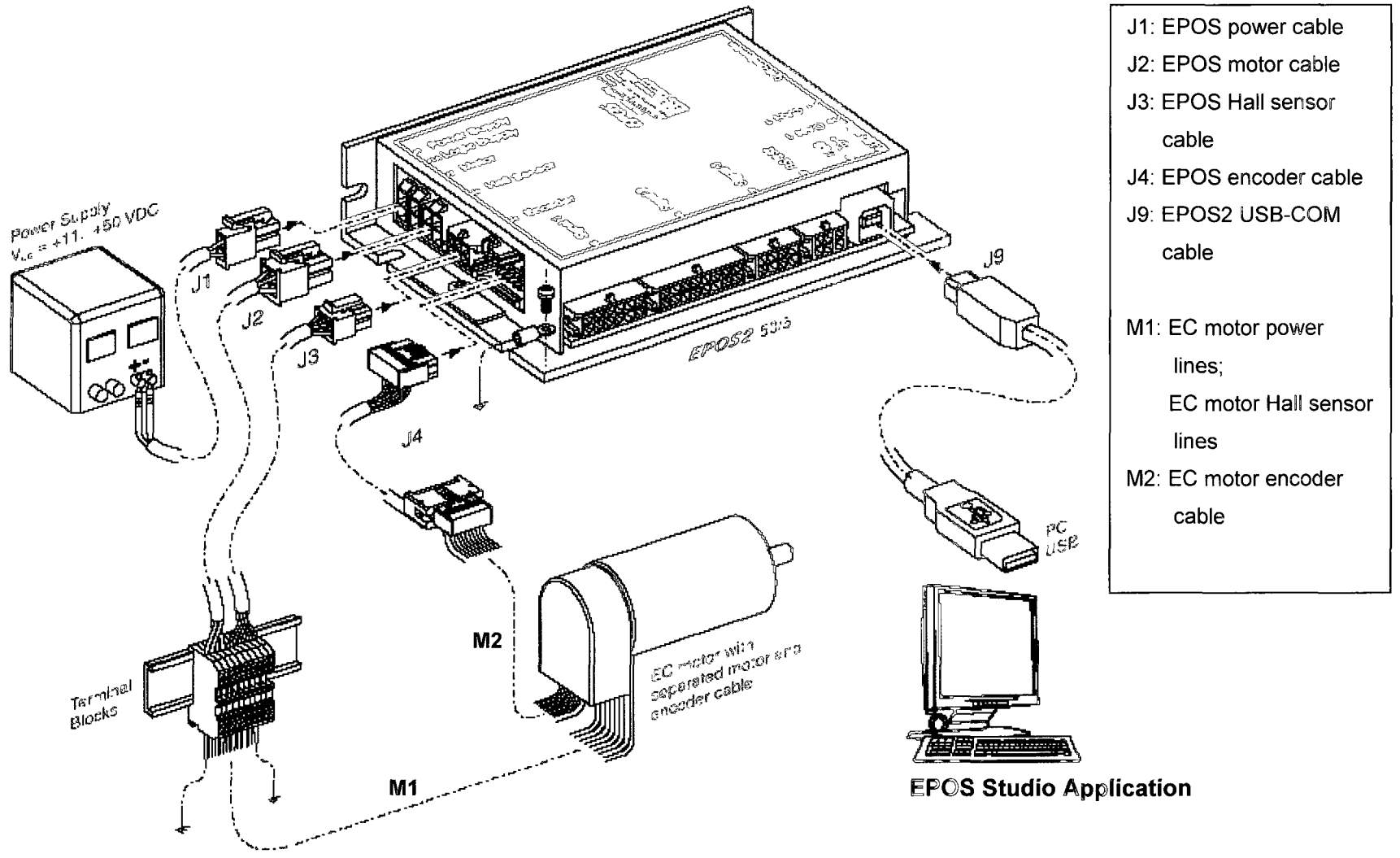

Figure App.3.1: Wiring scheme for brushless EC motor (EPOS2 50/5 Positioning Controller Documentation, 821376-02)

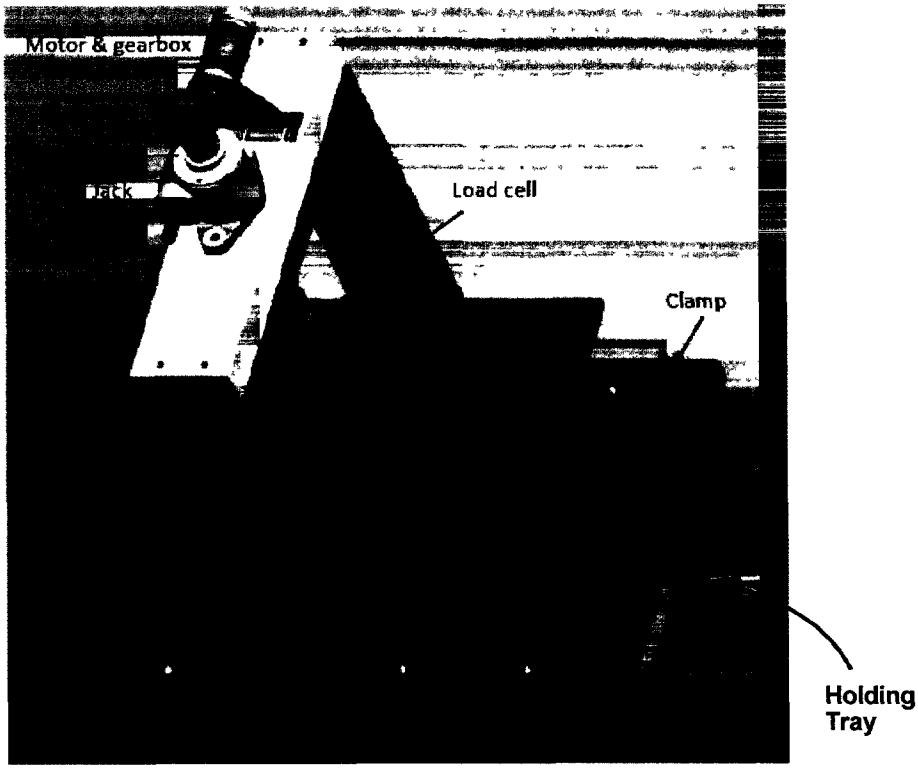

(a) Holding tray location

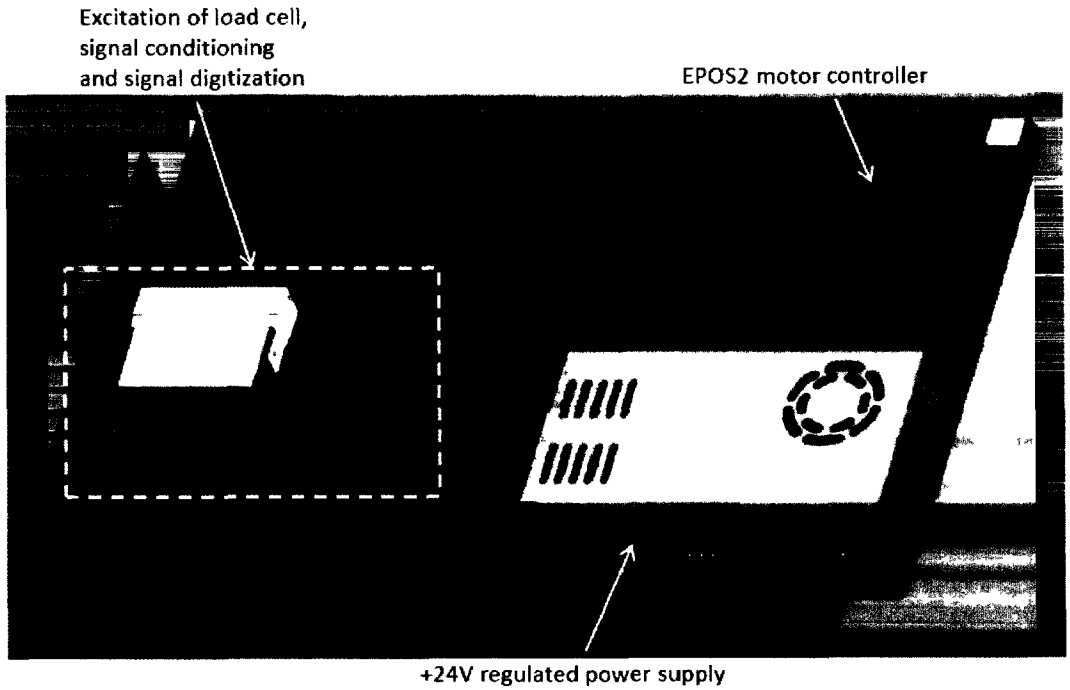

(b) Layout of parts on holding tray

Figure App.3.2: Holding tray underneath the testing platform (SAI Design Inc.)

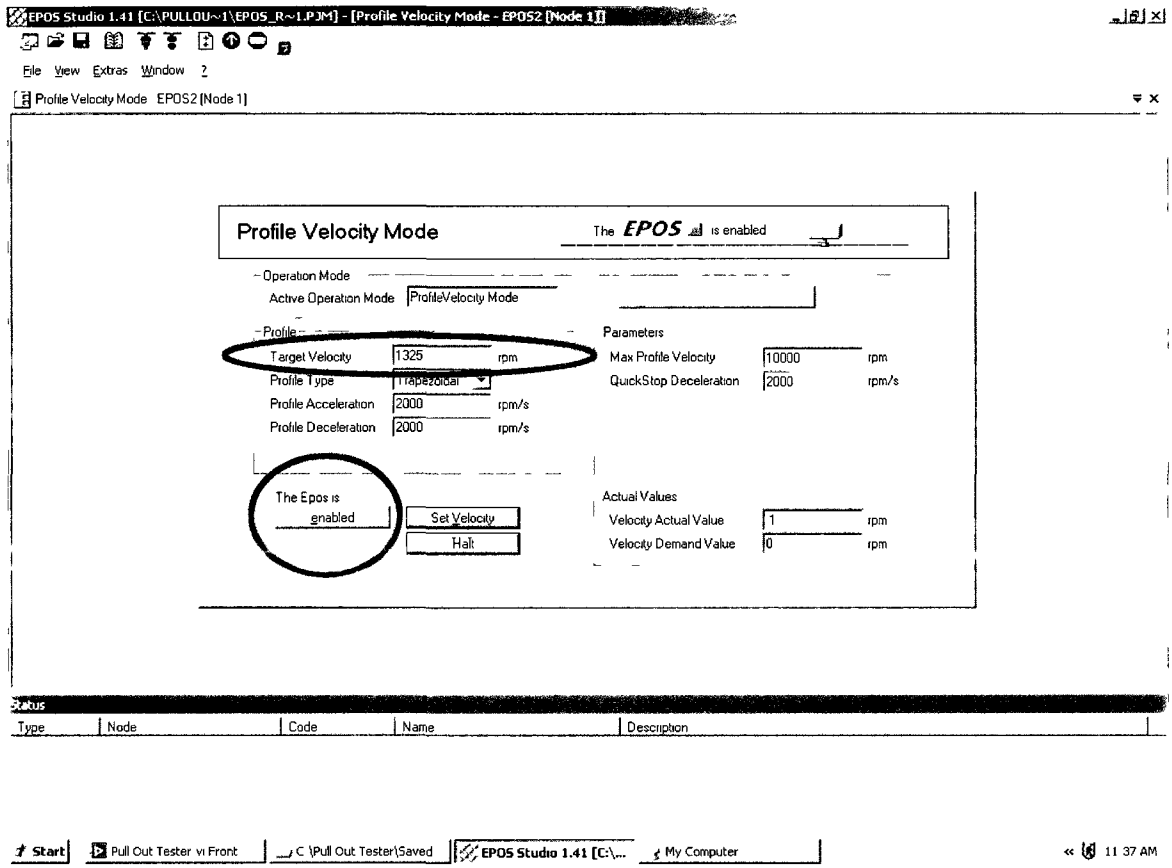

Figure App.3.3: Interface of EPOS Studio 1.41 with configured parameters (The motor positioning controller was in enabled status)

By entering either a positive or a negative speed in the "Target Velocity" field, the motor can be excited in rotating motion, immediately after, is the lifting screw on linear movement. A positive speed value causes the screw to move upwards. A negative speed value causes the screw to move downwards. The EPOS positioning controller ensures that the actual velocity value stays well within ±5% of the set-point value.

App.3.2 Data Acquisition System

An "S" beam load cell with the signal conditioning equipment located at the holding tray and a special LabVIEW application constitute the data acquiring and displaying system. A load cell is a transducer which converts force into a measurable electrical output. The LC101 – 1K load cell made by Omega Engineering was chosen to put in the portable tester to sense the extensile force and convert the deformation (strain) to electrical signals. The capacity is 1000 lbf (4.448 kN). Its designed Safe Overload is 150% and Ultimate Overload is 300% of the capacity. A customized LabVIEW application is configured to excite, acquire, display, and store data obtained from the load cell and processed by the signal conditioning equipment. Figure App.3.4 shows the operation interface of the software.

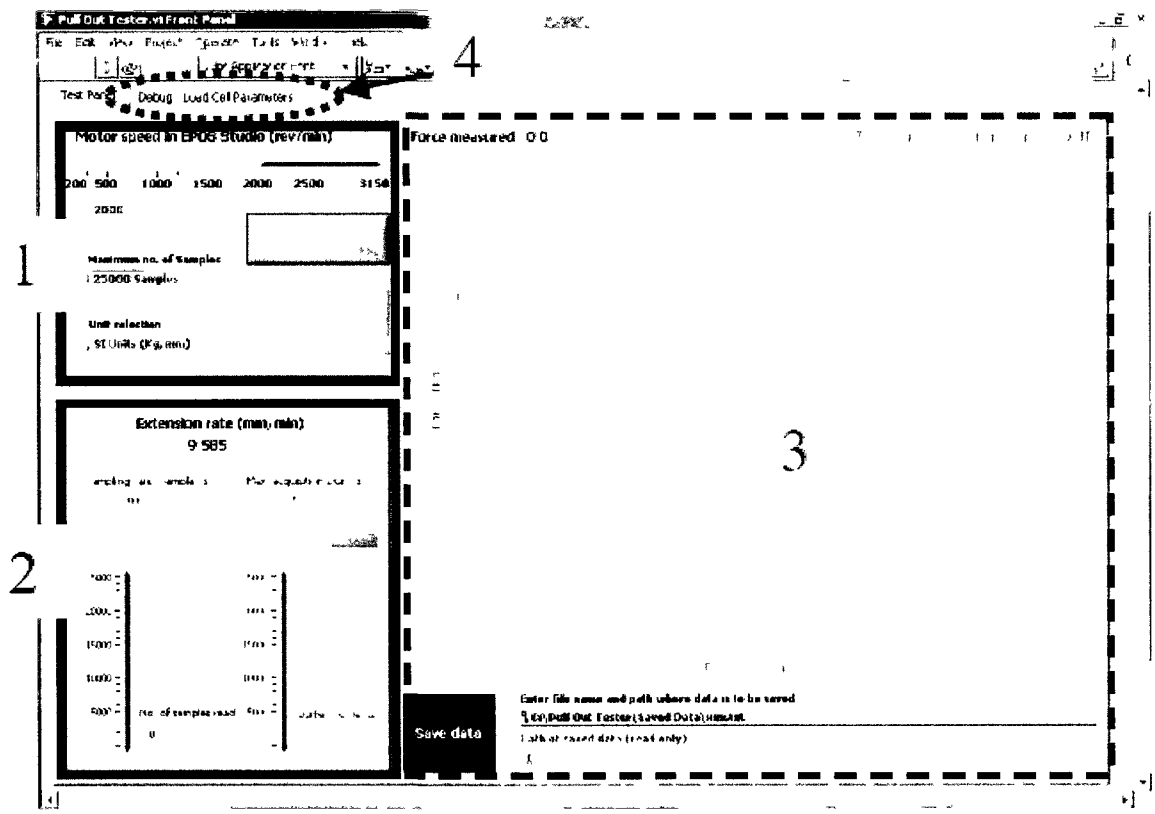

Figure App.3.4: Front panel of LabVIEW application for portable tester

The frequency of hardware used to carry out the data acquisition can make up to 50,000 samples per second. A sampling rate of 2,000 samples per second has been selected and hard coded in the LabVIEW application for the portable tester. Therefore, from selecting the "Maximum no. of Samples" field will gain the data acquiring duration through dividing by 2,000 and the result is revealed in the field of "Max. acquisition Dur. (s)". There are 10 different durations can be selected for each testing process. To an uncertain characteristic specimen, it is proper to choose the highest duration level. Out of the 2,000 samples per second, 10 samples are saved for every second in a text file as raw data for subsequent analysis.

The adjustable value of "Motor speed in EPOS Studio" can be reflected in the "Extension rate" field simultaneously. It helps the user to identify the correct motor speed for the specific test. Once a value is selected, the "Extension rate" field gets automatically updated to confirm the desired linear moving speed of the screw jack.

Section "3" displays the test results in a graphic approach. It records the collected data of the tested specimen with Load – Extension relationship. The units of the X and Y scales could be either Imperial or Metric system depends on the unit selection indicated.

Bibliography

Standards

National Building Code of Canada 2005, User's Guide – NBC 2005 Structural Commentaries (Part 4 of Division B)

Standard Test Procedure for Determining the Withdrawal Resistance of Roofing Fasteners, ANSI/SPRI FX – 1 – 2006

Wind Design Standard for Ballasted Single-ply Roofing Systems, ANSI/SPRI RP-4 2008

American Society for Testing and Materials (1996), "Standard Test Method for Tensile Strength of Adhesive by Means of Bar and Rod Specimens", ASTM D 2095-96, USA

American Society for Testing and Materials (2005), "Standard Test Method for Pull-Off Adhesion Strength of Coatings on Concrete Using Portable Pull-Off Adhesion Testers" ASTM D 7234-05, USA

American Society for Testing and Materials (2002), "Standard Test Method for Measuring Adhesion of Organic Coatings to Plastic Substrates by Direct Tensile Testing", ASTM D 5179-02, USA

A Guide for the Wind Design of Mechanically Attached Flexible Membrane Roofs (2005), A. Baskaran & T.L. Smith

European Standards (2007), "Adhesives for tiles – Determination of tensile adhesion strength for cementitious adhesives", BE EN 1348

Factory Mutual Global (2007) "Field Uplift Tests", FM 1-52

The International Organization for Standardization (2001), Determination of the bond strength of engineering plastic joints", ISO 15509

Single Ply Roofing Industry (2005), "Standard Field Test Procedure for Determing the Mechanical Uplift Resistance of Insulation Adhesives over Various Substrates" ANSI/SPRI IA-1-2005

Single Ply Roofing Industry (2006) "Standard Field Test Procedure for Determining the Withdrawal Resistance of Roofing Fasteners" ANSI/SPRI FX-1-2006

Resources

Theodore Stathopoulos, Rajan Marathe, Hanqing Wu, "Mean wind pressures on flat roof corners affected by parapets: field and wind tunnel studies", Journal of Engineering Structures 21 (1999) pp629–638

C.W. Letchford, P.P. Sarkar, "Mean and fluctuating wind loads on rough and smooth parabolic domes", Journal of Wind Engineering and Industrial Aerodynamics 88 (2000) pp101-117

Building Science for a Cold Climate

C. W. Griffin, "The manual of low-slope roof systems", Third Edition, 2000

Gregory A. Kopp, David Surry, Christian Mans, "Wind effects of parapets on low buildings: Part 1. Basic aerodynamics and local loads", Journal of Wind Engineering and Industrial Aerodynamics 93 (2005) pp817–841

A. Baskaran, T. Stathopoulos, "Roof corner wind loads and parapet configurations", Journal of Wind Engineering and Industrial Aerodynamics 29 (1988) 79–88

R.N. Sharma, P.J. Richards, "Net pressures on the roof of a low-rise building with wall openings", Journal of Wind Engineering and Industrial Aerodynamics 93 (2005) pp267–291

A. Baskaran , "Top 10 quest ions and answers on static vs. dynamic wind testing for commercial roofs", NRCC-48676, Sept., 2006

Baskaran, B.A., Molleti, S., "Air intrusion vs. air leakage - the dilemma for low sloped mechanically attached membrane roofs", The Journal of RCI Interface, November 2009, pp4–10

National Roofing Contractors Association (USA) and the National Research Council of Canada, Institute for Research in Construction, "Investigating the Cause of Blistering in SBS Polymer Modified-Bitumen Roofing Membranes", March 1998

RICOWI, Inc. (Roofing Industry Committee on Weather Issues, Inc.), "Hurricane Katrina Wind Investigation Report", August, 2007

RICOWI, Inc. (Roofing Industry Committee on Weather Issues, Inc.), "Hurricanes Charley and Ivan Wind Investigation Report", March, 2006

Baskaran, A., Desjarlais, A., Roodvoets and D., "Hurricane Katrina Wind Investigation Report, Powder Springs, Georgia: Roofing Industry Committee on Weather Issues", Inc. pp. 183, August 01, 2007 (NRCC-50024)

Baskaran, A. and Lei, W. (1997), "New Facility for Dynamic Wind Performance Evaluation of Roofing Systems", Proceedings of the Fourth International Symposium on Roofing Technology, (Gaithersburg, MD., USA, September 17, 1997), pp. 168 -179.

Baskaran, A., Molleti, S., Sexton, (2006) M. "Wind performance evaluation of fully-bonded roofing assemblies" Journal of Construction and Building Materials 22, pp 343-363

Banks D. (2000) "The suction induced by conical vortices on low-rise buildings with flat roofs", Ph.D. Thesis, Department of Civil Engineering, Colorado State University, Fort Collins, Colorado,

Banks, D., Meroney, R.N., Sarkar p.P., Zhao, Z., Wu, F. (2000) "Flow visualization of conical vortices on flat roofs with simultaneous surface pressure measurement", Journal of Wind Engineering and Industrial Aerodynamics. 84 pp 65-85

Current, J, Murty, B., Wu, J., Baskaran, A., Tanaka, H. "Wind uplift resistance data for adhesive applied roofing systems - Part 1," pp. 1-236, January 01, 2007 (IR-876)

Murty, B.; Current, J., Wu, J., Baskaran, A.; Tanaka, H. "Wind uplift resistance data for adhesive applied roofing systems - Part 2," pp. 1-180, January 01, 2008 (IR-877)

Murty, B., Current, J., Davelay, C., Baskaran, A., Tanaka, H. "Wind uplift resistance data for adhesive applied roofing systems - Part 3," pp. 1-120, August 01, 2008 (IR-878)

Wu, J (2008) "Development of a Peel Test Procedure for Adhesive Applied Roofing Systems." M.A.Sc. Thesis, Department of Civil Engineering, University of Ottawa, Ottawa, Ontario.

Current, J (2009) "Development of a Pullout Test Method for Adhesive Applied Roofing Systems" M.A.Sc. Thesis, Department of Civil Engineering, University of Ottawa, Ottawa, Ontario.

Websites

www.instron.us/wa/product/ (January, 2010)
www.maxonmotor.com (June, 2009)
www.allsteel-buildings.com (March, 2009)
http://cmroof.com/ (March, 2009)
www.ddinstallations.com (March, 2009)
www.milleniumadhesives.com (March, 2009)
www.reliantroofingsystems.com (March, 2009)
www.yourguardianroof.com (March, 2009)
http://conestogaroofing.com/FlatRoofSystems.html
http://products.construction.com
http://greensolinc.com
http://building.dow.com
www.bellaremodeling.net
www.deerparkroofing.com
www.nrca.net/
www.soprema.ca